

Universität Potsdam
Arbeitsgruppe Prof. Dr. A. Laschewsky

**The multifarious self-assembly of triblock copolymers:
From multi-responsive polymers and multi-compartment micelles**

*Dissertation zur Erlangung des akademischen Grades
„doctor rerum naturalium“ (Dr. rer. nat.)
in der Wissenschaftsdisziplin „Kolloid- und Polymerchemie“*

eingereicht an der Mathematisch-Naturwissenschaftlichen Fakultät
der Universität Potsdam

von Katja Skrabania, geboren am 9. Februar 1979 in Stralsund

Potsdam, im November 2008

This work is licensed under a Creative Commons License:
Attribution - Noncommercial - Share Alike 3.0 Germany
To view a copy of this license visit
<http://creativecommons.org/licenses/by-nc-sa/3.0/de/>

Published online at the
Institutional Repository of the University of Potsdam:
<http://opus.kobv.de/ubp/volltexte/2009/3076/>
[urn:nbn:de:kobv:517-opus-30764](http://nbn-resolving.org/urn:nbn:de:kobv:517-opus-30764)
[<http://nbn-resolving.de/urn:nbn:de:kobv:517-opus-30764>]

I wish to express my gratitude to all the people that contributed with their professional and personal support to the successful completion of this PhD project.

I owe my greatest thanks to Prof. Dr. A. Laschewsky (University of Potsdam (UP) and Fraunhofer Institute for Applied Polymer Research, Potsdam) for giving me the opportunity to prepare my PhD thesis under his supervision working on this multifaceted and challenging research topic. At all times he has been amenable to discussions and I am grateful to him for sharing his scientific knowledge and experience and for his ongoing support. I greatly appreciate his confidence in me and the freedom he gave me to follow my ideas. Finally, I am grateful for the opportunities to present the results of this PhD thesis at conferences.

My sincere thanks go to all the members of the Fraunhofer Institute of Applied Polymer Research in Potsdam-Golm for the friendly environment. In particular, I would like to thank Dr. H. P. Fink and Dr. U. Buller who permitted me to conduct my research in the laboratories of the institute.

I gratefully acknowledge the help of Dr. V. Strehmel (UP) for TGA and DSC measurements, Dr. M. Heydenreich and A. Krtitschka (UP) for NMR measurements, B. Hannemann (UP) for elemental analyses and IR measurements and Dr. H. Wetzel (Fraunhofer IAP) for fluoride ion chromatography. Moreover, I would like to thank Dr. H. Schlaad and M. Gräwert (Max-Planck-Institute of Colloids and Interfaces) for their help with SEC measurements.

I am indebted to Dr. H. von Berlepsch and Dr. C. Böttcher (Research Center for Electron Microscopy, Freie Universität, Berlin) for the cryo-TEM measurements and cryo-electron tomography measurements that made the wealth of multi-compartment micelles visible.

I gratefully acknowledge J. Kristen (UP) for the synthesis of monomer *N*-acryloyl pyrrolidine (M3) and A. M. Bivigou Koumba and D. Zehm (both UP) for the synthesis of the trithiocarbonates CTA3, CTA4, CTA9 and CTA11. Many thanks go to S. Eidner (UP) for his valuable comments on the UV-vis spectroscopic investigations of thiocarbonylthio compounds.

I would like to thank the scientists and technicians of the water-borne polymer systems department ("FB4") at the Fraunhofer IAP for the great atmosphere and their kind support. In particular, I would like to thank Dr. J. Bohrisch, Dr. S. Bruzzano, V. Jentzen, Dr. A. Lieske and Dr. J. Storsberg for their friendship and help - I could not have wished for better colleagues. I am deeply indebted to Dr. M. Päch who not only provided me with valuable feedback and suggestions concerning my thesis but became a great friend, too. Special thanks to Dr. M. Mertoglu, Dr. L. Wattebled, Dr. D. Schütt, Dr. N. Sieverling, A. M. Bivigou Koumba, P. Ott and C. Wieland who have been wonderful office and lab mates and friends.

Special thanks to F. Salles (Ecole Nationale Supérieure de Chimie, Montpellier, France) and Li Wen (Master of Polymer Science program, Technische Universität, Berlin) for their practical help during their internships at the Fraunhofer IAP and while preparing their master theses. Their placements for several months not only gave me the great opportunity to learn more about their cultures but also to develop my skills as supervisor.

Finally, I wish to express my heartfelt thanks to M. Steude and K. Okulla (Fraunhofer IAP) for their friendship and for providing me with insights into PR and marketing.

Last, but by no means least, I am grateful to the support, patience, and understanding of my family.

New ABC triblock copolymers were synthesized by controlled free-radical polymerization via Reversible Addition-Fragmentation chain Transfer (RAFT). Compared to amphiphilic diblock copolymers, the prepared materials formed more complex self-assembled structures in water due to three different functional units. Two strategies were followed: The first approach relied on double-thermoresponsive triblock copolymers exhibiting Lower Critical Solution Temperature (LCST) behavior in water. While the first phase transition triggers the self-assembly of triblock copolymers upon heating, the second one allows to modify the self-assembled state. The stepwise self-assembly was followed by turbidimetry, dynamic light scattering (DLS) and ^1H NMR spectroscopy as these methods reflect the behavior on the macroscopic, mesoscopic and molecular scale. Although the first phase transition could be easily monitored due to the onset of self-assembly, it was difficult to identify the second phase transition unambiguously as the changes are either marginal or coincide with the slow response of the self-assembled system to relatively fast changes of temperature.

The second approach towards advanced polymeric micelles exploited the thermodynamic incompatibility of “triphilic” block copolymers – namely polymers bearing a hydrophilic, a lipophilic and a fluorophilic block – as the driving force for self-assembly in water. The self-assembly of these polymers in water produced polymeric micelles comprising a hydrophilic corona and a microphase-separated micellar core with lipophilic and fluorophilic domains – so called multi-compartment micelles. The association of triblock copolymers in water was studied by ^1H NMR spectroscopy, DLS and cryogenic transmission electron microscopy (cryo-TEM). Direct imaging of the polymeric micelles in solution by cryo-TEM revealed different morphologies depending on the block sequence and the preparation conditions. While polymers with the sequence hydrophilic-lipophilic-fluorophilic built core-shell-corona micelles with the core being the fluorinated compartment, block copolymers with the hydrophilic block in the middle formed spherical micelles where single or multiple fluorinated domains “float” as disks on the surface of the lipophilic core. Increasing the temperature during micelle preparation or annealing of the aqueous solutions after preparation at higher temperatures induced occasionally a change of the micelle morphology or the particle size distribution.

By RAFT polymerization not only the desired polymeric architectures could be realized, but the technique provided in addition a precious tool for molar mass characterization. The thiocarbonylthio moieties, which are present at the chain ends of polymers prepared by RAFT, absorb light in the UV and visible range and were employed for end-group analysis by UV-vis spectroscopy. A variety of dithiobenzoate and trithiocarbonate RAFT agents with differently substituted initiating R groups were synthesized. The investigation of their absorption characteristics showed that the intensity of the absorptions depends sensitively on the substitution pattern next to the thiocarbonylthio moiety and on the solvent polarity. According to these results, the conditions for a reliable and convenient end-group analysis by UV-vis spectroscopy were optimized. As end-group analysis by UV-vis spectroscopy is insensitive to the potential association of polymers in solution, it was advantageously exploited for the molar mass characterization of the prepared amphiphilic block copolymers.

Abbreviations	vii
1 Introduction	1
1.1 Block copolymers in selective solvents	2
1.1.1 Micellization of block copolymers	2
1.1.2 Applications of amphiphilic block copolymers	4
1.2 Increasing the complexity of block copolymer micelles	7
1.2.1 ABC triblock copolymers	7
1.2.2 Stimuli-responsive block copolymers	8
1.2.3 Multi-compartment micelles - A new class of polymeric micelles	10
1.3 Methods of controlled radical polymerization (CRP)	13
1.3.1 Introduction to CRP methods	13
1.3.2 Nitroxyl-mediated polymerization (NMP)	14
1.3.3 Atom transfer radical polymerization (ATRP)	15
1.3.4 Polymerization by reversible addition fragmentation chain transfer (RAFT)	16
1.4 Objectives and motivation	22
2 Synthesis of chain transfer agents	23
2.1 The most used synthetic routes to thiocarbonylthio compounds	24
2.2 Synthesis of chain transfer agents	26
3 UV-vis absorptions of chain transfer agents & Their potential for end-group analysis	30
3.1 Motivation for studying UV-vis absorptions of chain transfer agents	31
3.2 Introduction: Electronic spectra of thiocarbonyl compounds	32
3.3 Influence of R groups on the electronic spectra of CTAs	33
3.4 Influence of solvent polarity on the electronic spectra of CTAs	35
3.5 Model compounds for macroCTAs	38
3.6 CTAs with chromophore-labeled R groups	41
3.7 Summary and guidelines for an optimized end-group analysis	43
4 Double-thermoreponsive ABC triblock copolymers & Their self-assembly in water	44
4.1 Challenges and strategies of the studied system	44
4.2 Synthesis and molecular characterization of double-thermoreponsive ABC triblock copolymers	47
4.3 Self-assembly of double-thermoreponsive polymers in water	53
4.3.1 Turbidimetric analysis	54

4.3.2	Survey by ^1H NMR spectroscopy	59
4.3.3	Study of the double thermoresponsive self-assembly by DLS	61
4.3.4	Summary	68
5	Triphilic ABC triblock copolymers & Their self-assembly into multi-compartment micelles	70
5.1	Challenges and strategies of the studied system	70
5.2	Synthesis and molecular characterization of macroCTAs	73
5.3	Synthesis and characterization of di- and triblock copolymers	75
5.4	Thermal analysis of the triphilic ABC triblock copolymers	81
5.5	Self-assembly of triphilic ABC block copolymers in water	83
5.5.1	Preparation of micellar solutions	84
5.5.2	Study of the micelle size by DLS	88
5.5.3	Survey of the micelle morphology by cryo-TEM	93
5.5.4	Summary	101
6	General conclusions	102
7	Experimental part	104
7.1	Analytical methods	104
7.2	Synthesis of chain transfer agents (CTA)	106
7.2.1	Naphthalene-2-ylmethyl dithiobenzoate (CTA2)	106
7.2.2	Butyl 2-(butylsulfanylthiocarbonylsulfanyl) propionate (CTA5)	107
7.2.3	<i>N,N</i> -dimethyl 2-(butylsulfanylthiocarbonylsulfanyl) propionamide (CTA6)	108
7.2.4	2-(butylsulfanylthiocarbonylsulfanyl)-2-methyl propionic acid (CTA7)	110
7.2.5	Methyl 2-(butylsulfanylthiocarbonylsulfanyl)-2-methyl propionate (CTA8)	111
7.2.6	S-butyl-S'-naphthalen-2-ylmethyl trithiocarbonate (CTA10)	112
7.2.7	1,4-bis(butyl trithiocarbonato methyl) benzene (CTA12)	112
7.2.8	1,4-bis(octadecyl trithiocarbonato methyl) benzene (CTA13)	113
7.2.9	PEO monomethyl ether 2-(butylsulfanylthiocarbonylsulfanyl)-2-methyl propionate (CTA14)	114
7.3	UV-vis spectroscopic analysis of CTAs	115
7.3.1	Determination of λ_{max} and the molar absorptivity ϵ	115
7.3.2	Synthesis of polymers for the evaluation of end-group analysis	115
7.4	Polymerizations	116
7.4.1	Reagents	116
7.4.2	Synthesis of double-thermoresponsive block copolymers	116
7.4.3	Synthesis of triphilic block copolymers	117
7.5	Preparation and analysis of micellar solutions	120

7.5.1 Solutions of thermoresponsive polymers	120
7.5.2 Micellar solutions of amphiphilic block copolymers	120
8 Bibliography	121
 Appendix	
1 NMR spectra of chain transfer agents	I
2 IR spectra of chain transfer agents	XIII
3 Cryo-TEM micrographs	XVIII
4 List of figures	XIX
5 List of tables	XXIV
6 Structures of the CTAs, monomers and initiators	XXV

A	absorption
AIBN	azobis(isobutyronitrile)
AM	acrylamide
AN	acrylonitrile
ATRP	atom transfer radical polymerization
BuA	n-butyl acrylate
BuAc	n-butyl acetate
cmc	critical micellization concentration [mol/L]
CRP	controlled radical polymerization
cryo-TEM	cryogenic transmission electron microscopy
CTA	chain transfer agent for RAFT polymerization
<i>D</i>	diameter
<i>D_h</i>	hydrodynamic diameter
DLS	dynamic light scattering
DMA	<i>N,N</i> -dimethyl acrylamide
DP	degree of polymerization
DSC	differential scanning calorimetry
FC	fluorocarbon
FRP	free-radical polymerization
HC	hydrocarbon
<i>L_{corona}</i>	thickness of the micellar corona
LCST	lower critical solution temperature
M	molar mass
<i>M_n</i>	number-average molar mass
<i>M_{theory}</i>	theoretically expected molar mass
<i>M_w</i>	weight-average molar mass
MA	methyl acrylate
MADIX	macromolecular design via the interchange of xanthates
MMA	methyl methacrylate
MW	molecular weight
<i>N_{Agg}</i>	aggregation number
NIPAM	<i>N</i> -isopropyl acrylamide
N-MP	<i>N</i> -methyl pyrrolidone
NMP	nitroxyl mediated polymerization
NMR	nuclear magnetic resonance
NVP	<i>N</i> -vinyl pyrrolidone
PB	polybutadiene
PD	polydispersity index for DLS
PDI	polydispersity index for SEC (<i>M_w</i> / <i>M_n</i>)
PEE	poly(ethyl ethylene)
PEO	poly(ethylene oxide)

PI	polyisoprene
PMMA	poly(methyl methacrylate)
PRE	persistent radical effect
PS	polystyrene
PTC	phase transfer catalyst
PVP	poly(vinyl pyridine)
RAFT	reversible addition fragmentation chain transfer
SEC	size exclusion chromatography
T	absolute temperature
T_g	glass transition temperature
T_m	melting temperature
T_r	recrystallization temperature
TEM	transmission electron microscopy
TEMPO	2,2,6,6-tetramethyl-piperidinyl-1-oxy
THF	tetrahydrofuran
TGA	thermal gravimetric analysis
UCST	upper critical solution temperature
VAc	vinyl acetate
X	fractional monomer conversion
ϵ	molar absorptivity
ΔG_{mic}°	standard free energy of micellization
ΔH_{mic}°	standard enthalpy of micellization
ΔS_{mic}°	standard entropy of micellization
λ_{max}	maximum absorption wavelength

1. INTRODUCTION

The expression self-organization or self-assembly refers to a process in which the components of a disordered system arrange spontaneously and form an ordered structure or pattern due to specific, local interactions. The spontaneous formation of structures - without any guidance - contradicts our usual perception that things rather fall apart than arrange themselves. Nevertheless, self-organization is widespread in nature and is observed on all scales. From galaxies to hurricanes, from schools of fish or flocks of birds to cells and folded proteins, self-organization is the prevailing principle around us which generates structural order.

In chemistry, molecular self-assembly is defined as the spontaneous and reversible organization of molecular units into ordered structures by non-covalent interactions, such as hydrogen bonding, Van der Waals-forces or π - π -interactions. The final structure of the self-assembled system is 'encoded' in the functional units of the molecule as they are able to create such weak bonds. The folding of proteins exemplifies how complex and three-dimensional structures are generated by the spontaneous folding of linear precursors. In principle, self-assembly requires neither input of information nor energy but proceeds spontaneously towards thermodynamic equilibrium or at least towards a free-energy minimum. Although self-assembling systems attract the interest of fundamental researchers due to their fascinating interplay of weak forces, the development of these systems has also been driven by the need for advanced materials due to the rise of nanotechnology and by the miniaturization of computer circuitry. Self-assembly is referred to as a 'bottom-up' manufacturing technique, as the desired structure is built according to the shape and properties of the molecule. Examples include self-assembled monolayers, micelles, surfactant bilayer membranes, Langmuir-Blodgett films, alternatively deposited polyelectrolyte multilayers and microphase-separated block copolymers.

Block copolymers are generally defined as (linear) macromolecules where two or more polymer blocks of different chemical structure are covalently attached to each other. The simplest case is a diblock copolymer AB consisting of a homopolymer block A and homopolymer block B linked to each other. In comparison to statistical or alternating copolymers, block copolymers retain and combine the individual properties of the constituting blocks. For example, rigid and soft blocks or blocks with coiled and helical conformation can be combined, resulting in materials with unique properties. In bulk, block copolymers segregate into a variety of ordered structures if the blocks are immiscible with each other. The connectivity of the blocks prevents macrophase separation and thus, the block copolymer chains organize in such a way that unfavorable A-B contacts are minimized without over-stretching the block copolymer chains.¹

Chapter 1.1 provides a general overview on the field of self-assembling amphiphilic polymers and highlights selected applications. Chapter 1.2 presents how the complexity of polymeric micelles formed from amphiphilic block copolymers can be increased by the introduction of a third functional block and how smart materials are created by stimuli-responsive polymers.

The field of amphiphilic block copolymers has received much attention in the younger past due to recent developments of controlled free radical polymerization (CRP). In contrast to ionic polymerization methods, controlled radical polymerization allows the direct synthesis of block copolymers bearing highly

polar moieties. In chapter 1.3, a general overview of these methods is provided, with special emphasis on RAFT polymerization. Chapter 1.4 presents the objectives and motivation of the present work.

1.1. Block copolymers in selective solvents

1.1.1. Micellization of block copolymers

When block copolymers are dissolved in a selective solvent, i.e. any solvent which is good for only one of the blocks, the insoluble blocks will associate to form micellar aggregates (Fig. 1.1). The aggregates form as a result of the attractive forces between the insoluble blocks and the repulsive forces between the soluble blocks which prevent the unlimited growth of the aggregates into a macroscopic phase. Especially water as selective solvent is an intriguing case. In analogy to classical surfactants, amphiphilic block copolymers associate in water to form aggregates with a hydrophobic core and a hydrophilic corona. In contrast to polysoaps, where each repeating unit is amphiphilic by itself, macro surfactants obtain their amphiphilicity only by connecting hydrophilic and hydrophobic blocks. In addition to their ability to self-assemble even in organic solvents, block copolymers are superior to classical surfactants as they allow for a much larger degree of compositional and architectural control and can be precisely designed to fulfill particular applications.

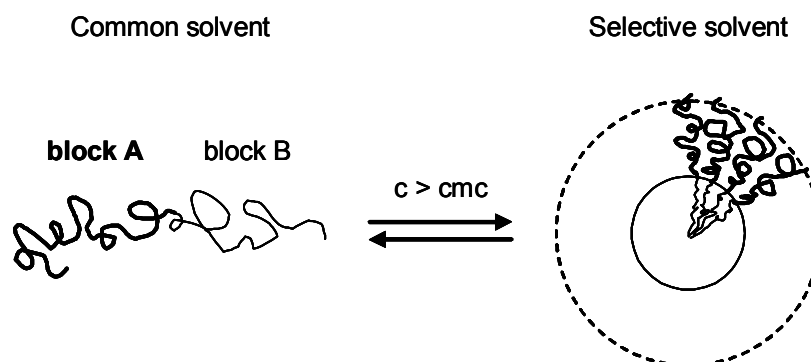


Figure 1.1 Association of AB diblock copolymers into spherical micelles in a selective solvent for the A block

Several theoretical studies of the association of block copolymers have been published.²⁻⁵ The driving forces for the micellization of block copolymers depend on the selective medium. Considering the dominating contributions to the free energy of micellization, one has to distinguish between micellization in organic solvents and in water. In organic solvents, the micellization of block copolymers is driven by enthalpy. The replacement of polymer/solvent interactions by polymer/polymer and solvent/solvent interactions upon formation of the micellar core is an exothermic process which involves negative changes of ΔH_{mic}° . However, micellization is disfavored by entropy (negative change of ΔS_{mic}°) as the copolymer chains are less swollen in the micelles than in the unassociated state. Furthermore, the number of possible conformations of the chains is decreased due to the block junctions at the core/shell interface of the micelles. Nevertheless, ΔH_{mic}° dominates over ΔS_{mic}° leading to a negative standard Gibbs energy ΔG_{mic}° :

$$\Delta G_{mic}^{\circ} = \Delta H_{mic}^{\circ} - T\Delta S_{mic}^{\circ} \quad \text{Equation 1.1}$$

For PI-b-PS block copolymers in n-hexadecane, $\Delta G_{\text{mic}}^\circ$ and $\Delta H_{\text{mic}}^\circ$ were found to be strongly dependent on the molar mass of the insoluble PS block, both becoming more negative with increasing chain length.⁶ Thus, the enthalpy-driven association of block copolymers in organic solvents normally requires lengthy insoluble blocks, typically 20,000 g/mol or more. In water, the micellization of amphiphilic block copolymers is driven by entropy as the water structure next to the polymer chains is changed and as a consequence of hydrophobic interactions.

In principle, the micellization of block copolymers in selective solvents is considered to be similar to that of low-molar mass amphiphiles. At very low concentrations, the block copolymer chains exist as unimers in solution. The insoluble block might be collapsed to form so-called monomolecular micelles. When the concentration reaches a critical value - namely the critical micellization concentration (cmc) - the polymer chains associate to form micellar aggregates in which the insoluble blocks form the micellar core and the soluble blocks the corona. With increasing concentration of block copolymer the equilibrium is shifted to the micellar form.

Deviations in the micellization behavior of block copolymers⁵ compared to classical surfactants arise first of all from the fact that block copolymers are usually polydisperse materials with respect to molar mass and composition. Moreover, the process of association into aggregates is expected to be different due to the collapsed insoluble blocks. Amphiphilic block copolymers exhibit in general a lower cmc and lower diffusion rates than low-molar mass surfactants, rendering the micellar aggregates stable upon extreme dilution.² However, the cmc is influenced by the polydispersity of the sample in organic solvents as well as in water and decreases with increasing polydispersity.^{5, 7} Although the concentration of unimers above the cmc is constant for low-molar mass surfactants, it is not necessarily true for block copolymers. Accordingly, methods that are sensitive to the concentration of unimers such as surface tensiometry and conductivity are not suited for the determination of the cmc of amphiphilic block copolymers.

The micellar aggregates of block copolymers in a selective solvent are characterized by:⁸

- the equilibrium constant unimers \leftrightarrow micelles
- the cmc
- the morphology; which is spherical in the simplest case
- N_{Agg} ; the aggregation or association number, e.g. the average number of polymer chains in a micelle,
- R_g , the radius of gyration of the micelle;
- R_h , the hydrodynamic radius of the micelle; i.e. radius of the equivalent sphere which would exhibit the same diffusion coefficient as the aggregate
- the ratio R_g/R_h which is informative of the shape
- R_c ; the micellar core radius
- L ; the thickness of the shell (corona) formed by the soluble blocks

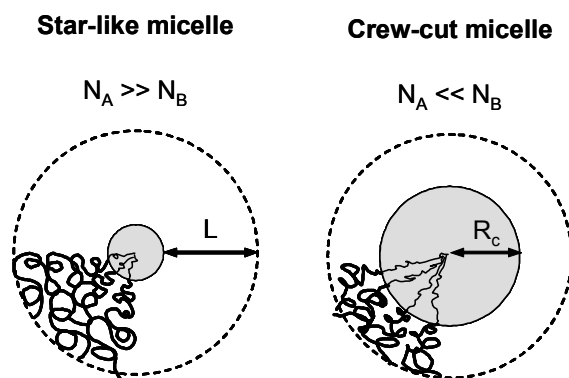


Figure 1.2 Morphologies of spherical block copolymer micelles

The morphology and size of polymeric micelles is influenced by both, molecular and solution parameters. The molecular parameters comprise the chemical structure of the blocks, their ratio, the overall molar mass and the architecture of the macromolecule. These parameters proved to be the most important influences on the micelle morphology.^{9, 10} Only recently¹¹⁻¹³ it has been recognized that the micellar morphology is influenced by the history of the polymer solution, too. Solution parameters include type of solvent, the solvent/non-solvent ratio, the copolymer concentration, the pH value, impurities such as salts and homopolymer, the method of preparation and temperature. In some cases, the micelle morphology is determined by specific interactions like hydrogen bonding or excess chirality in the monomer units.¹⁴ Micellar morphologies that were obtained from amphiphilic block copolymers include but are not limited to spheres, cylinders, worm-like micelles and vesicles.¹⁵

1.1.2. Applications of amphiphilic block copolymers

Due to their unique properties amphiphilic block copolymers hold a great potential for advanced technological applications. In contrast to low-molar mass surfactants, they offer a much higher flexibility and diversity as each polymeric system can be tailor-made according to the desired application. Furthermore, they allow to introduce a great variety of functionalities such as moieties for complexation of metal ions or targeting moieties for drug delivery applications. The field of amphiphilic block copolymers is rapidly growing and was strongly supported by the development of the methods of controlled free radical polymerization (CRP) as they allow to polymerize monomers bearing highly polar functionalities.

Still, there are also drawbacks concerning the use of amphiphilic block copolymers. First of all, they are not as well-defined as their low-molar mass counterparts. Especially in the case of CRP methods, polydisperse samples with homopolymer impurities cannot be excluded. Moreover, the direct solubility of amphiphilic block copolymers is decreased requiring (extensive) dispersion methods. Nevertheless, the combined advantages have established the use of amphiphilic block copolymers in numerous applications of which some will be highlighted in the following section.

Applications employing the surface activity of amphiphilic block copolymers

Block copolymers behave as typical amphiphiles in solvents which are selective for only one block. Depending on their affinity to different phases they are able to accumulate at interfaces leading to a decrease of interfacial tension. Due to their surface activity block copolymers are of increasing

importance in many industrial and pharmaceutical applications and are employed as dispersants, emulsifiers, wetting agents, foam stabilizers, flocculants, demulsifiers, etc.

Block copolymers are known to adsorb on solid surfaces, too.¹⁶⁻¹⁸ The various possibilities, how a block copolymer can interact physically with a solid surface in a selective solvent, are depicted in Figure 1.3. If the soluble block has an affinity to the surface, a monolayer of micelles will cover the surface above the cmc, especially in cases of micelles with frozen cores ((a) in Fig. 1.3). If the insoluble block is able to interact with the substrate, it will adsorb on the surface forming a molten film and the swollen soluble block will build up a brush¹⁹ (Fig. 1.3b). The adsorption behavior of amphiphilic diblock copolymers at interfaces plays an important role in the stabilization of colloidal particles in inks, paints, coatings and pharmaceuticals.

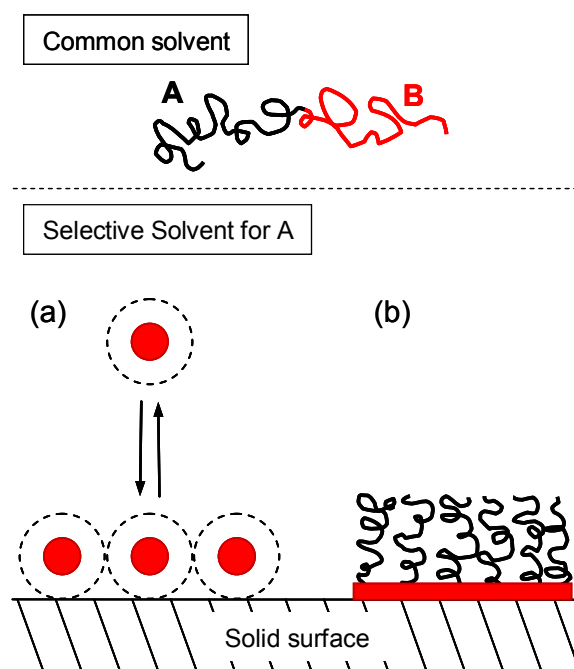


Figure 1.3 Modification of solid surfaces by block copolymers and block copolymer micelles: (a) Soluble block A interacts with surface (b) Insoluble block B interacts with surface.

Amphiphilic block copolymers have been shown to efficiently stabilize polymer dispersions²⁰ and emulsions.²¹⁻²⁶ Their advantages compared to conventional surfactants lie in their low cmc, their better compatibility with the polymer particles and their lower migration rate due to the good anchorage of the hydrophobic block to the latex particle. By forming a dense hydrophilic shell around the particle they provide steric as well as electrostatic stabilization if a polyelectrolyte is employed as hydrophilic segment. The difficulties in dissolving the polymeric surfactant in water prior to polymerization can be overcome by using stimuli-responsive polymeric surfactants²⁷⁻²⁹ or by using a reactive hydrophilic precursor polymer that gains its amphiphilicity during polymerization of the hydrophobic monomer.²²

Colloidal nanostructures and nanomaterial fabrication

Creating materials with dimensions of the nano scale that are uniform in size and shape is one of the most important topics of current research.³⁰⁻³³ There is a growing demand for such materials for numerous applications such as heterogeneous catalysis,^{34, 35} separation media, biopolymer tagging and

quantum dots^{36, 37} (light-emitting semiconductor nano crystals, e.g. CdS) due their special size-dependent chemical and physical properties. Nanoparticles are classically prepared by a so-called top-down approach starting from bulk material. However, the top-down approach is difficult to control regarding uniformity of size and shape and causes high costs. For optimal control, such nanoparticles are synthesized in preformed structures such as micellar cores³⁸ or shells³⁹ of self-assembled block copolymers in apolar solvents⁴⁰ and in water.⁴¹ Metal salts are selectively accumulated in the micellar core by complexation, and then reduced or oxidized to form the desired nanoparticles while the micellar shell restricts the uncontrolled growth of the aggregates. Poly(vinyl pyridine) (PVP) is the most studied polymer in this context due to its excellent metal complexation properties.⁴¹ A number of metal colloids such as Au⁴², Ag⁴², Pd^{38, 42, 43}, Rh⁴² and Co⁴⁴ were prepared in this way.

The coating of metal⁴⁵ and semiconductor nanoparticles with polymers increases their stability towards aggregation as well as their solubility. Furthermore, they are protected against oxidation and can exhibit a much higher catalytic activity.³⁸ In addition, such systems allow the recovery of the catalytic nanoparticles by ultrafiltration or precipitation of the polymer.

Amphiphilic block copolymers for drug delivery

In the field of biomedical applications block copolymers have found increasing interest in their colloidal form as controlled drug delivery systems,⁴⁶⁻⁵⁰ as carriers of diagnostic agents and more recently in gene delivery.⁵¹ As their most important property, amphiphilic block copolymers enhance the solubility of poorly water-soluble therapeutic compounds since the micellar cores serve as a compatible microenvironment. Micelles formed from amphiphilic block copolymers are much more stable upon dilution than those from classical surfactants. This is an important property to avoid the premature dissociation of micelles and thus, the release of the drug. Being resistant against protein adsorption⁵² and cell adhesion, poly(ethylene oxide) (PEO) is often employed as hydrophilic shell. Accordingly, the contents of the micellar core are protected against hydrolysis and enzymatic degradation. The PEO corona also avoids the elimination of the micelles from the blood stream⁵³ as they are not recognized by the reticuloendothelial system. According to these properties, the circulation times of the polymeric micelles are increased and the drugs are administered for a prolonged time. Another important advantage of block copolymers for drug delivery applications is the possibility to modify the design of polymeric micelles by changing the composition, the molar mass and the architecture of the respective polymers.

Although amphiphilic block copolymers have been proven to be efficient drug delivery devices their performance regarding temporal and distribution control still needs optimization. These aspects are especially important for administering of peptide drugs and for gene therapy. Control of the drug release profile is generally achieved by cross-linking either of the micellar core or the shell. In order to cross-link the micellar core, polymerizable groups can be introduced either at the end or along the hydrophobic chain. However, this approach also decreases the drug loading capacity. Cross-linking of the hydrophilic shell⁵⁴ enables the fine-tuning of the drug release profile as it depends on the density of cross-links. Hydrophilic shells made of poly(methacrylic acid), poly(vinyl pyridine) and poly(dimethylaminoethyl acrylate) have been cross-linked by amide bonds or by quaternization. The removal of the hydrophobic core after cross-linking produces nanocages⁵⁵ with a much higher drug loading capacity for rather hydrophilic drugs.

The biodistribution of an administered drug can be controlled by functionalization of the shell for site targeting. An example of passive drug targeting is the enhanced permeability and retention effect (EPR)⁵⁶ which is exploited for the efficient treatment of solid tumors as it takes advantage of the enhanced vascular permeability of tumor tissue compared to healthy tissue. As a result, high-molar mass substances can be preferentially accumulated at these sites. Active targeting⁵⁷ - the transportation of drugs to a specific site - is achieved by modification of the hydrophilic shell with ligands that are recognized by cell receptors. Such ligands include saccharides⁵⁸ and most notably folate, since receptors for this vitamin are frequently overexpressed in tumors.^{59, 60}

1.2. Increasing the complexity of block copolymer micelles

1.2.1. ABC triblock copolymers

Block copolymers that contain two blocks of distinct monomers A and B can have various architectures, such as linear diblock (AB), triblock (ABA), multiblock (AB)_n or star diblocks (AB)_nX. Beside the architecture, control over the self-assembled structure of diblock copolymers in bulk and in solution is typically achieved by variation of the molar mass or the composition of the polymer. The introduction of a third component C in ABC triblock copolymers⁶¹ modifies the self-organization in bulk compared to the diblock AB and results in a much larger variety of mesomorphic structures^{62, 63} due to two independent compositional order parameters and three Flory-Huggins interaction parameters.⁶⁴

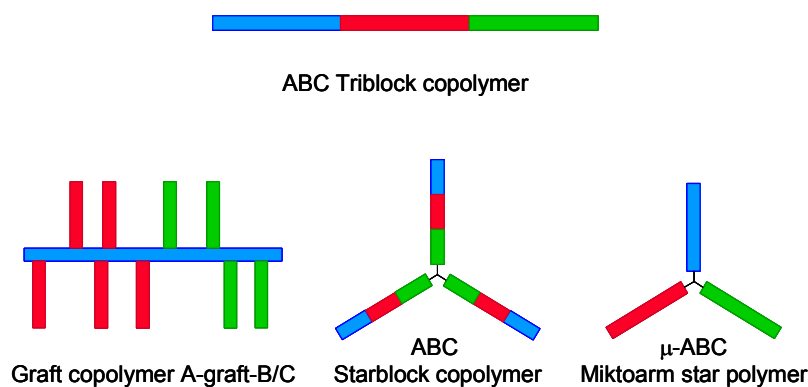


Figure 1.4 Various architectures of ABC triblock copolymers

Although the synthesis of ABC triblock copolymers is well documented, the number of studies that deal with their self-assembly in selective solvents is limited. The introduction of a third block results in morphologies with a structured core^{39, 65-70} or shell, such as three-layer^{65, 67, 71} or onion as well as Janus micelles.^{70, 72, 73} The so-called Janus micelles

are reported to consist of a cross-linked polybutadiene (PB) core with a northern polystyrene (PS) and a southern poly(methyl methacrylate) (PMMA) hemisphere. Their distinctive feature is the generation of the structure in bulk which persists in solution after cross-linking of the core.

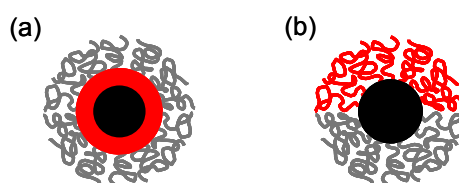


Figure 1.5 Micelle morphologies of ABC triblock copolymers in selective solvents: (a) "onion" micelle (b) Janus micelle.

1.2.2. Stimuli-responsive block copolymers

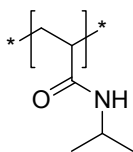
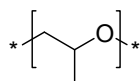
Response to stimulus is a phenomenon found in living nature. Inspired by this, increasing efforts are made to develop "smart" materials that dynamically respond to external stimuli by a dramatic change of their key properties. In the strict sense, the induced property changes should be reversible if the stimulus is suppressed, or if a second, "reverse" stimulus is applied. Recently, much attention has been focused on stimuli-responsive amphiphilic block copolymers whose amphiphilicity can be altered by the afore mentioned environmental changes, i.e. they can be reversibly switched from hydrophilic to hydrophobic.⁷⁴ Due to their switchable amphiphilic behavior they can self-assemble "on demand" in aqueous solution and form polymeric micelles with hydrophobic nano-domains. Various stimuli - such as pH,^{29, 75-78} light,⁷⁹⁻⁸² pressure,⁸³ ionic strength,^{84, 85} selective ion binding,²⁹ magnetic fields⁸⁶ or redox reactions^{87, 88} - can be used to trigger the switching (cf. Fig. 1.6).

Temperature is especially suitable as stimulus because the changes are intense, fully reversible, and no reagents have to be added or to be removed. Two kinds of thermoresponsive polymers may be distinguished: First, polymers that are insoluble at low temperatures but become soluble at higher temperatures, i.e. the system shows a behavior that is characterized by an Upper Critical Solution Temperature (UCST). Such a behavior is rarely found in aqueous solution, and has been observed mainly for polyzwitterions⁸⁹ or poly(vinyl alcohol).⁹⁰ The second type are polymers that are soluble at low temperatures but become insoluble at high temperatures, i.e. such which are characterized by a Lower Critical Solution Temperature (LCST).

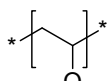
The occurrence of a LCST is known for many nonionic polymers. It is found in systems where the solubility of the polymer depends on specific, directed interactions (e.g. hydrogen bonds) leading to negative entropy changes. With increasing temperature the entropic term dominates which results in positive contributions to the free energy of mixing.⁹¹ This phenomenon is particularly important in aqueous media where a further negative entropy change is contributed by the hydrophobic effect. A thermoresponsive behavior which is characterized by a LCST in aqueous media is not restricted to a certain class of polymers. Many examples are known: polymers of substituted (meth)acrylamides,⁹²⁻⁹⁸ polyvinylether,⁹⁹ poly(*N*-vinylalkylamide)s¹⁰⁰ and poly(*N*-vinylcaprolactam),¹⁰¹⁻¹⁰³ methyl- and hydroxypropylcellulose,¹⁰⁴ poly(ethylene oxide) (PEO) and poly(propylene oxide) (PPO)¹⁰⁵, polymers with alkyl end-capped oligo(ethylene oxide)s side chains¹⁰⁶ and poly(2-alkyl-2-oxazoline)s.¹⁰⁷ A relatively new class of thermoresponsive polymers are poly(amino acid)s¹⁰⁸ which are not only biocompatible but also biodegradable and therefore promising materials for drug delivery applications. Within the mentioned examples the substituted poly(meth)acrylamides are very versatile since their LCST can be varied over the whole temperature range of liquid water at ambient pressure by appropriate substitution of the amide nitrogen. Poly(*N*-isopropyl acrylamide) (polyNIPAM) is the most widely used polymer in this class since its LCST of 32°C is convenient for studying the thermoresponsive behavior. Moreover, its clouding temperature is rather insensitive to variations of molar mass and concentration.

(a) temperature

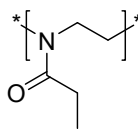
LCST

poly(*N*-isopropylacrylamide)

poly(propylene oxide)

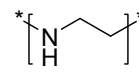
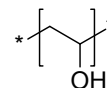


poly(methyl vinyl ether)

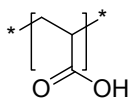


poly(2-ethyl-2-oxazoline)

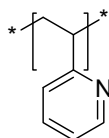
UCST

poly(ethylene imine)
(+ pH)

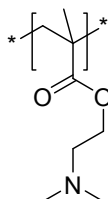
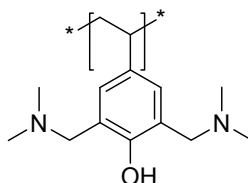
poly(vinyl alcohol)

(b) pH

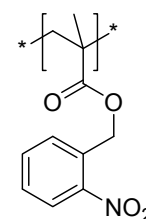
poly(acrylic acid)



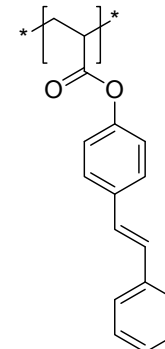
poly(2-vinyl pyridine)

poly(dimethylaminoethyl methacrylate)
(+ LCST)

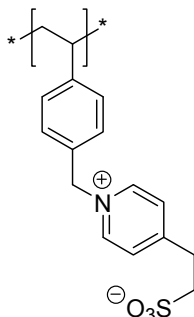
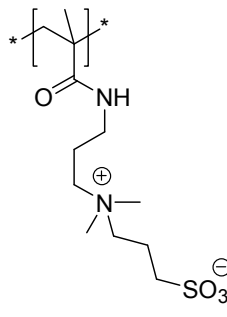
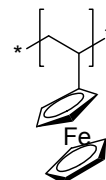
poly[3,5-bis(dimethylamino)methylene] hydroxystyrene

(c) light

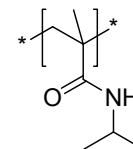
poly(2-nitrobenzyl methacrylate)



poly(4-phenylazo-phenyl acrylate)

(d) ionic strength4-(2-sulfoethyl)-1-(4-vinylbenzyl) pyridinium betain
(+ UCST)3-[N-(3-methacrylamidopropyl)-N,N-dimethyl] ammoniopropane sulfonate
(+ UCST)**(e) redox reaction**

poly(vinyl ferrocene)

(f) pressurepoly(*N*-isopropylmethacrylamide)
(+ LCST)**Figure 1.6** Repeating units of stimuli-responsive polymers

Various amphiphilic block copolymers with thermoresponsive blocks have been studied, but most examples are polymers that combine a classical hydrophobic block with a thermoresponsive one.¹⁰⁹ Double-hydrophilic block copolymers¹¹⁰ comprising a stimuli-responsive block are a minority so far. However, this combination is especially useful if a “surfactant on demand” is looked for, as this approach avoids the extensive procedures that are often necessary to disperse amphiphilic block copolymers in water.¹¹¹⁻¹¹³

1.2.3. Multi-compartment micelles - A new class of polymeric micelles

Nanotechnology is one of the biggest topics in research today and there is an increased need for new/advanced nano materials for a diversity of applications. In chapter 1.1.2, amphiphilic block copolymers were shown to be employed in many nano scale applications and especially polymeric micelles made from such polymers have attracted great interest. However, in most cases they only exhibit a single hydrophobic domain in the micellar cores which can be addressed.

In biological systems - such as cells, enzymes, etc. - distinct functional and structural units enable reactions to proceed in close proximity but without mutual interference. In front of this background the concept of multi-compartment micelles has emerged which was proposed originally by H. Ringsdorf in the 1990ies. Since then several research groups have dealt with this topic using different approaches to realize such a compartmented micellar system. First of all, hydrophobic domains have to be stabilized in water. Although this could be achieved by low-molar mass surfactants, too, the use of amphiphilic block copolymers is the preferred approach since they are more stable upon dilution. The most important feature of a multi-compartment system is a hydrophobic micellar core which is compartmentalized due to microphase-separation. Additionally, these compartments have to be substantially different so that they selectively solubilize low-molar mass solubilizates. Therefore, the use of polymers that are thermodynamically incompatible - such as polystyrene and polybutadiene - is not sufficient.

Hydrocarbons (HC) and fluorocarbons (FC) are known to be hardly miscible with each other. The enhanced hydrophobicity and lipophobicity of fluorocarbons is a consequence of their low cohesiveness and their larger surface area. The mutual immiscibility is even observed for low-molar mass systems, e.g. for surfactants. When hydrocarbon and fluorocarbon surfactants are co-dissolved in water, they tend to form not mixed but separate micelles.¹¹⁴ When they are present simultaneously in bilayer membranes, they form phase-separated microdomains (cf. Fig. 1.7).¹¹⁵ Most studied systems have used fluorocarbons to impart a second hydrophobic domain that is incompatible with the first one.

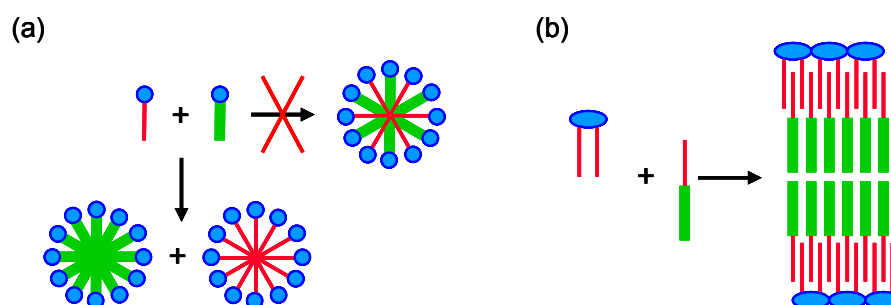
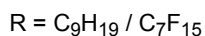
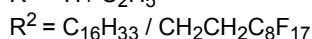
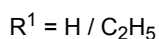
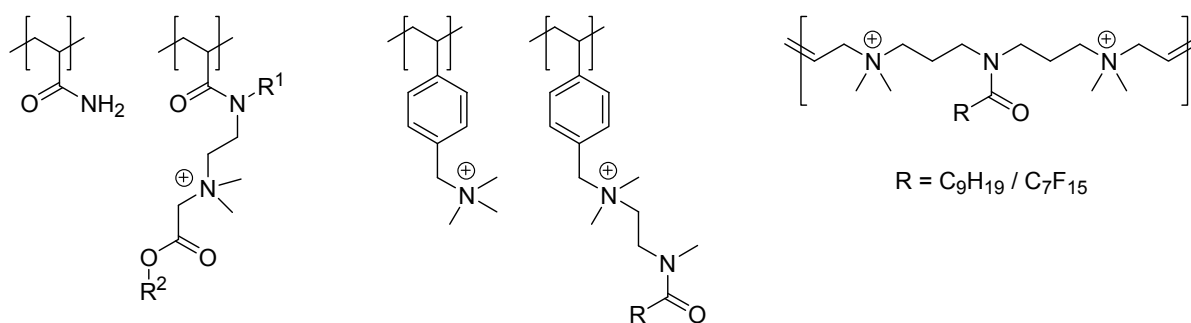


Figure 1.7 Phase separation in mixtures of hydrocarbon (HC) and fluorocarbon (FC) amphiphiles: (a) mixture of HC and FC surfactants (b) mixture of a standard phospholipid and a HC/FC diblock.

The selective uptake and release of different transport goods necessitates a dynamic system with a high mobility to assure exchange processes. As all the mentioned requirements are difficult to meet there are only a few studies available until today. The first approaches towards multicompartment micelles relied on polysoap systems (cf. Fig. 1.8).

(a) Polysoap Approach

statistical terpolymers

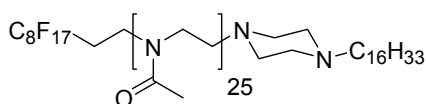
statistical and block copolymers

statistical and block copolymers

free-radical polymerization

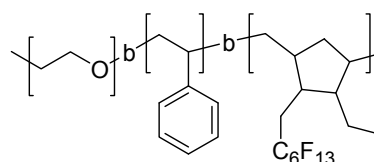
free-radical and RAFT polymerization

step-growth polymerization

(b) Triblockcopolymer Approach

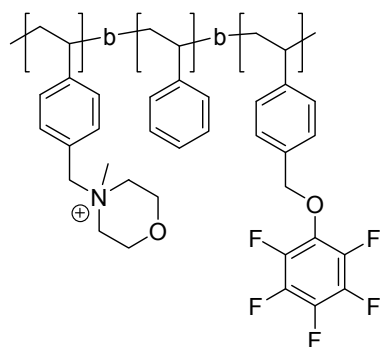
ABC triblock copolymer analogous telechelic

cationic ring-opening polymerization
and termination



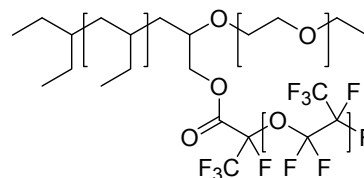
ABC triblock copolymer

anionic polymerization
and selective modification



ABC triblock copolymer

RAFT polymerization



ABC μ -arm star polymer

anionic polymerization
and polymer-analogous reaction

Figure 1.8 Macromolecular design of multi-compartment micellar systems

Polysoaps are micellar polymers where each monomeric unit is an amphiphile by itself (a so-called surfmer). Stähler et al.¹¹⁶ have synthesized acrylamide based polysoaps with hydrocarbon and fluorocarbon side chains by aqueous statistical terpolymerization aiming for a random distribution of F-domains along the hydrophilic backbone. As the molecular characterization of the obtained polymers was difficult, it could not be proven that multiblock polymers had been obtained. Furthermore, the content of

hydrophobic repeat units was very low rendering the domains very small with limited solubilizing power. However, the studied system behaved different compared to the mixture of homopolymers.

A similar approach used cationic polysoaps based on styrene with HC and FC chains.¹¹⁷ The polymers were obtained by free-radical as well as by Reversible Addition Fragmentation chain Transfer (RAFT) polymerization. The analysis by ¹⁹F NMR spectroscopy revealed a solid-like behavior of the aggregated FC chains indicating frozen micellar cores with a reduced mobility. Additionally, the system behaved somewhat like an associative thickener. Due to the sterically crowded backbone based on polystyrene, the intermolecular association of the polysoap was favored. Cationic polysoaps of the ionene type¹¹⁸ which were prepared by step-growth polymerization showed on the contrary a very different behavior. Statistical and block copolymers were studied and in the latter case a multi-compartment system was realized as the HC and FC domains were microphase-separated and the low viscosifying effect pointed to intramolecular association. The liquid-like state of the FC domains, which is preferred for a dynamic system that enables solubilization, was evidenced by ¹⁹F NMR spectroscopy.

Another approach towards multi-compartment micelles used amphiphilic block copolymers composed of one hydrophilic and two hydrophobic blocks. Linear ABC triblock copolymers are the simplest case. A triblock copolymer analogue was prepared by Weberskirch et al.¹¹⁹ by end-capping oligomeric poly(2-methyl-2-oxazoline) with a hydrocarbon and a fluorocarbon end-group, respectively. The studied telechelics exhibited low cmc's and ¹⁹F NMR relaxation experiments suggested pure FC and HC phases. The competition between intra- and intermolecular association was controlled by the polymer concentration. This system has to be regarded rather as a mixed population of HC and FC micelles since the oxazoline block is too short and too bulky to enable the presence of both hydrophobic end-groups in the same micellar core.

Lodge and coworkers⁶⁹ prepared a ABC triblock copolymer from a PEO-PS-PB precursor of intermediate molar mass and modified the PB block with perfluorohexyl iodide to obtain a fluorocarbon block. Remarkably, the micelle formed a sub-structured core after modification whereas it was a mixed PS/PB core before. Moreover, the modification changed the micellar shape from spherical to oblate elliptical. According to cryogenic transmission electron microscopy (cryo-TEM), a core-shell-corona micelle was obtained which is not optimal for an independent uptake and release of different solubilizates. In an approach to avoid this particular micelle structure, the same researchers have synthesized an ABC mikto-arm (μ -arm) star block copolymer based on PEO, poly(ethyl ethylene) (PEE) and poly(perfluoropropylene oxide).¹²⁰ The three blocks were all joined together at the same junction point and in aqueous solution the polymer formed micelles with a segmented worm-like morphology and distinct HC/FC microdomains. Blending the micellar solution of the μ -arm star terpolymer with the spherical micelles formed from a PEO-PEE diblock copolymer induced a change of the micellar shape.¹²¹ The new morphology, which was assumed to evolve according to a collision/fusion/fission mechanism,¹²² was referred to as a "hamburger" micelle.

While the aforementioned examples of multi-compartment micelles based on amphiphilic block copolymers were all prepared by ionic polymerization methods and polymer-analogous reactions, Kubowicz et al.¹¹² reported the first example of such a polymer prepared by controlled radical polymerization. The triblock copolymer based on styrene monomers probably evoked the problem of

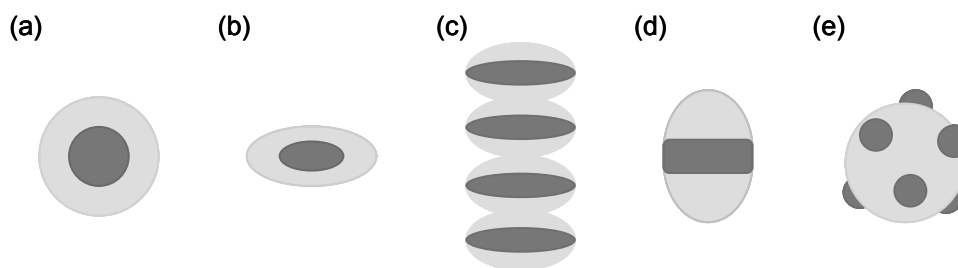


Figure 1.9 Morphologies of micellar cores found for multi-compartment polymeric micelles: (a) spherical and (b) disk-like core-shell-corona micelles (c) segmented worm-like micelle (d) “hamburger” micelle and (e) sphere-on-sphere morphology. For clarity, the hydrophilic corona is omitted.

frozen micelles. Still, cryo-TEM revealed very small micelles exhibiting a sphere-on-sphere morphology with separated HC and FC domains.

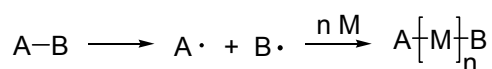
Lately, the experimental work on multicompartment micelles has been more and more supported by theoretical simulations. Monte Carlo¹²³ as well as dissipative particle dynamics simulations¹²⁴⁻¹²⁶ have been performed to study the influence of molecular architecture, block length and polymer concentration on the micellar morphology.

1.3. *Methods of controlled radical polymerization (CRP)*

1.3.1. *Introduction to CRP methods*

Free-radical polymerization (FRP) is today the most important technology for the production of polymeric materials on an industrial scale and has achieved this importance due to its versatility, synthetic ease and its compatibility with many functional groups. Polymers are formed in free-radical polymerization by the addition of vinylic monomers to an active radical species. Due to the high reactivity of the radicals a very broad range of vinylic monomers, such as (meth)acrylic, styrenic and many others can be polymerized by this method. Emulsion and suspension techniques, which are of high commercial significance today, have been developed due to the tolerance of FRP towards water and other protic media. However, classical free-radical processes have some major disadvantages. As radicals are constantly generated during the polymerization process and propagation is very fast, the chains grow in series leading to a broad molar mass distribution. Moreover, it is not possible to build directly complex polymeric architectures such as block copolymers with classical free-radical processes. Such complex macromolecules can be prepared by living polymerization processes, but these are incompatible with functional groups and very sensitive to impurities and thus, require mostly the use of ultrapure reagents and the total exclusion of water and oxygen. As nanotechnology and other applications demand functionalized, well-defined materials as building blocks, increasing efforts have been made to combine the virtues of living polymerization with the ease and versatility of conventional free-radical polymerization.

In the past, several strategies have been developed to moderate the molar masses of polymers in FRP and to introduce functionalities at the polymeric chain ends. Traditionally used compounds for this purpose are chain transfer agents such as halomethanes, disulfides, thiols and various other compounds with readily abstractable H atoms. In the 1950ies, Otsu et al.¹²⁷ found during their research for new photoinitiators that tetraethyl thiuram disulfide not only acts as efficient photoinitiator but also as retarder, terminator and transfer agent. In 1982, the name *iniferter*^{128, 129} (initiator transfer agent terminator) was proposed for compounds that react according to the following scheme:



A• is a reactive radical that participates in initiation and then propagation, and B• is a less reactive or non-reactive radical that principally enters into primary radical termination to give a polymer with A and B as α,ω -end-groups.

The iniferter concept constitutes the first attempt to establish a living/controlled radical polymerization process because some rudimentary characteristics of a living polymerization such as the increase of molar mass with time, predictable molar mass and the possibility to prepare block copolymers due to α,ω -functionalized chain ends were achieved. Still, the molar mass distributions obtained from iniferters such as benzyl *N,N*-diethyl dithiocarbamate were broad due to the ability of the thio radical to initiate polymerization.¹³⁰ The initial work of Rizzardo et al.¹³¹ in 1984 and of Georges et al.¹³² employing stable free radicals as mediators in free-radical polymerization constitute the basis for the development of a living free-radical polymerization technique.

Controlled radical polymerization (CRP)¹³³ methods enable the synthesis of polymers with predetermined molar masses, low polydispersities, and well-defined end groups from a large variety of monomers and under a wide range of polymerization conditions. CRP also provides a facile access to complex polymeric architectures such as block, graft, star and hyperbranched polymers. The major advantage of CRP lies in the fact that new block copolymers can be prepared that were not accessible using existing living techniques. Nowadays, CRP methods mainly include nitroxyl-mediated polymerization (NMP), atom transfer radical polymerization (ATRP) and polymerization by reversible addition fragmentation chain transfer (RAFT). While ATRP and NMP are based on a dissociation-combination and an atom transfer mechanism, respectively, RAFT relies on a degenerative chain transfer. Each of these methods is described briefly in the following section.

1.3.2. Nitroxyl-mediated polymerization (NMP)

Nitroxyl mediated polymerization^{134, 135} - as one method of CRP - involves stable free radicals. The polymerization is believed to proceed according to the mechanism depicted in Figure 1.10. The radicals formed during initiation are trapped by stable free radicals which are assumed to be stable enough to undergo no reaction other than the combination with P•. Furthermore, ideal stable free radicals do not react with themselves, do not initiate polymerization and do not undergo disproportionation. The best known examples of stable free radicals are nitroxyls, such as TEMPO (cf. Fig. 1.10 b). As the formed C-O-N bond is weak, it can be homolytically cleaved by thermolysis to release again the propagating

radical which in turn can add monomer. Control over the polymerization process is achieved in nitroxyl-mediated polymerization by a phenomenon termed persistent radical effect (PRE).^{136, 137} Transient ($R\cdot$) and persistent ($Y\cdot$) radicals are produced from the same or different sources at equal rates. While per definition the persistent radicals do not self-terminate, the transient radicals are trapped by self-termination or cross-termination with $Y\cdot$. As a consequence, the concentration of $Y\cdot$ builds up and accelerates in turn the cross-termination at the expense of self-termination. Due to this reversible combination/dissociation of propagating radicals self-termination is minimized and the polymeric chains grow in parallel.

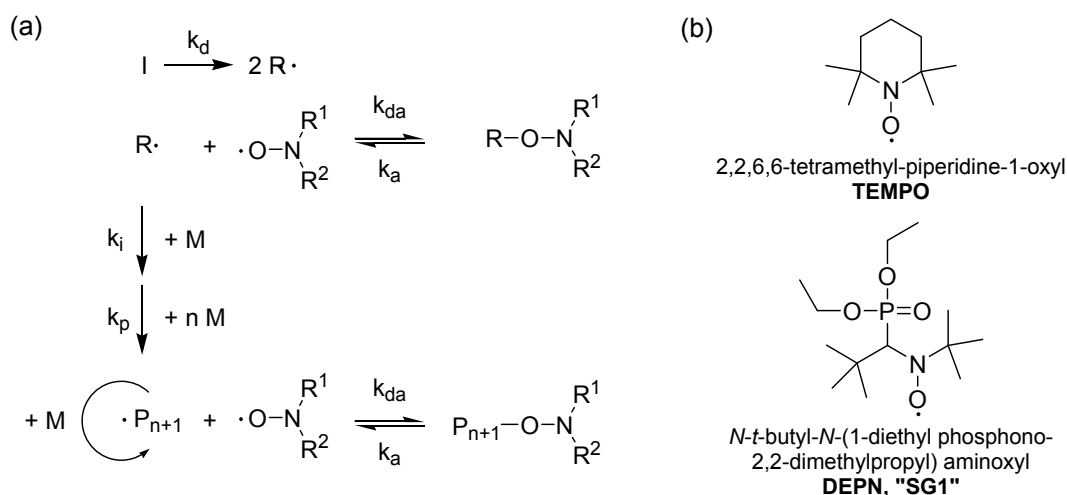


Figure 1.10 Nitroxyl-mediated polymerization: (a) Mechanism (b) Examples of typical nitroxyls.

The problems related to the polymerization of other monomers than styrenics with TEMPO have been overcome by the introduction of new examples of nitroxyls, such as the phosphonate derivatives, introduced by Gnanou and Tordo^{138, 139} and the family of arenes introduced by Hawker.¹⁴⁰ These nitroxyls have been shown to be superior to TEMPO as they allow the controlled polymerization of a wide variety of monomer families, such as acrylates,^{141, 142} acrylamides,¹⁴³⁻¹⁴⁵ 1,3-dienes¹⁴⁶ and acrylonitrile¹⁴⁷ and allow also shorter reaction times and lower temperatures. Even acrylic acid which was supposed to give side reactions with the nitroxyl can be polymerized using NMP.¹⁴⁸ The drawbacks of NMP are the high polymerization temperatures and the long polymerization times as well as the limited range of monomers which can be polymerized.

1.3.3. Atom transfer radical polymerization (ATRP)

In 1995, atom transfer radical polymerization¹⁴⁹ was introduced independently by Sawamoto¹⁵⁰ and Matyjaszewski.^{151, 152} The name is derived from the atom transfer step, which is the key reaction responsible for the uniform growth of polymeric chains. This polymerization method originates in atom transfer radical addition (ATRA) reactions, which target the formation of 1:1 adducts of alkyl halides and alkenes catalyzed by transition metal complexes. The general accepted mechanism for ATRP is shown in Figure 1.11. The initiating radicals $R\cdot$ are generated from an alkyl halide through a reversible redox process catalyzed by a transition metal complex. Although a variety of transition metals such as Ru, Ni, Rh, Pd, and Fe can be used for the catalyst, Cu is superior concerning versatility and cost.

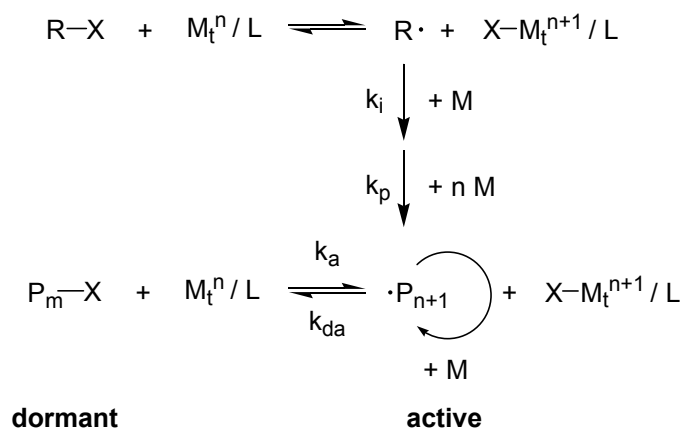


Figure 1.11 Mechanism of ATRP polymerization

While ATRP works well for (meth)acrylates, styrene and acrylonitrile, some problems are encountered for (meth)acrylamides and monomers containing acid functionalities. These difficulties are related to the inactivation of the catalyst by complex formation between copper and the monomer/polymer and the displacement of the terminal halogen bond by the amide group.¹⁵³ Nevertheless, by employing appropriate catalysts and reaction conditions these problems can be overcome.¹⁵⁴ A major drawback of this method is the catalyst of which residual amounts remain in the polymer samples even after purification. The employed transition metals are often toxic and in addition may interfere with the properties of the studied polymers.

1.3.4. Polymerization by reversible addition fragmentation chain transfer (RAFT)¹⁵⁵

In 1998, the polymerization by reversible addition-fragmentation chain transfer was invented by Rizzardo et al.¹⁵⁶⁻¹⁵⁸ in Australia. A related polymerization process termed MADIX^{159, 160} (Macromolecular Design via the Interchange of Xanthates) was invented by Rhodia in France at the same time. RAFT polymerization works under conditions very similar to those of conventional free-radical polymerization. The major difference is the addition of certain thiocarbonylthio derivatives to an otherwise conventional polymerization mixture. These compounds contain an activated C=S double bond and act as reversible Chain Transfer Agents (termed CTA or RAFT agent). The general structure of a CTA is depicted in Fig. 1.12. Polymerization by RAFT is probably the most versatile among CRP methods regarding types of monomers and reaction conditions.

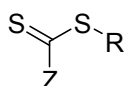


Figure 1.12 General structure of a RAFT agent

(1) Mechanism of RAFT polymerization

The general accepted mechanism of RAFT polymerization is depicted in Figure 1.13.

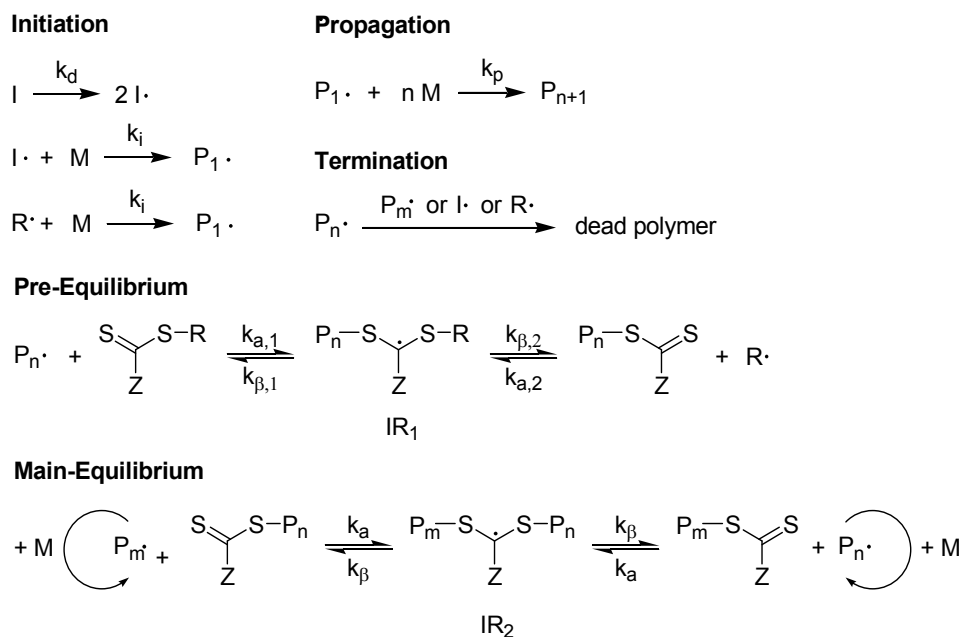


Figure 1.13 Mechanism of RAFT polymerization

Initiation, propagation and termination reactions are the same as in conventional free-radical polymerization.¹⁶¹ The polymerization process is controlled by the equilibrium between propagating and dormant chains. In the pre-equilibrium - during the early stages of the RAFT polymerization - the oligomeric radical species $P_n \cdot$ adds to the CTA to form an intermediate radical (IR_1). The intermediate radical (IR_1) then fragments into an oligomeric thiocarbonylthio compound [$P_nS(Z)C=S$], which constitutes the dormant species, and a new radical ($R \cdot$). The $R \cdot$ radical re-initiates the polymerization to generate a new propagating radical $P_m \cdot$. In the main-equilibrium - after all of the initial RAFT agent is consumed - the polymer chains change between the active state (during which they can add monomer) and the dormant state. As a result of this equilibrium, the polymer chains grow in parallel, and the polymers have predictable molar masses and narrow molar mass distributions. An effective RAFT agent is characterized by the following parameters:

- a high rate constant for the addition of propagating radicals to the thiocarbonyl bond of the RAFT agent ($k_{a,1} \gg k_p$);
- the intermediate radical IR_1 fragments in favor of the products ($k_{\beta,2} \geq k_{\beta,1}$);
- the fragmentation of the intermediate radical is fast compared to propagation;
- the expelled radicals ($R \cdot$) re-initiate the polymerization fast.

The ideal RAFT process - as depicted in Figure 1.13 - does not change the concentration of propagating radicals, as for every radical addition to the CTA a new radical is released by fragmentation. Thus, the rate of polymerization in the steady state should remain unchanged compared to a conventional radical polymerization system. However, non-ideal kinetic phenomena are often encountered in RAFT

polymerizations such as an induction period in the initial phase of polymerization (with virtually no polymerization activity) and/or an overall rate retardation caused by a lower propagating radical concentration than in the polymerization system in absence of a CTA. Several theories on the origins of induction and retardation have been developed and are still the subject of intense scientific discussions.¹⁶² It is commonly agreed, that the retardation effect is observed for RAFT agents that form stable intermediate radicals in the pre- and main equilibrium, such as dithiobenzoates ($Z = \text{phenyl}$). The high stability is caused by the delocalization of the radical site into the aromatic system (cf. Figure 1.14) and results in a high chain transfer constant for this class of RAFT agents.

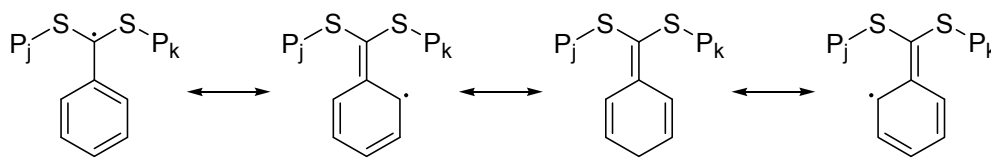


Figure 1.14 Resonance structures of the intermediate radical in dithiobenzoate-mediated RAFT polymerization

Initially, the CSIRO team explained the effect of rate retardation by:¹⁵⁸ (a) slow fragmentation of the intermediate radical, (b) slow re-initiation by the expelled radical R^\bullet , and (c) specificity of R^\bullet and the propagating radical P_n^\bullet to add to the RAFT agent rather than to monomer. Shortly after, Monteiro and de Brouwer¹⁶³ proposed that irreversible termination of intermediate radicals with propagating radicals - termed cross-termination - causes the rate retardation (cf. Fig. 1.15a). The increased stability of the intermediate radical leads to its accumulation until the addition-fragmentation equilibrium is established and thus, the probability for recombination with propagating radicals or themselves is increased.

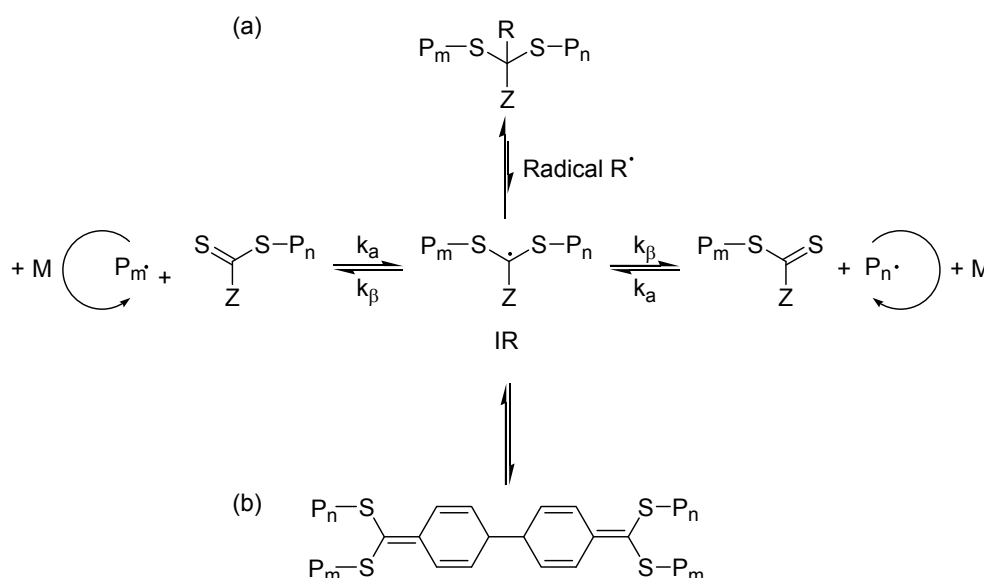


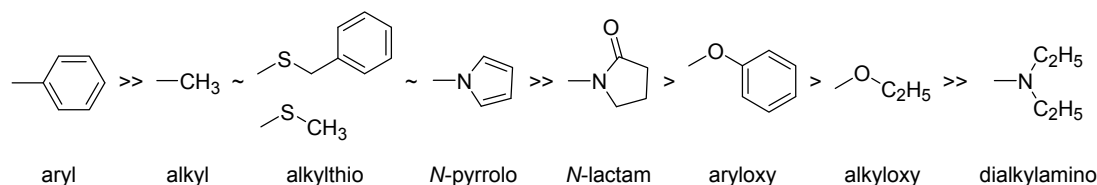
Figure 1.15 Models for rate retardation in RAFT polymerization by: (a) irreversible and (b) reversible cross-termination.

The model of cross-termination is consistent with the experimentally determined radical concentration. Although cross-termination should result in significant amounts of termination products, such species could not be detected by mass spectrometry.¹⁶⁴ On the other hand, the model of slow

fragmentation agrees with the non-stationary polymerization rate in the pre-equilibrium and is able to explain the observed radical storage effect.¹⁶⁵ Still, the concentration of radicals found by ESR spectroscopy is lower than expected for a long-lived intermediate radical. At present, a conclusive kinetic picture, which is capable to explain all the observed effects, has not yet emerged. A composite model, that assumes a reversible cross-/self-termination (cf. Fig. 1.15b), could harmonize the low radical concentration detected by ESR with the long life-times of the intermediate radicals in the slow fragmentation model.¹⁶²

(2) Types of RAFT agents

Since the invention of the RAFT process, the structures of CTAs have been adapted to a broad range of monomers as well as to the desired polymerization conditions (temperature, medium), so that today a vast variety of RAFT agents is accessible and a suitable CTA for a given system can be found. As the thiocarbonylthio moiety is the crucial structural element, the structure of the CTA can be varied concerning R and Z group (cf. Fig. 1.12). The Z group should on one hand activate the thiocarbonyl bond towards radical addition but on the other hand should not stabilize the intermediate radical too much as this contributes to slow fragmentation and thus retardation. The effect of various Z groups on the chain transfer activity of RAFT agents has been discussed.¹⁶⁶ For the RAFT polymerization of styrene, the chain transfer constants were found to decrease in the following order:



The low chain transfer activity of dithiocarbamates and xanthates has been attributed to their zwitterionic resonance structures, where the conjugation of the lone pair of electrons with the thiocarbonyl bond reduces its double bond character making the addition of radicals less favorable (cf. Fig. 1.16).¹⁶⁶ While these RAFT agents provide poor control in the polymerization of less reactive monomers such as styrene or MMA, they control the polymerization of highly reactive monomers such as vinyl esters.

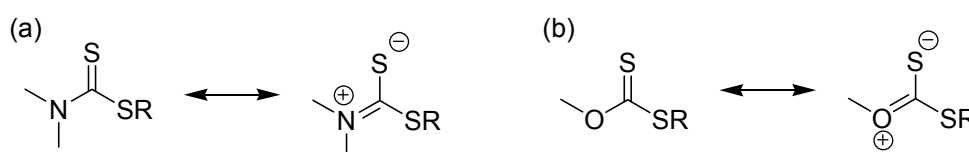
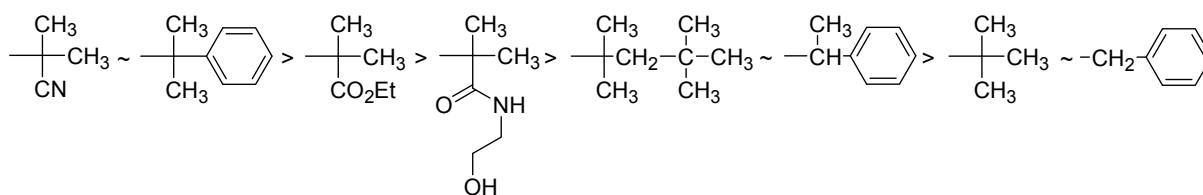


Figure 1.16 Resonance structures of (a) dithiocarbamates and (b) xanthates

The R group plays an important role during fragmentation in the pre-equilibrium and during re-initiation. To achieve fragmentation of the intermediate radical in favor of the products in the pre-equilibrium, the R group is preferentially a better homolytic leaving group than the propagating radical. However, R• should not be too stable to ensure a fast and efficient re-initiation of new chains. The effect of the R group on the chain transfer activity of RAFT agents was studied for the polymerization of MMA with dithiobenzoates.¹⁶⁷ The leaving group ability of R was found to decrease in the following order:



Interestingly, only the first two leaving groups in this row were found to be effective in the polymerization of MMA. That means, even for the third R group which is structurally similar to the MMA propagating radical, the obtained polydispersities were broad, an effect which possibly reflects the higher chain transfer activity of polymeric RAFT agents.

(3) Optimization of the RAFT process and strategies for the synthesis of block copolymers¹⁶⁸

The most important advantage of CRP methods is the synthesis of block copolymers which contain functional moieties that are incompatible with the active species of living polymerization methods. The homopolymers synthesized by RAFT can be employed as macromolecular CTAs (macroCTAs) in the polymerization of a second monomer to produce a diblock copolymer. In order to achieve efficient blocking, the thiocarbonylthio moieties have to be preserved at the polymer chain ends. Since polymers without thiocarbonylthio endgroup arise from initiator-derived chains, high ratios of RAFT agent to initiator are preferred in order to maintain a low radical flux. Typically, molar ratios [CTA]/[initiator] between 5 and 10 lead on one hand to acceptable rates of polymerization and on the other hand guarantee a high degree of end-group functionalization.

By increasing the polymerization temperature, the rate of polymerization can be increased for systems showing rate retardation (e.g. dithiobenzoates) as the fragmentation is accelerated. However, a parallel increase of radical concentration has to be avoided as it leads to lower control. Therefore, another initiator with a higher half-life time for decomposition has to be used in such a case. Since the probability for termination events increases with decreasing monomer concentration, intermediate monomer conversions are preferred in RAFT polymerization. A marked increase of viscosity during polymerization might favor the heterogeneous growth of chains and should be avoided. According to these requirements, block copolymers cannot be prepared by sequential monomer addition as in anionic polymerization but they have to be isolated after each block copolymerization step.

In the preparation of block copolymers the precursor macroCTA acts as re-initiating R group. Consequently, it is necessary that its leaving group ability is better or comparable to that of the second block. Otherwise, the intermediate radical fragments in favor of the educts and the blocking efficiency is low. In general, the homolytic leaving ability decreases in the following order: methacrylyl > styryl > acrylyl. Accordingly, the preparation of a methacrylate-acrylate block copolymer is only successful if the methacrylate block is synthesized first as exemplified in Figure 1.17.

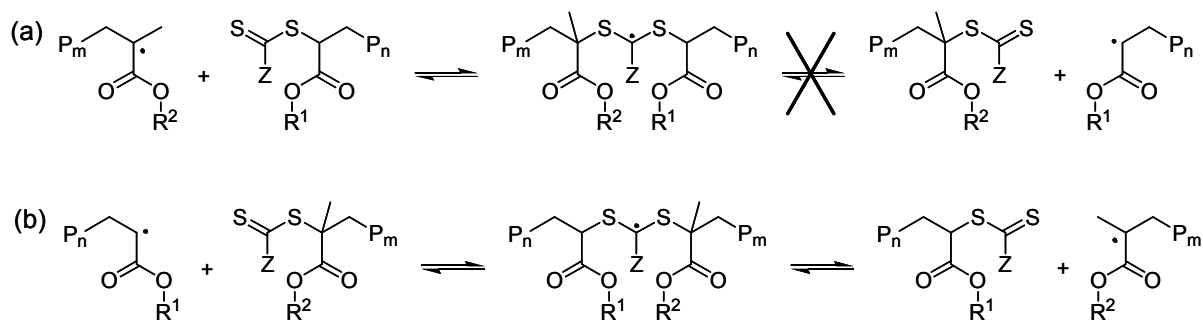


Figure 1.17 Effect of the block sequence on the chain transfer step in the synthesis of block copolymers by RAFT polymerization: (a) polymerization of a methacrylate monomer using a polyacrylate macroCTA (b) polymerization of an acrylate monomer with a polymethacrylate macroCTA.

To summarize, by careful selection of the CTA according to the monomer structure and the required reaction conditions well-defined polymers of complex architectures can be successfully synthesized by RAFT polymerization. Due to its tolerance towards functional groups the RAFT process enables the synthesis of a large variety of polymers that could not be prepared by living polymerization techniques.

1.4. Objectives and motivation

In the introductory chapters, amphiphilic block copolymers were shown to be versatile materials for a variety of applications. Most systems are based on diblock copolymers while ABC terpolymers comprising three functional blocks are still rare. Inspired by biological systems, the amphiphilic ABC triblock copolymers synthesized in this work were designed in such a way that their self-assembly in water allowed for gradual transitions between different self-organized structures. Or, they were able to self-assemble in water under formation of sub-structures.

The first studied system was based on double-responsive block copolymers whose self-assembly is triggered and modified by the temperature stimulus. In the second system, amphiphilic block copolymers self-assembled under formation of micelles with sub-structured cores by the introduction of a highly fluorinated block, so-called multi-compartment micelles. In order to understand the influence of polymer architecture on the self-assembly, the block sequence ABC was systematically varied (BAC, ACB). Overall molar masses of the polymers were targeted to be between 10.000 and 100.000 g/mol. The chosen hydrophilic blocks were nonionic polymers due to the difficulties in finding a common solvent for polyelectrolytes and hydrophobic polymers.

The key objectives of this work were:

- Synthesis of new double-thermoreponsive triblock copolymers exhibiting LCST behavior.
- Study of their temperature-induced self-assembly in water which is characterized by a cascade of phase transitions instead of an all-or-nothing response. Correlation of the self-organization behavior to the macromolecular structure.
- Synthesis of new amphiphilic ABC triblock copolymers comprising a nonionic hydrophilic, a classical hydrophobic and a fluorinated block.
- Study of the self-assembly in water and its relation to the polymer architecture. Realization of a multicompartment micellar system that is characterized by a sub-structured micellar core originating from the mutual immiscibility of the hydrophobic and the fluorinated block.
- Synthesis of the desired ABC terpolymers by reversible addition fragmentation chain transfer polymerization (RAFT) as it is probably the most versatile of all CRP methods.
- Study of the UV-vis absorptions of thiocarbonylthio end-groups of (macro)CTAs. Evaluation of these absorptions as analytical tool for the end-group analysis and alternative molar mass determination of the synthesized triblock copolymers.

The monomers and chain transfer agents used in this work are listed in Appendix 6.

2.1. The most used synthetic routes to thiocarbonylthio compounds

Dithiocarboxylic and trithiocarbonic acids or their salts are intermediates in the preparation of dithioester and trithiocarbonate RAFT agents (Fig. 2.2). Dithiocarboxylic acids are frequently prepared from Grignard reagents and CS₂ as many Grignard reagents are commercial products or readily prepared (Fig. 2.2a). An alternative route to dithiobenzoic acid and its derivatives is the oxidation of benzyl halides with a mixture of sulfur and base in a polar solvent (Fig. 2.2b).^{176, 177} Dithiobenzoic acid cannot be stored as it is unstable and should be used immediately for further reactions. Trithiocarbonic acid salts are synthesized by the nucleophilic addition of thiolates or inorganic sulfides to CS₂ (Fig. 2.2c).¹⁷⁸

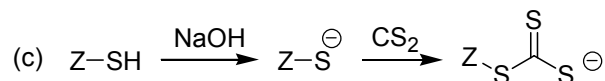
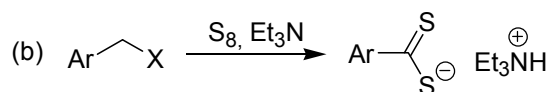
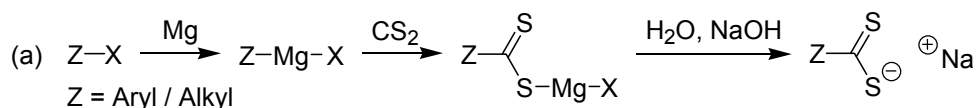
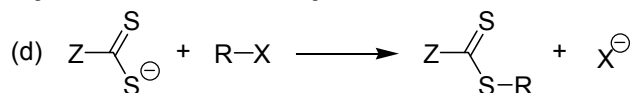
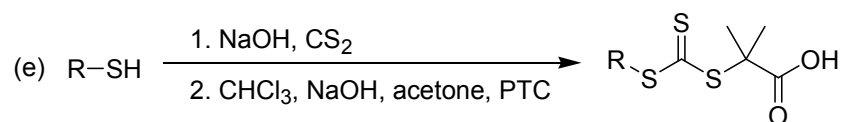
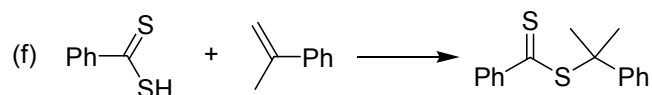
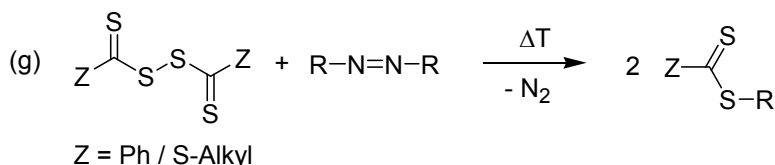
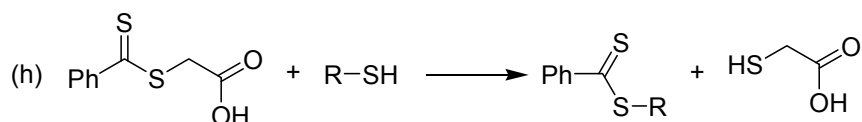
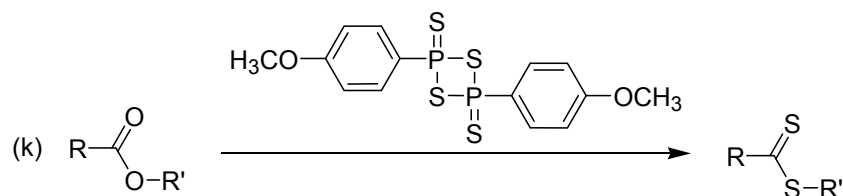
A popular route towards dithioester and trithiocarbonate RAFT agents is the alkylation of the anionic salts of dithiocarboxylic and trithiocarbonic acids with suitable alkyl halides (Fig. 2.2d). The reaction proceeds smoothly and fast for many alkyl halides without sterically hindering groups. Only for tertiary alkyl halides the yields are low and the reaction requires elevated temperatures depending on the bulkiness of the alkyl group. Furthermore, higher temperatures favor elimination of the halide instead of substitution.

Consequently, CTAs bearing tertiary leaving groups are mostly accessed by other routes. A straight-forward and facile way to synthesize tertiary trithiocarbonates from commercial and inexpensive chemicals was first described by Lai and coworkers.¹⁷⁹ The procedure comprises a ketoform reaction using a phase transfer catalyst (PTC) (Fig. 2.2e). Deprotonation of chloroform with 50 wt% NaOH gives trichloromethanide ions which attack acetone under formation of an oxirane. The oxirane ring is opened by the reaction with the nucleophilic trithiocarbonate which is formed *in situ* by the addition of CS₂ to the deprotonated thiol. Acidification yields the carboxyl-functionalized trithiocarbonate.

Another route to tertiary CTAs is the addition of dithiocarboxylic acid to olefins (Fig. 2.2f). Dithiocarboxylic acids can add to electrophilic olefins such as acrylonitrile and vinyl pyridine, as well as to nucleophilic olefins such as styrene, α -methylstyrene and vinyl ether. For electrophilic olefins the reaction follows Michael type addition resulting in ineffective RAFT agents for (meth)acrylic and styrenic monomers. The addition of dithiobenzoic acid to nucleophilic olefins obeys Markovnikov's rule¹⁸⁰ and yields effective RAFT agents. This procedure is applied to the synthesis of the frequently used cumyl dithiobenzoate by reacting dithiobenzoic acid with α -methylstyrene.

Dithioesters with tertiary leaving groups can also be synthesized via the free-radical coupling between radicals derived from conventional azoinitiators and bis(thiocarbonyl) disulfides.^{181, 182} The frequently employed 4-cyano-4-thiobenzoylsulfanyl pentanoic acid (**CTA1**) is synthesized by this method (cf. Fig. 2.2g).

Transesterification between dithiocarboxylates and thiols is a practicable and alternative route to dithioesters (Fig. 2.2h). Carboxymethyl dithiobenzoate is a commercially available dithioester and can be used as starting material for more efficient RAFT agents by transesterification. This method is especially useful if hydrophobic thiols are employed. In this case, the synthesis is facilitated by conducting the reaction in a two phase system, where the equilibrium is shifted towards the product by extracting the thioglycolic acid into the aqueous and the product into the oil phase, respectively.^{183, 184}

Synthesis of dithioates / trithiocarbonates**Alkylation of dithiocarboxylic / trithiocarbonic acid salts****Ketoform reaction****Addition of dithiocarboxylic acids to olefins****Free radical coupling between bis(thiocarbonyl) disulfides and azoinitiators****Transesterification****Conversion of thioesters to dithioesters by Lawesson's reagent****Figure 2.2** Frequently used synthetic routes to thiocarbonylthio compounds

Esters and thioesters can be converted into their respective dithio analogs by reacting them with Lawesson's reagent (2,2-Bis-(4-methoxy-phenyl)-1,3,2,4-dithiodiphosphetane-2,4-disulfide) or phosphorous pentasulfide (P_4S_{10}).¹⁸⁵ Lawesson's reagent is compared to P_4S_{10} more reactive and relatively well soluble in organic solvents at elevated temperature so that reactions can be run

homogenously. Furthermore, it can be prepared readily and in high yield starting from P_4S_{10} and methoxybenzene.

2.2. *Synthesis of chain transfer agents*

The synthesis of chain transfer agents in this thesis followed two objectives. First, the preparation of ABC triblock copolymers required effective chain transfer agents (chapters 4 and 5). Second, as the thiocarbonyl moieties of RAFT end-groups are chromophores which absorb light in the UV and visible range, their utility for end-group analysis of polymers was explored (cf. chapter 3). Thus, a variety of dithiobenzoates and trithiocarbonates was synthesized and their UV-vis characteristics studied. Relating the UV-vis absorptions with the particular CTA structure should elucidate which parameters allow for an accurate end-group analysis and thus, for a reliable molar mass determination. The following chapter presents the RAFT agents that were studied and their synthesis.

Presentation of the studied CTAs

Dithiobenzoates ($Z = Ph$) are very effective chain transfer agents for many monomers but they often cause retardation resulting in long polymerization times. Trithiocarbonates are less effective chain transfer agents than dithioesters, yet provide good control in the polymerization of (meth)acrylic and styrenic monomers. Above all, they lead to substantially less retardation, are more stable towards hydrolytic degradation and, last but not least, are more readily synthesized. Consequently, only two dithiobenzoates but a larger variety of trithiocarbonates were synthesized in this thesis (cf. Fig. 2.3).

CTA1 is one of the most widely used chain transfer agents in RAFT polymerization. The reason for the popularity of **CTA1** is its versatility, as it controls the polymerization of acrylic, styrenic and methacrylic monomers. Additionally, the carboxyl R-group located on the α -chain end of the polymer, allows a variety of modifications.

CTA7 is a derivative of the frequently employed 2-(1-dodecylsulfanylthiocarbonylsulfanyl)-2-methyl propionic acid.¹⁷⁹ Chain transfer agents with 2-methyl propionic acid leaving groups give only partial control in the polymerization of methacrylic monomers.¹⁶⁷ Nevertheless, they find widespread use as they can be synthesized from inexpensive chemicals in large quantities with moderate to high yields by a one-pot procedure and are readily purified. Similar to **CTA1**, these trithiocarbonate RAFT agents have been used for the synthesis of end-functionalized polymers by chemical modification of the CTA.^{186, 187} Both, **CTA1** and **CTA7** become water-soluble after deprotonation of the carboxylic acid functionality and can be employed for aqueous polymerizations. **CTA1** and **CTA7** were used in this work for the synthesis of thermoresponsive and amphiphilic block copolymers with fluorinated blocks, respectively (cf. chapters 4 and 5).

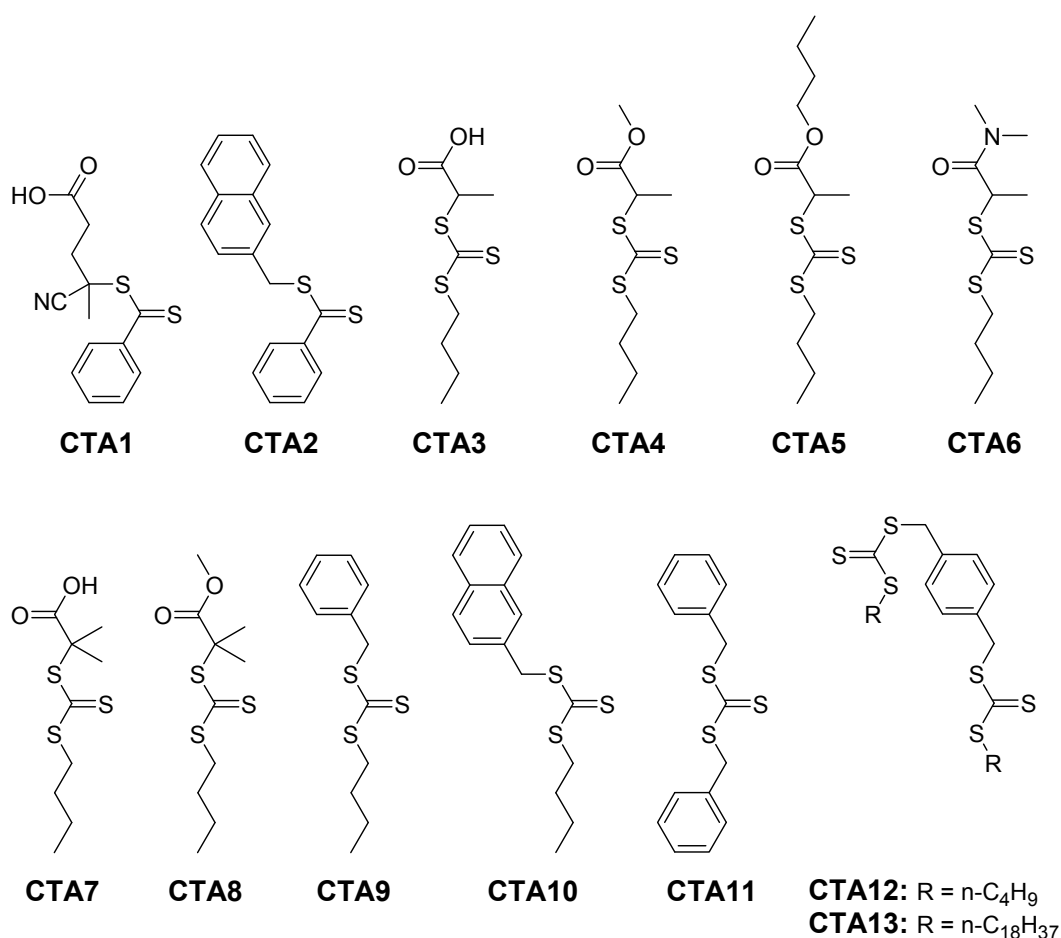


Figure 2.3 CTAs studied by UV-vis spectroscopy

Synthesis of model compounds for macroCTAs (CTA3-CTA8)

In order to understand how the UV-vis absorption characteristics (λ_{\max} , $\epsilon(\lambda_{\max})$) of the thiocarbonyl moiety are influenced by the substitution pattern in the R group, trithiocarbonates bearing secondary and tertiary R groups were synthesized. These trithiocarbonates served as model compounds for n-butyl trithiocarbonate moieties attached to the chain end of common (meth)acrylic polymers such as poly(n-butyl acrylate) or PMMA.

The trithiocarbonates with secondary R groups were synthesized by reacting a commercially available (**CTA3-CTA4**) or a previously prepared (**CTA5-CTA6**) alkyl halide with the sodium salt of n-butyl trithiocarbonate. This procedure works excellently at ambient temperature with high yields. Despite its polar R moiety the trithiocarbonate **CTA6** is not water-soluble at ambient and high temperatures, underlining the strongly hydrophobic character of the trithiocarbonate group.

CTA7 was synthesized according to the ketoform reaction described by Lai et al.¹⁷⁹ 1-Dodecanthiol is frequently employed for the synthesis of tertiary trithiocarbonates via this route in order to facilitate purification but also to avoid problems related to the odor of more volatile thiols. Here, however, 1-butanethiol was deliberately chosen for the synthesis of the trithiocarbonates as it is on one hand not too volatile but on the other hand not too hydrophobic.

As was discussed in chapter 2.1, the substitution of dithiobenzoate or trithiocarbonate anions by tertiary alkyl halides is difficult. Therefore, **CTA8** was synthesized from **CTA7** by methylation of the deprotonated carboxyl group with dimethylsulfate. As they are liquids, **CTA5** and **CTA8** were purified by column chromatography, while **CTA6** and **CTA7** were recrystallized from n-hexane.

Synthesis of benzylic (and bifunctional) chain transfer agents (CTA9-CTA13)

Benzylic R groups are a frequently used structural motif in all classes of CTAs. Their attractiveness is on one hand related to the availability of the corresponding starting materials (e.g. benzyl halides). On the other hand, they effectively control the polymerization of acrylic monomers. **CTA9** is the basic structure of the studied benzylic trithiocarbonates (**CTA10-CTA13**). In this study, **CTA11** is the only example of a symmetrically substituted trithiocarbonate bearing two homolytic leaving groups. Thus, it can be used to synthesize symmetrical ABA triblock copolymers in two successive polymerization steps where the active trithiocarbonate moiety is located in the center of the macromolecule. As this moiety is hydrolytically labile¹⁵⁷, cleavage of this group is possible especially in an aqueous environment with dramatic effects on the molar mass and its distribution. These limitations can be overcome by using a CTA that bears two trithiocarbonate moieties on the leaving group R, as for example in **CTA12** and **CTA13**. By employing these CTAs the polymer propagates from the R group in two directions and in the final polymer the trithiocarbonate moieties are located at the chain termini. **CTA13** was synthesized to study the effect of chain end polarity on the absorption of the thiocarbonyl moiety. Furthermore, it can be used to synthesize water-soluble polymers that self-assemble in water due to the highly apolar n-octadecyl chains. Both CTAs were synthesized by alkylation of the respective monoalkyl trithiocarbonate (starting from butyl or octadecyl thiol) with 1,4-bis(chloromethyl) benzene. In contrast to a previously reported procedure¹⁸⁸ the synthesis of **CTA12** was carried out without a phase transfer catalyst at room temperature, to give the bis(trithiocarbonate) in high purity.

Synthesis of chain transfer agents with a chromophore-labeled R group (CTA2, CTA10)

Although the chain transfer agents for RAFT polymerization are already inherently labeled with the thiocarbonyl chromophore, it might prove helpful for end-group analysis by UV-vis spectroscopy to introduce a chromophore into the re-initiating R group, too. The R group is attached to the polymer chain by a C-C bond and cannot be cleaved e.g. by hydrolysis. Ideally, the absorptions of the chromophore do not coincide with those of the thiocarbonyl moiety. The molar absorptivity should be high to achieve a high sensitivity. Moreover, the chromophore is preferentially not too hydrophobic as this may alter the properties of water-soluble or thermoresponsive polymers. And last but not least, it should be rather inexpensive as considerable amounts are needed for the synthesis of the CTA.

The naphthalene chromophore was explored for this purpose. **CTA2** and **CTA10** contain both a naphthylmethyl moiety as re-initiating R group and are of the dithiobenzoate and trithiocarbonate class, respectively. **CTA2** was synthesized in a one-pot procedure via the Grignard route to dithiobenzoates. The raw product contained substantial amounts of by-products and required extensive purification by column chromatography. **CTA10** was synthesized by alkylation of the monobutyl trithiocarbonate with 2-bromomethyl naphthalene. As for the synthesis of all trithiocarbonates in this work, the reaction proceeded smoothly at ambient temperature and the product was obtained in high purity.

The synthesis of all CTAs is described in detail in chapter 7.2. Their ^1H and ^{13}C NMR as well as their IR spectra are presented in Appendices 1 and 2. All synthesized RAFT agents were used for extensive studies by UV-vis spectroscopy in order to explore their usefulness for end-group analysis, as presented in the following chapter.

Summary

The alkylation of dithiobenzoate and trithiocarbonate salts is probably the most versatile method for the synthesis of chain transfer agents for RAFT polymerization as many alkylating agents are commercially available and the reactions can be run under mild conditions. In the case of dithiobenzoates, the route via Grignard reagents leads to side products which complicate the purification. In contrast, the synthesis of trithiocarbonates is compatible with aqueous environments and functional groups. Moreover, less side products are formed and most products were readily purified by recrystallization.

3. UV-VIS ABSORPTIONS OF CHAIN TRANSFER AGENTS & THEIR POTENTIAL FOR END-GROUP ANALYSIS

The design and synthesis of materials with unique properties is a rapidly growing field of polymer chemistry. Polymers attain their properties by their chemical structure as well as their molar mass and its distribution. In order to establish structure-property relationships, it is indispensable to know about these parameters as many macroscopic properties are related to the polymer's molar mass and molar mass distribution. Various methods have been developed to assess the molar mass of polymeric materials, from which size exclusion chromatography (SEC) and matrix-assisted laser desorption/ionization mass spectrometry (MALDI-MS)^{189, 190} are the most widely used today.

One of the classical methods of molar mass determination is end-group analysis. Assuming that each polymer chain bears a defined amount of specific end-groups, the molar mass is derived from the concentration of end-groups in the polymer sample. They can be typically quantified by:

- (a) titration of a special functional group (e.g. acid¹⁹¹ or amine¹⁹² functionality),
- (b) elemental analysis of element-specific end-groups,
- (c) measurement of radioactive-tagged end-groups, or
- (d) spectroscopic determination of end-groups (e.g. by NMR^{193, 194})

Classically, the method of end-group analysis has been applied to polymers obtained in condensation reactions where a functional end-group such as the carboxyl group is present and can be titrated. Due to the generally low concentrations of end-groups within a polymer sample, the method of end-group analysis suffers from limitations regarding sensitivity and precision with increasing molar mass. Therefore, end-groups producing high signal intensities - such as chromophores with specific absorptions in the UV-vis or IR range - are desirable. If the molar absorptivity ϵ of the chromophore is known, the number-average molar mass of the polymer is calculated according to the Beer-Lambert law:

$$M_n = \frac{\epsilon \cdot m \cdot d}{A \cdot V} \quad \text{Equation 3.1}$$

ϵ is the molar absorptivity [$\text{L mol}^{-1} \text{cm}^{-1}$], m is the mass of polymer in the sample [g], d is the thickness of the sample cell [cm], A is the maximum absorption at λ_{max} , V is the volume of the sample [L].

End-group analysis by optical spectroscopy does neither require costly equipment nor complicated sample preparation. Instead, the molar mass of a polymer can be determined within minutes. Furthermore, this technique is *a priori* insensitive to the association of polymers as molecularly dissolved samples are not essential. Thus, end-group analysis by optical spectroscopy is even applicable to the characterization of (amphiphilic) block copolymers that associate in solution.

3.1. Motivation for studying UV-vis absorptions of chain transfer agents

Polymerization by reversible addition fragmentation chain transfer (RAFT) is a widely applied technique of controlled radical polymerization (CRP) today. The synthetic potential of the well-defined thiocarbonylthio end-groups has been recognized, for example in photopolymerizations¹⁹⁵ or the transformation of the thiocarbonylthio groups into thiol^{45, 157, 196-200} and a variety of other telechelic functionalities.²⁰¹⁻²⁰³

For analytical purposes the absorption of the thiocarbonylthio end-groups was exploited in studies of the RAFT pre-equilibrium,²⁰⁴ to confirm the presence or absence²⁰⁵ of RAFT end-groups and for SEC to prove the homogenous concentration of active end-groups over the whole molar mass distribution.¹⁸⁸ Nevertheless, studies that quantify the absorption of the RAFT active groups in order to derive a molar mass are rare.^{171, 172, 187, 206} In order to obtain meaningful results from end-group analysis, it is necessary that each polymeric chain bears exactly the amount of end-groups as dictated by the structure of the CTA. Consequently, any side reaction that destroys end-groups must be avoided. Under optimal polymerization conditions a high degree of end-group functionalization is generally achieved - in agreement with the RAFT mechanism.

Aiming for simple experimental conditions, the quantification of end-groups by using Lambert-Beer's law is usually based on the approximation that λ_{\max} and the molar absorptivity ϵ do not change when the thiocarbonyl moiety is transferred from the low-molar mass CTA to the polymer chain. However, the substitution pattern on the thiocarbonylthio moiety can change dramatically by this transfer (cf. Fig. 3.1) and therefore, the absorption characteristics may be modified. Moreover, the UV-vis absorptions of the thiocarbonyl moiety may be affected by the polarity of its microenvironment, too, to which the solvent as well as the polymer contribute as the local concentration of the latter is high.

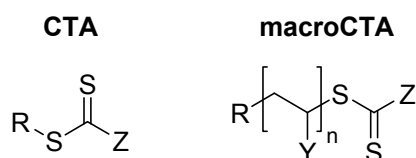


Figure 3.1 General structures of CTAs and macroCTAs

Based on the above-mentioned approximations, end-group analysis by UV-vis spectroscopy is occasionally performed for polymers obtained from RAFT. However, it has never been scrutinized whether these assumptions are in fact true. Hence, the effect of substitution pattern on the electronic spectra of dithiobenzoate and trithiocarbonate CTAs bearing secondary, tertiary and benzylic R groups was studied, complementing the obtained results with literature data. The effect of polarity on the absorption characteristics was studied by recording the electronic spectra in solvents of different polarity. Special emphasis was put on the synthesis and characterization of CTAs whose R groups are structurally similar to the repeating units of common polymers, such as poly(meth)acrylates and polyacrylamides.

3.2. Introduction: Electronic spectra of thiocarbonyl compounds

Thiocarbonyl compounds were synthesized and characterized concerning their electronic spectra^{207, 208} before they have been employed as chain transfer agents in RAFT polymerizations. Compounds with different substituents (e.g. Cl, -NH₂, -F, -CF₃, -CN, -CONH₂) next to the thiocarbonyl group have been extensively studied, as these compounds display pronounced and characteristic spectral shifts depending on the type of electronic transition and on the substituents.^{209, 210} Three types of bands are known:^{207, 209} I (~235 nm, strong), II (~300 nm, strong) and III (420-520 nm, weak). Type I is ascribed to allowed n-π*-transitions, type II to allowed π-π*-transitions and type III to forbidden n-π*-transitions of the thiocarbonyl bond.

A large variety of RAFT agents has been reported up to now. Their main categories according to the Z substituent are dithioesters¹⁶², trithiocarbonates,¹⁵⁷ xanthates^{159, 160} and dithiocarbamates²¹¹ (Fig. 3.2). Occasionally, more exotic RAFT agents such as phosphoryl dithioesters²¹² have been reported. The Z group of a CTA is the basic structural element that determines its chemical classification, activates or deactivates the C=S double bond towards radical addition and, additionally, determines its spectral characteristics. In Table 3.1, the spectral data of some examples taken from the literature are summarized.

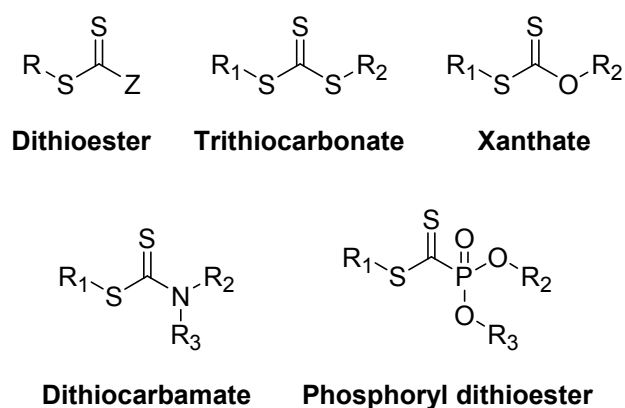


Figure 3.2 The categories of RAFT agents according to their Z group

The substitution of the S-CS-chromophore by strong electron-donating groups leads to a blue-shift of the π-π*- and n-π*-absorption (entries 11-13). The coupling of the phenyl moiety with the dithioester lowers the transition energy for both the n-π*- and π-π*-absorption and results in a pronounced red-shift for this class (entries 3-7). As thiocarbonyl compounds are cross-conjugated²¹³ two absorption maxima are observed, if the substituents of the thiocarbonyl group differ markedly, as e.g. in xanthates and dithiocarbamates (entries 11-13).

Table 3.1 Maximum absorption wavelengths (λ_{\max} , in nm) and molar absorptivities (ϵ , in $\text{L mol}^{-1} \text{cm}^{-1}$) for a variety of thiocarbonylthio compounds taken from the literature

Entry	Example	$\pi \rightarrow \pi^*$			$n \rightarrow \pi^*$			Ref.
		$\text{C}_6\text{H}_{12}^{\text{a}}$	$\text{C}_2\text{H}_5\text{OH}$	CH_3CN	$\text{C}_6\text{H}_{12}^{\text{a}}$	$\text{C}_2\text{H}_5\text{OH}$	CH_3CN	
1	MeCS-SMe	302 11500		302 11700	456 15.5		446 19.1	209
2	MeCS-SEt	306 12300						213
3	Ph-CSSH	298 10000	300 -	302 9800	538 70.8	518 -	522 70.8	207
4	Ph-CS-SEt	299 12900	299 14500	299 14800	508 117.5	501 117.5	497 125.9	207
5	Ph-CS-S-iPr	296 17400	299 15800	298 15100	509 117.5	503 114.8	500 128.8	207
6	Ph-CS-S-tBu	296 15100	298 12000	296 12000	526 102.3	520 93.3	515 75.9	207
7	Ph-CS-S-Bn	299 19000			504 107.0			214
8	HS-CS-SH	288 ^b 2400						213
9	MeS-CS-SMe	303 16200			429 28.2			209
10	PhS-CS-SPh	310 8900			460 53.7			209
11	NH₂-CS-SMe	241 6500	279 8100		357 39.8			213
12	(Et)₂N-CS-S-Bn		282 10500					215
13	EtO-CS-SEt	221 ^c 8700	278 ^c 13200		357 ^c 52.5			209, 213

^a in cyclohexane. ^b in petrol ether. ^c in iso-octane

3.3. Influence of R groups on the electronic spectra of CTAs

As has been discussed in chapter 3.1, end-group analysis of polymers by UV-vis spectroscopy is usually based on the approximation that λ_{\max} and ϵ remain unchanged compared to the low-molar mass CTA. In order to clarify to what extent a different substitution pattern modifies the electronic spectrum of the thiocarbonylthio moiety, λ_{\max} and ϵ were determined for a variety of CTAs (Tables 3.2 and 3.3). The studied CTAs were trithiocarbonates or dithiobenzoates bearing secondary, benzylic and tertiary R groups (cf. Fig. 2.3). As in this study only two dithiobenzoate CTAs were synthesized, the determined λ_{\max} values are complemented with literature data (Table 3.1).

The maximum absorption wavelength λ_{\max} of the $\pi\text{-}\pi^*$ -transition of trithiocarbonate CTAs with secondary, tertiary and benzylic R groups is found in n-hexane between 305 nm and 308 nm, while λ_{\max} of the unsubstituted trithiocarbonic acid is shifted to lower wavelengths ($\lambda_{\max} = 288$ nm) (Table 3.1). Compared to trithiocarbonates, λ_{\max} of the $\pi\text{-}\pi^*$ -transition is slightly shifted to lower wavelengths (294-297 nm) for dithiobenzoates. Thus, within a given category of thiocarbonylthio compound the influence of the various R groups on λ_{\max} of the $\pi\text{-}\pi^*$ -transition is small.

For the n- π^* -absorption band of trithiocarbonates and dithiobenzoates the obtained results reveal partially a different behavior. While trithiocarbonates with secondary (**CTA3-CTA6**, 429-433 nm) and benzylic (**CTA9-CTA13**, 432-433 nm) (cf. Table 3.2) R groups absorb approximately at the same wavelength, λ_{\max} of trithiocarbonates bearing tertiary R groups (**CTA7-CTA8**) is markedly red-shifted by about 10 nm (λ_{\max} = 440-442 nm). A similar red-shift is found in the visible range for dithiobenzoates bearing tertiary R groups (λ_{\max} ~ 520 nm) compared to primary, secondary and benzylic R groups (λ_{\max} = 504-509 nm).

Table 3.2 Maximum absorption wavelengths (λ_{\max}) of the π - π^* - and n- π^* -absorption band of the thiocarbonyl bond for the studied dithiobenzoates and trithiocarbonates in a variety of solvents

CTA	$\pi \rightarrow \pi^*$						n $\rightarrow \pi^*$					
	C ₆ H ₁₄	BuAc ^a	CH ₂ Cl ₂	CH ₃ CN	C ₄ H ₉ OH	CH ₃ OH	C ₆ H ₁₄	BuAc ^a	CH ₂ Cl ₂	CH ₃ CN	C ₄ H ₉ OH	CH ₃ OH
CTA1	297	300	303	302	301	301	- ^c	- ^b	514	- ^b	- ^b	516
CTA2	294	295	296	295	296	294	505	501	496	496	496	- ^c
CTA3	305	307	308	- ^b	- ^b	309	431	432	428	- ^b	- ^b	432
CTA4	305	306	307	- ^b	- ^b	305	432	433	432	- ^b	- ^b	432
CTA5	305	306	307	306	306	305	433	433	433	433	432	432
CTA6	308	309	309	309	308	307	429	430	430	431	429	430
CTA7	306	308	308	309	309	311	441	442	440	442	441	442
CTA8	307	307	308	307	307	307	442	441	440	440	440	439
CTA9	306	308	310	- ^b	- ^b	307	433	433	433	- ^b	- ^b	433
CTA10	307	309	310	308	308	308	433	432	433	433	432	- ^c
CTA11	306	308	309	- ^b	- ^b	308	433	433	433	- ^b	- ^b	433
CTA12	307	309	310	309	309	309	432	433	432	434	432	- ^c
CTA13	308	- ^c	310	- ^c	- ^c	- ^c	- ^c	- ^c	433	- ^c	- ^c	- ^c

^a n-butyl acetate ^b not determined ^c insufficient solubility to determine ϵ

According to these results, the assumption of an unchanged λ_{\max} for the n- π^* -absorption is only true for certain monomer-CTA combination. For instance, acrylic macroCTAs that were prepared with benzylic CTAs should absorb at the same wavelength in the polymer as in the CTA. The same applies to methacrylic monomers and CTAs bearing tertiary R groups. But if acrylic monomers are polymerized by CTAs with tertiary R groups, variations of λ_{\max} are observed. However, this combination is often employed in practice as tertiary R groups are excellent leaving groups compared to the propagating chains of acrylic polymers and thus, establish the main equilibrium of the RAFT polymerization fast. The shift of λ_{\max} in secondary compared to tertiary dithiobenzoates has been exploited in studies concerning the pre-equilibrium of RAFT polymerization.²⁰⁴ This blue shift can even be followed visually as initially pink polymerization mixtures - which contain an acrylic monomer and **CTA1** - turn red when the main equilibrium is established.

In contrast to the relatively constant λ_{\max} values for similar R substituents, the molar absorptivities for both transitions in n-hexane differed strongly depending on the substitution by the R group

(cf. Table 3.3). In the trithiocarbonate class, the values of ϵ range from 11,000 to 21,000 L mol⁻¹ cm⁻¹ for the π - π^* -transition, and from 31 to 61 L mol⁻¹ cm⁻¹ for the much weaker n - π^* -transition in n-hexane. Even for very similar R substituents such as the secondary R groups (**CTA3-CTA6**) the molar absorptivities can differ by up to \pm 15%.

Table 3.3 Molar absorptivities ϵ (in L mol⁻¹ cm⁻¹) due to the π - π^* - and n - π^* -transition of the thiocarbonyl bond for the studied dithiobenzoates and trithiocarbonates in a variety of solvents

CTA	$\pi \rightarrow \pi^*$						$n \rightarrow \pi^*$					
	C ₆ H ₁₄	BuAc ^a	CH ₂ Cl ₂	CH ₃ CN	C ₄ H ₉ OH	CH ₃ OH	C ₆ H ₁₄	BuAc ^a	CH ₂ Cl ₂	CH ₃ CN	C ₄ H ₉ OH	CH ₃ OH
CTA1	10900	11200	13600	13100	13200	13200	- ^c	- ^b	114.3	- ^b	- ^b	114.1
CTA2	16400	16200	15900	15800	16600	18700	129.7	134.0	138.0	141.3	134.8	- ^c
CTA3	14500	16000	14900	- ^b	- ^b	15800	37.4	38.4	31.9	- ^b	- ^b	37.8
CTA4	19200	17900	18300	- ^b	- ^b	17000	33.2	36.0	41.6	- ^b	- ^b	35.0
CTA5	16400	15300	14400	14000	15200	16400	35.2	36.1	40.9	36.3	38.2	35.7
CTA6	17800	17000	16000	15500	16800	15800	45.2	44.0	48.5	42.6	44.2	41.8
CTA7	15900	14600	13500	13400	14900	11900	35.4	32.6	37.9	33.4	33.1	32.0
CTA8	11400	13300	10400	13900	11700	14500	30.9	31.7	36.4	33.0	31.8	32.3
CTA9	17200	16500	16200	- ^b	- ^b	16500	46.7	47.7	53.0	- ^b	- ^b	48.4
CTA10	20600	17800	17600	15800	18200	17600	60.5	61.7	64.7	60.9	65.1	- ^c
CTA11	18600	17300	16900	- ^b	- ^b	16900	62.1	61.5	65.8	- ^b	- ^b	62.7
CTA12^d	37900	33300	33200	31200	34500	33600	109.7	113.1	120.1	105.0	113.1	- ^c
CTA13^d	40000	- ^c	34800	- ^c	- ^c	- ^c	- ^c	- ^c	124.7	- ^c	- ^c	- ^c

^a n-butyl acetate ^b not determined ^c insufficient solubility to determine ϵ ^d bifunctional CTA

The intensities of the π - π^* - as well as the n - π^* -transition of CTAs bearing benzylic R groups (**CTA9-CTA13**) were found to be slightly increased compared to secondary or tertiary R groups. Regarding the measurements in the visible range, the results have to be interpreted cautiously as in these very concentrated solutions mutual interactions of solute molecules cannot be excluded. The origins of the increased intensity for the UV-vis absorptions of benzylic CTAs were not object of this thesis but the observations underline that the approximation of a stable molar absorptivity ϵ at the maximum absorption wavelength λ_{\max} is not justified, but must be considered as a relatively rough estimation. Consequently, if the structure of the CTA and the synthesized macroCTA differ strongly, the determined concentration of end-groups can deviate markedly from the actual value if the molar absorptivity of the primary CTA is used for quantification.

3.4. Influence of solvent polarity on the electronic spectra of CTAs

In order to study how sensitive the absorptions of the thiocarbonyl bond are towards changes in the polarity of the micro-environment, solutions in solvents of varying polarity were prepared and measured, namely in n-hexane, n-butyl acetate (BuAc), dichloromethane, acetonitrile, 1-butanol and methanol. As the most apolar solvent, n-hexane was chosen while methanol constituted the most polar one. In order to clarify, whether hydrogen bonding affects the thiocarbonyl absorptions, 1-butanol was chosen as a second hydrogen bond-donating yet more apolar solvent. Acetonitrile was selected due to its highly polar, aprotic nature. As it dissolves nonionic hydrophilic as well as hydrophobic polymers, CH₂Cl₂ is a suitable solvent for the end-group analysis of amphiphilic block copolymers and thus, was included in this study. As it is structurally similar to the repeating unit of poly(n-butyl acrylate) (polyBuA) and thus, should exhibit a similar polarity as the corresponding polymer, n-butyl acetate was chosen. If the end-group analysis of a poly(BuA) macroCTA is performed in this solvent, effects on the thiocarbonyl absorptions that are caused by different polarities of solvent and polymer may be avoided. The determined maximum absorption wavelengths and respective molar absorptivities for **CTA1-CTA13** in the selected solvents are summarized in Tables 3.2 and 3.3.

In order to detect trends related to the polarity of the surrounding medium, the solvents must be evaluated according to their polarity. But polarity is not easy to be quantified. Parameters that have been used for this include dielectric constant, refractive index, heat capacity, etc. However, they are not suited to describe all the interactions that a given solute may experience when it is put into solution. Due to this reason a variety of empirical solvent polarity scales have been developed and they are based primarily on either kinetic and/or spectroscopic measurements.

One of the most widely used empirical scales of solvent polarity is known as the $E_T(30)$ scale²¹⁶ and is based on the charge-transfer absorption of 2,6-diphenyl-4-(2,4,6-triphenyl-N-pyridinio)-phenolate, also known as Dimroth or Reichardt's betaine. The $E_T(30)$ scale has been shown to be sensitive to both, the solvent dipolarity / polarizability as well as to the solvent's hydrogen bond donating ability. There also exist multi-parameter approaches to solvent polarity effects, as best exemplified by the work of Kamlet, Taft, and co-workers.²¹⁷⁻²¹⁹ The π^* scale²¹⁹ is an index of solvent dipolarity/polarizability, which measures the ability of a solvent to stabilize a charge or a dipole by virtue of its dielectric effect. While the $E_T(30)$ scale is based on solvent effects of a single indicator, the π^* scale is derived from a variety of properties involving many diverse types of indicators. Solvent polarity parameters of the chosen solvents according

Table 3.4 Solvent polarity parameters

solvent	$E_T(30)$	π^*
C ₆ H ₁₄	31.0	-0.08
BuAc	38.5	0.46
CH ₂ Cl ₂	40.7	0.82
CH ₃ CN	45.6	0.75
C ₄ H ₉ OH	49.7	0.47
CH ₃ OH	55.4	0.60

to the $E_T(30)$ and π^* scale are summarized in Table 3.4. The given values increase with increasing dipolarity/polarizability for both scales. It is noteworthy, that according to the two chosen scales, the sequences of increasing solvent polarity differ.

For the π - π^* -transition of the C=S-chromophore, the found wavelength shifts are rather small ($\lambda_{\max} = 2\text{-}5$ nm) and therefore, no clear solvatochromic trends are observed. The π - π^* -transition of dithiobenzoates was reported to be red-shifted in polar solvents.²⁰⁷ The results of this study confirm this as a general trend but partially deviations occur. In fact, most of the trithiocarbonates and dithiobenzoates exhibit the largest red-shift of the π - π^* -transition in CH_2Cl_2 , which is a solvent of intermediate polarity according to the $E_T(30)$ scale. On the other hand, the strong red-shift in CH_2Cl_2 correlates with its high dipolarity/polarizability according to the π^* -scale. The influence of solvent polarity in the visible range is negligible for trithiocarbonates as λ_{\max} is shifted by 2 nm only. The dithiobenzoates seem to be more sensitive towards changes of solvent polarity²⁰⁷ as λ_{\max} is red-shifted by about 10 nm in polar media.

While the solvent polarity has no remarkable effect on λ_{\max} of the π - π^* -transition, the situation is different concerning the molar absorptivities. Depending on the solvent, the intensities of both transitions can vary strongly for a given compound. However, clear trends following the solvent polarity according to the $E_T(30)$ or π^* scale were not found.

3.5. Model compounds for macroCTAs

Measuring the UV-vis spectra of a variety of dithiobenzoates and trithiocarbonates revealed that λ_{\max} and especially the molar absorptivity ϵ for both studied transitions are sensitive to changes of substitution in the R group. Due to this variations it should not be appropriate to use the molar absorptivity of the primary CTA as a measure to quantify the concentration of end-groups in the polymer and thus, to derive a molar mass. Ideally, calibration for a certain polymer is performed with macromolecular samples of known molar mass and which are completely functionalized with the respective end-group. However, this procedure is painstaking and impracticable. Instead, thiocarbonylthio compounds that serve as model compounds for trithiocarbonate end-groups attached to common polymers were synthesized and their UV-vis characteristics studied. The respective structures (**CTA3-CTA8**) together with their polymeric analogs are resumed in Figure 3.3. In the following, an example is given which illustrates the importance of choosing the appropriate ϵ -value for end-group quantification.

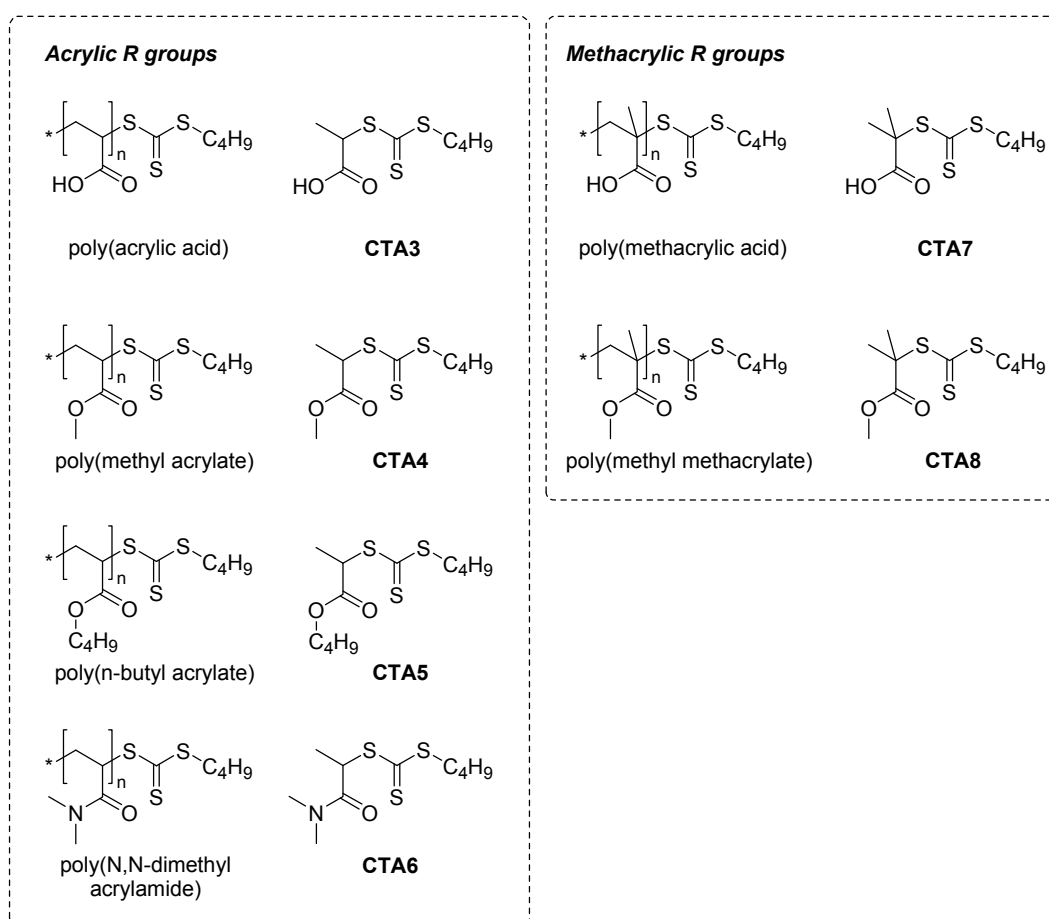


Figure 3.3 Macromolecular CTAs and their corresponding low-molar mass model compounds with a similar substitution pattern

Upon polymerization of *N,N*-dimethyl acrylamide (DMA) with **CTA7**, the substitution pattern next to the trithiocarbonate moiety changes from tertiary to secondary. **CTA6** is the model compound for the respective polyDMA macroCTA bearing *n*-butyl trithiocarbonate end-groups. As is shown in Figure 3.4, the UV-vis spectra of **CTA6** and **CTA7** differ markedly in intensity and λ_{\max} . The molar absorptivities of the π - π^* - as well as the n - π^* -transition deviate by approximately 25%.

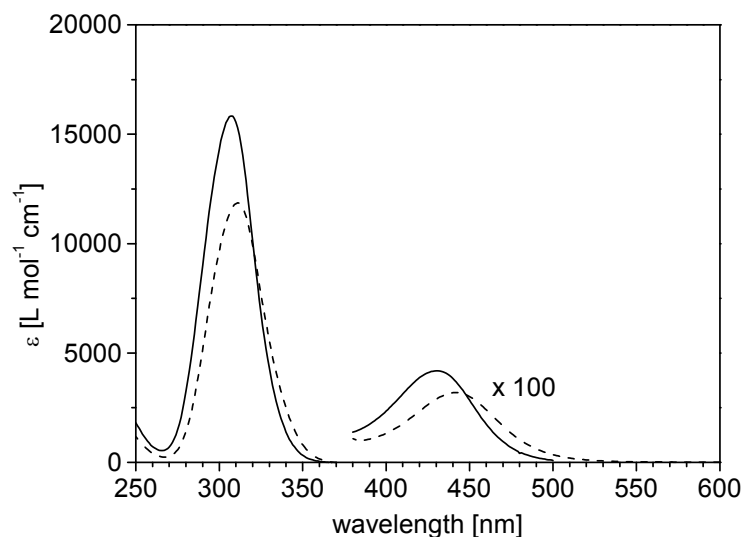


Figure 3.4 UV-vis spectra of **CTA6** (solid line) and **CTA7** (dashed line) in CH_3OH

Consequently, if the molar absorptivity of **CTA7** is used, the determined concentration of end-groups is overestimated. Accordingly, a loss of 25% of end-groups would not be recognized. However, for block copolymerizations it is desirable to know exactly the concentration of RAFT active end-groups in a polymer sample. A high degree of end-group functionalization is the most important prerequisite to obtain a high blocking efficiency in subsequent block copolymerizations. Furthermore, the concentration of end-groups must be known, in order to adjust the monomer/end-group and end-group/initiator ratios properly.

CTA5 and **CTA6** are the model CTAs for *n*-butyl trithiocarbonate-monofunctionalized poly(*n*-butyl acrylate) (polyBuA) and polyDMA macroCTAs. The overlays of the UV spectra of the model CTAs with those of respective polymer samples are depicted in Fig. 3.5. For better comparison, the spectra are normalized to their maximum height. The good agreement between the curves indicates that the substitution on the β -C-atom has no detectable influence on the shape of the UV spectrum for both model CTAs. Furthermore, the high concentration of polymer close to the thiocarbonyl moiety does not shift the absorption band compared to the model CTA alone. On the other hand, this possible effect was minimized in advance by recording the spectra in solvents which exhibit a comparable polarity as the

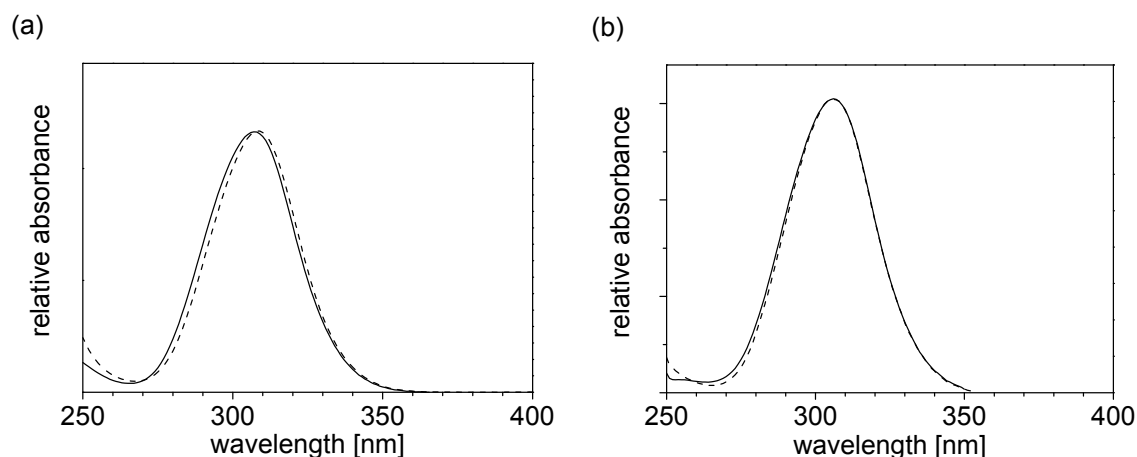


Figure 3.5 UV spectra of model CTAs and macroCTAs: (a) **CTA6** and a poly(*N,N*-dimethyl acrylamide) macroCTA in CH_3OH (b) **CTA5** and a poly(*n*-butyl acrylate) macroCTA in *n*-butyl acetate. Solid line: model CTA, dashed line: macroCTA.

respective polymer. Accordingly, n-butyl acetate was used for the UV-analysis of polyBuA and methanol for polyDMA.

Finally, the molar masses obtained by UV end-group analysis are compared to those obtained by SEC. Depending on their polarity, the polymers were analyzed by two different SEC systems. Although polyBuA can be analyzed by SEC in N-MP, too, the analysis was carried out in tetrahydrofuran (THF), as in this solvent polystyrene is a suitable standard for polyBuA²²⁰ and thus, the calibration gives meaningful molar masses.

Table 3.5 Molar mass determination of polymers used for the evaluation of end-group analysis

entry	polymer	SEC ^a		UV-1 ^b	UV-2 ^c
		$M_n \times 10^{-3}$ [g/mol]	PDI	$M_n \times 10^{-3}$ [g/mol]	$M_n \times 10^{-3}$ [g/mol]
1	polyBuA	15 ^d	1.11	13 ^f	14 ^f
2	polyDMA	14 ^e	1.19	11 ^g	15 ^g

^a (apparent) molar mass and PDI according to SEC traces ^b calculated by end-group analysis of UV band (trithiocarbonate absorbance at $\lambda \sim 305$ nm, employing ϵ of **CTA7**) ^c calculated by end-group analysis of UV band (trithiocarbonate absorbance at $\lambda \sim 305$ nm, employing ϵ of the model CTAs **CTA5** or **CTA6**, respectively) ^d eluent: THF, calibrated with PS standards ^e eluent: 0.05 M LiBr/N-MP, calibrated with PS standards ^f determined in n-butyl acetate ^g determined in CH₃OH.

The agreement of number-average molar masses determined by SEC and UV spectroscopy is better for both polymers, if the calculation is based on the molar absorptivity of the respective model CTA. Thus, the molar absorptivity of the model CTA proved to be the more appropriate measure to quantify the concentration of thiocarbonyl end-groups. Accordingly, a precise end-group analysis would necessitate the synthesis and UV-vis characterization of a model CTA for every employed monomer. At the beginning, this would be a laborious task, however, it provides a pool of data which can be referred to for identical monomer-Z group combinations.

Although the methacrylic model CTAs **CTA7** and **CTA8** were characterized by UV-vis spectroscopy, polymethacrylates could not be included in this study. The synthesis of poly(methacrylic acid) and poly(methyl methacrylate) macroCTAs exhibiting a high degree of end-group functionalization would have required the synthesis of more effective CTAs with better homolytic leaving groups (cf. Fig. 2.1). The polymerization of methacrylates with **CTA7** leads to incomplete end-group functionalization and thus, the basic requirement for end-group analysis is not met.

3.6. CTAs with chromophore-labeled R groups

The hydrolytic lability of the dithioester and trithiocarbonate Z groups can pose a problem to a reliable end-group analysis, as these moieties can be cleaved. Therefore, it is advantageous to extend the approach of end-group analysis by UV-vis spectroscopy to the R groups and to introduce a chromophore to the re-initiating moiety of a CTA. According to the general RAFT mechanism, this approach guarantees virtually 100% end-group functionalization. Moreover, the R group is connected to the polymer chain by a stable C-C-bond. Although several studies reported on initiating species for living / controlled polymerization techniques bearing a chromophore or fluorophore, these works focused mainly on imparting the chromophore characteristics to the polymer, not on using it as an analytical tool for molar mass determination. Examples include all methods of CRP, namely ATRP,²²¹ TEMPO²²² and RAFT^{185, 223-226} but also ROMP.²²⁷

The concept of introducing a chromophore in the re-initiating R group of a RAFT agent offers several advantages regarding end-group analysis: First of all, UV-vis spectroscopy is a convenient, low-cost and very sensitive method when using chromophores with a high molar absorptivity. Second, the comparison of the amount of R- and Z-groups allows to determine precisely the degree of end-group functionalization. Being essential for setting the appropriate $[M]/[\text{macroCTA}]$ and $[\text{macroCTA}]/[\text{initiator}]$ ratios, this information is difficult to be assessed by other methods. Third, end-group analysis allows for the determination of the true M_n since SEC mostly refers to polystyrene calibration. Noteworthy, end-group analysis is probably the best possibility to determine the molar mass of amphiphilic block copolymers, which tend to associate in solution.

An ideal chromophore - as part of the R group - should have a defined absorption band which does neither overlap with the absorption bands of common polymers nor with those of the thiocarbonyl moiety. Moreover, it should not be too big otherwise it might affect the properties of the polymer. This is a particular problem for thermoresponsive polymers exhibiting LCST behavior, as their phase transition temperatures are typically influenced by attached hydrophobic or hydrophilic end-groups.^{228, 229} Additionally, the respective absorption band of the chromophore should exhibit a high molar absorptivity in order to achieve a high sensitivity for molar mass determination and is preferred to be non-solvatochromic.

As these requirements are difficult to meet all together, a first focus was on the naphthalene chromophore. A dithiobenzoate (**CTA2**) and a trithiocarbonate (**CTA10**) - both bearing the naphthalenyl-2-methyl group as R group - were synthesized and their UV-vis spectra recorded (Fig. 3.6). For both CTAs, the absorptions of the naphthalene chromophore overlap unfavorably with the π - π^* -absorption band of the thiocarbonyl moiety. In Figure 3.7, the UV spectrum of **CTA10** is compared with those of **CTA5** and 2-ethyl naphthalene.²³⁰ The contribution of the naphthalene chromophore to the molar absorptivity of the C=S-absorption at the maximum absorption wavelength ($\lambda_{\text{max}} \sim 300$ nm) is negligible. However, the absorption band of the naphthalene chromophore ($\lambda_{\text{max}} = 275$ nm) is not resolved from that of the thiocarbonyl moiety rendering the quantification of R groups problematic. Still, the naphthalene absorption can be employed for end-group analysis, if the Z groups are cleaved from the polymer.

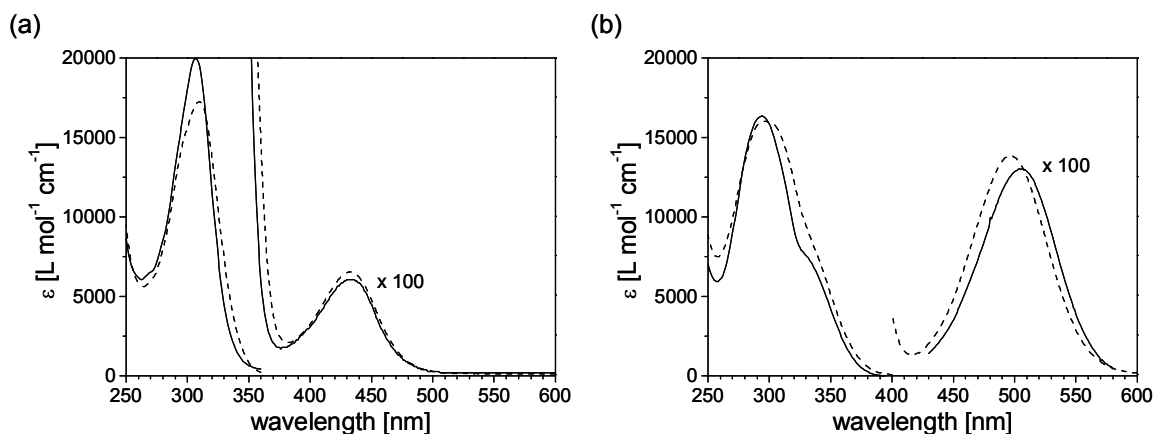


Figure 3.6 UV-vis spectra of CTAs with naphthalenyl-2-methyl R groups: (a) **CTA2** (b) **CTA10**. Solid line: in n-hexane, dashed line: in CH_2Cl_2 .

Several methods have been utilized for the removal or transformation of Z end-groups. Examples include aminolysis,^{202, 231, 232} hydrolysis²⁰⁰ in basic media and heating the polymer with an excess of azoinitiator.²³³ While in the latter case the thiocarbonylthio end-groups are replaced by an initiator fragment, hydrolysis produces thiol end-groups which should be protected or transformed²⁰³ in order to avoid oxidative coupling to disulfides.

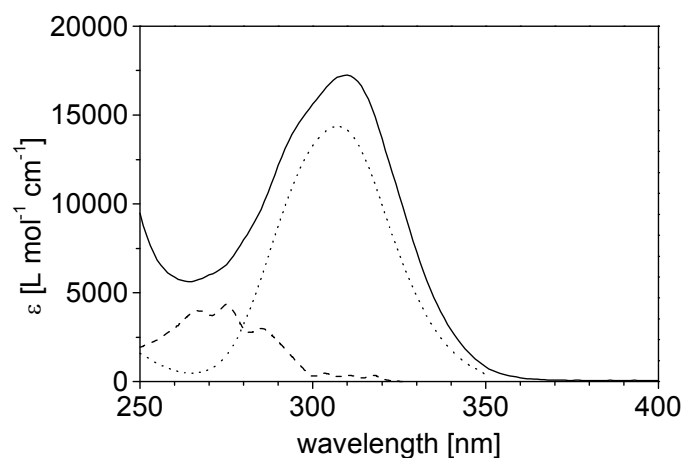


Figure 3.7 UV spectra of **CTA10** (solid line), **CTA5** (dotted line) (both in CH_2Cl_2) and 2-ethyl naphthalene (dashed line).

An alternative to UV-vis spectroscopy constitutes the end-group analysis by ^1H NMR spectroscopy, which offers the advantage of not requiring calibration as all protons exhibit the same absorptivity. However, the equal intensity of end-group and polymer signals reduces the sensitivity of this method and therefore, it is only suited for polymers of relatively low molar mass.

3.7. Summary and guidelines for an optimized end-group analysis

So far, the concentration of thiocarbonyl end-groups in polymers synthesized by RAFT polymerization has been determined by UV-vis spectroscopy employing the molar absorptivity of the primary CTA. The changed substitution and environment of the thiocarbonyl moiety in the polymer - compared to the primary CTA - was assumed to have a negligible influence on the absorption characteristics. In this study, it was shown that both, the substitution pattern next to the C=S bond and the polarity of the surrounding medium can have a distinct influence on the UV-vis absorptions of dithiobenzoates and trithiocarbonates.

In principle, both absorptions of the thiocarbonyl bond can be used for end-group analysis by UV-vis spectroscopy. However, the intensity of the $n-\pi^*$ -absorption in the visible range is very weak, rendering the measurement for polymers of high molar mass imprecise. Due to the high molar absorptivity of the $\pi-\pi^*$ -absorption band ($\sim 15000 \text{ L mol}^{-1} \text{ cm}^{-1}$) measurements in the UV range are much more sensitive.

In order to obtain meaningful results, it is necessary to consider some factors affecting the accuracy of the measurement: First of all, the substitution pattern on the R group has a marked influence on the absorption characteristics of a CTA. Therefore, it is preferred to employ the molar absorptivity of a model CTA - which exhibits the same or a similar substitution pattern as the macroCTA - for the quantification of end-groups. Secondly, the polarity of the surrounding medium was found to have a pronounced influence on the intensity of the thiocarbonyl absorptions in the UV and vis range, too. Thus, end-group analysis of the polymer should be performed in the same solvent in which the molar absorptivity of the CTA was determined. Preferentially, the solvent exhibits a similar polarity as the polymer in order to minimize polarity effects originating from the high concentration of polymer close to the thiocarbonyl moiety.

In conclusion, end-group analysis by UV-vis spectroscopy proved to be a convenient and reliable analytical method which complements the molar mass characterization by SEC or other methods. As samples are easily prepared and measurements performed quickly with standard equipment, this method can be adopted straightforwardly by any laboratory dealing with the synthesis of polymers by RAFT polymerization.

4. DOUBLE-THERMORESPONSIVE ABC TRIBLOCK COPOLYMERS & THEIR SELF-ASSEMBLY IN WATER

4.1. Challenges and strategies of the studied system

Compared to classical surfactants, amphiphilic block copolymers offer many advantages, e.g. lower cmc, higher stability of self-assembled structures, better control over properties by composition, architecture, etc. In some cases it may be desirable to tune additionally the amphiphilic state of the final block copolymer on demand. The hydrophilic-hydrophobic balance of amphiphilic triblock copolymers can be switched due to the incorporation of stimuli-responsive blocks.²³⁴⁻²³⁷ This strategy is particularly advantageous for the handling of amphiphilic block copolymers in selective solvents. Polymers with a low hydrophilic-hydrophobic balance are mostly not directly soluble in water and thus, require extensive dispersion procedures. Double-hydrophilic block copolymers comprising stimuli-responsive blocks can be readily dissolved and are then switched from the hydrophilic to the amphiphilic state by the stimulus. Compared to other stimuli, the temperature-stimulus is conveniently applied and in addition very versatile, as has been discussed in chapter 1.2.2.

Most thermoresponsive polymers studied so far respond to an external stimulus by an all-or-nothing response, i.e. multi-responsive system that respond gradually to one or more stimuli are rare. Multi-responsive systems are desirable as their amphiphilicity can be fine-tuned and they enable the switching between different self-assembled states. The ternary block copolymers synthesized in this work comprise two thermoresponsive blocks exhibiting LCST behavior and one permanently hydrophilic block. While the presence of two thermoresponsive blocks with different phase transition temperatures should allow to control the hydrophilic-hydrophobic balance, the permanently hydrophilic block provides steric stabilization of the aggregates formed. At low temperatures, the “triple” hydrophilic block copolymer can be homogeneously dissolved in water. Upon increasing the temperature of the aqueous solution, the polymer becomes amphiphilic with an accompanied two-step decrease of hydrophilic-hydrophobic balance and an anticipated stepwise self-assembly into polymeric micelles. In order to investigate the influence of the polymer architecture on the self-assembly, the block sequence ABC was systematically varied. Three permutations are possible: (a) the sequence corresponds to the one of increasing LCST, (b) the mid-block is formed by the permanently hydrophilic block and (c) the mid-block is formed by the polymer with the lowest LCST. A general scheme for the phase transitions upon heating and the resulting amphiphile architectures is given in Figure 4.1.

In the synthesis of block copolymers by RAFT, the sequence of monomer addition is crucial in order to achieve a high blocking efficiency (cf. chapter 1.3.4). The limitations regarding the sequence of monomer addition²³⁸ were eluded by selecting the monomers from the same class. As the stability of their propagating radicals is comparable, the sequence of the blocks can be chosen freely and polymers of the sequences ABC, BAC and ACB were synthesized with a high blocking efficiency. Substituted acrylamides are a known class of thermoresponsive polymers and their LCST can be varied from 0°C to 100°C by appropriate substitution of the amide nitrogen.^{94, 95}

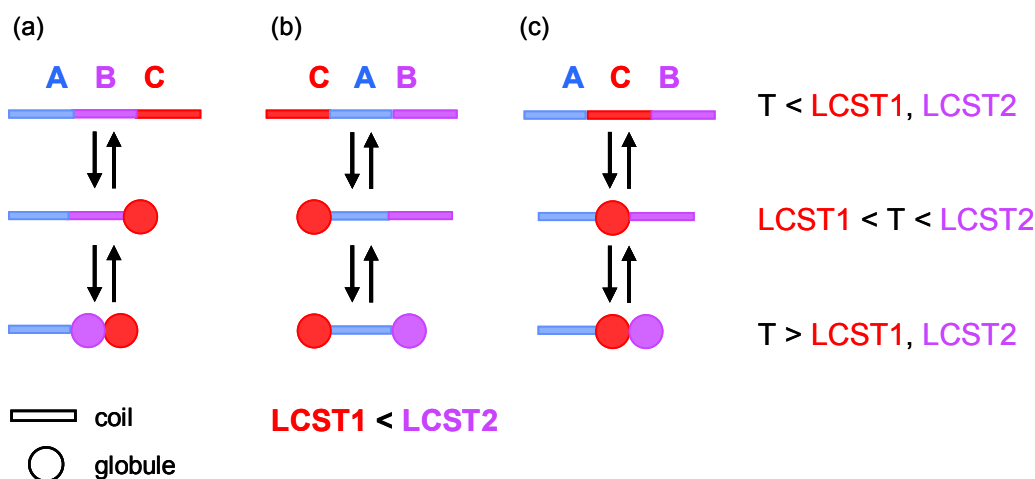


Figure 4.1 Effect of temperature on the amphiphile architectures of double-thermoresponsive triblock copolymers

Poly(*N*-isopropyl acrylamide) (**polyM4**) was chosen for the thermo-responsive block with the lower phase transition temperature. The temperature-responsive behavior of this polymer exhibiting a LCST at 32°C is well-studied.^{103, 104} Moreover, the clouding point of **polyM4** is relatively insensitive to variations of molar mass and concentration^{93, 228, 239} and 32°C is a convenient temperature to carry out studies. The coil-to-globule transition is sharp with only a small hysteresis.⁹³ Furthermore, **M4** can be polymerized in a controlled fashion by RAFT polymerization,²⁸ while by NMP and ATRP some difficulties occur.²⁴⁰ In fact, RAFT polymerization is generally tolerant towards functional groups, applicable to most classical monomers and can be carried out in a variety of solvents (organic and water) and in a large temperature window.

The monomer for the second thermo-responsive block was chosen such, that the phase transition temperature of its polymer is about 20 K higher than that of **polyM4**. Allowing on one hand for sufficient resolution of the two temperature-induced phase transitions, this strategy maintains on the other hand simple experimental conditions. Due to its reported phase transition temperature of 56°C, poly(*N*-acryloyl pyrrolidine) (**polyM3**) was selected from a variety of polyacrylamides exhibiting LCST behavior.⁹⁵ At present, poly(*N*-acryloyl pyrrolidine) is rarely studied in the context of thermo-responsive polymers.^{29, 111, 113, 241} As the permanently hydrophilic block, which stabilizes the self-assembled aggregates, poly(*N,N*-dimethyl acrylamide) (**polyM2**) (LCST > 100°C at 1 bar) was chosen, because it is frequently used as nonionic hydrophilic polymer and can be polymerized in a controlled fashion by RAFT polymerization.¹⁷³

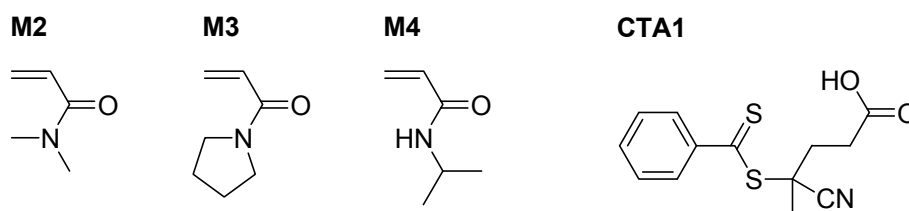


Figure 4.2 Monomers and CTA used for the synthesis of double-thermo-responsive triblock copolymers

RAFT polymerization was the method of choice for the synthesis of the double thermoresponsive polymers due to the highly polar monomer units. Despite the water-solubility of the chosen monomers, polymerizations were not carried out in water as elevated temperatures lead to the precipitation of the polymers - even in some water/organic solvent mixtures.²⁴²⁻²⁴⁵ The synthesis of well-defined triblock copolymers with a high blocking efficiency is the main challenge concerning the macromolecular design in this study. Thus, precursor polymers exhibiting a high degree of end-group functionalization are required. However, even under optimal polymerization conditions the loss of a small amount of end-groups is inherent to the RAFT process. New radicals are generated by a (thermal) initiator at each block copolymerization step. As a consequence of the RAFT mechanism, the number of lost end-groups corresponds at least to the number of formed radicals during initiation. To minimize this loss, the [CTA]/[Initiator] has to be as high as possible, taking into account the polymerization temperature and the decomposition rate of the initiator, too. The temperature should be chosen such that a constant flow of radical is established to balance the loss of radical species by inevitable termination reactions. If the polymerization conditions are optimized in such a way, it is possible to obtain block copolymers with no detectable homopolymer impurity (< 5%) while still maintaining a relatively fast polymerization.²³⁸

The choice of the CTA is essential to control the molar mass and the polydispersity and to obtain a high degree of end-group functionalization. The R group should be on one hand a good homolytic leaving group but on the other hand should re-initiate the polymerization efficiently in order to establish the main equilibrium quickly. Furthermore, the R and Z groups should not be too hydrophobic as the LCST of thermoresponsive polymers is influenced by attached hydrophilic or hydrophobic end-groups.^{201, 221, 229, 246} Dithiobenzoates are frequently utilized as CTAs in RAFT polymerization as they are characterized by a high transfer constant. However, the phenyl Z group is known to cause inhibition and retardation effects due to the stabilization of the intermediate radical. To minimize inhibition periods that are related to different reactivities/stabilities of the initiator radical, the R group of the CTA and the propagating radical, attempts were made to adopt the structure of the CTA to the one of initiator or monomer. For example, the R-group of the CTA 4-cyano-4-thiobenzoylsulfanyl pentanoic acid (**CTA1**) is the same as the radical generated from the initiator **V-501** (4,4-azobis(4-cyanopentanoic acid)).¹⁸² As **CTA1** is known to control efficiently the polymerization of a large variety of monomers¹⁶⁹ such as acrylic (acrylamide²⁴⁷⁻²⁴⁹ and acrylate¹⁷²), styrenic²⁵⁰ and methacrylic^{29, 156, 172} monomers including polymerizations in water,^{172, 247, 249, 250} it was used for the synthesis of the thermoresponsive triblock copolymers.

4.2. Synthesis and molecular characterization of double-thermoreponsive ABC triblock copolymers

The importance of a high degree of end-group functionalization in the synthesis of block copolymers by RAFT has been emphasized before. Consequently, termination events that produce dead polymer chains without active end-groups have to be minimized. Beside a low initiator concentration, it is desirable to choose solvents and initiators which give minimal irreversible chain transfer. AIBN was used as thermal initiator and the molar ratio [CTA]/[initiator] was set to 5 which is on one hand high enough to allow a relatively fast polymerization and on the other hand ensures a high degree of end-group functionalization. According to the half-life time of AIBN (10 h at 65°C), radicals are permanently generated throughout the polymerization process and thus, balance the loss of radical species. In order to investigate the influence of block sequence on the thermoresponsive self-assembly of triblock copolymers, equal degrees of polymerization ($DP \sim 100$) were targeted for each block. The polymerization mixtures were deoxygenated by flushing with N_2 for at least 20 min. Polymerizations were stopped at moderate conversions (50%) as with ongoing monomer consumption an increasing amount of thiocarbonyl end-groups is lost. In the synthesis of homopolymers, the polymerization mixtures showed a slight increase in solution viscosity after polymerization with toluene as the polymerization medium. As this increased viscosity might affect the polymerization kinetics, the syntheses of di- and triblock copolymers were carried out in THF. The double-thermoreponsive ABC triblock copolymers and their respective precursors were synthesized by RAFT polymerization under the conditions listed in Table 7.2. A typical procedure is described in chapter 7.4.2.

The prepared homopolymers and block copolymers were purified by repeated precipitations of the polymer solution into diethyl ether or n-hexane. Precipitation is a much faster purification method compared to dialysis and the risk of losing end-groups by hydrolysis is lower. Additionally, it gives a valuable indication whether the thiocarbonyl end-groups are attached to the polymer chains or not. The supernatant should remain uncolored after precipitation of the polymer in an excess of non-solvent. A colored supernatant indicates low-molar mass thiocarbonyl compounds and thus, the cleavage of RAFT moieties from the polymer. By dialyzing the polymer sample such cleaved thiocarbonyl end-groups are probably not noticed. After repeated precipitations, the polymers were dissolved in water and lyophilized to remove any trapped solvent molecules. Conversions were determined gravimetrically after lyophilization. All triblock copolymers are readily soluble in polar solvents such as THF, $CHCl_3$, *N*-methyl pyrrolidone and water at room temperature.

The synthesized macroCTAs were molecularly characterized before the next block copolymerization step, in order to verify the removal of residual monomer and to determine the number of active RAFT end-groups. As the polymer chains in RAFT polymerization grow linearly with conversion, a theoretical molar mass can be calculated under certain assumptions: (i) the amount of initiator derived polymer chains is negligible, (ii) all employed CTA molecules are attached to a polymer chain and (iii) the obtained yields correspond to the monomer conversion. Theoretically expected molar masses (M_{theory}) of the polymers were calculated according to the following equation:¹⁵⁶

$$M_{theory} = \frac{[M]}{[CTA]} \cdot \chi \cdot M_{Monomer} + M_{CTA} \quad \text{Equation 4.1}$$

[M] and [CTA] are the initial concentrations of monomer and CTA, respectively, χ is the fractional monomer conversion, $M_{Monomer}$ and M_{CTA} are the molar masses of the monomer and the CTA, respectively.

The good agreement between theoretically expected and experimentally determined molar masses is an indicator for a high degree of polymerization control. All homo- and block copolymers were characterized by ^1H NMR spectroscopy to verify the removal of monomer traces. The absence of peaks at 5.6 and 6.4 ppm – typical of olefinic protons – proved that the purified polymers do not contain any unreacted monomer.

The overall molar masses of the block copolymers were calculated from their composition according to ^1H NMR spectroscopy. The composition was not determined by elemental analysis as the three polymer blocks exhibit very similar CHN-ratios. The calculations of composition and molar mass of the block copolymers are based on the molar mass values of the homopolymer as determined by UV-vis spectroscopy assuming that the molar mass of the first block remains unchanged in the following block copolymerizations. The ^1H NMR spectra of block copolymers were recorded in D_2O which appeared to be a better solvent for substituted polyacrylamides than CDCl_3 as the proton signals were better resolved. Although the three polymer blocks are structurally very similar, they exhibit characteristic proton signals. The methyl, methylene and methine protons in α -position to the amide nitrogen were utilized to determine the composition of the block copolymers. Figure 4.3 depicts the ^1H NMR spectrum of $(\text{M4})_{110}$ - $(\text{M3})_{70}$ - $(\text{M2})_{64}$ as an example.

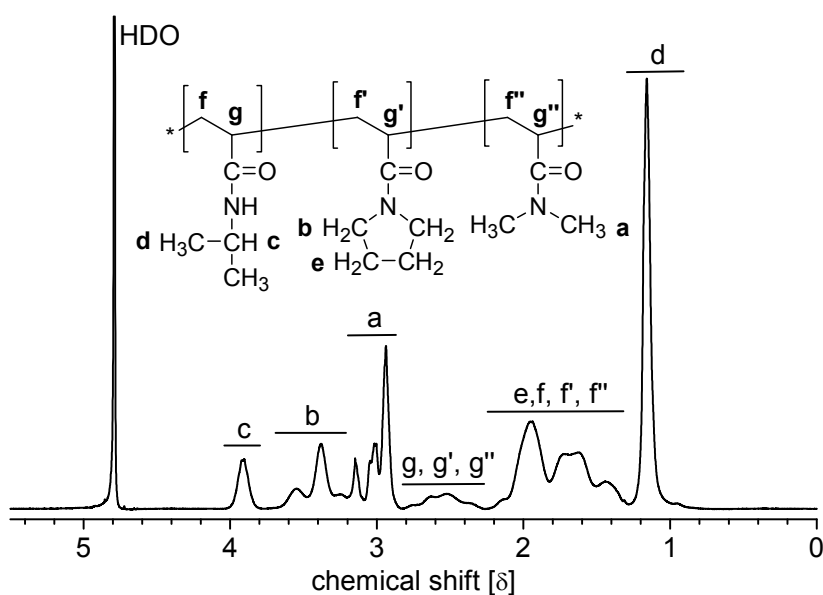


Figure 4.3 ^1H NMR spectrum of triblock copolymer $(\text{M4})_{110}$ - $(\text{M3})_{70}$ - $(\text{M2})_{64}$ in D_2O

The thiocarbonyl moiety of a RAFT agent is a chromophore with two distinct absorptions in the UV and visible range of light (cf. chapter 3). Accordingly, the number of end-groups was determined by UV-vis spectroscopy. As has been discussed in chapter 3, the concentration of RAFT-active end-groups within a polymer sample is an important information which cannot be assessed by other methods. The synthesis of well-defined block copolymers of controlled molar mass and with a high blocking efficiency requires the knowledge of this value as the appropriate $[M]/[\text{macroCTA}]$ and $[\text{macroCTA}]/[\text{initiator}]$ ratios have to be accurately set in the successive block copolymerizations. Here, end-group analysis by UV-vis spectroscopy was applied to determine the concentration of end-groups and to derive a molar mass by an alternative method to SEC.

The number-average molar masses of the polymers were calculated according to Equation 3.1 (chapter 3). The absorption band of the thiocarbonyl group in the visible range ($\lambda_{\text{max}}(\text{CTA1}) = 499 \text{ nm}$, $\epsilon = 113 \text{ L mol}^{-1} \text{ cm}^{-1}$ in THF) was utilized for the molar mass determination of the thermoresponsive polymers. Partially, theoretical molar masses and M_n values according to ^1H NMR deviate from those determined by vis-spectroscopy. Several reasons may be responsible for this: First of all, the sensitivity of end-group analysis is low due to the low molar absorptivity of the employed $n\text{-}\pi^*$ -transition and thus, high polymer concentrations are required to obtain sufficient signal intensity. With increasing molar mass, the concentration of end-groups – and thus the precision of the measurement decreases. Furthermore, it has to be kept in mind that even under optimal polymerization conditions the loss of a small amount of end-groups is inherent to block copolymerizations by the RAFT process. The molar masses of the triblock copolymers were not determined by vis-spectroscopy as their reduced color already indicated a very low concentration of end-groups.

Table 4.1 Characterization of the poly(acrylamide) homo- and block copolymers

Entry	Polymer	Theory ^a	SEC ^b			NMR ^c	vis ^d
		$M_n \times 10^{-3}$ [g/mol]	$M_n \times 10^{-3}$ [g/mol]	$M_w \times 10^{-3}$ [g/mol]	PDI	$M_n \times 10^{-3}$ [g/mol]	$M_n \times 10^{-3}$ [g/mol]
1	(M2) ₁₃₉	11	13	14	1.0	-	14
2	(M3) ₅₂	6	4	5	1.4	-	7
2	(M4) ₁₁₀	6	9	11	1.2	-	13
3	(M2) ₁₃₉ (M4) ₅₂	20	15	19	1.3	20	35
4	(M4) ₁₁₀ (M2) ₅₂	18	9	13	1.4	17	18
5	(M4) ₁₁₀ (M3) ₇₀	22	9	15	1.6	22	28
6	(M2) ₁₃₉ (M4) ₅₂ (M3) ₂₈	29	12	20	1.7	23	- ^e
7	(M4) ₁₁₀ (M2) ₅₂ (M3) ₆₉	27	9	15	1.7	26	- ^e
8	(M4) ₁₁₀ (M3) ₇₀ (M2) ₆₄	26	9	16	1.7	28	- ^e

^a theoretical molar mass based on the obtained yield assuming 100% end-group functionalization (cf. equation 4.1) ^b PS-equivalent molar mass and PDI according to SEC (eluent: 0.05 M LiBr/N-MP at 25°C) ^c M_n determined from the averaged compositional data according to ^1H NMR spectroscopy, assuming that $M_n(\text{vis})$ of the first block is preserved in the block copolymers ^d calculated by end-group analysis of visible band (absorption band of **CTA1** at $\lambda_{\text{max}} = 499 \text{ nm}$, $\epsilon = 113 \text{ L mol}^{-1} \text{ cm}^{-1}$ in THF) ^e many end-group lost, analysis not conclusive.

Size exclusion chromatography (SEC) was employed for the characterization of the synthesized polymers in order to verify the controlled character of the RAFT polymerizations and to prove the successful formation of block copolymers. Moreover, SEC is an indispensable tool to detect homopolymer or block copolymer impurities. Although the acrylamide-based block copolymers are fully water-soluble at room temperature, aqueous SEC (TSK gel columns from Tosoh Bioscience with 0.2 M Na₂SO₄ + 1 wt% CH₃COOH as eluent) was not conclusive, as the polymers interacted strongly with the column material leading to complete retention on the SEC column. The SEC analysis of the polyacrylamides was therefore carried out at 25°C using 0.05 M LiBr/*N*-methyl pyrrolidone as the eluent. The employed SEC system used only concentration sensitive detectors (RI and UV) and was calibrated with PS standards. Consequently, the determined molar masses are not true, but PS-equivalent molar masses. Figure 4.4 depicts the SEC elugrams for the two precursor homopolymers.

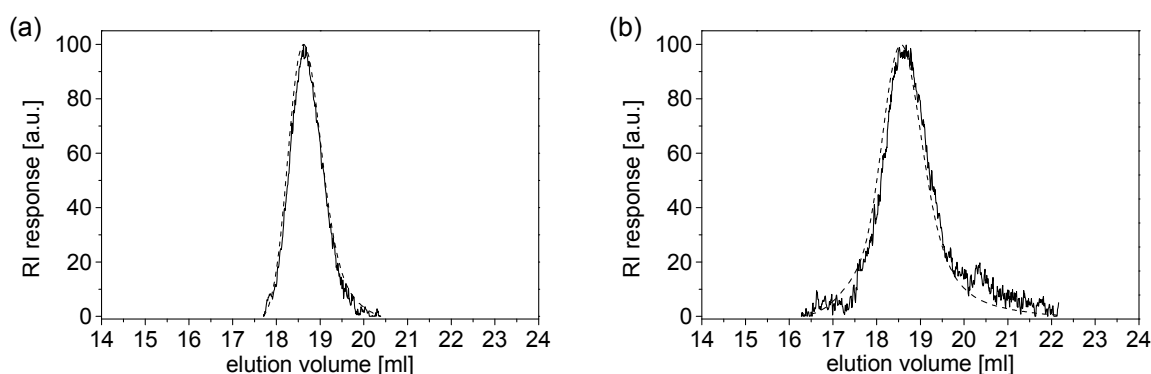


Figure 4.4 SEC elugrams of macroCTAs: (a) **(M2)**₁₃₉ and (b) **(M4)**₁₁₀ according to RI (dashed line) and UV (solid line) detection. Eluent: *N*-methyl pyrrolidone (0.05 M LiBr).

The UV detection at 270 nm identifies residual intensity of the thiocarbonyl absorption ($\lambda_{\text{max}} \sim 300$ nm). The SEC traces according to RI and UV detection superpose and thus, prove the homogenous distribution of the thiocarbonyl end-group throughout the molar mass distribution. Moreover, both homopolymer peaks are narrow and nearly symmetrical. The theoretical molar mass and the number-average molar masses determined by SEC and vis-spectroscopy agree well for polymer **(M2)**₁₃₉ (cf. Table 4.1) and evidence a high degree of polymerization control and end-group functionalization. For polymer **(M4)**₁₁₀ the number-average molar mass M_n determined by SEC is lower than the value according to end-group analysis by vis-spectroscopy. Either, some end-groups were already lost during polymerization. Or, PS is less suited as calibration standard for **polyM4**. Additionally, interactions of the polymer with the stationary phase might cause a shift of the SEC trace to higher elution volumes and thus, to apparently lower molar masses.

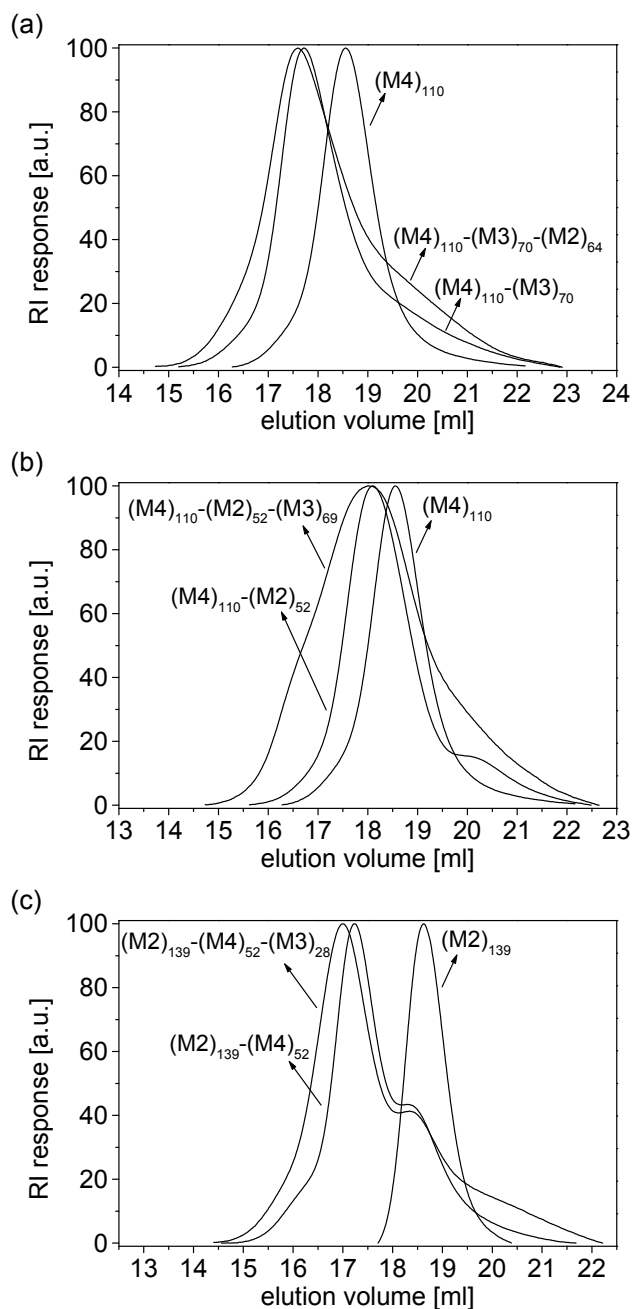


Figure 4.5 SEC elugrams of acrylamide-based ABC triblock copolymers and their respective precursors according to RI response (eluent: 0.05 M LiBr in *N*-methyl pyrrolidone): (a) $(\mathbf{M4})_{110}\text{-}(\mathbf{M3})_{70}\text{-}(\mathbf{M2})_{64}$ (b) $(\mathbf{M4})_{110}\text{-}(\mathbf{M2})_{52}\text{-}(\mathbf{M3})_{69}$ (c) $(\mathbf{M2})_{139}\text{-}(\mathbf{M4})_{52}\text{-}(\mathbf{M3})_{28}$.

That homopolymer or block copolymer impurities are produced to a low extent is an inherent feature of block copolymerizations by RAFT. In order to detect such impurities, the synthesized di- and triblock copolymers were analyzed by SEC under the same conditions as the homopolymers. The respective elugrams are depicted in Figure 4.5, and for a better comparison the traces of the precursor polymers are included in the presentation. For polymers $(\mathbf{M2})_{139}\text{-}(\mathbf{M4})_{52}$ and $(\mathbf{M2})_{139}\text{-}(\mathbf{M4})_{52}\text{-}(\mathbf{M3})_{28}$ the position of the shoulder is indicative for a small amount of **polyM2** without RAFT active chain ends. Being somewhat in contradiction to the high degree of end-group functionalization found before for $(\mathbf{M2})_{139}$ (see discussion above) this result can only be explained by a loss of end-groups during the second

polymerization step. This homopolymer impurity could not be separated by dialysis or precipitation due to its high molar mass.

Compared to the precursor diblock and homopolymers, the triblock copolymers generally showed broader molar mass distributions with pronounced tailings on the low molar mass side of the elugram. Such a tailing of the SEC trace is indicative for interactions of the analyte polymer with the stationary phase, but could also be the result of oligomeric impurities, that were formed in the initial stage of block copolymerization. In order to test this hypothesis, the triblock copolymer samples were dialyzed for several days (nominal molar mass cut-off: 4000-6000 D). As dialysis did not change the composition of the polymers according to ^1H NMR, the tailing in the SEC trace is attributed to interactions with the column material. Additionally, SEC analysis of the particular block polymers might be troubled by the potential association of the blocks due to hydrogen bonding, since **polyM3** and **polyM2** are hydrogen bond acceptors while **polyM4** is a hydrogen bond donor. Although SEC analysis of the acrylamide-based triblock copolymers is connected with difficulties, the obtained elugrams appear quite well-behaved and prove the successful formation of ABC triblock copolymers.

Summary

The monomers that were employed for the synthesis of thermoresponsive ABC triblock copolymers were all *N*-substituted acrylamides. Thus, their propagating radicals were expected to show similar reactivities toward the employed dithiobenzoate CTA and more importantly, to exhibit comparable fragmentation rates in the pre-equilibria of RAFT block copolymerization. Accordingly, the polymerizations proceeded smoothly for any block sequence. Still, polymerization rates of **M2**, **M3** and **M4** differ and as conversions had to be kept low to minimize the loss of RAFT active end-groups, it was not possible to prepare triblock copolymers with identical compositions. Still, the degrees of polymerization are comparable for the respective blocks in the triblock copolymers, and thus should allow for meaningful comparisons in studying the thermoresponsive self-assembly.

4.3. Self-assembly of double-thermoreponsive polymers in water

The self-assembly of the synthesized double thermoresponsive triblock copolymers in aqueous solution was studied to address the following questions:

- (i) Do the phase transitions of both thermoresponsive blocks take place as anticipated, and are they resolved from each other?
- (ii) How are the phase transition temperatures of the individual blocks influenced by the other attached blocks?
- (iii) Do the two phase transitions lead to a stepwise change of the aggregate size?
- (iv) How is the thermoresponsive self-assembly influenced by the block sequence?
- (v) To what extent is the thermoresponsive self-assembly subject to kinetics?

The homopolymers, diblock copolymers as well as the ternary triblock copolymers of **M2**, **M3**, and **M4** are hydrophilic at ambient temperature. Thus, they form clear solutions upon dissolution in water. DLS measurements of dilute solutions (1.0 g/L) showed only the presence of particles with hydrodynamic diameters (D_h) below 10 nm which are interpreted as molecularly dissolved polymer coils. Upon heating, the two thermoresponsive blocks undergo a phase transition from hydrophilic to hydrophobic at different temperatures. The switching of the polymer block with the lower LCST triggers the self-assembly into micellar aggregates. Upon further heating, the switching of the second thermoresponsive block changes the hydrophilic-hydrophobic balance of the triblock copolymers with an anticipated change of particle size or shape. The association process is accompanied by a more or less intense clouding depending on the size and distribution of the formed aggregates. The self-assembly of the double-thermoreponsive triblock copolymers in aqueous solution was studied by turbidimetry, by ^1H NMR spectroscopy and by dynamic light scattering. Turbidimetry is sensitive to macroscopic phase separation occurring, while the signal intensities in ^1H NMR spectroscopy are influenced by the extent of solvation of the polymer chains and their molecular mobility. Thus, ^1H NMR provides a straightforward, qualitative picture for the coil-to-globule transition in D_2O , as the proton signals of desolvated and associated blocks become strongly attenuated or even vanish, whereas the signals of the water-soluble block persist. Changes in the amphiphilic character of the block copolymers should translate in changes of their hydrodynamic diameters as a consequence of self-assembly. Thus, the thermoresponsive behavior was studied by dynamic light scattering.

4.3.1. Turbidimetric analysis

The phase transition of thermoresponsive polymers in water can be conveniently followed by monitoring the changes of transmittance vs. temperature. Turbidimetric measurements of aqueous solutions of the synthesized block copolymers were carried out with heating and cooling rates of 1.0°C/min. As has been shortly discussed in chapter 4.1, poly(*N*-acryloyl pyrrolidine) (**polyM3**) is rarely utilized as thermoresponsive polymer. The turbidimetric curve of a homopolymer sample that was previously prepared by RAFT polymerization employing cumyl dithiobenzoate as the CTA (cf. chapter 7.4.2) is depicted in Figure 4.6a. Additionally, the sensitivity of its clouding temperature to added salt was studied. The results of a preliminary test with NaCl are presented in Figure 4.6b.

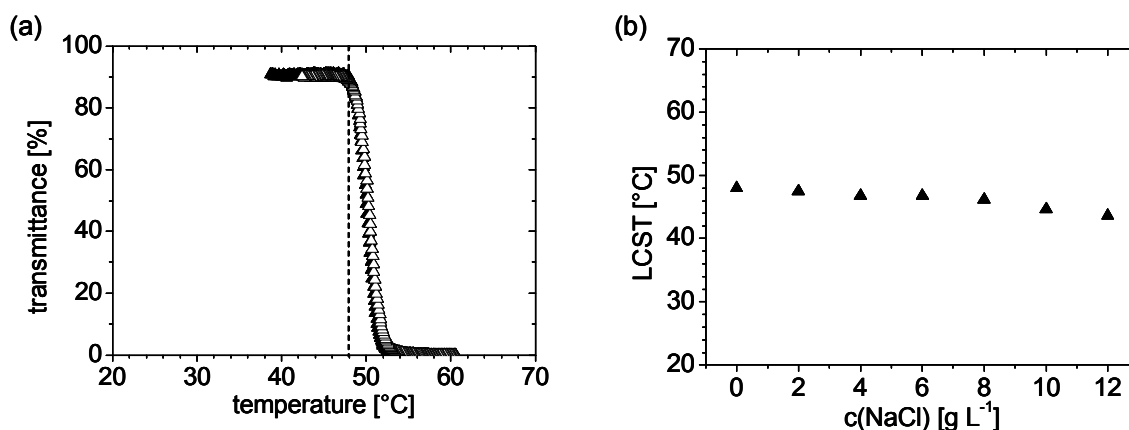


Figure 4.6 Thermoresponsive behavior of polymer (**M3**)₅₂ in water: (a) Temperature dependent transmittance of an aqueous solution (0.3 wt%) at 670 nm. Closed triangles: heating (1.0°C/min); open triangles: cooling (1.0°C/min) (b) Clouding temperatures for aqueous solutions of (**M3**)₅₂ (0.3 wt%) as a function of NaCl concentration.

The clouding of the aqueous solution of (**M3**)₅₂ took place in a narrow temperature interval and with a very small hysteresis between the heating and cooling run. Such a behavior is expected for a homopolymer of narrow molar mass distribution (or of low molar mass dependence of the cloud point), and is similar to the behavior of the well-established thermoresponsive **polyM4**. The hydrophobic cumyl end-group probably lowers the cloud point of (**M3**)₅₂ to 48°C. Such end-group effects on the LCST are also known for **polyM4** and are especially observed for polymers of low to moderate molar mass.^{228, 229}

The evolution of cloud points with increasing concentrations of NaCl shows that **polyM3** is similar to **polyM4** relatively insensitive to added salt. In advance to the turbidimetric measurements of triblock copolymers, it was interesting to learn which behavior a system shows whose double-thermoreponsiveness is purely additive. A physical mixture of the three homopolymers **polyM2**, **polyM3** and **polyM4** was studied by turbidimetry as in dilute solution (0.1 wt%), their individual phase transitions were expected to show minimal mutual interactions. The obtained turbidimetric curve is shown in Figure 4.7. The cloud point at 33°C is attributed to the phase transition of (**M4**)₁₁₀, which appeared to be hardly affected by the presence of the other two homopolymers. The second inflection point in the turbidimetric curve upon heating is attributed to the phase transition of (**M3**)₅₂. Surprisingly, the cloud point is markedly increased compared to the pure (**M3**)₅₂ solution. Although the reason for this shift of clouding temperature is not clear yet, the result indicates that already for a mixture of the three

homopolymers mutual interactions are possible. Hence, such effects can influence the behavior of the triblock copolymers, too, and might complicate the interpretation of the results. The direct comparison of single and double-thermoreponsive block copolymers can help to understand the observed behavior. Thus, the precursor diblock copolymers were included in this turbidimetric study (Fig. 4.8).

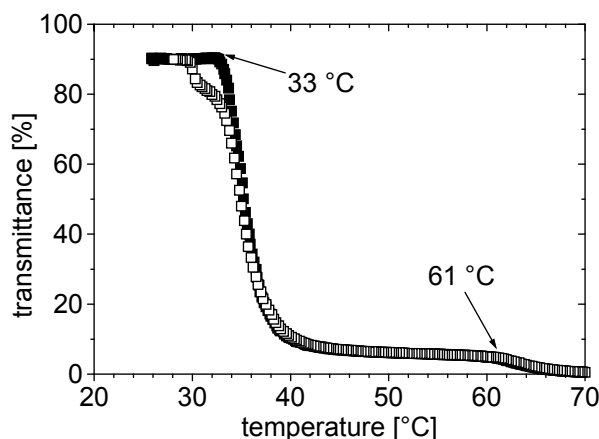


Figure 4.7 Thermoresponsive behavior of a 0.1 wt% aqueous solution of a 1:1:1 (by weight) mixture of $(\mathbf{M4})_{110}$, $(\mathbf{M3})_{52}$ and $(\mathbf{M2})_{139}$ as followed by turbidimetry. Solid squares: heating (1.0°C/min); open squares: cooling (1.0°C/min).

The onset temperatures for the clouding of diblock copolymers solutions is shifted to higher temperatures with increasing incorporation of monomer **M2**. Polymers $(\mathbf{M2})_{139}\text{-}(\mathbf{M4})_{52}$ and $(\mathbf{M4})_{110}\text{-}(\mathbf{M2})_{52}$ are composed of the same polymer blocks, yet differ in their ratios of **M2** to **M4**. Polymer $(\mathbf{M2})_{139}\text{-}(\mathbf{M4})_{52}$ with a large hydrophilic-hydrophobic balance above the LCST of **polyM4** should self-assemble into star-like micelles upon heating, while $(\mathbf{M4})_{110}\text{-}(\mathbf{M2})_{52}$ is expected to form crew-cut micellar aggregates. Indeed, the aqueous solution of $(\mathbf{M4})_{110}\text{-}(\mathbf{M2})_{52}$ became more cloudy than the solution of $(\mathbf{M2})_{139}\text{-}(\mathbf{M4})_{52}$, indicating the formation of larger aggregates. Furthermore, a local minimum was observed in the transmittance curve of $(\mathbf{M4})_{110}\text{-}(\mathbf{M2})_{52}$ upon heating which was not detected in the cooling run. This clouding-clearing effect was explained before by different temperatures for the onset of (micro)phase separation of a polymer block, which causes the clouding, and for a sufficient degree of dehydration, to produce strongly collapsed chains.^{251, 252}

The third diblock copolymer in this study, $(\mathbf{M4})_{110}\text{-}(\mathbf{M3})_{70}$, should already be a double thermoresponsive block copolymer. However, only one cloud-point can be distinguished in the turbidimetric curve. By attaching **polyM3** to **polyM4**, the cloud point was slightly shifted to higher temperatures and the clouding took place over a wider range (35-46°C). Despite comparable degrees of polymerization for both block copolymers, the thermoresponsive behavior of $(\mathbf{M4})_{110}\text{-}(\mathbf{M3})_{70}$ differs from that of $(\mathbf{M4})_{110}\text{-}(\mathbf{M2})_{52}$. Upon heating, the solution of $(\mathbf{M4})_{110}\text{-}(\mathbf{M3})_{70}$ became very turbid and transmittance dropped to 0%. Either, the aggregates which are stabilized by the **polyM3** block at intermediate temperature are extremely large and scatter the light so strongly that the phase transition of the **polyM3** block is concealed. Or, the **polyM3** block collapses before the coil-to-globule transition of the **polyM4** block is completed, and thus the resolution between both transitions is lost.

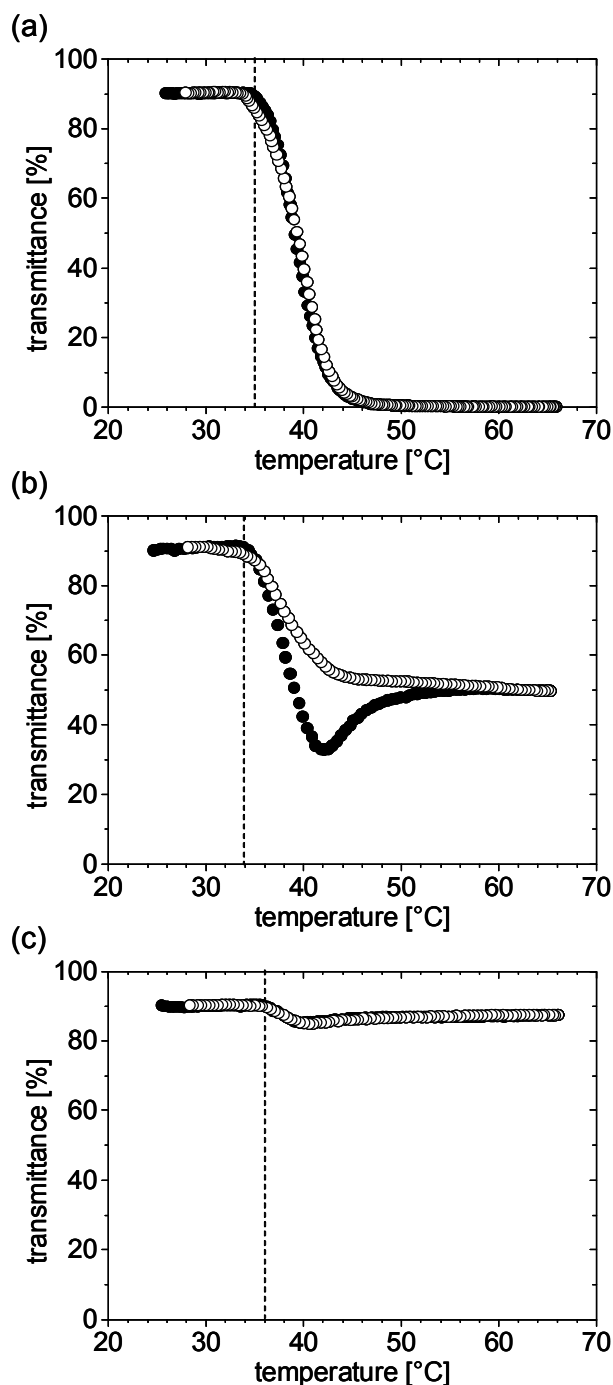


Figure 4.8 Thermoresponsive behavior of 0.1 wt% aqueous solutions of diblock copolymers as followed by turbidimetry: (a) $(\mathbf{M4})_{110}\text{-}(\mathbf{M3})_{70}$ (b) $(\mathbf{M4})_{110}\text{-}(\mathbf{M2})_{52}$ (c) $(\mathbf{M2})_{139}\text{-}(\mathbf{M4})_{52}$. Closed circles: heating ($1.0^\circ\text{C}/\text{min}$); open circles: cooling ($1.0^\circ\text{C}/\text{min}$).

Compared to their diblock precursor polymers, the onset temperatures for the clouding of the triblock copolymer solutions were slightly shifted to higher temperatures (Fig. 4.9). This shift is attributed to a higher hydrophilic-hydrophobic balance in the triblock copolymers. A two-step decrease of transmittance is indeed observed for triblock copolymer $(\mathbf{M4})_{110}\text{-}(\mathbf{M3})_{70}\text{-}(\mathbf{M2})_{64}$, although it was not possible to distinguish between both phase transitions in the corresponding precursor diblock copolymer $(\mathbf{M4})_{110}\text{-}(\mathbf{M3})_{70}$.

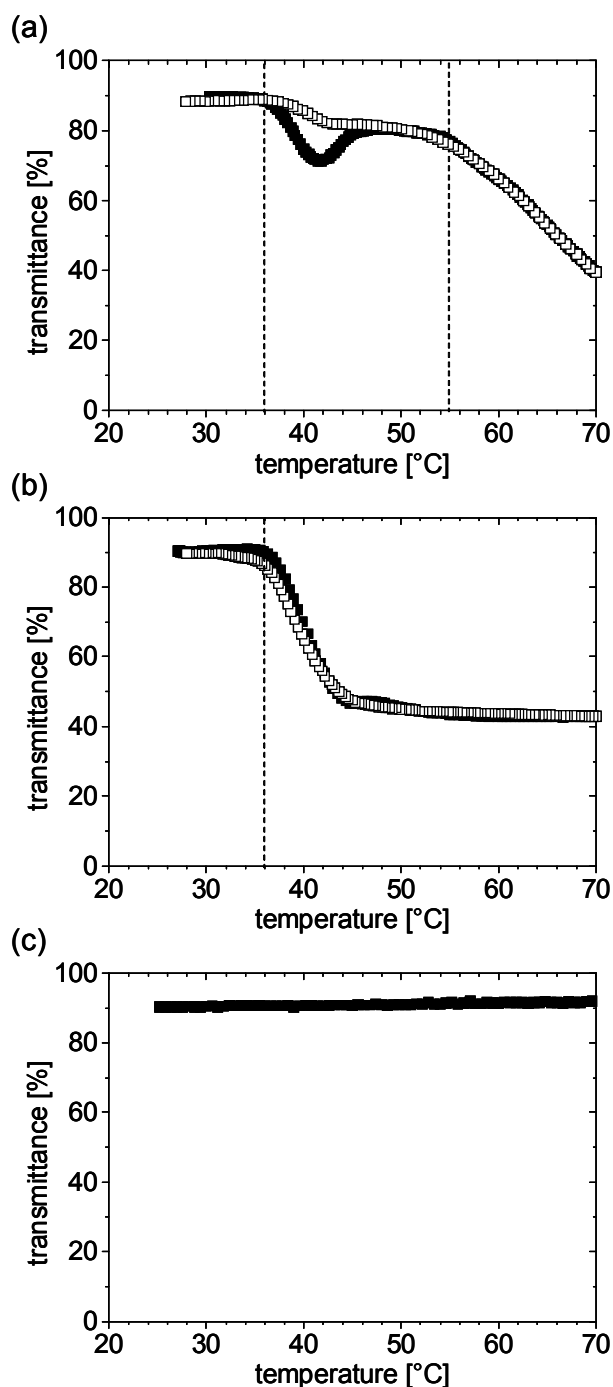


Figure 4.9 Thermoresponsive behavior of 0.1 wt% aqueous solutions of triblock copolymers as followed by turbidimetry: (a) $(\mathbf{M4})_{110}\text{-}(\mathbf{M3})_{70}\text{-}(\mathbf{M2})_{64}$ (b) $(\mathbf{M4})_{110}\text{-}(\mathbf{M2})_{52}\text{-}(\mathbf{M3})_{69}$ (c) $(\mathbf{M2})_{139}\text{-}(\mathbf{M4})_{52}\text{-}(\mathbf{M3})_{28}$. Closed squares: heating (1.0°C/min), open squares: cooling (1.0°C/min).

In the heating run, the transmittance curve passed through a local minimum at $\sim 42^\circ\text{C}$ which did not occur in the cooling run. After passing the minimum, the transmittance stabilized at $\sim 80\%$ before it dropped again at 55°C . The second cloud point - which is attributed to the phase transition of the **polyM3** block - is raised compared to $\sim 50^\circ\text{C}$ of the homopolymer **polyM3** as it is attached to the hydrophilic **polyM2** block.

Only one cloud point can be identified in the turbidimetric curve of polymer $(\mathbf{M4})_{110}\text{-}(\mathbf{M2})_{52}\text{-}(\mathbf{M3})_{69}$, i.e. the polymer in which the two thermoresponsive blocks are separated by the permanently hydrophilic one. The marked clouding-clearing effect that was observed in the heating run for the precursor polymer is not found for the triblock copolymer. For polymer $(\mathbf{M2})_{139}\text{-}(\mathbf{M4})_{52}\text{-}(\mathbf{M3})_{28}$ the turbidity curve shows no decrease of transmittance up to 90°C. That means either, that for this particular block sequence and composition the phase transitions of **polyM4** and **polyM3** are subdued. However, this seems not probable. Or, the method of turbidimetry misses here completely the phase separation and subsequent self-assembly of the polymer upon raising the temperature due to the formation of very small particles.

As in the case of homopolymers, a physical mixture of $(\mathbf{M2})_{139}\text{-}(\mathbf{M4})_{52}$ and $(\mathbf{M3})_{52}$ (1:1 by weight) was studied by turbidimetry (Fig. 4.10). A stepwise decrease of transmittance is observed upon heating with a small hysteresis. It is noteworthy, that the clouding temperature of the thermoresponsive block in $(\mathbf{M2})_{139}\text{-}(\mathbf{M4})_{52}$ is raised in presence of $(\mathbf{M3})_{52}$ from 36°C to 38°C (cf. Fig. 4.8c). Furthermore, the phase transition and subsequent self-assembly of $(\mathbf{M2})_{139}\text{-}(\mathbf{M4})_{52}$ causes a much stronger decrease of transmittance in the mixture than in the solution of the diblock copolymer alone. The second decrease of transmittance which is attributed to the phase separation of the $(\mathbf{M3})_{52}$ homopolymer occurs at 67°C which is remarkably higher than the clouding temperature of the pure homopolymer in solution.

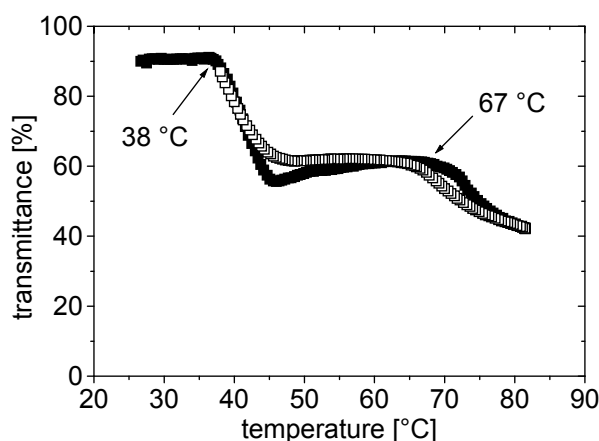


Figure 4.10 Thermoresponsive behavior of a 0.1 wt% aqueous solution of a 1:1 (by weight) mixture of $(\mathbf{M2})_{139}\text{-}(\mathbf{M4})_{52}$ and $(\mathbf{M3})_{52}$ as followed by turbidimetry. Closed squares: heating (1.0°C/min), open squares: cooling (1.0°C/min).

At the moment, such findings can only be explained by mutual interactions between the diblock copolymer and the homopolymer, whatever nature they are. Furthermore, it is difficult to deduce from the macroscopic behavior - as studied by turbidimetry - on the processes at the mesoscopic or molecular level. Thus, in the next step the thermoresponsive behavior of triblock copolymers was studied by temperature-dependent ^1H NMR spectroscopy which perceives the coil-to-globule transition on the molecular scale.

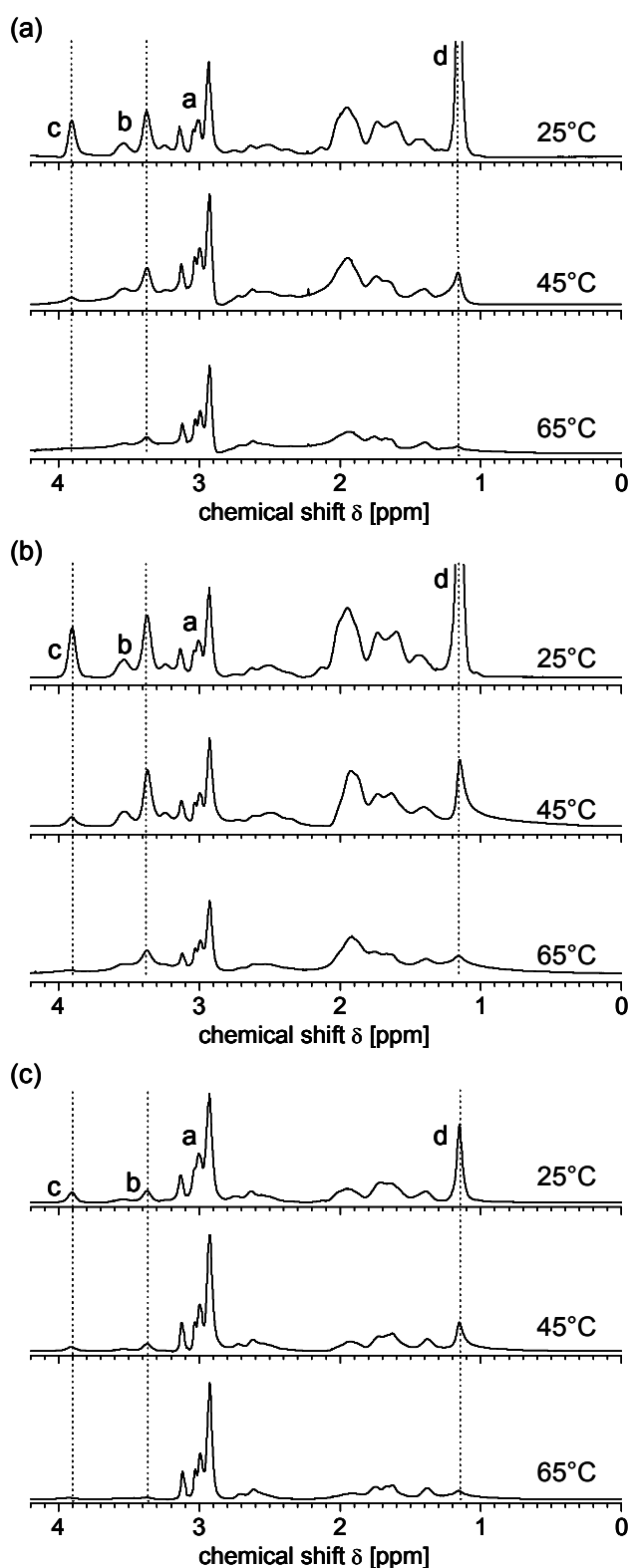
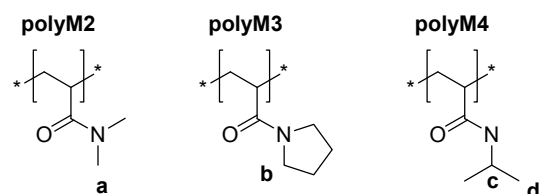
4.3.2. Study by ^1H NMR spectroscopy

Figure 4.11 Temperature dependent ^1H NMR spectra of double-thermoreponsive triblock copolymers in D_2O at 25°C, 45°C, and 65°C. (a) $(\text{M4})_{110}\text{-(M3)}_{70}\text{-(M2)}_{64}$ (b) $(\text{M4})_{110}\text{-(M2)}_{52}\text{-(M3)}_{69}$ (c) $(\text{M2})_{139}\text{-(M4)}_{52}\text{-(M3)}_{28}$.

Due to the reduced mobility of the collapsed thermoresponsive blocks, the switching from double-hydrophilic to amphiphilic block copolymers can be followed by monitoring the variations in relative peak intensities with temperature by ^1H NMR spectroscopy. Characteristic signals of **polyM2** at ca. 3.0 ppm (indicated "a"), of **polyM3** at ca. 3.5 ppm (indicated "b") as well as of **polyM4** at ca. 3.8 ppm (indicated "c") and 1.0 ppm (indicated "d") were used for this purpose:



As was mentioned before, ^1H NMR spectroscopy provides a qualitative picture of the phase transition on the molecular scale. Although turbidimetry shows a sharp decrease of transmittance for homopolymers, the phase transition on the molecular level is expected to be a gradual process. The coil-to-globule transition of thermoresponsive polymers is accompanied by dehydration and the formation of a dense hydrophobic structure. Due to this rigid environment the proton signals of the collapsed blocks become strongly broadened or even vanish completely.

The ^1H NMR spectra of the three triblock copolymers at 25°C, 45°C and 65°C are depicted in Figure 4.11. At 25°C all polymer blocks are molecularly dissolved. At 45°C, homopolymer **polyM3** is not phase-separated yet, while the coil-to-globule transition of the **polyM4** homopolymer is

completed according to the results of turbidimetry. The third measurement was carried out at 65°C as this temperature is well above the phase transition temperatures of both thermoresponsive homopolymers. The proton signals of the permanently hydrophilic **polyM2** block are assumed to be unaffected by higher temperatures and were used as internal reference.

The discussion is again started with triblock copolymer **(M4)₁₁₀-(M3)₇₀-(M2)₆₄**. Although the proton signals of **polyM4** are strongly decreased at 45°C, some intensity is retained. Noteworthy, the proton signals of **polyM3** are declined, too, although this temperature is below the cloud-point of the **polyM3** homopolymer. At 65°C, the signal of the methine-protons in the **polyM4** side chains cannot be detected anymore and only a very weak signal of the methyl protons in the side chain persists. The proton signals of **polyM3** are remarkably attenuated in comparison to 25°C but also retain some intensity.

For polymer **(M4)₁₁₀-(M2)₅₂-(M3)₆₉** the situation at 45°C is as follows: The proton signals of **polyM4** are strongly reduced but some intensity persists as was seen before. In contrast to the sample mentioned before, the intensity of **polyM3** signals is the same at 45°C as at 25°C. At 65°C the signals of the **polyM3** block are broadened. Obviously, the phase transitions of the two thermo-responsive blocks take place independently for this particular block sequence as they are separated by the permanently hydrophilic block.

For polymer **(M2)₁₃₉-(M4)₅₂-(M3)₂₈** a similar picture as for the first example is seen, i.e. the signals of **polyM3** are already broadened at 45°C while the protons of the **polyM4** block are not in a fully rigid environment. Compared to the signal intensity at 25°C and 45°C, the intensity of the **polyM3** block is further decreased at 65°C.

Although the ¹H NMR spectra were recorded for three different temperatures only, they provided valuable information about the state of solubility on the molecular level. ¹H NMR spectroscopy revealed that for all thermoresponsive blocks the respective phase transitions take place as expected, although turbidimetry missed such events in certain cases (see discussion above).

4.3.3. Study of the double-thermoreponsive self-assembly by DLS

The self-assembly of double thermoresponsive triblock copolymers can be studied by monitoring the changes of the hydrodynamic diameter (D_h) of aggregates using dynamic light scattering. In the heating procedure applied, aqueous solutions were heated in steps of 1.0°C and equilibrated for 10 min prior to each measurement. The evolution of particle sizes with temperature is presented in Figure 4.12. The given hydrodynamic diameters are Z-averaged values based on the intensity distribution. While the Z-average provides reliable values for a monodisperse sample, the amount of larger particles is overestimated for a multimodal and/or polydisperse distribution of particles. Nonetheless, this presentation is useful to display the changes of particle size upon changes of temperature due to the increased sensitivity of the Z-average towards the formation of larger aggregates.

The thermoresponsive self-assembly of triblock copolymers in aqueous solution is indicated by the sudden increase of particle sizes (Fig. 4.12). For all studied triblock copolymers the onset temperatures of self-assembly were shifted to higher values (36-38°C) compared to the LCST of the **polyM4** homopolymer (32°C). After passing a maximum of particle size upon heating, the aggregate sizes dwindled to a relatively stable state. The abrupt increase of particle size – followed by a strong decrease – correlates with the clouding-clearing effect observed by turbidimetry. Such a behavior was explained by Yusa et al.²⁵³ either to a decrease of aggregation number upon heating, or to the shrinking of polymeric micelles due to increasing dehydration. When phase separation starts upon heating, it appears that the initially formed aggregates are large but loose, as the solvent quality is relatively high yet and the **polyM4** chains in the core remain partially solvated. A similar situation is observed for classical amphiphilic block copolymers at the cmc, when the micellar core is highly swollen by the solvent.⁵ With increasing temperature the residual water content in the aggregates decreases and thus, smaller but more compact aggregates form. The occurrence of large particles at the initial stage of self-assembly was observed before for thermoresponsive systems²⁵⁴ and appears to be a common effect independent from the block copolymer composition or architecture.

Heating of aqueous solutions above the second phase transition temperature decreases the hydrophilic-hydrophobic balance of the copolymers and might translate into changes of the size or shape of aggregates which are detectable by DLS. Depending on the respective block sequence different morphologies result for the polymeric amphiphiles (cf. Figure 4.1). For block copolymer **(M4)₁₁₀-(M3)₇₀-(M2)₆₄** - where the LCST of the constituting blocks increases along the chain - the phase transition of the **polyM3** block decreases the hydrophilic-hydrophobic balance, but the amphiphile's morphology remains linear. If spherical core-shell-corona micelles with a solvated shell of **polyM3** were formed upon the first phase transition, the second phase transition would cause the **polyM3** chains to collapse upon the **polyM4** core. Consequently, the particle size is expected to decrease as far as the aggregation number remains constant. In contrast to this theoretical considerations, the DLS measurement revealed an increase of particle sizes for copolymer **(M4)₁₁₀-(M3)₇₀-(M2)₆₄** at 53°C (Fig. 4.12a), which might be explained by clustering of micelles or by the rearrangement into larger micellar aggregates. As the temperature at which this change of particle size happens is close to the LCST of the homopolymer of

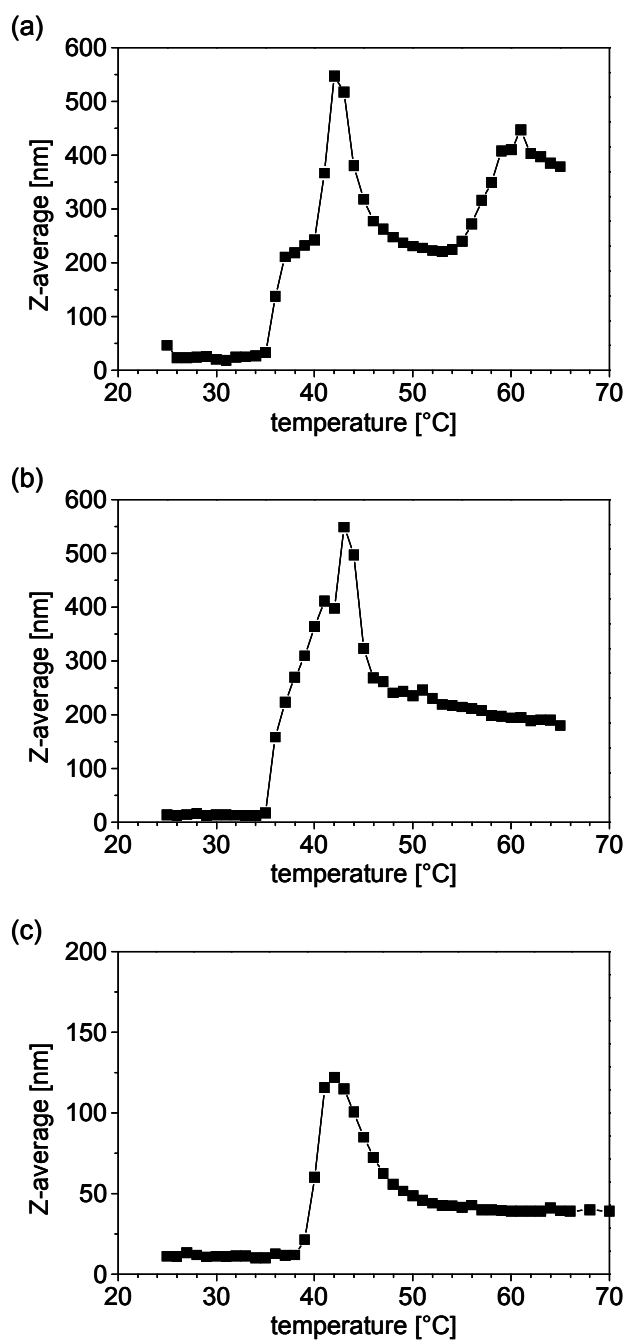


Figure 4.12 Temperature dependent evolution of particle sizes (Z-average) of 0.1 wt% aqueous solutions of ternary block copolymers as followed by DLS: (a) $(\mathbf{M4})_{110}\text{-}(\mathbf{M3})_{70}\text{-}(\mathbf{M2})_{64}$ (b) $(\mathbf{M4})_{110}\text{-}(\mathbf{M2})_{52}\text{-}(\mathbf{M3})_{69}$ (c) $(\mathbf{M2})_{139}\text{-}(\mathbf{M4})_{52}\text{-}(\mathbf{M3})_{28}$.

M3, it is reasonable to attribute this increase of particle size to the coil-to-globule transition of the **polyM3** block.

Heating above the phase transition temperature of **polyM3** modifies the morphology of copolymer $(\mathbf{M4})_{110}\text{-}(\mathbf{M2})_{52}\text{-}(\mathbf{M3})_{69}$ from a linear amphiphile to an amphiphile with two collapsed, hydrophobic end-blocks (cf. Fig. 4.1b). This amphiphile architecture can self-assemble into a variety of aggregates: If the collapsed blocks are compatible with each other and the back-folding of the hydrophilic block is entropically allowed, flower-like micelles with mixed cores may be formed (Fig. 4.13a). Alternatively, the collapsed end-blocks can be incorporated into separate micellar cores leading to clustered micelles

(Fig. 4.13b). Above a certain polymer concentration the formation of interconnected micelles leads to gelation, as has been observed before for multi-thermoreponsive polyvinyl ethers.²⁵⁵ As a third possibility, the collapsed chains might not be part of a micellar core, but exist as dangling chain ends (Fig. 4.13c).

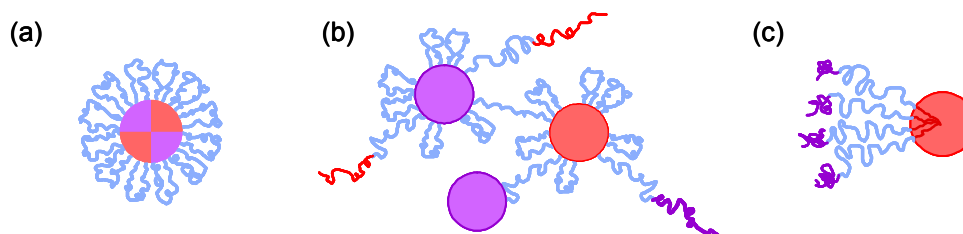


Figure 4.13 Chain topologies of triblock copolymers with associating end blocks: (a) flower-like micelle (b) interconnected micelles (c) dangling chain ends.

According to the Z-averaged D_h presented in Figure 4.12b, the aggregates of $(\mathbf{M4})_{110}$ - $(\mathbf{M2})_{52}$ - $(\mathbf{M3})_{69}$ continue to shrink slowly upon heating above 45°C. Here, the Z-averaged value is somewhat misleading as the size distribution became bimodal above this temperature, comprising small ($D_h \sim 40$ nm) and large ($D_h \sim 400$ nm) aggregates (cf. Fig. 4.14). With increasing temperature the fraction of small particles grows at the expense of large aggregates. It is difficult to decide whether the appearance of this bimodality is a result of the phase transition of the **polyM3** block. On one hand, the second phase transition alters the hydrophilic-hydrophobic balance and might trigger a reorganization of micellar aggregates. On the other hand, the appearance of the second population of aggregates might be a mere result of slow kinetics. Although the temperature dependent ^1H NMR measurements clearly disclosed that the **polyM3** block is collapsed at 65°C, neither turbidimetry nor DLS indicated explicitly the occurrence of a second thermally induced association process for this block copolymer.

In copolymer $(\mathbf{M2})_{139}$ - $(\mathbf{M4})_{52}$ - $(\mathbf{M3})_{28}$, the middle block exhibits the lower LCST. Upon heating above the first phase transition temperature a "bola-shaped" linear amphiphile with a high hydrophilic-hydrophobic balance forms (cf. Fig. 4.1c). The self-assembled particles are assumed to consist of a hydrophobic core of **polyM4** and a mixed corona of **polyM2** and **polyM3**. While neither visual inspection nor turbidimetry disclosed any clouding upon heating up to 90°C, DLS revealed the formation of small particles above 38°C. As for the other block copolymers, the size of the colloids passed through a maximum upon heating, here at about 45°C, before the aggregate's sizes stabilized above 50°C. Compared to the other block sequences, the architecture with the **polyM4** block in the middle exhibited the highest onset temperature for self-assembly. Similar observations regarding onset temperatures and particle sizes were made by Convertine et al.,²⁵⁴ who studied the thermoresponsive self-assembly of AB diblock copolymers in comparison to ABA triblock copolymers comprising **polyM2** and **polyM4** as A and B blocks, respectively. They found that critical micellization temperatures are higher and particle sizes are smaller for ABA triblock copolymers. Although the self-assembly of block copolymer $(\mathbf{M2})_{139}$ - $(\mathbf{M4})_{52}$ - $(\mathbf{M3})_{28}$ due to the phase transition of **polyM4** was clearly discernible by DLS, no indications for a change of particle size due to the phase transition of the **polyM3** block were found upon heating up to 70°C.

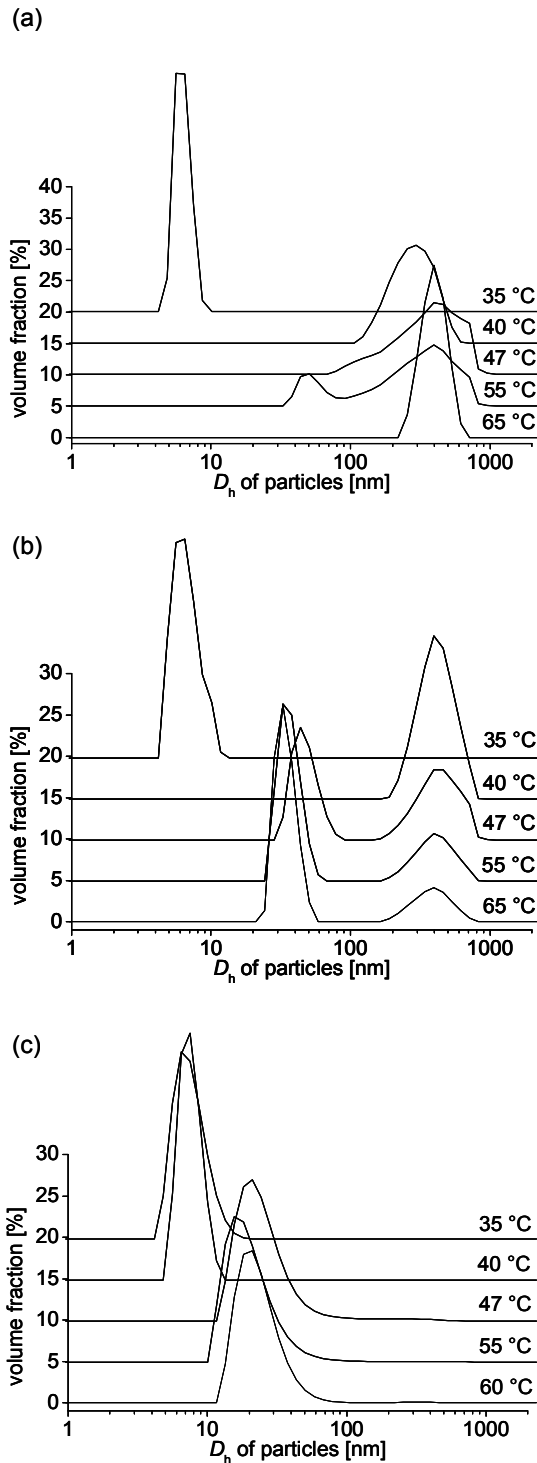


Figure 4.14 Evolution of particle size distributions for 0.1 wt% aqueous solutions of triblock copolymers according to the slow heating protocol: (a) $(M4)_{110}-(M3)_{70}-(M2)_{64}$ (b) $(M4)_{110}-(M2)_{52}-(M3)_{69}$ (c) $(M2)_{139}-(M4)_{52}-(M3)_{28}$.

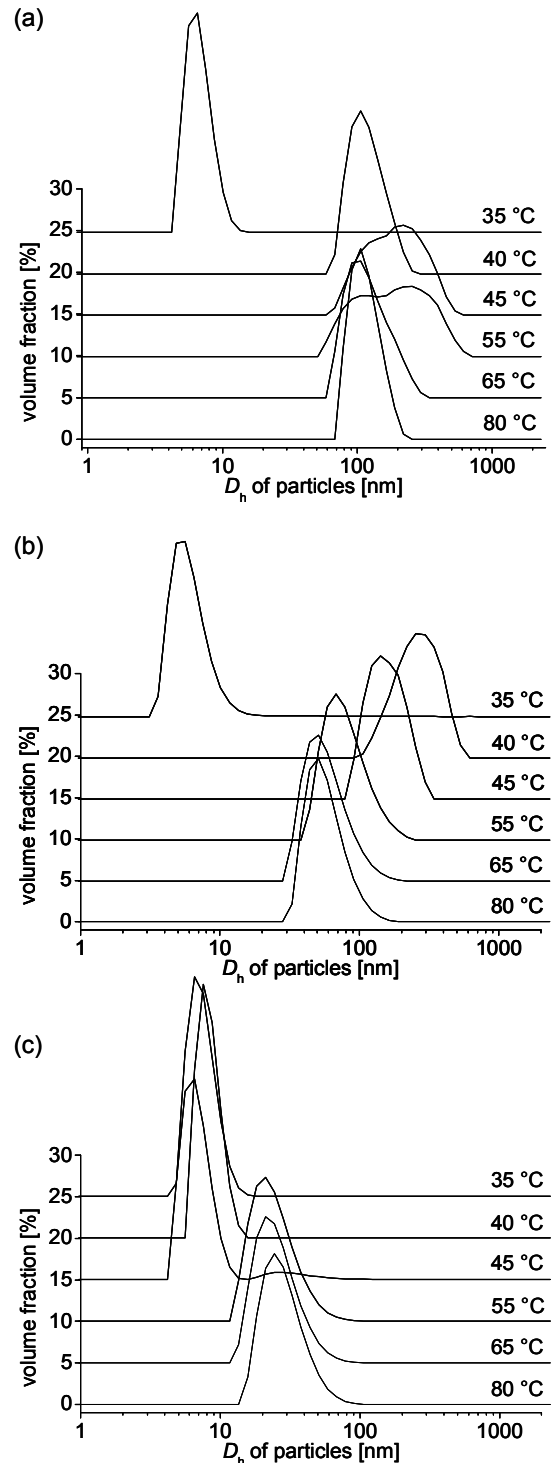


Figure 4.15 Evolution of particle size distributions for 0.1 wt% aqueous solutions of triblock copolymers according to the fast heating protocol: (a) $(M4)_{110}-(M3)_{70}-(M2)_{64}$ (b) $(M4)_{110}-(M2)_{52}-(M3)_{69}$ (c) $(M2)_{139}-(M4)_{52}-(M3)_{28}$.

Table 4.2 Dynamic light scattering analysis of 0.1 wt% aqueous solutions of double-thermoreponsive triblock copolymers prepared by the slow and fast heating protocol

Polymer	Temp. [°C]	Slow heating				Fast heating			
		Z-Avg	PD	$D_h(1)^a$	$D_h(2)^b$	Z-Avg	PD	$D_h(1)$	$D_h(2)$
		[nm]		[nm]	[nm]	[nm]		[nm]	[nm]
(M4)₁₁₀-(M3)₇₀-(M2)₆₄	25	47	0.51	7 (100)					
	35	33	1.00	6 (100)		15	0.74	7 (100)	
	40	242	0.12	292 (100)		127	0.04	123 (100)	
	45	318	0.31	499 (82)	97 (18)	186	0.16	228 (100)	
	47	263	0.26	389 (100)					
	55	240	0.25	365 (80)	56 (20)	167	0.22	272 (63)	103 (37)
	60	410	0.21	489 (100)					
	65	387	0.04	401 (100)		129	0.10	127 (100)	
	80					120	0.05	116 (100)	
(M4)₁₁₀-(M2)₅₂-(M3)₆₉	25	14	0.67	6					
	35	17	1.00	7		32	1.00	6 (99)	49 (1)
	40	364	0.10	425 (100)		225	0.11	267 (100)	
	45	323	0.27	55 (21)	464 (79)	156	0.07	162 (100)	
	47	261	0.34	48 (48)	444 (52)				
	55	214	0.55	37 (69)	418 (31)	93	0.11	81 (100)	
	60	194	0.61	35 (76)	414 (24)				
	65	180	0.64	35 (78)	395 (22)	73	0.12	60 (100)	
	80					70	0.10	59 (100)	
(M2)₁₃₉-(M4)₅₂-(M3)₂₈	25	11	0.44	8 (100)					
	35	10	0.40	8 (100)		14	0.59	8 (100)	
	40	60	0.76	8 (100)		46	1.00	8 (100)	
	45	85	0.55	9 (85)	31 (14)	45	0.43	7 (95)	39 (5)
	47	63	0.49	27 (98)					
	55	42	0.38	22 (100)		32	0.18	25 (100)	
	60	39	0.37	24 (100)					
	65	39	0.35	22 (100)		34	0.17	27 (100)	
	80					37	0.16	29 (100)	

^a hydrodynamic diameter (D_h) of micellar aggregates according to the volume distribution. 7 (100) means that 100% of particles (by volume) have a mean hydrodynamic diameter of 7 nm.

^b hydrodynamic diameter of a second population of aggregates.

The values of D_h given in Figure 4.12 are averaged values which provide no information about the particle size distribution. Figure 4.14 and Table 4.2 present the evolution of the aggregate sizes and distribution of the self-assembled triblock polymers for selected temperatures according to the volume distribution. At 25°C polymers are molecularly dissolved with hydrodynamic diameters of 6-8 nm. When the polymers start to self-assemble, the initially formed particles are except for **(M2)₁₃₉-(M4)₅₂-(M3)₂₈** very large (400-600 nm). With increasing temperature the particle size distribution becomes broad, or even

bimodal with a growing fraction of small particles (30-50 nm). In contrast, polymer $(\mathbf{M2})_{139}-(\mathbf{M4})_{52}-(\mathbf{M3})_{28}$ did not form very large aggregates at the initial state of self-assembly and the particles retain their original small size upon heating above the second LCST.

The interpretation of the results obtained from the temperature dependent DLS study is complicated by the possibility of marked kinetic effects: The size and distribution of aggregates may be strongly influenced by the applied heating rate as well as by ageing. Therefore, a fast heating protocol was applied, too (Fig. 4.15). In this protocol, polymer solutions were directly transferred from ambient temperature to a heating bath of the desired measuring temperature. The fast heating rate changed markedly the size and distribution of the formed aggregates. Generally, smaller aggregates with narrower size distributions - independent of the final temperature - were obtained (cf. Table 4.2). In particular, the fast heating protocol seemed to reduce the tendency to form very large aggregates at the initial stage of self-assembly.

Although the particle size distributions for polymer $(\mathbf{M4})_{110}-(\mathbf{M3})_{70}-(\mathbf{M2})_{64}$ became narrower in the fast heating protocol, a broadening was observed at 45°C and 55°C - similarly to the observations in the slow heating protocol. However, the effect was less pronounced and when the samples were heated immediately to 65°C and 80°C the particle size distribution was again narrow. In contrast to the slow heating rate, particle sizes decreased above 55°C for $(\mathbf{M4})_{110}-(\mathbf{M3})_{70}-(\mathbf{M2})_{64}$. Such a behavior is anticipated for the formation of core-shell-corona micelles, if the shell-forming block collapses upon heating and the original aggregation number is preserved.

For polymer $(\mathbf{M4})_{110}-(\mathbf{M2})_{52}-(\mathbf{M3})_{69}$ - with the permanently hydrophilic **polyM2** as central block - the particle size distributions were monomodal at all temperatures in the fast heating protocol. Although the aggregates, which had formed at intermediate temperatures (40-45°C), were very large (200-300 nm), they shrunk continuously with increasing final temperature. At 65°C and 80°C only small aggregates ($D_h = 60$ nm) were detected, although both thermoresponsive outer blocks are hydrophobic at these temperatures and the bridging between micellar cores would be possible (cf. Fig. 4.13b). While such a behavior would ultimately lead to gelation at high polymer concentrations, clustered micelles are assumed to form in dilute solution. Notwithstanding, the formed particles are small and their distribution is narrow which precludes multi-micellar aggregates. The ^1H NMR measurement at 65°C disclosed broadened **polyM3** signals, proving that the phase transition of the **polyM3** block took place as anticipated.

For copolymer $(\mathbf{M2})_{139}-(\mathbf{M4})_{52}-(\mathbf{M3})_{28}$ - comprising the block with the lowest LCST in the middle - no marked differences were found for the particle sizes obtained in the slow and fast heating protocol. For both heating rates, the polymer chains associated to form small micellar aggregates which were 20-30 nm in size. As the thermoresponsive blocks are rather short, they are possibly not subject to pronounced kinetic effects. Based on the size analysis by DLS, the second switching due to the phase transition of **polyM3** was neither in the slow nor in the fast heating protocol perceived. This observation might be a result of the particular polymer architecture and composition. Resulting from the first phase transition, the **polyM4** blocks associate to form the micellar core while the **polyM2** and **polyM3** blocks build a mixed corona. Upon further heating, the **polyM3** block collapses - as was seen by ^1H NMR - and is assumed to form a shell upon the **polyM4** core. Since the **polyM3** block is rather short, the formation of the shell should not affect the size of the micelle markedly.

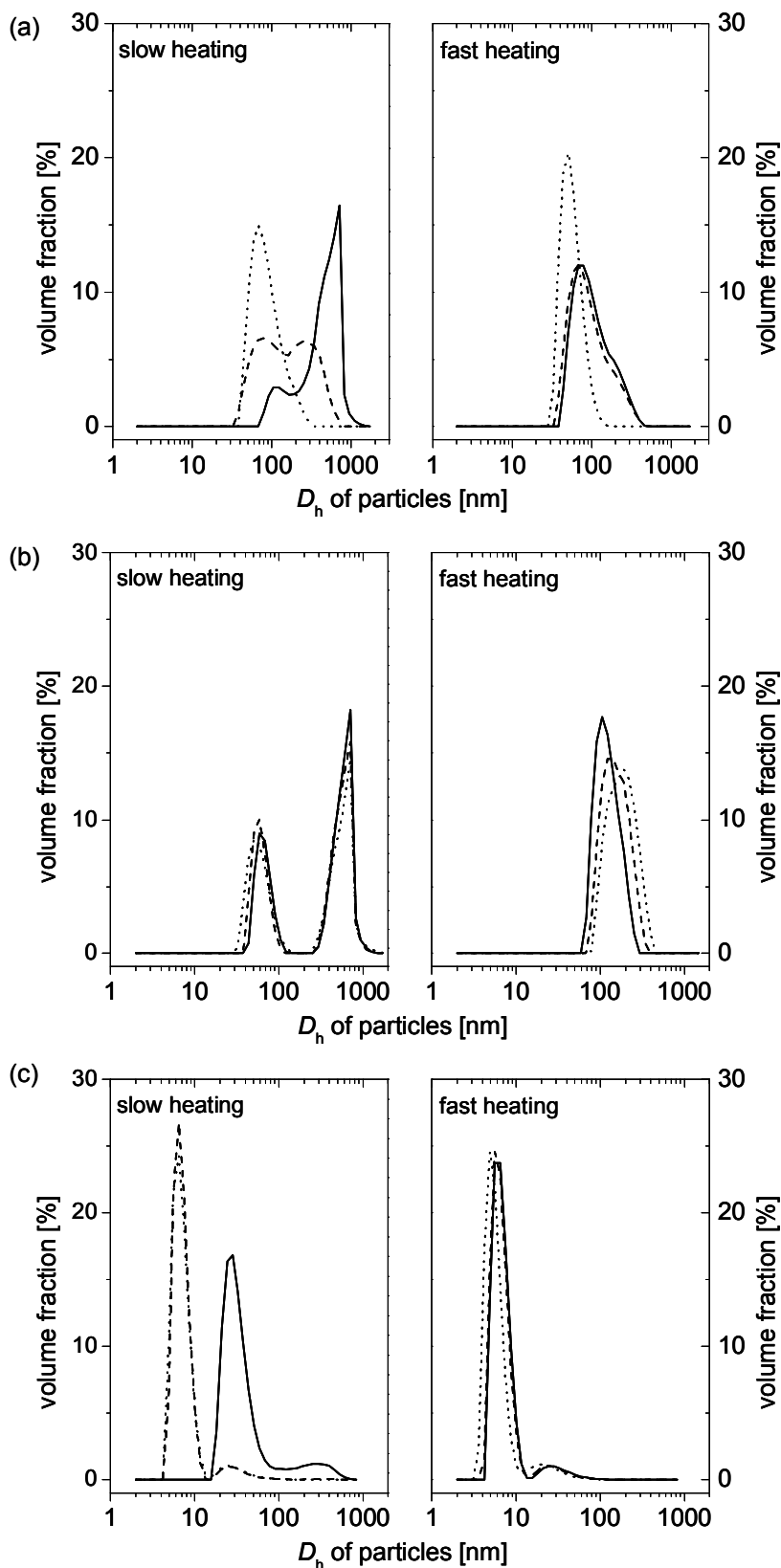


Figure 4.16 Annealing of 0.1 wt% aqueous solutions of triblock copolymers obtained by the slow and fast heating protocol at 45°C: (a) $(M4)_{110}-(M3)_{70}-(M2)_{64}$ (b) $(M4)_{110}-(M2)_{52}-(M3)_{69}$ (c) $(M2)_{139}-(M4)_{52}-(M3)_{28}$. Particle size distributions after thermal equilibration (solid line), after annealing for 24 h (dashed line) and 48 hours (dotted line).

In order to learn more on possible ageing effects, the samples that were obtained by the fast and slow heating protocol were annealed at 45°C over several days, and their size distributions were reanalyzed by DLS (Fig. 4.16). The annealing experiments were performed in order to elucidate whether the appearance of a bimodal distribution during the slow heating of **(M4)₁₁₀-(M3)₇₀-(M2)₆₄** and **(M4)₁₁₀-(M2)₅₂-(M3)₆₉** solutions is a result of the second phase transition or merely the result of a slow rearrangement. Therefore, the annealing temperature was set to 45°C which is between both phase transition temperatures and corresponds to the temperature where the bimodality arises.

Annealing the sample of **(M4)₁₁₀-(M3)₇₀-(M2)₆₄** obtained by the slow heating protocol had a pronounced effect on the size and distribution of the particles (Fig. 4.16a). The bimodal distribution disappeared completely. The bimodality which occurred at 45°C in the fast heating protocol vanished upon annealing, too, and small, narrowly distributed particles were obtained after 48 h. Consequently, slow kinetics play a role in the self-assembly of this polymer.

For polymer **(M4)₁₁₀-(M2)₅₂-(M3)₆₉** - with the hydrophilic block in the middle - the situation was different: Here, the bimodal distribution did not evolve measurably over 5 days. Either, the equilibrium situation is already attained. Or - more probably - the observed stability is only apparent as the aggregates are “frozen”.

In the slow heating protocol, polymer **(M2)₁₃₉-(M4)₅₂-(M3)₂₈** formed self-assembled aggregates at 45°C. Upon annealing for several days the particles disintegrate and very small aggregates or unimers predominate in solution. Although ¹H NMR spectroscopy evidenced the presence of collapsed **polyM4** blocks the driving force for self-assembly is obviously not yet strong enough at this temperature. The particle size distribution obtained by the fast heating protocol - comprising mainly unimers - is stable upon annealing for several days.

4.3.4. Summary of the self-assembly of double-thermoreponsive block copolymers

Ternary block copolymers comprising one permanently hydrophilic, namely poly(*N,N*-dimethyl acrylamide), and two thermoresponsive blocks, namely poly(*N*-isopropyl acrylamide) and poly(*N*-acryloyl pyrrolidine), aggregate at elevated temperatures in aqueous solution. The thermoresponsive association is a convenient method to prepare micelle-like aggregates of amphiphilic block copolymers, as their ready solubility in water at ambient temperature precludes complicated dispersion procedures. Moreover, the incorporation of a second thermoresponsive block allows to modify the hydrophilic-hydrophobic balance by changing the temperature. The self-assembly of three double-thermoreponsive ABC triblock copolymers with permuted block sequence was studied by turbidimetry, dynamic light scattering and ¹H NMR spectroscopy. These three analytical methods provided a complementary picture of the complex thermoresponsive behavior representing the behavior on the macroscopic, mesoscopic and molecular scale, respectively. The two monomers for the thermoresponsive blocks were chosen according to the phase transition temperatures of the respective homopolymers which differ by about 20K. This difference was expected to provide sufficient resolution of the two thermal transitions upon heating. Although the first phase transition and the consequent self-assembly could be easily followed by all applied analytical methods, the second phase transition was not clearly identified. In fact, only for the block sequence of increasing phase transition temperature, i.e. low LCST block - high LCST block - permanently hydrophilic

block, two distinct phase transition temperatures and the formation of different particles at intermediate and high temperatures were recognized unambiguously. For the block sequence with the permanently hydrophilic block in the middle, several indications for the second phase transition were found but the detection of the second phase transition temperature is complicated by the fact that attached polymer blocks affect each other in their coil-to-globule transitions. Additionally, the self-assembly of thermoresponsive block copolymers is subject to slow kinetics, despite the fast response of individual blocks to changes of temperature. Especially, for the block sequence with the permanently hydrophilic block in the middle, the polymer tends to form frozen aggregates. Beside the block sequence, the self-assembly of the double thermoresponsive block copolymers depended sensitively on the applied heating rate. In general, fast heating resulted in smaller aggregates and narrower distributions. The studied double thermoresponsive block copolymers exhibited a complex association behavior in aqueous solution which is not fully understood yet. Especially, the identification of the second phase transition requires more investigations.

5. TRIPHILIC ABC TRIBLOCK COPOLYMERS & THEIR SELF-ASSEMBLY INTO MULTI-COMPARTMENT MICELLES

5.1. Challenges and strategies of the studied system

Serum albumin is a transport protein in the blood that bears specific binding sites for poorly water-soluble compounds such as long-chain fatty acids, vitamins, hormones and drugs. Its complex structure and multi-fold binding functionalities make it an inspiring model for scientists aiming at synthetic materials, which mimic biological behavior. In this context, the idea of multi-compartment micelles has recently emerged.²⁵⁶ Although multi-compartmentalization is elegantly brought about by nature, the realization of synthetic counterparts is challenging. The basic requirements for a multi-compartment micellar system and the approaches that have been realized to date were presented in chapter 1.2.3. The macromolecular design chosen in this work relied on amphiphilic ABC triblock copolymers comprising two hydrophobic, yet mutually incompatible fragments to generate a microphase-separated micellar core and a third, hydrophilic fragment which stabilizes the hydrophobic domains in an aqueous environment.

The monomers for the first core-forming block were chosen according to their glass transition temperature (T_g), which has been proven to be an important parameter controlling the dynamics of the micelles in water. Polymers with high T_g 's such as polystyrene or PMMA are known to form micelles with so-called frozen cores at ambient temperature,^{8, 67} meaning that the glassy micellar core reduces markedly the exchange between unimers and micelles. As a consequence, the micellar characteristics are to a large extent controlled by the conditions of the micelle preparation and the micelles are trapped in non-equilibrium structures.⁸ Poly(*n*-butyl acrylate) (**polyM5**) ($T_g = -54$ °C) and poly(2-ethylhexyl acrylate) (**polyM6**) ($T_g = -50$ °C)²⁵⁷ are frequently employed lipophilic polymers of technical importance and exhibit glass transition temperatures far below ambient temperature. Both acrylates are known to be polymerizable in a controlled fashion by RAFT polymerization.^{164, 188, 258}

The second hydrophobic block is preferred to be strongly incompatible with the first one in order to achieve compartmentalization of the micellar core. However, the thermodynamic incompatibility of polymer blocks leading to microphase separation in bulk is not sufficient to realize a multicompartment system since such a system would not allow to solubilize different transport goods in separate domains. As has been discussed in chapter 1.2.3, fluorocarbon and hydrocarbon fragments are adequately distinct so that low-molar mass compounds are expected to be selectively partitioned between the two compartments. An acrylate monomer with a long perfluorinated side chain (**M7**) was selected for the second hydrophobic block. Both, the high fluorine content and the terminal $-CF_3$ group enhance the mutual immiscibility with the lipophilic block. It has been shown for anionic and nonionic fluorinated surfactants that switching from $-CF_3$ to $-CF_2H$ terminal chain ends induces a permanent dipole moment and that the surfactants are less effective in terms of cmc, limiting surface tension and limiting molecular area.^{259, 260} A perfluoroalkyl ester is an activated ester which is labile due to the electron-withdrawing effect of fluorine. In order to avoid hydrolysis of the ester in aqueous media, the perfluorocarbon side chain is linked to the acrylate moiety by a hydrocarbon spacer. Two methylene groups between the fluoroalkyl and the carboxyl moiety provide enough stability that the material can be handled like a typical

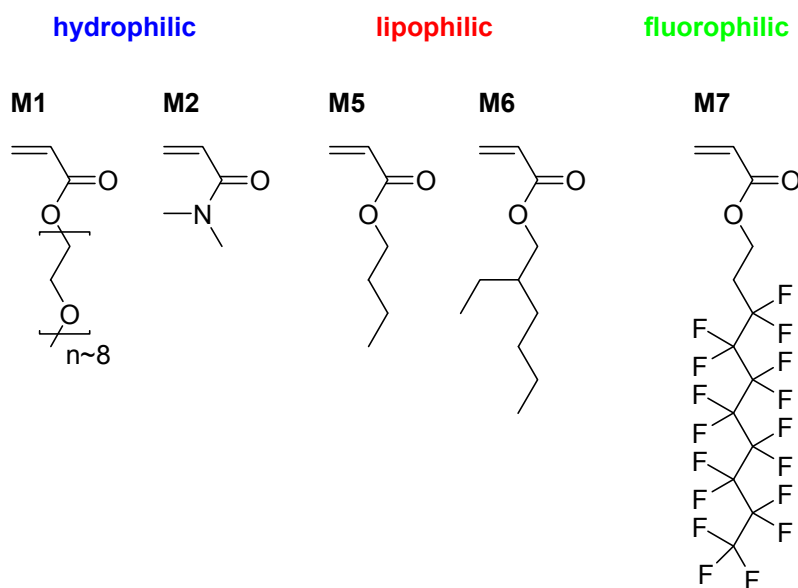


Figure 5.1 Monomers used for the synthesis of triphilic ABC block copolymers

acrylate. As the spacer also increases the mobility of the side chains, the solubility of the polymer in conventional organic solvents is improved.

To build the water-soluble block, non-ionic polymers were preferred over ionic ones due to the difficulties in handling and characterization of polyelectrolytes. Additionally, a common solvent which dissolves equally ionic, lipophilic and fluorophilic polymers, could not be found, however, a homogeneous polymerization medium is important for an optimal control in the synthesis of block copolymers. Therefore, the polymers of *N,N*-dimethyl acrylamide (**M2**) and oligoethylene oxide monomethyl ether acrylate (**M1**) were chosen for the hydrophilic block as they are classical hydrophilic polymers, which have been widely used in the synthesis of amphiphilic^{111, 261} and double-hydrophilic block copolymers by RAFT^{111, 173} and other CRP methods.²⁶²

A linear ABC triblock copolymer is the most simple polymer architecture that comprises three different fragments. Besides variations of molar mass and composition, the self-assembly of ABC triblock copolymers in selective solvents can be controlled by the block sequence leading to a larger variety of micellar structures compared to diblock copolymers. Since the polymerization of macromonomer **M1** produces a comb polymer with oligo(ethylene oxide) side chains, the final triblock copolymers comprise a mixed comb/block copolymer architecture.

The methods of controlled radical polymerization permit to access a large diversity of amphiphilic block copolymers containing highly polar or even ionic moieties. Among them especially RAFT polymerization is very versatile as it can be performed under a wide range of reaction conditions. As a consequence of their highly amphiphilic nature, the synthesis and characterization of triblock copolymers was expected to be challenging. A polymerization medium, which dissolves homogeneously the propagating polymer chains, is essential for the control of polymerization. Association or even precipitation of growing chains will markedly influence the polymerization kinetics. However, highly fluorinated polymers are rarely soluble in conventional organic solvents.²⁶³ While **polyM7** can be readily dissolved in fluorinated solvents - such as hexafluorobenzene or hexafluoroisopropanol - these solvents

precipitate the desired hydrophilic and lipophilic blocks. In order to minimize these difficulties, the syntheses of amphiphilic triblock copolymers were not started from a **polyM7** macroCTA. The molecular characterization of amphiphilic polymers was expected to be even more challenging as the usual methods of molar mass characterization, e.g. size exclusion chromatography or static light scattering, can be substantially disturbed in the case of associative polymers.²⁶⁴

As discussed in chapter 1.3.4, the structure of the CTA influences the control of the polymerization. Not all CTAs are equally suited for the polymerization of certain monomers. Instead, the structure of the CTA has to be adapted to the monomer. As was discussed before, the Z group should be activated towards the addition of propagating radicals. Preferentially, the R group is a better homolytic leaving group than the propagating radical and should re-initiate the polymerization fast so that the main-equilibrium is established rapidly.

Dithioesters are the most active chain transfer agents for RAFT polymerization. However, inhibition and retardation effects are observed in the polymerization of acrylates when CTAs are employed whose Z group is phenyl (cf. chapter 1.3.4). Trithiocarbonates are more and more used in the synthesis of block copolymers by RAFT polymerization as they are effective CTAs but usually show no retardation. Additionally, they are more easily synthesized and purified compared to dithiobenzoates prepared by the classical Grignard routes. Due to the higher rate of trithiocarbonate-mediated polymerizations, a lower concentration of initiator can be employed which is in turn beneficial for the preservation of end-groups. 2-(Butylsulfanylthiocarbonylsulfanyl)-2-methyl propionic acid (**CTA7**) was employed as RAFT agent in the synthesis of the amphiphilic ABC triblock copolymers. The Z group of **CTA7** cannot stabilize the intermediate radical of the RAFT equilibrium by mesomeric stabilization and thus, no retardation effect occurs. The 2-carboxy-prop-2-yl group is a good homolytic leaving group and is reported to control the polymerization of acrylic and styrenic monomers.¹⁷⁹

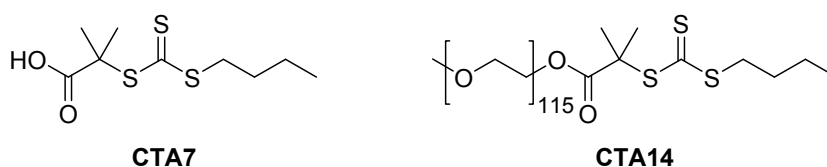


Figure 5.2 CTAs used for the synthesis of triphilic ABC block copolymers

The loss of a certain amount of thiocarbonyl end-groups at every block copolymerization step is inherent to the RAFT mechanism due to re-initiation and gives rise to homopolymer or block copolymer impurities. In order to reduce such impurities, the synthesis of triblock copolymers starting from a linear PEO macroCTA was explored, too. Poly(ethylene oxide) monomethyl ether was esterified with **CTA7** and the resulting macroCTA **CTA14** employed for the synthesis of amphiphilic triblock copolymers in only two successive block copolymerization steps.

5.2. Synthesis and molecular characterization of macroCTAs

As the influence of polymer architecture on the micellar morphologies was to be studied, different block sequences had to be realized and thus, homopolymers of hydrophilic and hydrophobic monomers were prepared. However, the synthesis of block copolymers was deliberately not started from a **polyM7** macroCTA due to the difficulties in finding a common solvent for **polyM7** and the other monomers. Instead, homopolymers of **M1**, **M2** and **M6** were prepared by RAFT polymerization under the experimental conditions summarized in Table 7.3. A typical procedure is described in chapter 7.4.3. As the trithiocarbonate-mediated RAFT polymerization of acrylic monomers is relatively fast, lower concentrations of initiator can be used and therefore, ratios of CTA to initiator were set to a value of ~ 10-20. Additionally, the low amount of generated radicals is advantageous for the preservation of end-groups. For the preservation of RAFT active end-groups, polymerizations were stopped at ~ 50% conversions.

Polymerizations of the hydrophilic oligo(ethylene oxide) macromonomer (**M1**) were conducted in 1:1 mixtures (by weight) of deionized water and methanol. The RAFT agent **CTA7** is not water-soluble without deprotonation of the carboxyl moiety, but readily soluble in mixtures of methanol and water. The polymerization was initiated by a water-soluble azoinitiator (**V-501**) and the polymerization temperature was set to 69°C according to the decomposition rate of **V-501**. After polymerization, the aqueous polymerization mixtures were directly transferred to dialysis tubes for purification.

The homopolymer of **M6** was prepared in toluene at 65°C with AIBN as thermal initiator and purified by precipitation. The removal of residual **M6** in the vacuum is difficult due to its high boiling point (215-219°C). Although purification of gluey polymers by precipitation is usually tedious, the strongly apolar nature of **polyM6** enabled its precipitation into cold methanol. The polymer settled on the bottom of the beaker as a viscous and intensely yellow-colored paste. As the employed CTA (**CTA7**) dissolves in CH₃OH, the colorless supernatant verified the presence of end-groups on the polymer. The methanol solution was decanted and the polymer was extracted several times under stirring with methanol. Finally, the polymer was lyophilized from benzene solution.

CTA7 was attached to PEO monomethyl ether (MW ~ 5000 g/mol) via azeotropic esterification of the hydroxyl group to produce a monofunctional PEO macroCTA (**CTA14**) according to a procedure reported by Ma and Lacroix-Dezmaces et al.²⁶⁵ Noteworthy, the trithiocarbonate is stable under the reaction conditions applied (110°C, acid catalyst) and the PEO was esterified quantitatively to introduce a trithiocarbonate moiety at the ω -chain ends as was evidenced by ¹H NMR and UV spectroscopy. Conversions of all prepared homopolymers were determined gravimetrically after purification.

The synthesized hydrophilic and hydrophobic macroCTAs were characterized to confirm the absence of residual monomer and to determine their molar mass as well as the concentration of RAFT active end-groups. The techniques applied were ¹H NMR spectroscopy in CDCl₃, end-group analysis by UV spectroscopy and SEC. The results of the various characterization methods are presented in Table 5.1 (entries 1-5). Theoretical molar masses based on monomer conversion were calculated according to equation 4.1.

Table 5.1 Characterization of triphilic ABC triblock copolymers and their precursors

entry	polymer ^a	theory ^b	SEC			NMR ^c	UV ^d	[wt.% M7]	
		M _n × 10 ⁻³ [g/mol]	M _n × 10 ⁻³ [g/mol]	M _w × 10 ⁻³ [g/mol]	PDI	M _n × 10 ⁻³ [g/mol]	M _n × 10 ⁻³ [g/mol]	IC ^q	NMR ^r
1	(M1) ₇₀	28	8 ^f	9 ^f	1.17	-	32 ⁱ		
2	(M1) ₈₅	21	12 ^f	14 ^f	1.17	-	39 ⁱ		
3	(M2) ₁₄₃	10	14 ^h	17 ^h	1.19	-	15 ^k		
4	(M2) ₃₈₄	26	19 ^h	26 ^h	1.39	-	38 ^k		
5	(M6) ₁₂₀	21	15 ^f	19 ^f	1.27	-	22 ⁱ		
6	(M1) ₇₀ -(M5) ₈₃	41	13 ^f	17 ^f	1.26	42	53 ⁱ		
7	(M1) ₇₀ -b-(M6) ₁₄₀	45	15 ^f	23 ^f	1.54	58	78 ⁱ		
8	(M1) ₈₅ -b-(M7) ₂₄	44	13 ^f	15 ^f	1.16	51	59 ⁱ		
9	(M2) ₁₄₃ -(M5) ₆₂	20	-	-	-	23	- ^p		
10	(M2) ₃₈₄ -(M6) ₁₉	- ^o	-	-	-	42	- ^p		
11	(M6) ₁₂₀ -(M1) ₅₀	45	13 ^f	17 ^f	1.31	45	47 ⁱ		
12	(M6) ₁₂₀ -(M1) ₁₀₉	82	10 ^f	14 ^f	1.43	72	80 ⁱ		
13	(M1) ₇₀ -(M5) ₈₃ -(M7) ₁₃	60	14 ^f	18 ^f	1.30	49	74 ⁱ	17.6	13.7
14	(M1) ₇₀ -(M6) ₁₄₀ -(M7) ₁₃	- ^o	16 ^f	23 ^f	1.43	64	165 ⁱ	9.5	10.5
15	(M6) ₁₂₀ -(M1) ₅₀ -(M7) ₄₀	- ^o	14 ^f	19 ^f	1.33	66	73 ⁱ	19.0	31.6
16	(M6) ₁₂₀ -(M1) ₁₀₉ -(M7) ₂₅	88	12 ^f	16 ^f	1.37	85	- ^p	18.1	15.3
17	PEO macroCTA (CTA14)	-	6 ^f	7 ^f	1.17	5	5 ^m		
18	PEO-(M5) ₂₂	7	6 ^f	9 ^f	1.37	8	15 ^l		
19	PEO-(M6) ₂₄	9	7 ^f	10 ^f	1.50	9	16 ⁱ		
20	PEO-(M5) ₂₂ -(M7) ₂	16	7 ^f	9 ^f	1.37	9	18 ⁱ	12.1	11.6
21	PEO-(M6) ₂₄ -(M7) ₂	18	8 ^f	10 ^f	1.35	11	23 ⁱ	11.4	9.8

^a DP_n according to combined UV and ¹H NMR spectroscopy, cf. ^c. ^b theoretical molar mass based on the obtained yield assuming 100% end-group functionalization (cf. equation 4.1) ^c M_n of di- and triblock copolymers determined by ¹H NMR spectroscopy from averaged compositional data assuming that M_n(UV) of the first block is preserved in the block copolymers ^d calculated by UV spectroscopic end-group analysis ^f PS-equivalent molar mass and PDI according to SEC (eluent: THF at 25°C, 1.0 mL/min) ^g aqueous SEC (eluent: 0.2 M Na₂SO₄, 1% CH₃COOH, 25°C, 1.0 mL/min): M_w determined by MALLS detection, PDI calculated according to pullulan calibration ^h PS-equivalent molar mass and PDI according to SEC (eluent: 0.05 M LiBr/N-MP at 25°C, 0.5 mL/min) ⁱ based on absorption band of **CTA5** at λ_{max} = 307 nm, ε = 14400 L mol⁻¹ cm⁻¹ in CH₂Cl₂ ^k based on absorption band of **CTA6** at λ_{max} = 307 nm, ε = 15800 L mol⁻¹ cm⁻¹ in CH₃OH ^l based on absorption band of **CTA5** at λ_{max} = 306 nm, ε = 15300 L mol⁻¹ cm⁻¹ in n-butyl acetate ^m based on absorption band of **CTA8** at λ_{max} = 308 nm, ε = 10400 L mol⁻¹ cm⁻¹ in CH₂Cl₂ ^o due to loss of material during purification M_n(theory) could not be calculated from the yield ^p loss of Z groups, end-group analysis not conclusive ^q determined by fluoride ion chromatography after combustion ^r determined by ¹H NMR spectroscopy.

The concentration of RAFT active end-groups in the synthesized macroCTAs could not be determined by ¹H NMR spectroscopy as either the proton signals of the employed **CTA7** coincide with those of the polymers, and/or as the relative amount of end-groups is too small to be determined precisely due to the high molar mass of **polyM1** samples. Consequently, the thiocarbonyl end-groups were quantified by UV spectroscopy. The study concerning the spectral properties of CTAs (cf. chapter 3) showed that end-group analysis employing the UV absorption band is very sensitive and that

quantification using the molar absorptivity of an appropriate model CTA is very reliable. Therefore, the molar absorptivity of the model CTA **CTA6** was used to calculate the molar mass of **polyM2** macroCTAs. As the respective polyacrylate model CTAs for each monomer were not prepared, end-group analysis of the polyacrylate macroCTAs relied on the molar absorptivity of the poly(*n*-butyl acrylate) model CTA (**CTA5**). As discussed in chapter 4.2, the molar masses of polymers were calculated based on the determined concentration of end-groups under the idealized assumption that each polymer chain bears exactly one thiocarbonyl end-group.

The theoretical molar masses of the hydrophilic homopolymers are smaller than those determined by UV spectroscopy. Two reasons might be responsible for this: The low-molar mass fraction in the samples might have been eliminated by dialysis. Thus, the theoretical molar masses would be underestimated if their calculation is based on the obtained yield. Second, it cannot be excluded that some thiocarbonyl end groups were lost during the purification by dialysis due to hydrolysis. Good agreement between the theoretical molar mass and the molar mass by end-group analysis was found for the hydrophobic macroCTA (**M6**)₁₂₀ which indicates a high degree of polymerization control accompanied by a high degree of end-group functionalization. Due to their distinct polarities and molecular architectures, the prepared homopolymers were characterized by different SEC systems. For the highly polar repeating units of **polyM2**, the SEC analysis was carried out with 0.05 M LiBr in N-MP as the eluent using PS calibration for molar mass calculation. Homopolymers of **M1** and **M6** were characterized by SEC in THF with PS calibration. While polystyrene might be a suitable calibration standard for **polyM6**, it is definitely not appropriate for the comb polymer architecture of **polyM1**. Therefore, **polyM1** was additionally characterized by aqueous SEC (0.2 M Na₂SO₄/1 wt% CH₃COOH as eluent) using MALLS for molar mass sensitive detection. The refractive index increment of **polyM1** ($dn/dc = 0.125 \text{ mL/g}$ in 0.2 M Na₂SO₄/1 wt% CH₃COOH, 30°C, 632 nm) was taken from the report of Mertoglu et al.¹⁷²

5.3. Synthesis and characterization of di- and triblock copolymers

The experimental conditions for the synthesis of block copolymers are listed in Table 7.3 and a typical procedure is described in chapter 7.4.3. The use of nonionic hydrophilic monomers facilitated the synthesis of block copolymers as it is possible to find a solvent that homogeneously dissolves the hydrophilic as well as the hydrophobic blocks. Examples include solvents of intermediate polarity such as toluene or THF. The polymerization mixtures were deoxygenated by flushing with N₂ for at least 45 min before polymerizations were performed under stirring at 65°C with AIBN as thermal initiator.

The purification of diblock copolymers was not trivial due their amphiphilic nature. In general, purification of amphiphilic polymers by precipitation is difficult as non-solvents for one block are often good solvents for the other. Thus, micellization or emulsification instead of precipitation occurs. The two diblock copolymers that were prepared from **polyM2** macroCTAs could be purified by precipitation in *n*-hexane as the non-soluble **polyM2** blocks were much larger than the hydrophobic blocks. The polymers precipitated as light yellow, soft flakes. However, the supernatants were yellow after filtration which indicates either that the block copolymer was not precipitated quantitatively. Or, that a notable amount of trithiocarbonate end-groups was cleaved from the initial macroCTA. The solvent was

evaporated from the supernatant and a yellow paste was obtained for both samples. The ^1H NMR spectra of these residues revealed the presence of pure **polyM5** and **polyM6** homopolymer, respectively, without any trace of **polyM2**. Although the reason is not clear yet, the results indicate a low blocking efficiency for the sequence acrylamide-acrylate in the trithiocarbonate-mediated polymerization. On one hand, acrylates are reported to be better leaving groups than acrylamides¹⁶⁷ which would result in a lower blocking efficiency. On the other hand, the leaving ability of **polyM2** propagating radicals in the pre-equilibrium is markedly increased due to steric reasons. Due to the low conversions of the second monomer and the pronounced loss of thiocarbonyl end-groups these polymer samples were not used for further syntheses.

As precipitation proved to be a fruitless procedure for the other prepared diblock copolymers, they were purified by dialysis. Toluene was removed from the polymerization mixtures for which macroCTA (**M6**)₁₂₀ had been employed. The residues were then dissolved in THF and dialyzed against deionized water to remove unreacted monomer **M1**. The diblock copolymers that were prepared starting from macroCTA (**M1**)₇₀ were purified first by dialysis against ethanol to remove the unreacted monomers **M5** and **M6** and low-molar mass fractions of lipophilic homopolymer impurity. Subsequently, the solutions were dialyzed against water and lyophilized. The diblock copolymers were obtained as very viscous, yellow pastes.

The polymerization conditions had to be modified for the synthesis of the hydrophilic-fluorophilic diblock copolymer (**M1**)₈₅-(**M7**)₂₄. A lower [monomer]:[macroCTA] ratio was employed as short fluorinated blocks were desired in order to maintain the solubility of the diblock copolymer in conventional solvents. α,α,α -trifluorotoluene (TFT) was used as the solvent to improve the solubility of the block copolymer in the polymerization medium. A previously performed RAFT-controlled homopolymerization trial of the fluorinated monomer **M7** at 65°C showed that its polymerization is retarded in comparison to the other employed acrylates. Guyot et al.²⁶⁶ studied the free-radical polymerization of fluorinated (meth)acrylates and observed in comparison to their hydrogenated homologues a lower reactivity. They attributed the lower polymerizability of fluoroacrylates to the electron-withdrawing effect of the perfluoroalkyl chain which decreases with increasing spacer length between the ester function and the perfluorinated chain. In order to enhance the rate of polymerization for monomer **M7**, the polymerization temperature was increased (88°C) for the synthesis of copolymer (**M1**)₈₅-(**M7**)₂₄. The less active azoinitiator **V-40** was employed for thermal initiation, which decomposes at 88°C with a comparable rate as AIBN at 65°C. The diblock copolymer was isolated by dialyzing the polymerization mixture first against ethanol followed by dialysis against water. After lyophilization of the aqueous solution, the polymer was obtained as yellow and opaque paste.

The preparation of diblock oligomers from the linear PEO macroCTA (**CTA14**) was carried out analogously to the block copolymerizations described above. Due to the lower molar mass of the PEO chain (MW = 5000 g/mol) the degrees of polymerization of the hydrophobic blocks had to be kept low in order to guarantee the steric stabilization of the hydrophobic micellar cores by the hydrophilic corona. Both, monomers **M5** and **M6** were polymerized under identical conditions using **CTA14** in order to obtain comparable degrees of polymerization. Addition of the polymerization mixture to diethyl ether did not precipitate the diblock copolymer but produced a milky dispersion. Therefore, the diblock copolymers

were purified by dialysis against ethanol to remove unreacted monomer. After dialysis against water, solutions of the amphiphilic oligomers were lyophilized and the products were obtained as light yellow, sticky powders.

The fluorinated block was synthesized for all prepared triblock polymer samples in the last polymerization step. In order to minimize microphase separation, the partially fluorinated solvent α,α,α -trifluorotoluene was employed as polymerization medium. Because of the low reactivity of **M7**, copolymerizations of the fluorinated block were carried out at 65°C for a prolonged time to attain nearly full conversions. While the fluorinated monomer **M7** dissolves in methanol as well as in diethyl ether, these solvents are selective for the hydrophilic or the lipophilic block. Attempts to remove unreacted monomer by precipitating the triblock copolymer in one of these solvents, gave in both cases a milky, stable dispersion. Thus, the polymerization mixtures were purified against ethanol and deionized water. Finally, the aqueous polymer dispersions were lyophilized.

Although ethanol is a non-solvent for **polyM7** and dissolves **polyM6** only partially, the diblock and triblock copolymer solutions remained transparent upon dialysis against ethanol. When these solutions were dialyzed against water, bluish or milky aqueous solutions were obtained, but no macrophase separation occurred. These observations are strong indicators for the amphiphilicity of the prepared materials and thus, for the successful formation of di- and triblock copolymers with a high blocking efficiency.

Attempts were made to corroborate the observed behavior with SEC analysis although the analysis of (amphiphilic) block copolymers is connected with several difficulties. Usually, SEC is a convenient and rapid method to evaluate the degree of control/livingness in the synthesis of standard polymers. Narrow molar mass distributions and the absence of shoulders or additional peaks are regarded as key parameters of a well-defined polymer sample. However, the SEC analysis of the prepared block copolymers was found to be complex and the results have to be interpreted cautiously.

The SEC elugrams of the prepared homopolymers confirmed the controlled polymerization of monomers **M1** and **M6** as their elugrams showed narrow and relatively symmetrical peaks. Upon polymerization of the second block, however, pronounced shoulders appeared in the elugrams. Although all determined polydispersity indices ranged from 1.2 to 1.5, such effects are mostly interpreted as results of a less controlled block copolymerization. Looking at the elugram of polymer **(M6)₁₂₀-(M1)₅₀**, for example, one would normally argue that homopolymerization instead of block copolymerization was achieved since the main peak did not shift towards lower elution volumes and a shoulder appeared on the low molar mass side. However, the excellent agreement of the theoretical molar mass and the molar masses determined by ¹H NMR and UV spectroscopy (cf. Table 5.1) - in addition to the observed amphiphilic properties - strongly suggest the controlled synthesis of polymer **(M6)₁₂₀-(M1)₅₀**. Another example is provided by diblock copolymer **(M6)₁₂₀-(M1)₁₀₉**: According to its elugram one would assume a mixture of two homopolymers. However, the molar masses determined by ¹H NMR and UV spectroscopy agree reasonably well with the theoretical molar mass and thus, corroborate the successful formation of the block copolymer. An even more corroborating evidence for a high blocking efficiency is, that polymer **(M6)₁₂₀-(M1)₁₀₉** self-assembled in water into small and narrowly distributed spherical micelles as will be seen in chapter 5.5 (see also Fig. A3.3 in Appendix 3).

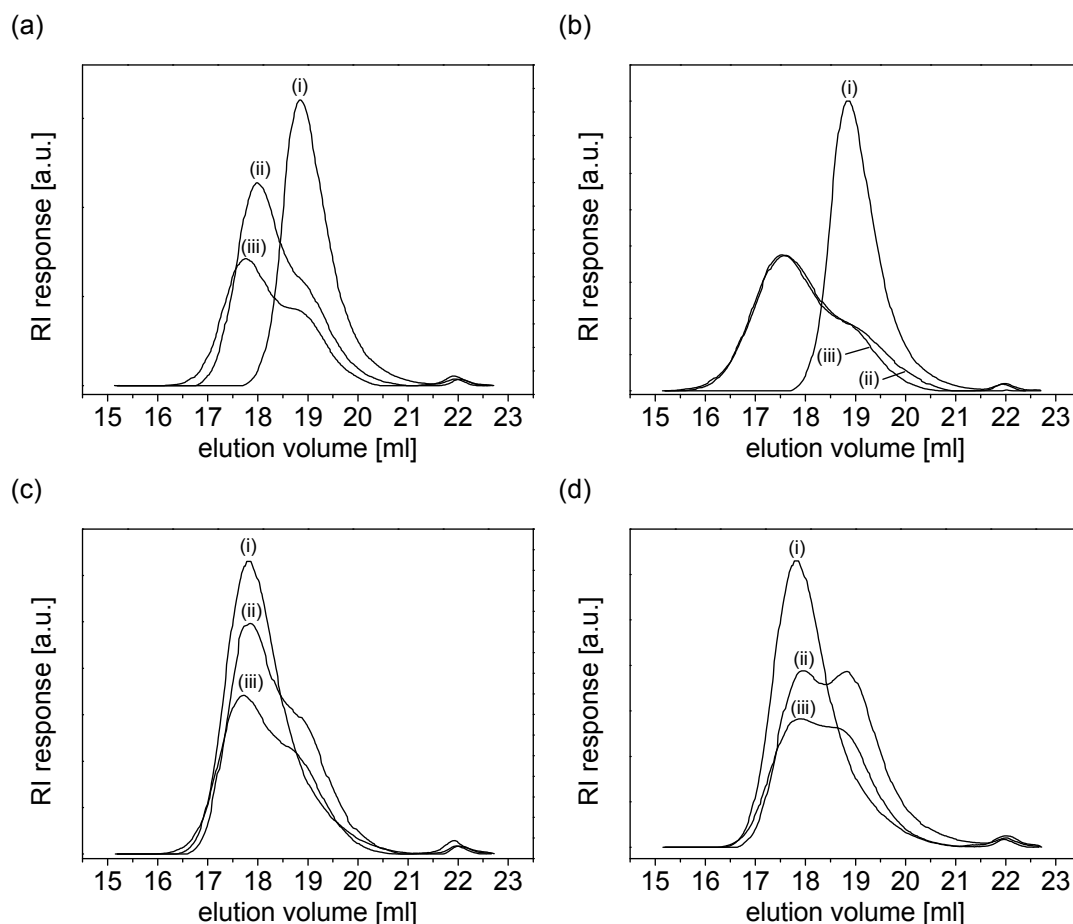


Figure 5.3 SEC elugrams of triphilic ABC triblock copolymers and their precursors (eluent: THF, flow rate: 1.0 mL/min, RI detection): (a) $(\mathbf{M1})_{70}$ - $(\mathbf{M5})_{83}$ - $(\mathbf{M7})_{13}$ (b) $(\mathbf{M1})_{70}$ - $(\mathbf{M6})_{140}$ - $(\mathbf{M7})_{13}$ (c) $(\mathbf{M6})_{120}$ - $(\mathbf{M1})_{50}$ - $(\mathbf{M7})_{40}$ (d) $(\mathbf{M6})_{120}$ - $(\mathbf{M1})_{109}$ - $(\mathbf{M7})_{25}$. (i), (ii) and (iii) are homopolymer, di- and triblock copolymer, respectively.

These peculiar observations can be in part explained by the polymer architecture. Upon polymerization of the second block, the polymer architecture changes from either a linear or comb polymer to a mixed block/comb copolymer. In fact, the separation of macromolecules by SEC does not occur according to their molar mass but to their hydrodynamic volume, $V_h = M \cdot [\eta]$, with M being the molar mass and $[\eta]$ the intrinsic viscosity. As the intrinsic viscosity of a comb polymer is lower than that of a linear polymer chain, V_h might not increase linearly with molar mass for a mixed linear block/comb architecture. Still, the attachment of the comb block should lead to an increase of M_n , however, it was found to decrease for diblock copolymers $(\mathbf{M6})_{120}$ - $(\mathbf{M1})_{50}$ and $(\mathbf{M6})_{120}$ - $(\mathbf{M1})_{109}$. The decrease of the hydrodynamic volume of diblock copolymers $(\mathbf{M6})_{120}$ - $(\mathbf{M1})_{50}$ and $(\mathbf{M6})_{120}$ - $(\mathbf{M1})_{109}$ might indicate intramolecular interactions of the polymer blocks. Furthermore, interactions of the polymers with the stationary phase cannot be excluded.

Although some aspects of the SEC elugrams can be explained by the hydrophilic comb polymer block, this argumentation is not applicable to the oligomers with a linear PEO chain. However, a bimodal distribution is observed in their elugrams, too. As has been described above, attempts were made to separate residual monomer and possible homopolymer impurities by precipitation in selective solvents. However, only stable emulsions were obtained due to the amphiphilic character of the polymers.

Therefore, the polymers were first dialyzed against ethanol and then against water by using a dialysis membrane with a molar mass cut off of 4000-6000 D. This purification procedure was presumed to remove homopolymer impurities, too. Still, the macroscopic behavior of polymer **PEO-(M6)₂₂-(M7)₂** strongly suggested the successful formation of block copolymer. Although polymer **PEO-(M6)₂₂-(M7)₂** did not spontaneously dissolve in water, it dissolved slowly in the course of one month forming a bluish dispersion.

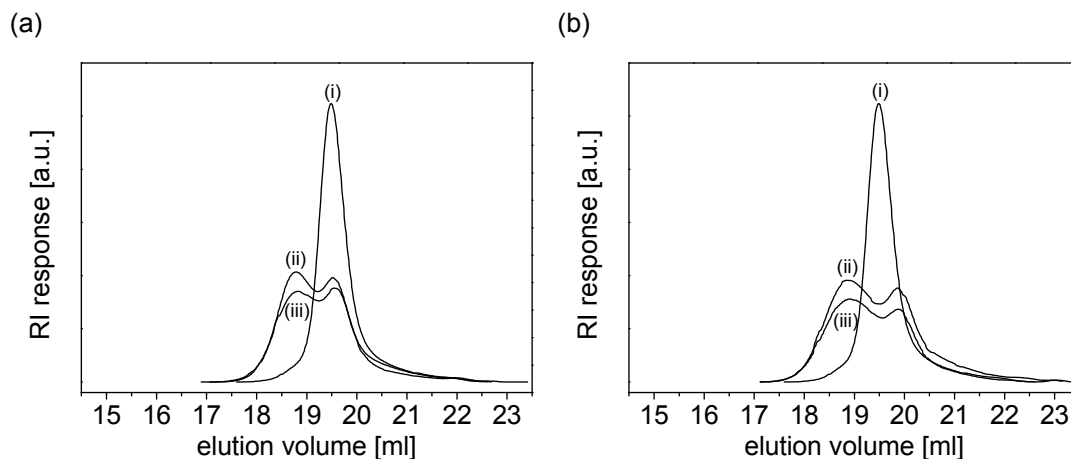


Figure 5.4 SEC elugrams of ABC triblock oligomers prepared from a linear PEO macroCTA (eluent: THF, flow rate 1.0 mL/min, RI detection). (a) **PEO-(M5)₂₂-(M7)₂** (b) **PEO-(M6)₂₄-(M7)₂**. (i), (ii) and (iii) are homopolymer, di- and triblock copolymer, respectively.

The synthesis of the third, fluorinated block had no marked effects on the elugrams of triblock copolymers in comparison to their parent diblock copolymers. While no shift of elution volume was observed for the triblock copolymer, the intensity of the RI detector signal decreased in most cases. In principle, the association of triblock copolymers via their fluorinated blocks is possible, but no indications for such behavior were found in the elugrams.

The amphiphilic di- and triblock copolymers were characterized by ¹H NMR and UV spectroscopy to determine their composition, their molar mass and the concentration of thiocarbonylthio end-groups. The overall molar masses of di- and triblock copolymers were calculated from their composition according to ¹H NMR spectroscopy in CDCl₃. The calculations of composition and molar mass of the block copolymers are based on the molar mass values of the precursor homopolymers as determined by UV spectroscopy assuming that the molar mass of the first block remained unchanged in the following block copolymerization steps. The methylene protons in α-position to the ester functionality were utilized to determine the composition of the block copolymers. Figure 5.5 depicts the ¹H NMR spectrum of **(M6)₁₂₀-(M1)₅₀-(M7)₄₀** as an example.

Determination of the composition by ¹H NMR is best performed in a solvent which dissolves all polymer blocks. While CDCl₃ is a good solvent for the polymers of **M1**, **M5** and **M6**, it is a non-solvent for the homopolymer of **M7**. Still, the triblock copolymers dissolved completely in CDCl₃ and formed transparent solutions. Nevertheless, the fluorinated blocks might still be associated leading to attenuation/broadening of the respective ¹H NMR signals. For the determination of composition by ¹H NMR only one proton signal of the fluorinated block can be employed, namely the α-methylene protons of the ester groups as the other proton signals overlap with the backbone or side chain signals of

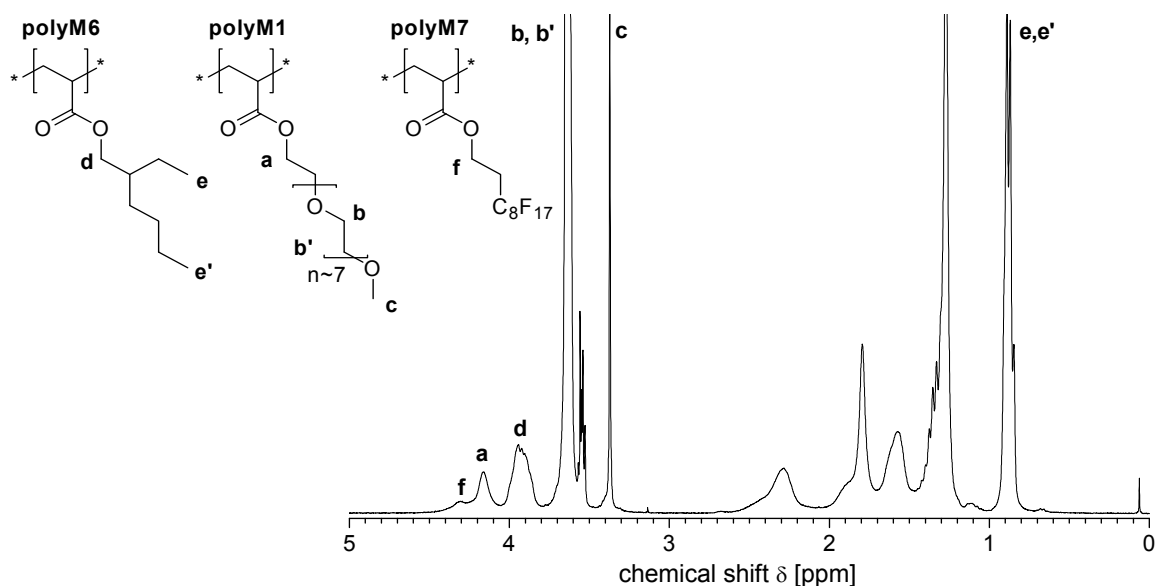


Figure 5.5 ^1H NMR spectrum of polymer $(\text{M6})_{120}\text{-}(\text{M1})_{50}\text{-}(\text{M7})_{40}$ in CDCl_3

the hydrophilic and the lipophilic block. The analysis by ^1H NMR spectroscopy is complicated further by the low degrees of polymerization of the fluorinated block. The contents of fluorinated repeating units were determined after combustion (Schöniger method) and ion chromatography of fluoride. The obtained results agree reasonably well with the values determined by ^1H NMR spectroscopy.

Summary

The synthesis as well as the characterization of the desired amphiphilic triblock copolymers proved to be a challenging task due to the disparate “philicities” of the constituting blocks. Because SEC did not provide reliable molar masses, the prepared polymers were characterized by a combination of UV and ^1H NMR spectroscopy. In this respect, RAFT polymerization was demonstrated to be superior to the other techniques of controlled radical polymerization, as the RAFT end-groups can be advantageously exploited for molar mass determination by UV spectroscopic end-group analysis. The good agreement between the experimentally determined and theoretically expected molar masses demonstrated the controlled character of the polymerizations.

5.4. Thermal analysis of the amphiphilic triblock copolymers

As microphase separation between the core-forming blocks is an essential requirement for multi-compartment micelles, the compatibility of the three polymer blocks in bulk was investigated by thermal analysis. Thermal gravimetric analysis (TGA) showed that neither the homopolymer nor the block copolymers of **M7** are thermally more stable than other polyacrylates as they all undergo degradation above 250°C. That means, the increased thermal stability of materials with a fluorinated backbone is not observed here. Thermal characterization by differential scanning calorimetry (DSC) was performed applying a temperature program of heating-cooling-heating from -120°C to 120°C with rates of either 10 or 20 K/min. Data analysis was carried out during the second heating ramp and the results are summarized in Table 5.2.

Table 5.2 Thermal analysis of homo- and triblock copolymers by differential scanning calorimetry (DSC)

polymer	T_g^a [°C]	T_r^b [°C]	T_m^c [°C]	T_m^d [°C]	heating rate [K/min]
(M1)₇₀	-62	-44	5		10
(M6)₁₂₀	-72				20
polyM7^e				77	10
(M1)₇₀-(M5)₈₃-(M7)₁₃	-67	-37	1	66	20
(M1)₇₀-(M6)₁₄₀-(M7)₁₃	-67	-32	0	65	20
(M6)₁₂₀-(M1)₅₀-(M7)₄₀	-67	-35	3	63	20
PEO macroCTA (CTA14)			60		20
PEO-(M5)₂₂	-58	-	57		20
PEO-(M5)₂₂-(M7)₂	-56	-	57	37	20

^a glass transition, onset temperature ^b recrystallization temperature ^c first melting temperature ^d second melting temperature ^e sample prepared by free radical polymerization.

The hydrophobic polymers **polyM5** and **polyM6** are reported to exhibit glass transition temperatures at -54°C and -50°C.²⁵⁷ The observed T_g of -62°C for **(M1)₇₀** correlates with $T_g = -63°C$ reported for PEO chains (MW = 400)²⁵⁷ and is thus attributed to the glass transition of the PEO side chains in **(M1)₇₀**. The glass transition of the side chains is followed by recrystallization at -44°C and melting at 5°C.

A glass transition is observed for all studied triblock copolymers at -67°C and is attributed to the T_g of the hydrophilic **polyM1** block. In the DSC traces of the block copolymers it is not possible to differentiate between the glass transition of **polyM1** and the hydrophobic block. However, the thermal behavior of homopolymer **polyM1** is preserved in the block copolymers giving a strong indication for the segregation of the hydrophilic and hydrophobic blocks.

Due to its rigid perfluorinated side chains, **polyM7** is a crystalline polymer for which a glass transition was not observed. A sample of **polyM7** which was prepared by free radical polymerization

exhibited a sharp melting peak at 77°C. In the triblock copolymers the melting temperature of the **polyM7** blocks was slightly decreased due to their low molar mass.

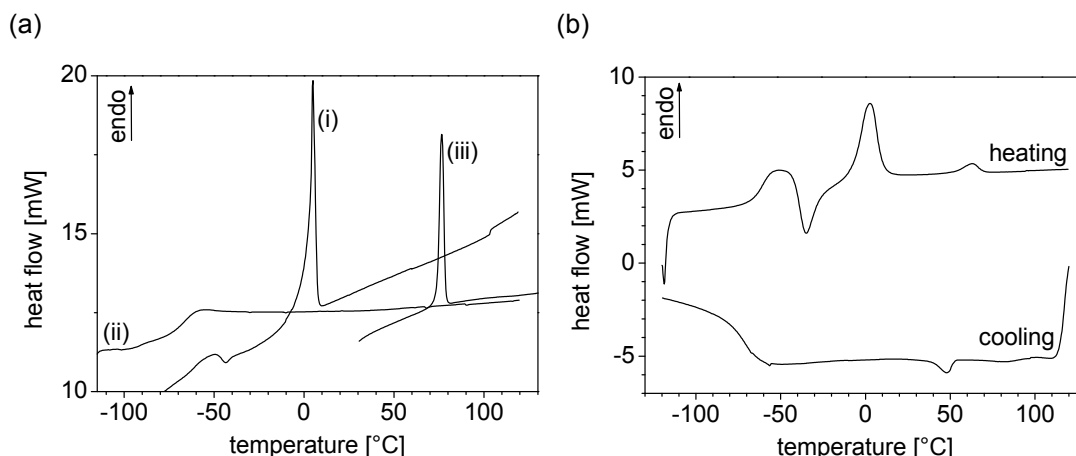


Figure 5.6 Differential scanning calorimetry (DSC) traces of (a) homopolymers: (i) **(M1)₇₀**, (ii) **(M6)₁₂₀**, (iii) **polyM7** and (b) triblock copolymer **(M6)₁₂₀-(M1)₅₀-(M7)₄₀**.

In the oligomeric triblock copolymer **PEO-(M5)₂₂-(M7)₂** the effect of molar mass on the melting point was even more pronounced. Due to the very low contents of fluorinated repeating units the melting temperature was depressed to 37°C.

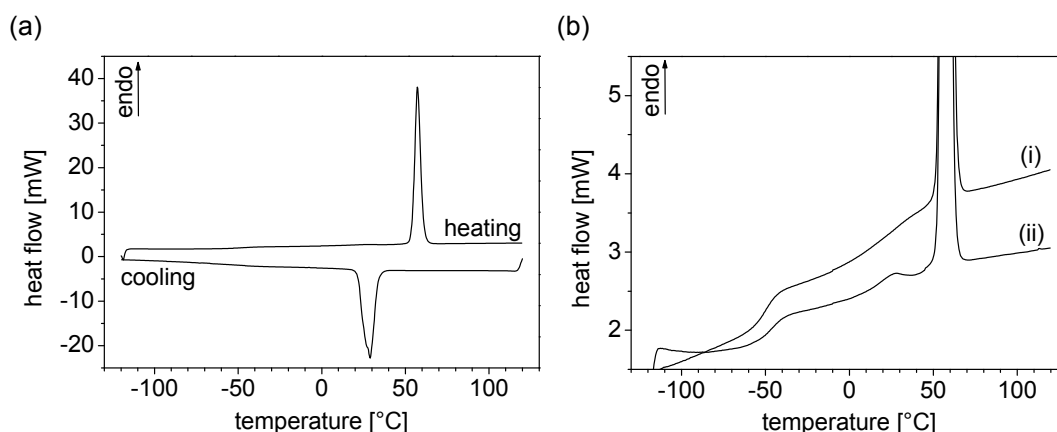


Figure 5.7 DSC analyses of block copolymers: (a) Traces of **PEO-(M5)₂₂-(M7)₂** (cooling and 2nd heating run, 20 K/min) (b) Magnified parts of the DSC traces (2nd heating, 20 K/min) of polymers (i) **PEO-(M5)₂₂** and (ii) **PEO-(M5)₂₂-(M7)₂**.

The thermal analysis of the prepared triblock copolymers revealed that all polymer blocks are thermodynamically incompatible with each other and microphase-separate in bulk. Consequently, these polymers are expected to microphase-separate in solution and form micellar aggregates with segregated cores.

5.5. Self-assembly of triphilic ABC block copolymers in water

The self-assembly of ABC triblock copolymers comprising a hydrophilic, a lipophilic and a fluorophilic block was studied in aqueous solution to address the following questions:

- (1) Do the triphilic block copolymers self-assemble into polymeric micelles?
- (2) To what extent is the micellization influenced by the preparation conditions?
- (3) Do they form aggregates with segregated cores?
- (4) How is the self-assembly influenced by the block sequence and the polymeric architecture?
- (5) Is the aggregate morphology suited as a multi-compartment micellar system?

The prepared ABC triblock copolymers were anticipated to self-assemble in water as well as in certain organic solvents due to the very disparate philicities of their constituting blocks. As the present study focused on their self-assembly in water, the micellization in organic solvents was not investigated in detail. Properties such as the critical micellization concentration and the surface activity - which are key parameters for low-molar mass amphiphiles - were not determined for the prepared block copolymers, due to the difficulties related to the typically very low cmc's of block copolymers and since equilibrium situations are usually not attained.

The self-assembly of amphiphilic block copolymers in a selective solvent can be studied by a variety of techniques. Nuclear magnetic resonance has been widely used to probe micellization or association.^{65, 267-269} The loss of fine structure or signal intensity compared to a molecularly dissolved sample is attributed to the reduced mobility of polymer chains located in the micellar cores.

The sizes of micellar aggregates formed from block copolymers are typically in the order of 20-100 nm. Dynamic light scattering is a rapid method to determine the mean size and the size distribution of such colloidal samples. Although the method is well adapted for routine measurements, its results should be interpreted cautiously, since the calculation of the hydrodynamic diameter from the determined diffusion coefficient assumes compact spheres. For morphologies that deviate from spherical micelles, accuracy in size determination can be improved by working with variable angle systems. Although DLS can rapidly determine the overall particle size, no conclusions regarding the size or morphology of the micellar core can be drawn. As the prepared amphiphilic triblock copolymers were designed to form sub-structured micellar cores, direct imaging by cryogenic transmission electron microscopy²⁷⁰ (cryo-TEM) was the method of choice.

The measurements of micellar solutions by cryo-TEM were realized in cooperation with the Research Center for Electron Microscopy at the Freie Universität, Berlin. Cryo-TEM is a technique allowing for near *in situ* imaging of nano objects in solution. While in classical TEM the complete removal of the solvent from the sample, e.g. by air drying, can deform or even destroy the structures to be studied, they are physically fixed for cryo-TEM by freezing the solution rapidly in a suitable cryogen. The very rapid cooling preserves on one hand the delicate self-assembled structures and on the other hand prevents the crystallization of ice which could destroy them. Another important advantage of cryo-TEM is the possibility to observe complex and/or polydisperse objects.

5.5.1. Preparation of micellar solutions

Essentially, there are two methods to prepare micellar solutions of amphiphilic block copolymers in water.^{8, 271, 272} Block copolymers comprising large and strongly hydrophilic blocks (e.g. polyelectrolytes) can be often directly dispersed in water and small, relatively monodisperse micelles are obtained at concentrations above the cmc. Still, the direct dissolution method can suffer from long equilibration times and requires annealing, e.g. by thermal treatment. Besides, the micelle morphology might be predetermined by the morphology in bulk. With increasing relative length of the hydrophobic block, the copolymer becomes less water-soluble and will not self-assemble into monodisperse nanoparticles through direct dissolution. In an alternate dispersion procedure, water as the precipitant solvent for the hydrophobic block is slowly added to the block copolymer dissolved in a common solvent. Above a critical water content micellization occurs. Residues of the common solvent are then removed either by evaporation or by dialysis. If block copolymer solutions are directly dialyzed against water, large aggregates were found to evolve in addition to micelles and were attributed to the fast exchange of solvent.²⁷³ As different common solvents interact differently with the core- and corona forming blocks, the common solvent exerts a strong influence on the micelle morphology.²⁷⁴

The prepared amphiphilic ABC triblock copolymers were not directly soluble in water due to their low hydrophilic/hydrophobic balance. Therefore, aqueous micellar solutions had to be prepared starting from a common solvent. For optimal results, the solvent to be employed was preferred to dissolve all polymer blocks and to be fully miscible with water. In most reported procedures²⁷⁴ of block copolymer micellization by solvent exchange, the common solvent is removed by dialysis after the micelle morphology has been locked in by the addition of the selective solvent. However, the micellar solution is uncontrollably diluted by dialysis and its concentration must be determined and adjusted afterwards. The concentration of the micellar solution can be better controlled during preparation, if the chosen common solvent is more volatile than water and thus, evaporates preferentially from the micellar solution.

Several water-miscible organic solvents were tested as common solvents for the dispersion of amphiphilic triblock copolymers. Solubility tests with the respective homopolymers showed that ethanol, acetone, *N,N*-dimethyl formamide (DMF) and *N,N*-dimethyl acetamide (DMAc) are not suited for the desired dispersion procedure as they do not dissolve the apolar **polyM6** and **polyM7** blocks. Moreover, the high boiling points of DMF and DMAc render them unsuited for the solvent evaporation procedure. Highly fluorinated solvents such as perfluorobenzene or hexafluoroisopropanol were found to be the only solvents for a high molar mass sample of **polyM7**. However, these solvents are not water-miscible and in addition precipitants for the polymers of **M1** and **M6**. Within the conventional, non-fluorinated organic solvents tested, THF was the only one in which the fluorinated homopolymer was at least swollen. Although the homopolymer of **M7** did not dissolve in CHCl₃ or THF, all prepared triblock copolymers were readily soluble in these solvents and formed transparent homogeneous solutions. Still, the fluorinated blocks might be associated in the common solvent and thus, micellization would not start from a molecularly dissolved block copolymer. In order to elucidate this issue, DLS measurements of two representative triblock copolymer samples and their precursor macroCTAs were carried out in THF and CHCl₃ (cf. Table 5.3).

Table 5.3 Dynamic light scattering analysis of homo- and block copolymer solutions (4.0 g/L) in various organic solvents

entry	sample	THF D_h [nm] ^a	CHCl ₃ D_h [nm] ^a
1	(M1) ₇₀	7 (100)	7 (100)
2	(M1) ₇₀ -(M5) ₈₃	11 (100)	10 (100)
3	(M1) ₇₀ -(M5) ₈₃ -(M7) ₁₃	11 (97)	167 (100)
4	(M6) ₁₂₀	5 (100)	
5	(M6) ₁₂₀ -(M1) ₅₀	7 (100)	
6	(M6) ₁₂₀ -(M1) ₅₀ -(M7) ₄₀	8 (100)	

^a mean hydrodynamic diameter according to the volume distribution. 7 (100) means that 100% of particles (by volume) have an average D_h of 7 nm.

The hydrodynamic diameter of homopolymer (M1)₇₀ is the same in THF and CHCl₃ solution and the size is typical for molecularly dissolved polymer coils. The amphiphilic diblock copolymer (M1)₇₀-(M5)₈₃ showed an increase of D_h which is attributable to its higher molar mass. Except for a very small fraction of larger aggregates, triblock copolymer (M1)₇₀-(M5)₈₃-(M7)₁₃ exhibited the same mean hydrodynamic diameter as its precursor diblock copolymer in THF and is obviously molecularly dissolved in THF. In contrast, large monodisperse particles were detected for this polymer in CHCl₃ solution and are ascribed to the association of fluorinated blocks. Provided that the aggregates in CHCl₃ are spherical, particles should comprise a small and dense fluorinated core and a well-solvated corona made of **polyM1** and **polyM5** blocks (core-shell-corona micelles with a swollen shell of **polyM5**). The particle size found by DLS was more than twice times larger than the contour length of the whole polymer chain. It has to be kept in mind that particles are treated as compact spheres in DLS analysis and that the determined size corresponds to the equivalent sphere exhibiting the same diffusion coefficient. Other morphologies such as cylindrical or worm-like micelles might account for such large apparent particle sizes. But since the DLS measurements were carried out at a single angle only, no conclusions regarding the shape of particles can be drawn.

NMR spectroscopy can provide indications for the association of polymers in selective solvents.^{267, 268} The broadening of ¹H NMR signals due to slowed-down molecular tumbling of desolvated or associated chains was already exploited as a qualitative indication for the self-assembly of thermoresponsive polymers (cf. chapter 4). Here, ¹⁹F NMR spectroscopy was utilized to study further the state of association of fluorinated chains in CHCl₃ and THF. Figure 5.8 depicts the ¹⁹F NMR spectra of polymer (M6)₁₂₀-(M1)₅₀-(M7)₄₀ in CDCl₃ and THF in comparison to the spectrum of monomer M7 in CDCl₃. Trifluorotoluene (0.5 wt%, $\delta(\text{Ph-CF}_3) = -63.72$ ppm vs. CFCI₃) was used as a secondary standard for chemical shifts. Although the solution of (M6)₁₂₀-(M1)₅₀-(M7)₄₀ in CDCl₃ was clear and gave no indication for association, the ¹⁹F NMR spectrum showed broadened signals which point to associated fluorinated side chains and consequently, corroborate the results of the DLS analysis. Especially the signal of the trifluoromethyl group (at $\delta = -83$ ppm) and the adjacent fluorinated methylene group (at $\delta = -128$ ppm) appear broadened. In contrast, the signals of the fluorinated side chains are narrower in THF and evidence - in agreement with the DLS measurements - a lower degree of association.

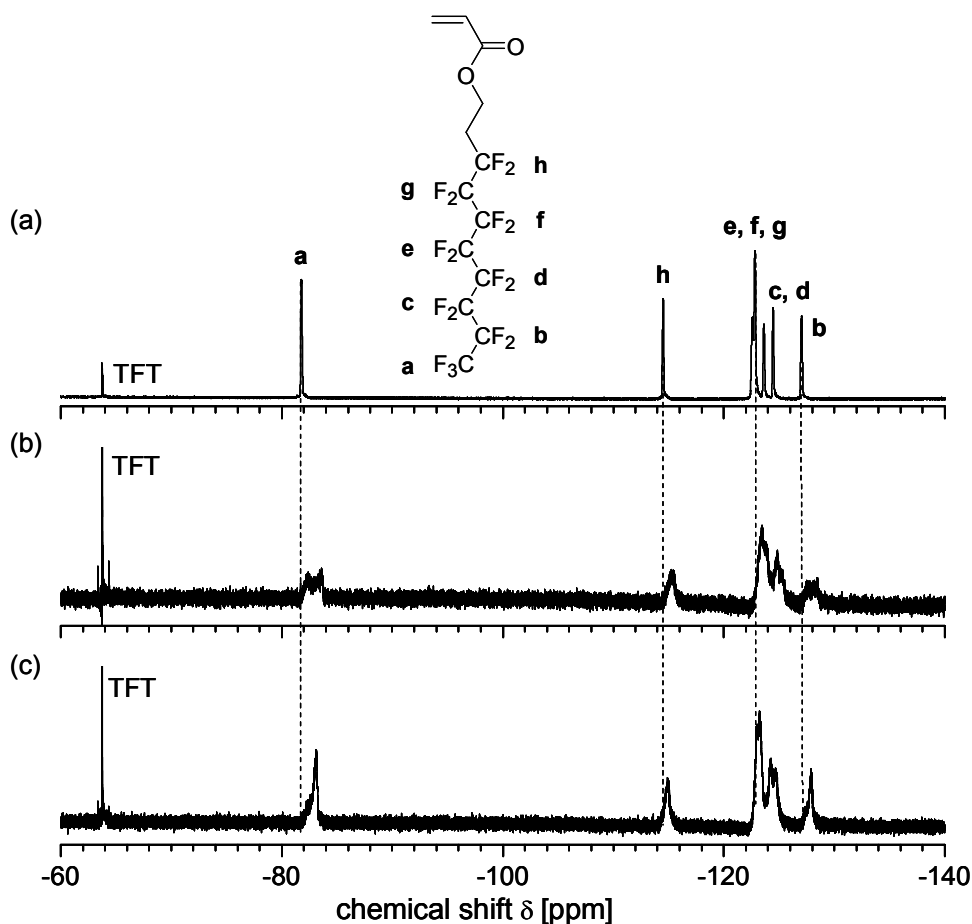


Figure 5.8 Comparison of the ^{19}F NMR spectra of the fluorinated monomer **M7** and an ABC triblock copolymer in different solvents: (a) monomer **M7** in CDCl_3 (b) $(\text{M6})_{120}\text{-(M1)}_{50}\text{-(M7)}_{40}$ in CDCl_3 (c) $(\text{M6})_{120}\text{-(M1)}_{50}\text{-(M7)}_{40}$ in THF. Internal reference: α,α,α -trifluorotoluene (TFT).

According to the results obtained by DLS and ^{19}F NMR spectroscopy, THF proved to be the most suitable common solvent for the dispersion of amphiphilic triblock copolymers in water. Accordingly, micellar solutions with a final concentration of 0.5 wt% were prepared by slowly adding water to a solution of the block copolymer in THF at ambient conditions. The detailed procedure is given in chapter 7.5.2. The polymer concentration in the common solvent THF was deliberately kept low in order to support the formation of simple spherical micelles instead of complex or mixed morphologies which are often reported for higher polymer concentrations.^{11, 275} In order to probe the micellization of amphiphilic block copolymers by ^1H NMR spectroscopy, micellar solutions of the triblock copolymers were prepared in D_2O with a concentration of 1.5 wt% to attain sufficient signal intensity. Figure 5.9 compares as an example - the ^1H NMR spectra of polymer $(\text{M1})_{70}\text{-(M5)}_{83}\text{-(M7)}_{13}$ in CDCl_3 and in D_2O .

The ^1H NMR spectra show that the signals of the protons **a**, **b**, **b'** and **c** of the hydrophilic block are intense and well-resolved in CDCl_3 as well as in D_2O . Thus, the **polyM1** block is well-solvated in both solvents. While the proton signals **d** and **e** of the poly(*n*-butyl acrylate) block are well resolved in CDCl_3 , they are strongly attenuated in D_2O . The broadening and or vanishing of ^1H NMR signals is due to the respective protons being in a rigid environment, thus implying the formation of micellar aggregates. The proton signal **f** of the fluorinated block was not found in D_2O . Even in the ^{19}F NMR spectrum (secondary

standard: CF_3COONa) the respective signals vanished completely and their absence indicated a strongly decreased mobility for the fluorinated block.

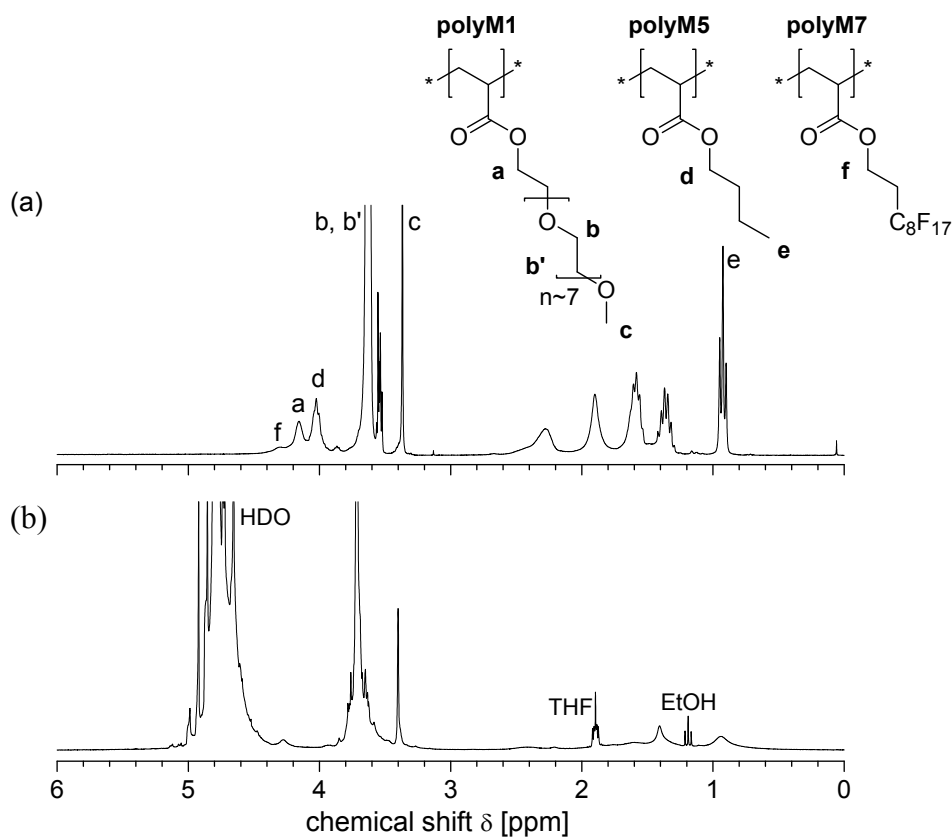


Figure 5.9 ^1H NMR spectra of triblock copolymer $(\text{M1})_{70}-(\text{M5})_{83}-(\text{M7})_{13}$ in (a) CDCl_3 and in (b) D_2O

In advance to the investigations of micellar characteristics, the conditions for the preparation of micellar solutions by the solvent evaporation procedure were optimized. ^1H and ^{19}F NMR spectroscopy provided a first qualitative picture on the self-assembly in water. In the next step, the size and distribution of the self-assembled polymeric nanoparticles was studied by DLS.

5.5.2. Study of the micelle size by dynamic light scattering

Aqueous solutions of di- and triblock copolymers were systematically studied by DLS in order to confirm the formation of polymeric micelles by the dispersion procedure applied and to determine their size and distribution. The amphiphilic diblock copolymers were included in the DLS study to compare their self-assembly characteristics with those of the triblock copolymers and to study whether the incorporation of the fluorinated block changes notably the micellization behavior. Micellar solutions of di- and triblock copolymers in water were prepared at ambient conditions with a concentration of 0.5 wt% according to protocol A as described in chapter 7.5.2.

The amphiphilic diblock copolymers were anticipated to self-assemble in water into spherical micellar aggregates comprising a lipophilic or fluorophilic core, respectively, and a hydrophilic corona. The DLS analysis of their aqueous solutions disclosed particles with mean hydrodynamic diameters (D_h) in the range of 14 nm to 55 nm and in most cases with a monomodal size distribution (cf. Table 5.4). In DLS, the ratio $\mu_2 / \bar{\Gamma}$ (PD) provides a measure of the size distribution (“mobility dispersity”) where $\bar{\Gamma}$ is the first cumulant or average decay rate and μ_2 is the second cumulant, both derived from the cumulant fit of the intensity correlation functions. Although a PD value < 0.1 is usually regarded as an indicator for a high homogeneity in the particle population, the PD value has to be considered as a supportive rather than a conclusive information on the particle size distribution since discrepancies between the PD value and the size distribution observed by SEM were found.²⁷⁶

Diblock copolymers **(M1)₇₀-(M5)₈₃** and **(M1)₇₀-(M6)₁₄₀** self-assembled into small nanoparticles with relatively narrow, monomodal distributions in water. Both polymers comprise identical hydrophilic blocks but differ in the nature and length of their hydrophobic blocks. That polymer **(M1)₇₀-(M6)₁₄₀** formed larger aggregates than polymer **(M1)₇₀-(M5)₈₃** is attributed to the higher DP and the larger molar volume of the hydrophobic **polyM6** block.

It is noteworthy that diblock copolymer **(M1)₈₅-(M7)₂₄** formed smaller particles in water than the oligomers **PEO-(M5)₂₂** and **PEO-(M6)₂₄** despite similar degrees of polymerization for their hydrophobic blocks and a larger hydrophilic block. Apparently, the architecture of the hydrophilic block exerts a pronounced influence on micelle formation and the result may be rationalized as follows: The strong osmotic crowding caused by the PEO comb polymer in the hydrophilic corona may be reduced in small spherical micelles with a larger interfacial curvature. In contrast, the linear PEO chains cause less coronal chain crowding and thus, larger micellar aggregates relative to the molar mass of the unimers are formed. Provided that aggregation numbers are comparable for polymers **PEO-(M5)₂₂** and **PEO-(M6)₂₄**, the larger particle size found for **PEO-(M6)₂₄** is consistent with the higher molar volume of **M6** repeating units.

A bimodal distribution with mean particle diameters of 55 nm and 300 nm, respectively, was found for micellar aggregates self-assembled from polymer **(M6)₁₂₀-(M1)₅₀**. As the polymer chain cannot stretch beyond its contour length in order to fill the micellar core homogeneously, the latter particle size would not be compatible with the diameter of a spherical micelle. Such large aggregates have been observed before for block copolymers with long insoluble blocks and have been attributed, for example, to large compound micelles formed by the secondary aggregation of (reverse) micelles.^{10, 11}

As block copolymers exhibit much lower rates of micellar exchange compared to low-molar mass surfactants and the micellar aggregates might not be equilibrated 24 h after preparation yet, some of the aqueous solutions of diblock copolymers were reanalyzed after two weeks of aging at ambient conditions. The results of the size analysis by DLS were reproducible within the experimental error and thus, the particle sizes and distributions appeared to be unaffected by aging (Table 5.4). Apparently, the equilibration between micelles is already attained one day after preparation. Alternatively, the exchange of macromolecules might be extremely slowed down. Although the absence of micelle equilibration for block copolymers was originally attributed to the high T_g of the core-forming blocks (PS or PMMA),^{8, 67} block copolymers comprising short hydrophobic blocks with a low T_g (PB) are reported to form “frozen” micelles, too.²⁷⁷ Hence, the observed stability of particle size distributions is attributed to the very slow equilibration of micelles.

Table 5.4 Dynamic light scattering analysis of 0.5 wt% aqueous solutions of diblock copolymers prepared at 25°C

entry	sample	1d after preparation			2 weeks after preparation		
		$D_h(1)^a$ [nm]	$D_h(2)^b$ [nm]	PD	$D_h(1)$ [nm]	$D_h(2)$ [nm]	PD
1	(M1) ₇₀ -(M5) ₈₃	19 (99.9)		0.18	21 (99.8)		0.18
2	(M1) ₇₀ -(M6) ₁₄₀	42 (100)		0.11	42 (100)		0.10
3	(M1) ₈₅ -(M7) ₂₄	14 (99.5)		0.71			
4	PEO-(M5) ₂₂	29 (100)		0.42			
5	PEO-(M6) ₂₄	36 (100)		0.13			
6	(M6) ₁₂₀ -(M1) ₅₀	55 (56)	311 (44)	0.30	51 (52)	281 (48)	0.28
7	(M6) ₁₂₀ -(M1) ₁₀₉	51 (84)	1637 (16)	0.33	54 (100)		0.14

^a mean hydrodynamic diameter D_h of a first population of aggregates. 19 (99.9) means that 99.9 % of particles (by volume) have a D_h of 19 nm. ^b D_h of a second population of aggregates.

While control over the self-assembly in bulk as well as in solution is accomplished for diblock copolymers by the variation of molar mass and/or composition, linear ABC triblock copolymers can self-assemble into a greater variety of structures due to three Flory-Huggins interaction parameters (χ_{AB} , χ_{BC} , χ_{AC}) and the possibility to permute the block sequence. Although it was initially intended to prepare the sequences ABC, BAC and ACB of hydrophilic-lipophilic-fluorophilic block copolymers, samples with the fluorinated blocks as central block could not be prepared (cf. chapter 5.3) and hence, only the architectures comprising either lipophilic or hydrophilic central blocks could be analyzed.

The discussion is started with those polymers where the hydrophobicity increases stepwise along the chain, i.e. those with the sequence hydrophilic-lipophilic-fluorophilic. According to DLS the incorporation of the fluorinated block had no distinct effect on the size distributions of nanoparticles self-assembled from triblock copolymers (M1)₇₀-(M5)₈₃-(M7)₁₃, (M1)₇₀-(M6)₁₄₀-(M7)₁₃ and PEO-(M6)₂₄-(M7)₂ compared to the polymeric micelles of their diblock precursor polymers (cf. Figures 5.10a-b and 5.10d). Still, they exhibited mostly a broader distribution according to the PD value. The small changes of the particles size distribution compared to the precursor diblock copolymer are consistent with the low DP's for their fluorinated blocks. Assuming a fully stretched chain for the fluorinated block and identical

aggregation numbers, the mean hydrodynamic diameter would increase by about 6-7 nm only. In contrast, the hydrodynamic diameter of particles formed from triblock copolymer **PEO-(M5)₂₂-(M7)₂** increased dramatically compared to its precursor polymer micelles (Figure 5.10c). It is reasonable to assume that this particle size is only apparent, as it is too large for regular spherical micelles. Furthermore, the attachment of the very short fluorinated block should cause rather small changes of the micelle size. The origins of such large aggregates were already discussed above for diblock copolymer micelles. The presence of a few very large aggregates can interfere strongly with an accurate DLS analysis as it increases markedly the mean particle size, while concealing the small particle fraction. Under such circumstances, the particle size distributions may be misleading.

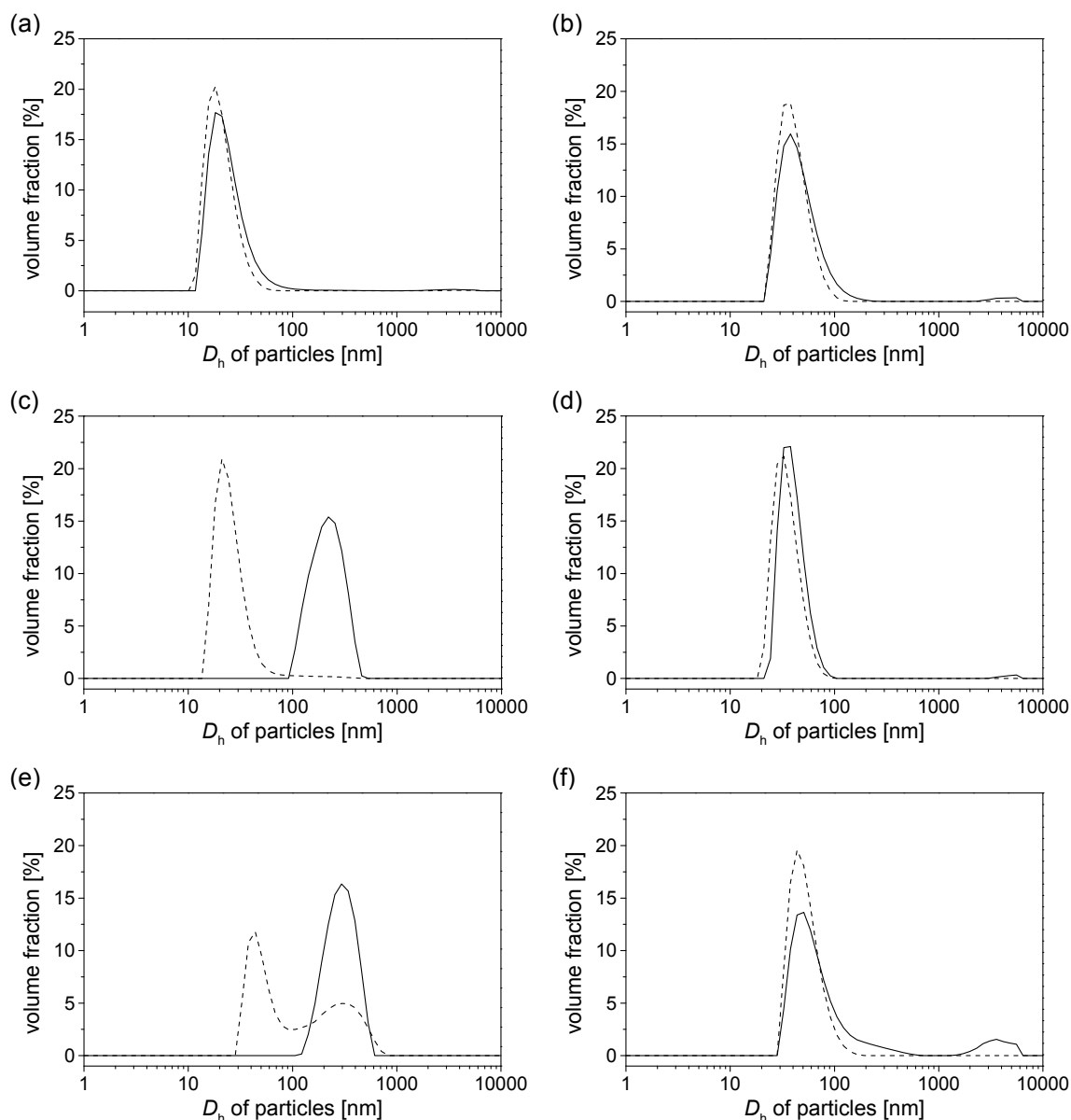


Figure 5.10 Comparison of particle size distributions in 0.5 wt% aqueous solutions of triblock copolymers (solid line) compared to the aggregates of their precursor diblock copolymers (dashed line) as studied by DLS: (a) **(M1)₇₀-(M5)₈₃-(M7)₁₃** (b) **(M1)₇₀-(M6)₁₄₀-(M7)₁₃** (c) **PEO-(M5)₂₂-(M7)₂** (d) **PEO-(M6)₂₄-(M7)₂** (e) **(M6)₁₂₀-(M1)₅₀-(M7)₄₀** (f) **(M6)₁₂₀-(M1)₁₀₉-(M7)₂₅**.

The second polymer architecture which was realized in the prepared triblock copolymers comprised the hydrophilic block in the centre of the macromolecule. Two samples with this block sequence and varied length of the hydrophilic block were prepared. The self-assembly of polymers bearing hydrophobic end-blocks usually results in the formation of more complex structures such as flower-like or interconnected micelles (cf. Fig. 4.13). Network formation would result for the prepared triblock copolymers in two populations of micellar cores (hydrocarbon and fluorocarbon domains) within a hydrophilic network. However, the low concentrations of block copolymer should preclude from physical cross-linking during micelle preparation and favor the formation of flower-like micelles.

For polymer **(M6)₁₂₀-(M1)₅₀-(M7)₄₀** - comprising a shorter hydrophilic middle block - a pronounced growth of particle size was observed compared to the micelles of the precursor polymer. Again, the determined particle size of 240 nm is too large to be the hydrodynamic diameter of a spherical micelle, as the contour length of the fully stretched polymer chain of **(M6)₁₂₀-(M1)₅₀-(M7)₄₀** would be 53 nm.

Table 5.5 Dynamic light scattering analysis of 0.5 wt% aqueous solutions of triblock copolymers prepared at 25°C (protocol A) and 70°C (protocol B)

entry	sample	prep. protocol	1d after preparation		2 weeks after preparation		4-6 weeks after preparation	
			$D_h(1)^a$ [nm]	PD	$D_h(1)$ [nm]	PD	$D_h(1)$ [nm]	PD
1	(M1)₇₀-(M5)₈₃-(M7)₁₃	A	22 (99.4)	0.44	26 (99.2)	0.36	28 (99.2)	0.35
2		B	23 (99.9)	0.24				
3	(M1)₇₀-(M6)₁₄₀-(M7)₁₃	A	39 (100)	0.24	47 (100)	0.21	47 (100)	0.18
4		B	38 (100)	0.20				
5	PEO-(M5)₂₂-(M7)₂	A	222 (100)	0.15				
6		B	30 (100)	0.11				
7	PEO-(M6)₂₄-(M7)₂	A	40 (99)	0.17				
8		B	43 (100)	0.24				
9	(M6)₁₂₀-(M1)₅₀-(M7)₄₀	A	239 (100)	0.15	292 (100)	0.07	295 (100)	0.08
10		B	82 (100)	0.09				
11	(M6)₁₂₀-(M1)₁₀₉-(M7)₂₅	A	72 (84) ^b	0.28	77 (90.9) ^b	0.26	72 (95.2) ^b	0.26
12		B	119 (100)	0.05				

^a mean hydrodynamic diameter D_h of a first population of aggregates. 22 (99.4) means that 99.4 % of particles (by volume) have a D_h of 22 nm. ^b second population were aggregates with dimensions >1 μ m and are attributed to micellar clusters.

According to the mean hydrodynamic diameter, the micelle size of polymer **(M6)₁₂₀-(M1)₁₀₉-(M7)₂₅** - comprising a much longer hydrophilic middle block - increased from 50 nm for the precursor diblock copolymer to 70 nm. However, this mean value is misleading as no shift of the particle size is observed but the distribution becomes broader with a higher percentage of large aggregates (cf. Fig. 5.10f). Additionally, a second population of very large aggregates with dimensions larger than 1 μ m was detected. These very large aggregates could not be removed by filtration prior to the DLS measurement

and are attributed to clusters which form by the interconnection of micelles via their hydrophobic end-blocks.

Some of the micellar solutions of triblock copolymers were reanalyzed after two weeks and once more after 4-6 weeks. Virtually, no changes of size or distribution were observed in the studied time interval. Thus, the polymeric micelles appeared to be very stable. As has been discussed before, it is difficult to judge whether this stability originates from the system being in thermodynamic equilibrium or from the frozen micellar exchange. The equilibration of micelles might be strongly hindered due to the crystalline fluorinated blocks. Therefore, a modified protocol for the preparation of micelles (denoted B) was exploited in which the temperature was increased to 70°C. Contrary to protocol A, the polymer solutions in THF were added dropwise to purified water (cf. chapter 7.5.2), however, the concentrations were the same as in protocol A. The temperature was chosen according to the results of thermal analysis by DSC which disclosed that the fluorinated blocks are molten in bulk at this temperature. The liquid state of the fluorinated block was expected to enhance the equilibration of micellar structures. The high temperature also led to an increased rate of solvent exchange as the common solvent THF was evaporated approximately within 1 h at 70°C compared to 24 h at ambient conditions. In the investigation of double-thermoreponsive polymers (chapter 4), the fast heating protocol produced smaller and more narrowly distributed particles. A similar effect was anticipated here due to the faster solvent exchange.

Although the preparation of micellar solutions at 70°C did not change the size of the particles self-assembled from polymers **(M1)₇₀-(M5)₈₃-(M7)₁₃**, **(M1)₇₀-(M6)₁₄₀-(M7)₁₃** and **PEO-(M6)₂₄-(M7)₂**, the size distributions became narrower according to the PD value (Table 5.5). For polymer **PEO-(M5)₂₂-(M7)₂**, the particle size decreased markedly and the calculated hydrodynamic diameter is close to the particle size found for its precursor polymer. For the two polymers with the hydrophilic block in the middle the higher temperature during micelle preparation affected markedly the particle size. Compared to the preparation at ambient conditions, the mean particle size decreased from 239 nm to 82 nm for polymer **(M6)₁₂₀-(M1)₅₀-(M7)₄₀**, while for polymer **(M6)₁₂₀-(M1)₁₀₉-(M7)₂₅** - with a larger hydrophilic middle block - the mean particle size increased. For both polymers, very narrow size distributions were found for the higher temperature preparation. Reanalyzing the micellar aggregates prepared by protocol B after one month showed that - as for protocol A - the self-assembled particles are very stable and no changes of particle size or size distribution were observed.

To summarize, the prepared di- and triblock copolymers self-assembled in water to form polymeric micelles. While large aggregates are sometimes formed from amphiphilic block copolymers by direct dissolution, such aggregates were mostly avoided by the dispersion procedure applied. The incorporation of the fluorinated block did not change notably the micellar characteristics for the block sequence hydrophilic-lipophilic-fluorophilic as studied by DLS. As the analysis of micellar characteristics by DLS provides an overall particle size, the formation of multi-compartment micelles with separate domains in their micellar cores could not be observed. Therefore, direct imaging by cryo-TEM was applied in the next step.

5.5.3. Survey of the micelle morphology by cryogenic transmission electron microscopy

In the past decade, cryogenic transmission electron microscopy (cryo-TEM) has evolved as one of the most powerful characterization tools in studying the self-assembly of amphiphiles.²⁷⁰ While the interpretation of results obtained by experimental techniques such as small-angle neutron (SANS), X-ray (SAXS) and light scattering (static and dynamic) is ambiguous, if structures of different size or morphology coexist, cryo-TEM provides detailed information about single aggregates by direct imaging. Recent developments – such as controlled devices for specimen preparation and the development of CCD cameras²⁷⁸ – facilitated the use of this technique regarding sample preparation and image processing.

Micellar aggregates of diblock copolymers

The precursor diblock copolymers were included in the study by cryo-TEM for several reasons. First of all, the formation of spherical micelles which are usually anticipated for amphiphilic diblock copolymers can be verified by direct imaging. Additionally, cryo-TEM helps to clarify the origins of the bimodality observed for some diblock copolymer micelles by DLS. More importantly, the comparison of di- and triblock copolymer micelles allows to evaluate the impact of the fluorinated block on the micelle formation. For example, the incorporation of the fluorinated block might not only be accompanied by a change of the size and/or distribution of particles, but might lead to a transition between different micelle morphologies, too.

Two examples of micellar aggregates formed in 0.5 wt% aqueous solutions of amphiphilic diblock copolymers are depicted in Figure 5.11. The dark grey spheres represent the micellar cores made of **polyM6** and **polyM7** with apparent core diameters of approximately 29 nm and 12 nm, respectively, embedded in a less electron-dense water matrix. As the hydrophilic coronas of polymeric micelles are well-solvated, their electron density is comparable to vitrified water. Accordingly, they usually give only marginal contrast and are invisible in the TEM micrographs. In the case of PEO-PB block copolymers, however, the hydrophilic corona became visible in cryo-TEM images at maximum phase contrast using digital imaging and processing techniques.^{279, 280} and was explained by the collapse of PEO chains in the vicinity of the hydrophobic PB interface.²⁸¹

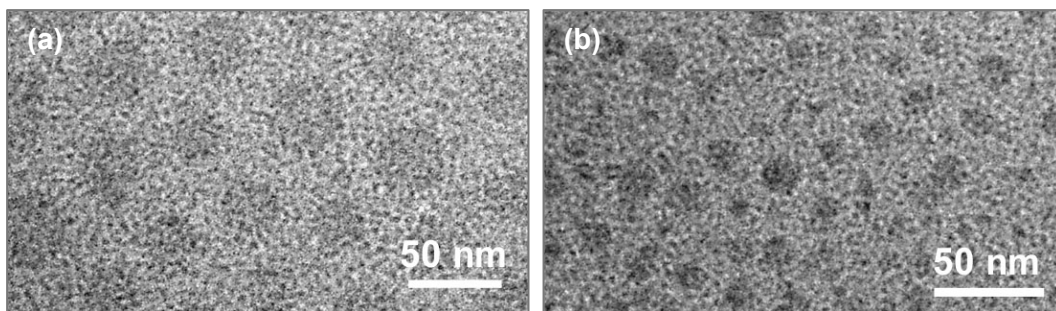


Figure 5.11 Cryo-TEM micrographs of 0.5 wt% aqueous solutions of amphiphilic diblock copolymers: (a) **(M6)₁₂₀-(M1)₅₀** (b) **(M1)₈₅-(M7)₂₄**.

In the micrographs of the prepared micellar solutions, the hydrophilic corona consisting of **polyM1** is partially visible as some sort of fibrous shell close to the surface of the micellar core. Most probably, this finding is due to the dense comb polymer architecture of **polyM1**. To further investigate this effect, a solution of pure **(M1)₇₀** was studied by cryo-TEM and compared to a sample of linear PEO ($M \sim 20,000$ g/mol). While in the case of the linear PEO sample no polymer could be discerned in the micrograph, a fine speckled pattern was found for the polyacrylate with oligo(ethylene oxide) side chains (see Fig. A3.1 in Appendix 3).

The corona thickness L of the polymeric micelles can be derived from the characteristic distance between the cores of closely packed micelles, as the repulsive interactions between polymer brushes on spherical interfaces were calculated to correspond closely to hard spheres.²⁸² That means, the coronas of star-like micelles penetrate each other only to a small extent. Consequently, the overall size of polymeric micelles can be determined from their micrographs and compared to the results from DLS (cf. Table 5.6). The particle sizes of the diblock copolymer micelles calculated from DLS and cryo-TEM measurements agree very well. Deviations were only found for very small particles (~ 20 nm) and are probably related to the decreasing resolution of cryo-TEM with decreasing particle size.

The DLS analysis of a 0.5 wt% aqueous solution of diblock copolymer **(M6)₁₂₀-(M1)₅₀** had revealed the presence of two populations of aggregates with hydrodynamic diameters of 55 nm and 300 nm, respectively. As the measurements were performed at a single angle only, it could not be clarified whether the second population of large particles is due to isotropic or anisotropic aggregates. The direct imaging by cryo-TEM showed the presence of a few large spherical aggregates with core diameter ranging from 100 nm to 200 nm (cf. Fig. A3.2a in Appendix 3). These objects were not vesicles as the contrast is homogeneous over the entire spheres while vesicles give maximum contrast for the bilayered wall. Although these aggregates are very large, they are still smaller than the mean hydrodynamic diameter determined by DLS. It has to be kept in mind that the sample thickness, through which the electron beam can penetrate (about 100-200 nm), is the size limiting factor for cryo-TEM measurements. That means, if larger objects are present, they cannot be observed by cryo-TEM and the micrographs might not reflect a representative picture of the bulk sample.

Block copolymer micelles proceed from the strong to the superstrong segregation limit with increasing interfacial tension. As a consequence, the morphology of micelles changes from spherical to disk-like.²⁸³⁻²⁸⁵ As the interfacial tension between water and the fluorinated **polyM7** block is very high, the hydrophilic-fluorophilic diblock copolymer **(M1)₈₅-(M7)₂₄** was expected to form disk-like micelles, too. Nevertheless, the TEM micrograph showed spherical objects (Fig. 5.11b). The osmotic chain crowding of the corona may preclude a disk-like morphology and favor the formation of small spherical micelles with a large interfacial curvature to relieve the chain crowding. However, the determined mean core diameter of the aggregates of polymer **(M1)₈₅-(M7)₂₄** ($D_{\text{core}} = 12$ nm) corresponds to the maximum diameter assuming a fully stretched chain and thus, is consistent with the super strong segregation limit.

Table 5.6 Characteristics of the micellar aggregates of amphiphilic di- and triblock copolymers as studied by cryo-TEM

sample	prep. ^a protocol	D_{core} ^b [nm]	$D_{\text{FC domain}}$ [nm]	$L_{\text{corona}} \times 2$ [nm]	D_{particle} [nm]	D_{h} by DLS [nm]
(M1) ₇₀ -(M5) ₈₃	A	~13 ^c 28	-	~18 ^c 17	~31	21
(M1) ₇₀ -b-(M6) ₁₄₀	A	(17-33, 100) 12	-	(11-22, 50) 13	45	42
(M1) ₈₅ -b-(M7) ₂₄	A	(4-17, 100) 12	-	(4-17, 30) 15	25	14
PEO-(M5) ₂₂	A	(8-31, 100) 21	-	(12-19, 50) 14	27	29
PEO-(M6) ₂₄	A	(13-26, 100) 29	-	(9-17, 50) 30	35	36
(M6) ₁₂₀ -(M1) ₅₀	A	(18-41, 100) 25	-	(14-41, 50) 18	59	55
(M6) ₁₂₀ -(M1) ₁₀₉	A	(15-35, 100)	-	(10-25, 50)	43	54
(M1) ₇₀ -(M5) ₈₃ -(M7) ₁₃	A	16 (9-18, 50)	- ^d	22 (14-32, 50)	38	22
	B	~14 ^c	- ^d	~7 ^c	21	23
	C	28 (20-35, 100)	11 (5-15, 40)	13 (10-15, 50)	41	-
(M1) ₇₀ -(M6) ₁₄₀ -(M7) ₁₃	A	32 (21-42, 100)	14 (8-25, 20)	18 (13-25, 50)	50	39
	B	28 (19-39, 40)	~13 ^e	27 (16-39, 50)	55	38
	C	34 (18-62, 40)	22 (13-35, 10)	30 (15-39, 30)	64	-
PEO-(M5) ₂₂ -(M7) ₂	A	12 (8-17, 100)	- ^d	9 (4-13, 50)	21	222
	B	15 (11-18, 100)	- ^d	18 (14-21, 50)	33	30
PEO-(M6) ₂₄ -(M7) ₂	A	21 (14-32, 100)	- ^d	15 (9-23, 50)	36	40
	B	20 (11-53, 100)	~4 ^f	15 (11-21, 50)	35	43
(M6) ₁₂₀ -(M1) ₅₀ -(M7) ₄₀	A	66 (31-150, 100)	~20 / ~8 ^h	- ^g		239
	B	46 (25-83, 100)	~20 / ~8 ^h	21 (8-25, 50)	67	82
	C	46 (25-120, 20)	~20 / ~8 ^h	- ^g		-
(M6) ₁₂₀ -(M1) ₁₀₉ -(M7) ₂₅	A	29 ⁱ (13-45, 50)	- ^l	30 ⁱ (19-39, 30)	59	72
	B	- ^k	- ^k	- ^k	- ^k	119
	C	36 (20-61, 100)	- ^l	16 (12-22, 50)	52	-

^a micelle preparation by solvent exchange at 25°C (A) and 70°C (B); solutions prepared by protocol A were annealed for 9-25 d at 78°C (C). ^b **28** (17-33, 100) means 100 counted micellar cores ranged from 17 to 33 nm and had a mean diameter of 28 nm. ^c due to very small aggregates and low contrast only approximate values are given. ^d segregated FC domains were not visible within the micellar cores. ^e FC domain was only partially visible. ^f thickness of single or multiple stacked domains within the micellar core. ^g as the micellar cores were irregularly packed, the corona thickness could not be determined from their interstitial distance. ^h fluorinated domains are disks which are about 20 nm in diameter and ~8 nm thick. ⁱ dimensions of irregularly shaped spherical aggregates. ^k no usable micrographs obtained. ^l thin FC “caps” partially covering the micellar core (cf. Fig. 5.16), dimensions difficult to determine due to 2D projection.

Micellar aggregates of triblock copolymers

While only an averaged particle size and size distribution could be determined for the self-assembled triblock copolymers by DLS, cryo-TEM visualizes individual micelles including their segregated domains. Thus, the morphology and dimensions of micellar aggregates self-assembled from triphilic block copolymers can be directly investigated and correlated with the molecular parameters of the polymers such as the block sequence or the length of their hydrophilic and hydrophobic blocks.

The discussion of cryo-TEM results for triblock copolymers is started with the polymers whose block sequence is hydrophilic-lipophilic-fluorophilic. From the samples prepared, those two with the hydrophilic blocks comprising oligo(ethylene oxide) side chains are considered first. Typical cryo-TEM images of 0.5 wt% micellar solutions of polymers $(\mathbf{M1})_{70}\text{-}(\mathbf{M5})_{83}\text{-}(\mathbf{M7})_{13}$ and $(\mathbf{M1})_{70}\text{-}(\mathbf{M6})_{140}\text{-}(\mathbf{M7})_{13}$ which were prepared by the solvent exchange procedure at ambient temperature are depicted in Figures 5.12.

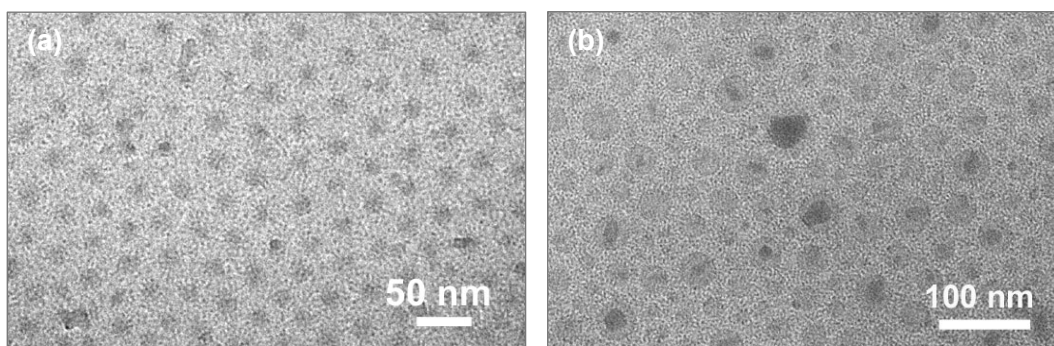


Figure 5.12 Cryo-TEM micrographs of 0.5 wt% aqueous solutions of amphiphilic triblock copolymers prepared at ambient conditions: (a) $(\mathbf{M1})_{70}\text{-}(\mathbf{M5})_{83}\text{-}(\mathbf{M7})_{13}$ (b) $(\mathbf{M1})_{70}\text{-}(\mathbf{M6})_{140}\text{-}(\mathbf{M7})_{13}$.

Both polymers self-assembled in water into spherical nanoparticles with the electron-dense spheres constituting the micellar cores, surrounded by the less electron-dense, speckled pattern of the hydrophilic corona. For polymer $(\mathbf{M1})_{70}\text{-}(\mathbf{M6})_{140}\text{-}(\mathbf{M7})_{13}$, further domains with a very strong contrast are visible within the micellar cores and the increased contrast is ascribed to the high electron density of the fluorinated block. The morphology of this triphilic block copolymer self-assembled in water is a core-shell-corona micelle with segregated lipophilic and fluorophilic domains. The core-shell-corona morphology emerges as a result of the polymer architecture, the mutual incompatibilities of the three blocks and their interfacial tension. Contacts between the lipophilic as well as the fluorinated domain and water are highly unfavorable. Furthermore, the lipophilic and the fluorophilic block are not compatible (as studied by DSC, cf. chapter 5.4) but covalently linked. Thus, the fluorinated domain is buried in the inner part of the micelle.

The presence of a fluorinated domain within the micellar aggregates of polymer $(\mathbf{M1})_{70}\text{-}(\mathbf{M5})_{83}\text{-}(\mathbf{M7})_{13}$ cannot be discerned. However, the cores of the aggregates are very small ($D_{\text{core}} \sim 16$ nm, cf. Table 5.6) for this polymer and the fluorophilic domain should even be smaller due to the low relative amount of the fluorinated block. Moreover, the difference in electron contrast between the lipophilic and the fluorophilic block is rather small, which complicates the detection of the fluorinated sub-domain within the aggregates of this polymer. The larger micellar core of polymeric micelles formed by polymer $(\mathbf{M1})_{70}\text{-}$

(M6)₁₄₀-(M7)₁₃ - compared to the aggregates of polymer **(M1)₇₀-(M5)₈₃-(M7)₁₃** - is consistent with its higher DP of the hydrophobic block.

Although the hydrophobic micellar cores of the aggregates of polymer **(M1)₇₀-(M6)₁₄₀-(M7)₁₃** appeared relatively uniform, their inner FC domains were irregularly shaped and showed a broad size distribution. In other words, while for some micelles no or only minute fluorinated domains were perceived, others contained large fluorinated cores. This finding could owe to the polydispersity in molar mass and composition of the block copolymer or to the non-equilibrated state of polymeric micelles. As has been discussed in the preceding chapter, the crystalline fluorinated block might prevent the equilibration of micellar structures. Therefore, the micellar solutions that were prepared above T_m of the fluorophilic block (protocol B) were also studied by cryo-TEM. In addition to this modified preparation procedure, the samples prepared according to protocol A were annealed at 75°C for several days and reanalyzed (protocol C).

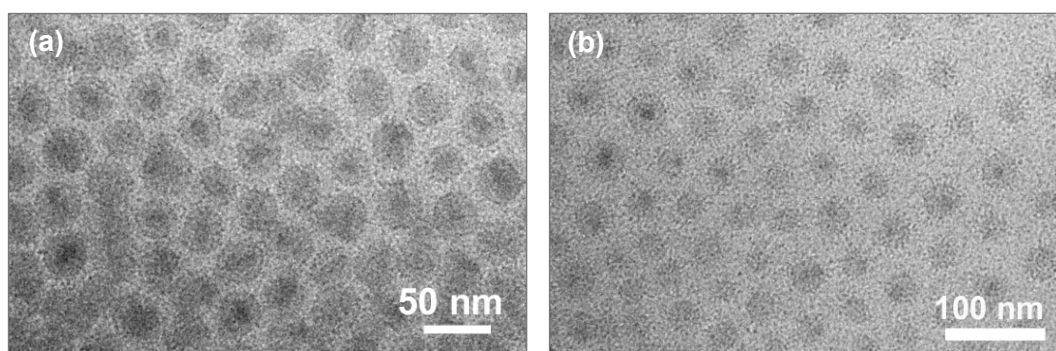


Figure 5.13 Cryo-TEM micrographs of 0.5 wt% aqueous solutions of amphiphilic triblock copolymers after thermal treatment: (a) **(M1)₇₀-(M5)₈₃-(M7)₁₃** after preparation by protocol A and annealing for 25 d at 78°C (= protocol C) (b) **(M1)₇₀-(M6)₁₄₀-(M7)₁₃** dispersed by protocol B.

While preparation protocol B did not affect the self-assembled state of polymer **(M1)₇₀-(M5)₈₃-(M7)₁₃**, annealing at higher temperatures had a pronounced effect on the appearance of the aggregates. Not only increased the average diameter of micellar cores from ~16 nm to ~28 nm, but the growth of micelles made also the fluorinated domains visible and a spherical core-shell-corona morphology emerged for this polymer, too. On the contrary, the thermal treatment at 78°C hardly affected the morphology or the size and distribution of aggregates formed by polymer **(M1)₇₀-(M6)₁₄₀-(M7)₁₃**. Instead protocol B resulted in a more homogeneous distribution of fluorinated domains.

Two more samples with the block sequence hydrophilic-lipophilic-fluorophilic had been prepared, namely polymers **PEO-(M5)₂₂-(M7)₂** and **PEO-(M6)₂₄-(M7)₂**. The block ratios of these oligomeric samples are comparable to the above discussed triblock copolymers, yet comprise a linear PEO chain (MW = 5000 g/mol) as the hydrophilic block. According to the cryo-TEM micrographs of their aqueous solutions, the oligomers formed small spherical micelles which were about 20 -40 nm for both preparation protocols (cf. Table 5.6). It is noteworthy that the hydrophilic corona is not visible in their micrographs. This supports the assumption given above that the dense comb polymer architecture of the **polyM1** block is responsible for the spotted halo seen around the micellar cores.

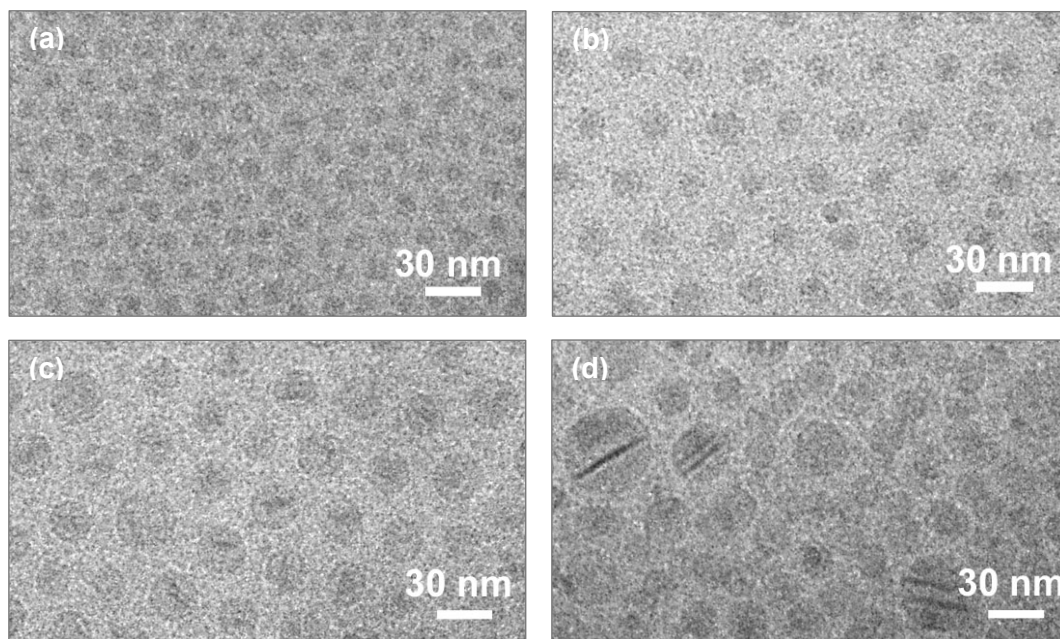


Figure 5.14 Cryo-TEM micrographs of ABC triblock oligomers with a linear PEO chain (0.5 wt% in water): **PEO-(M5)₂₂-(M7)₂** dispersed at (a) 25°C and (b) 70°C. **PEO-(M6)₂₄-(M7)₂** dispersed at (c) 25°C and (d) 70°C.

Although very large particles ($D_h \sim 200$ nm) were found by DLS when polymer **PEO-(M5)₂₂-(M7)₂** was dispersed at ambient temperature, the micrographs revealed that the overwhelming majority of objects were small polymeric micelles with $D_{\text{core}} \sim 10$ nm (Fig. 5.14a). Only a few large spherical objects with diameter of ~ 200 nm were found (cf. Fig. A3.2b in Appendix 3) which are probably responsible for the large mean particle size seen by DLS. As they exhibit an increased contrast at their edges, they might be vesicles. When the micellar solutions were prepared at 70°C applying protocol B, these large structures disappeared completely and the micrographs showed a very homogeneous distribution of small hexagonally packed micelles (Fig. 5.14b). The regular packing of micelles is probably a consequence of their narrow size distribution. However, no fluorinated domain could be discerned within the micellar cores, although the content of fluorinated repeating units in this polymer samples is 12 wt% according to fluoride ion chromatography (cf. Table 5.1). Similarly to the aggregates formed by polymer **(M1)₇₀-(M5)₈₃-(M7)₁₃**, the fluorinated domains might be too small to be resolved from their lipophilic environment.

Occasionally, elongated dark domains were observed within the micellar aggregates self-assembled from polymer **PEO-(M6)₂₄-(M7)₂** at ambient conditions (protocol A) (Fig. 5.14c), which point to the formation of segregated FC domains. Although preparation protocol B was intentionally employed to improve micellar equilibration, the self-assembled particles of polymer **PEO-(M6)₂₄-(M7)₂** exhibited a broader distribution of sizes compared to preparation method A (Fig. 5.14d). Nonetheless, protocol B made the fluorinated domains more clearly visible. Single or multiple stacked bands were observed within the lipophilic micellar cores but which were seen only in the larger polymeric micelles. It has to be kept in mind that cryo-TEM provides only a two-dimensional projection of a three-dimensional situation. Therefore, it is hypothesized that the dark domains are not rods or cylinders but flat disks which appear

as dark stripes only in the side-on view. However, this hypothesis needs to be verified by cryo electron tomography under tilted angles.

As has been confirmed before by experiment^{39, 69} and simulation,¹²⁴ linear ABC block copolymers form frequently micelles with a core-shell-corona morphology. However, this morphology must be regarded as not ideal for a multi-compartment system which is characterized by its ability to solubilize different substances in the respective compartments. If one hydrophobic compartment is enclosed in the other, the independent uptake and release of different solubilizates via the aqueous phase is expected to be obstructed.

The second polymeric architecture which was studied comprised the hydrophilic block in the middle of the macromolecule. The micrographs of the micellar aggregates formed from polymers **(M6)₁₂₀-(M1)₅₀-(M7)₄₀** and **(M6)₁₂₀-(M1)₁₀₉-(M7)₂₅** after application of the various preparation protocols are depicted in Figures 5.15 and 5.16. Polymer **(M6)₁₂₀-(M1)₅₀-(M7)₄₀** - comprising the shorter hydrophilic central block - formed spherical micelles with microphase-separated lipophilic and fluorophilic domains. Reminiscent of a soccer ball, the fluorinated domains were located as small disks predominately on the surface of the lipophilic micellar core. However, the fluorinated domains might be embedded within the lipophilic core, too. Conventional cryo-TEM cannot clarify this issue as it yields only a two-dimensional projection of three-dimensional objects. Using cryo electron tomography it was possible to show²⁸⁶ that the fluorinated domains are located at the surface as well as in the lipophilic core of larger micellar aggregates.

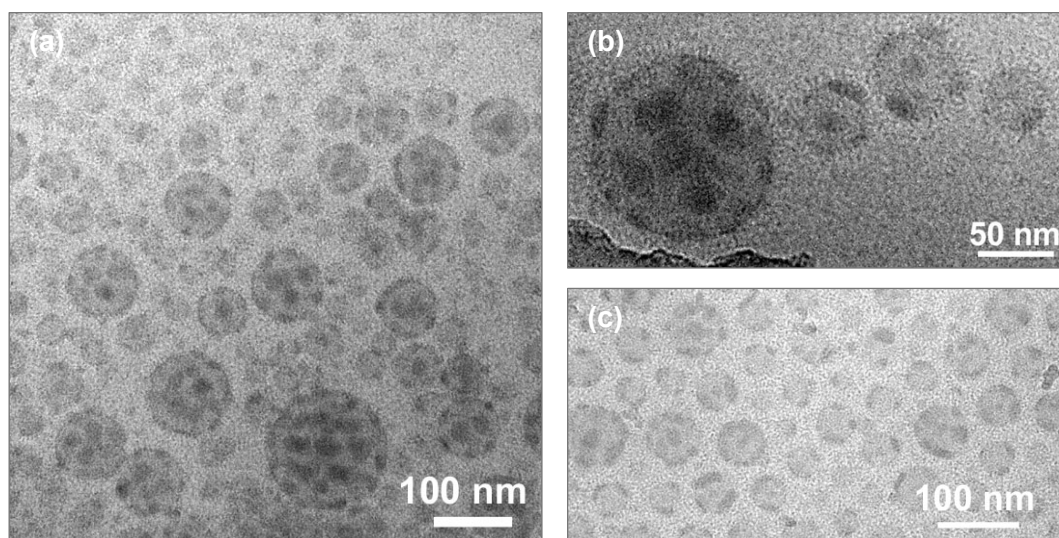


Figure 5.15 Cryo-TEM micrographs of triblock copolymer **(M6)₁₂₀-(M1)₅₀-(M7)₄₀** (0.5 wt% in water): (a) dispersed at 25°C (protocol A) (b) after dispersion at 25°C and annealing for 21 d at 78°C (protocol C) (c) dispersed at 70°C (protocol B).

The flat morphology of the fluorinated domain might be the consequence of the superstrong segregation limit which applies to the self-assembly of fluorinated materials. As another possibility, the disk-like domains could result from the crystalline fluorinated block.²⁸⁷ Although the micellar solution prepared by method A showed a broad distribution of sizes, the morphology is identical for all particle sizes.

Due to the solid-like fluorinated block, the polymeric micelles prepared from polymer **(M6)₁₂₀-(M1)₅₀-(M7)₄₀** at ambient conditions might be far from equilibrium. However, annealing of the aqueous solutions at 78°C had no visible effect on the morphology, size or distribution of aggregates. In agreement with the DLS result, the polymeric micelles prepared by method B were smaller and their size distribution narrower.

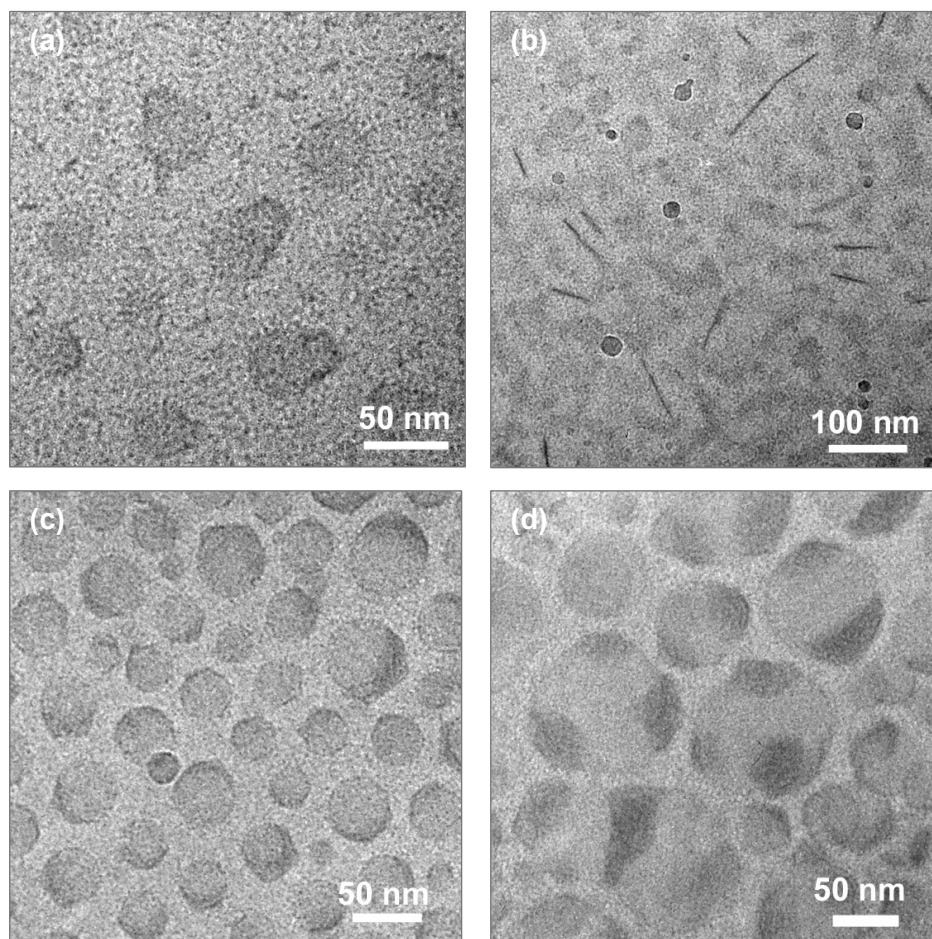


Figure 5.16 Micellar aggregates of triblock copolymer **(M6)₁₂₀-(M1)₁₀₉-(M7)₂₃** (0.5 wt% in water): Morphologies (a) and (b) were found for protocol A. Morphologies (c) and (d) evolved after annealing for 25 d at 78°C (protocol C).

Polymer **(M6)₁₂₀-(M1)₁₀₉-(M7)₂₅** with the same block sequence but with a longer hydrophilic block in the middle formed irregularly shaped spherical micelles (Fig. 5.16a) in addition to ribbon-like aggregates (Fig. 5.16b) after application of preparation protocol A. The cross-sectional diameter of the ribbon-like aggregates was approximately 10 nm and some of these aggregates contained a fluorinated domain. For the spherical aggregates, very thin but dark domains could be discerned on parts of the surface of the micellar core and were attributed to the FC domain. These thin domains appeared angular which might be a result of the crystallinity of the fluorinated block.

Dramatic changes of morphology occurred for polymer **(M6)₁₂₀-(M1)₁₀₉-(M7)₂₅** upon annealing. The irregularly shaped and ribbon-like aggregates disappeared while spherical micelles (Fig. 5.16c) and much larger aggregates (Fig. 5.16d) emerged. The smaller spherical micelles exhibited a core diameter of approximately 40 nm. In contrast to the polymeric micelles of polymer **(M6)₁₂₀-(M1)₅₀-(M7)₄₀**, the set of

smaller isolated fluorinated domains is replaced by one single, but larger domain on the lipophilic core (Fig. 5.16c). Located on the surface of the micellar core the fluorinated domain showed frequently edges. The angular shape could be an indication of the propensity of the fluorinated domains to undergo crystalline ordering.

The larger aggregates which evolved upon annealing of aqueous solutions of polymer **(M6)₁₂₀-(M1)₁₀₉-(M7)₂₅** have a shape which is similar to the above-mentioned soccer ball morphology. Being much larger than the aggregates with a single FC domain these aggregates are hypothesized to evolve by the fusion of smaller micelles.

5.5.4. Summary

Despite the high contents of hydrophilic block comprising either linear or comb PEO chains, the prepared amphiphilic triblock copolymers could not be directly dissolved in water. Instead, the polymers were dispersed via an optimized solvent exchange procedure starting from a common solvent for all polymer blocks. A variety of solvents was tested and THF was found to give optimal results - as was evidenced by DLS and ¹⁹F NMR spectroscopy. Upon the exchange of THF against water, all amphiphilic triblock copolymers self-assembled into micellar aggregates.

The particle sizes and distributions of self-assembled triblock copolymers were determined by DLS. The polymeric micelles exhibited mostly monomodal distributions with hydrodynamic diameters below 100 nm and the aggregates were found to be very stable upon annealing at ambient conditions. Due to the strong incompatibility of the hydrophobic blocks with the aqueous environment the exchange of micelles and unimers is probably extremely slowed down. The survey of the thermal properties of the bulk polymers revealed that the fluorinated blocks are crystalline at ambient temperature and might prevent the equilibration of micelles. According to these results, micelles were prepared above the melting temperature of the fluorinated block, and partially, remarkable changes of micelle sizes were observed. The higher temperature during micelle preparation produced in general smaller and more narrowly distributed aggregates.

Although the DLS analysis allowed the assessment of overall sizes of polymeric micelles, no conclusions regarding the micellar morphologies could be drawn. Direct imaging by cryo-TEM was the preferred method owing to the complex morphologies which were anticipated for the prepared materials. The fluorine atoms provided high electron contrast and therefore, the segregated lipophilic and fluorophilic domains were discernible without additional staining. Two polymeric architectures were studied, namely the sequence hydrophilic-lipophilic-fluorophilic (ABC) and its permutation with the hydrophilic block as central block (BAC). The ABC triblock copolymers formed in general core-shell-corona micelles with concentric fluorophilic and lipophilic domains. Indications for a novel version of this morphology – namely single or multiple fluorophilic disks within a lipophilic sphere were found but need to be confirmed by cryo electron tomography under tilted angles. For the BAC polymeric architecture a new micelle morphology was found, too, which comprised fluorophilic disks floating on the surface of the spherical lipophilic core. Increasing the length of the hydrophilic block for this polymer architecture resulted in changes of the relative sizes of lipophilic and fluorophilic domains but the principal micelle morphology was retained.

6. GENERAL CONCLUSIONS

New ABC triblock copolymers that self-assemble into complex micellar aggregates in water were synthesized by Reversible Addition Fragmentation chain Transfer (RAFT) using the chain transfer agents (CTAs) 4-cyano-4-thiobenzoylsulfanyl pentanoic acid and 2-(butylsulfanylthiocarbonylsulfanyl)-2-methyl propionic acid. RAFT was the method of choice due to its great versatility regarding monomers and reaction conditions. The polymers prepared by RAFT bear thiocarbonylthio end-groups at the chain ends which absorb light in the UV and visible range. Thus, the concentration of RAFT active end-groups is conveniently determined by UV-vis spectroscopy and the molar mass can be calculated assuming 100% end-group functionalization.

Despite their crucial role for the control of polymerization, the RAFT active end-groups are hitherto rarely quantified by UV-vis spectroscopy. In principle, both absorptions of the thiocarbonyl bond can be utilized for end-group analysis, but the absorption in the UV range is more suited due to its much higher intensity. In the rare cases of end-group analysis by UV-vis, it has been assumed that the thiocarbonylthio end-groups at the polymer chain ends exhibit the same absorption characteristics as the primary CTA which was employed for the polymerization. In order to scrutinize this hypothesis, a variety of dithiobenzoate and trithiocarbonate RAFT agents with secondary, tertiary and benzylic re-initiating R groups was synthesized and studied by UV-vis spectroscopy. The investigation showed that the intensities of the absorptions depend sensitively on both, the substitution pattern next to the thiocarbonylthio moiety and the solvent. Hence, model compounds for polyacrylamide and polyacrylate macroCTAs bearing trithiocarbonate end-groups were synthesized and their absorption characteristics were used as basis for the end-group analysis of the prepared amphiphilic triblock copolymers. With these provisions met, end-group analysis by UV-vis spectroscopy proved to be a reliable and convenient alternative method of molar mass determination.

Two different approaches to the advanced self-assembly of ABC triblock copolymers in water were explored. The first studied system relied on double-thermoresponsive triblock copolymers whose self-assembly is triggered and modified “on demand” by an increase of temperature as the constituting blocks exhibit lower critical solution temperature (LCST) behavior. The prepared triblock copolymers comprised poly(*N,N*-dimethyl acrylamide) as the permanently hydrophilic and poly(*N*-isopropyl acrylamide) and poly(*N*-acryloyl pyrrolidine) as the two thermoresponsive blocks. Since the phase transition temperatures of the latter polymers differ by about 20 K, switching between different self-assembled structures as a function of temperature was anticipated. Double-thermoresponsive polymers exhibit certain advantages compared to classical amphiphilic block copolymer. First, they can be synthesized under homogeneous conditions and second, their dispersion in water precludes from arduous procedures. The block sequence ABC of the prepared triblock copolymers was systematically varied (BAC, ACB) in order to study the influence of the polymer architecture on the self assembly.

While the phase transition of the block with the lower LCST switches the polymer from the double-hydrophilic to the amphiphilic state, the second phase transitions should decrease its hydrophilic-hydrophobic balance. The onset of self-assembly due to the first phase transition could be followed straightforwardly by turbidimetry and dynamic light scattering, but the changes evoked by the second

phase transition were not as easily discerned. Still, both thermoresponsive blocks collapsed upon heating – as was evidenced by ^1H NMR spectroscopy in D_2O . However, attached polymer blocks appeared to affect each other in their coil-to-globule transitions. Noteworthy, not even physical mixtures of the respective homopolymers showed a purely additive behavior since the clouding temperatures were partly shifted in presence of the other homopolymers. Moreover, the self-assembly of the double-thermoresponsive triblock copolymers is subject to slow kinetics and depends sensitively on the applied heating rate. In general, fast heating resulted in smaller aggregate sizes and narrower particle size distributions.

The second approach towards a more elaborate self-assembly of block copolymers exploited the thermodynamic incompatibility of three fragments with very disparate affinities. The prepared triblock copolymers comprised poly(oligoethylene oxide monomethyl ether acrylate) as the hydrophilic, either poly(*n*-butyl acrylate) or poly(2-ethylhexyl acrylate) as the lipophilic and poly(1,1,2,2-tetrahydroperfluorodecyl acrylate) as the fluorophilic block. As for the double-thermoresponsive triblock copolymers, the block sequence was varied. According to differential scanning calorimetry, the triblock copolymers were microphase-separated in bulk, which is an essential requirement for their self-assembly into micelle-like aggregates with sub-structured cores. The self-assembly of triblock copolymers was studied by ^1H and ^{19}F NMR spectroscopy, DLS and cryogenic transmission electron microscopy (cryo-TEM).

According to DLS, the triblock copolymers self-assembled into polymeric micelles with dimensions below 100 nm and which exhibited mostly a monomodal particle size distribution. The stability of these aggregates upon annealing at ambient conditions for 1-1.5 months was attributed to the strong incompatibility of the hydrophobic blocks with the aqueous environment and the crystalline state of the fluorinated block which precludes the equilibration of micelles. Changes of the particle size, its distribution and the aggregate's morphology occurred after annealing the micellar solutions above the melting temperature of the crystalline fluorinated block (70-75°C) or when the micelles were prepared at this temperature.

The polymeric micelles were studied by cryo-TEM in order to prove the formation of a multicompartiment micellar system comprising a sub-structured micellar core. The morphology of the micelle-like aggregates was found to be controlled by the block sequence as well as by the composition of the block copolymers. In general, the ABC triblock copolymers with the sequence hydrophilic-lipophilic-fluorophilic formed core-shell-corona micelles with concentric fluorophilic and lipophilic domains. Indications for another version of this morphology – namely single or stacked fluorophilic disks within a lipophilic sphere - were found but need to be confirmed by cryo electron tomography under tilted angles.

An unprecedented new micelle morphology was found for the block sequence lipophilic-hydrophilic-fluorophilic as the aggregates comprise flat fluorophilic disks on the surface of the spherical lipophilic core and are reminiscent of a soccer-ball. Such a micelle morphology constitutes an optimal starting point for studying the selective and independent uptake and release of lipophilic and fluorophilic solubilizates as both hydrophobic domains are in contact with the aqueous phase.

7. EXPERIMENTAL PART

7.1. Analytical methods

^1H (300 MHz), ^{13}C (75 MHz) and ^{19}F NMR (282 MHz) spectra were taken with a Bruker Avance 300 apparatus. Temperature dependent ^1H NMR spectra for thermoresponsive polymers were recorded with a Bruker Avance 500 (500 MHz). If not stated otherwise all spectra are referenced to the respective solvent residual peak (CHCl_3 7.26 ppm; HDO 4.79 ppm).

IR-spectra were taken from KBr pellets using a Bruker IFS 66/s FT-IR spectrometer.

Mass spectra were recorded by a GC/MS system Trace DSQ II (Thermo Scientific).

UV-vis spectra were recorded with a Cary 5000 UV-vis spectrophotometer (Varian) using quartz glass cuvettes (Suprasil, Hellma, Germany) with an optical path length of 1.0 cm. Solvents used for determination of molar absorptivities and molar mass by end-group analysis were all spectrophotometric grade.

Elemental analyses were carried out using a Vario ELIII microanalyzer (Elementar Analysensysteme, Germany).

The fluorine contents of the amphiphilic triblock copolymers were determined after combustion in oxygen (Schöniger method) which converted the organic fluorine into fluoride. Fluoride was quantified by **ion chromatography** using a 761 Compact IC apparatus (Metrohm AG, Herisau, Switzerland) equipped with suppressor technology, an autosampler and an electric conductivity detector. The column used was a Metrosep A Supp 5 (inner diameter 4 mm, length 250 mm, particle size 10 μm) with an eluent concentration of 3.2 mM sodium carbonate and 1.9 mM sodium hydrogen carbonate (flow rate: 0.7 mL/min).

Size exclusion chromatography (SEC) of the acrylamide based polymers was run at 25 °C in *N*-methyl pyrrolidone (N-MP (>99%, Fluka) with 0.05 M LiBr (flow rate: 0.500 mL/min) using a TSP apparatus (Thermo Separation Products from Thermo-Finnigan GmbH, Dreieich, Germany) equipped with a Shodex RI-71 refractive index detector, a TSP UV detector (270 nm), and a set of PSS GRAM columns (polyester, 100 Å and 1000 Å porosity, 7 μm particle size). Calibration was performed with polystyrene standards (PSS GmbH Mainz, Germany).

SEC of the acrylate based polymers was run at 25°C in THF (flow rate: 1.0 mL/min) using a TSP apparatus (Thermo Separation Products from Thermo-Finnigan GmbH, Dreieich, Germany) equipped with a Shodex RI-71 refractive index detector, a TSP UV detector (260 nm), and a set of PSS SDV columns (styrene/divinyl benzene, 100 Å and 1000 Å porosity, 5 μm particle size). Calibration was performed with polystyrene standards (PSS GmbH Mainz, Germany).

Aqueous size exclusion chromatography (ASEC) for **polyM1** homopolymers was performed using a Spectra Physics Instruments apparatus (Columns: TSK GEL® (polyglycidyl (meth)acrylate-gel) from TOSOH: Guard, 6000, 5000, 3000 and 40). Aqueous 0.2 M Na_2SO_4 containing 1 wt% of acetic acid was used as eluent at a flow rate of 1.0 mL/min. Evaluation was done by Multi-Angle Laser Light

Scattering (MALLS) (Wyatt DAWN DSP, Wyatt, Santa Barbara, CA/USA, laser wavelength 632 nm). Calibration was performed with pullulan standards (PSS GmbH Mainz, Germany).

Thermal properties of the amphiphilic polymers were measured with a TGA/SDTA 851 **thermal gravimetric** analyzer (TGA) (Mettler Toledo) and a DSC 822 **differential scanning calorimeter (DSC)** (Mettler Toledo) under nitrogen atmosphere.

Turbidimetry was performed using a temperature controlled turbidimeter (model TP1, E. Tepper, Germany) with heating and cooling rates of 1.0°C/min. Transmittance of polymer solutions was set automatically to 90 % prior to each measurement.

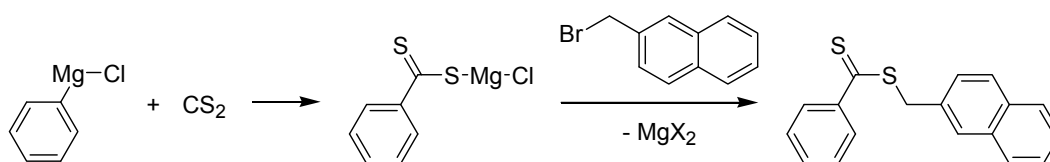
Dynamic Light Scattering (DLS) for the characterization of micellar solutions was performed with a High Performance Particle Sizer (HPPS-ET, from Malvern Instruments, UK) equipped with a He-Ne laser ($\lambda = 633$ nm) and a thermoelectric Peltier element for controlling the temperature (temperature control range: 10-90°C). The measurements were carried out at a scattering angle $\theta = 173^\circ$ ("backscattering detection"). The autocorrelation functions were analyzed with the CONTIN method. The apparent hydrodynamic diameters D_h of micelles or aggregates were calculated according to the Stokes-Einstein equation, $D_h = kT/3\pi\eta D_{app}$, with D_{app} being the apparent diffusion coefficient and η the viscosity of the solution. The polydispersity value PD of particle size distributions is calculated from the ratio $\mu_2 / \bar{\Gamma}$ where $\bar{\Gamma}$ is the first cumulant or average decay rate and μ_2 is the second cumulant, both derived from the cumulant fit of the intensity correlation functions. A PD value < 0.1 usually indicates a high homogeneity in the particle population. Prior to measurements, the polymer solutions were filtered into a quartz glass cuvette (Suprasil from Hellma, Germany) with an optical path length of 1.0 cm using a WICOM OPTI-Flow 0.45 μm disposable filter. Temperature dependent DLS measurements were run with a heating program from 25°C to 65°C in steps of 1.0°C, equilibrating the samples for 10 min at each step. For each measurement, the optimal measurement position, i.e. the optimal distance of the focal point from the cuvette wall, and the optimal attenuator was automatically determined by the HPPS software (Dispersion Technology Software 4.0).

Cryogenic Transmission Electron Microscopy (cryo-TEM) measurements were carried out in cooperation with Hans von Berlepsch and Christoph Böttcher at the Research Center for Electron Microscopy, Freie Universität Berlin. The samples for cryo-TEM were prepared at room temperature by placing a droplet (10 μL) of the solution on a hydrophilized perforated carbon filmed grid (60 s Plasma treatment at 8 W using a BALTEC MED 020 device). The excess fluid was blotted off to create an ultra thin layer (typical thickness of 100 nm) of the solution spanning the holes of the carbon film. The grids were immediately vitrified in liquid ethane at its freezing point (-184°C) using a standard plunging device. Ultra-fast cooling is necessary for an artifact-free thermal fixation (vitrification) of the aqueous solution avoiding crystallization of the solvent or rearrangement of the assemblies. The vitrified samples were transferred under liquid nitrogen into a Philips CM12 transmission electron microscope using the Gatan cryoholder and -stage (Model 626). Microscopy was carried out at -175°C sample temperature using the microscopes low dose mode at a primary magnification of 58300 x. The defocus was chosen to be 1.5 μm .

7.2. Synthesis of chain transfer agents

The chemicals used for the synthesis of chain transfer agents were used without further purification if not stated otherwise. Reagents and solvents were dried according to standard procedures when necessary. Solvents used for purification were analytical grade. **CTA3**, **CTA4** and **CTA11** were synthesized by Achille Mayelle Bivigou Kumba and **CTA9** by Daniel Zehm (both University of Potsdam, Golm). The CTA cumyl dithiobenzoate (CMDB) was a gift from Murat Mertoglu (University of Potsdam, Golm). 4-cyano-4-thiobenzoylsulfanyl pentanoic acid (**CTA1**) was synthesized as described by Thang et al.¹⁸²

7.2.1. Synthesis of naphthalene-2-ylmethyl dithiobenzoate (**CTA2**)



Materials

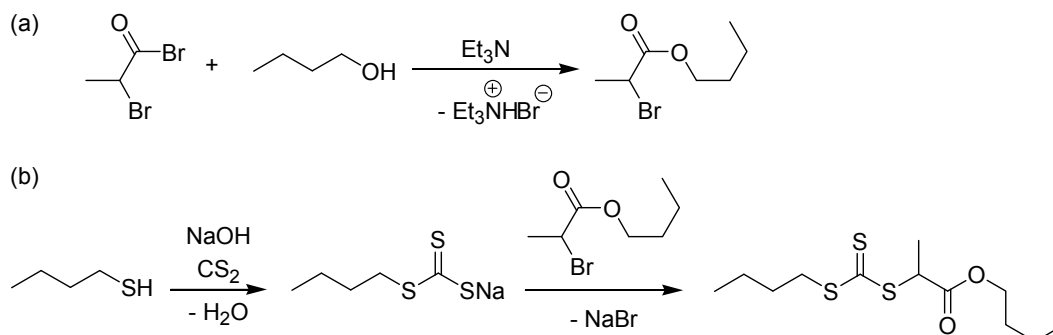
Phenylmagnesium chloride (Aldrich, 2 M in THF), CS₂ (Aldrich, 99+ %, anhydrous), 2-bromomethyl-naphthalene (Aldrich, 96%), THF (Merck, extra pure, dried and distilled over Na/K), MgSO₄ (Acros, anhydrous)

Procedure

CTA2 was synthesized by alkylation of the dithioacid salt according to a general procedure.²⁸⁸ Under nitrogen, 2.66 g (35 mmol) of CS₂ were added slowly to 16.5 ml (33 mmol) of phenylmagnesium chloride solution (2 M in THF) at ambient temperature. 11.21 g (50 mmol) of 2-bromomethyl naphthalene dissolved in 10 mL of THF were added at 30°C within 15 min. After maintaining the reaction mixture for 2 h at 50°C, 250 mL of cold water were added and the organic products were extracted in two portions with 300 mL of diethyl ether. The ether phase was washed with 250 mL of brine, dried over anhydrous MgSO₄ and concentrated. According to thin layer chromatography (n-hexane/CH₂Cl₂, 4:1 by volume) the raw material contained at least six by-products. The removal of all impurities necessitated two successive purification steps by column chromatography (silica gel 60, 0.040-0.063 mm) using first cyclohexane and then n-hexane/CH₂Cl₂ (4:1 by volume) as the eluent. Only fractions that were pure according to TLC were collected and combined. After removal of the solvent in vacuo the pure product was obtained as red solid (0.96 g).

m.p. 84 °C **Elemental analysis** (C₁₈H₁₄S₂, M_r = 294.43): Calc: **C** 73.43, **H** 4.79, **S** 21.78. Found: **C** 73.82, **H** 4.81, **S** 20.15. **MS** (EI, negative ions): m/z = 294. **¹H NMR** (300 MHz in CDCl₃, δ in ppm): δ = 4.78 (s, 2H, -CH₂-aryl), 7.36-7.41 (t, 2H, C(3)H phenyl), 7.47-7.56 (m, 1H + 3H, C(4)H phenyl, naphthyl), 7.82-7.88 (m, 4H, naphthyl), 8.02-8.04 (d, 2H, C(2)H phenyl). **¹³C NMR** (75 MHz in CDCl₃, δ in ppm): δ = 42.5 (-CH₂-aryl), 126.1, 126.4, 126.9, 127.0, 127.7, 128.2, 128.3, 128.5 (CH aryl), 132.4, 132.8, 133.3 (C aryl), 144.8 (C(1) phenyl), 227.5 (-C(=S)-S-). **FT-IR** (KBr, selected bands, wavenumber in cm⁻¹): 3053, 1593, 1444, 1225, 1041, 889, 822, 756.

7.2.2. Synthesis of butyl 2-(butylsulfanylthiocarbonylsulfanyl) propionate (CTA5)

**Materials**

2-bromopropionyl bromide (Fluka, purum $\geq 97.0\%$ AT), 1-butanol (Merck, extra pure), CH_2Cl_2 (Acros, pure, stabilized with 100 ppm amylene), triethylamine (Acros, pure), 1-butanethiol (Acros, 98%), NaOH (Fluka, puriss. p.a., ACS reagent, pellets), CS_2 (Aldrich, 99.9+%, ACS reagent), THF (Merck, extra pure), MgSO_4 (Acros, anhydrous)

Procedure**Synthesis of butyl 2-bromo-propionate**

Triethylamine (13 mL, 94 mmol) and 1-butanol (8.5 g, 115 mmol) were mixed with 100 mL of CH_2Cl_2 in a 500 mL round bottom flask equipped with a stir bar and a rubber septum. The mixture was cooled to 0°C and 10 mL (95 mmol) of 2-bromopropionyl bromide were added dropwise under stirring. The reaction mixture was maintained at 0°C for 30 min and then stirred at ambient temperature overnight. The precipitated triethylammonium bromide was filtered off and washed with CH_2Cl_2 . The collected organic phases were washed with dilute HCl and brine. After drying over MgSO_4 and evaporation of the solvent, the crude product was obtained as light yellow oil. Vacuum distillation at 65°C (2 mbar) gave 13.7 g (69%) of a colorless liquid.

$^1\text{H-NMR}$ (300 MHz in CDCl_3 , δ in ppm): $\delta = 0.92$ (t, 3H, $\text{CH}_3\text{-CH}_2\text{-}$), 1.32-1.44 (m, 2H, $-\text{O-C-CH}_2\text{-}$), 1.58-1.67 (m, 2H, $-\text{O-C-CH}_2\text{-}$), 1.80 (d, 3H, $\text{CHBr(CH}_3\text{)-}$), 4.08-4.21 (m, 2H, $-\text{O-CH}_2\text{-}$), 4.31-4.38 (m, 1H, $-\text{CHBr-}$). **$^{13}\text{C-NMR}$** (75 MHz in CDCl_3 , δ in ppm): $\delta = 13.6$ ($\text{CH}_3\text{-CH}_2\text{-}$), 18.9 ($-\text{O-C-CH}_2\text{-}$), 21.6 ($\text{CHBr(CH}_3\text{)-}$), 30.4 ($-\text{O-C-CH}_2\text{-}$), 40.2 ($\text{CHBr(CH}_3\text{)-}$), 65.7 ($-\text{O-CH}_2\text{-}$), 170.2 ($-\text{C(=O)-O-}$).

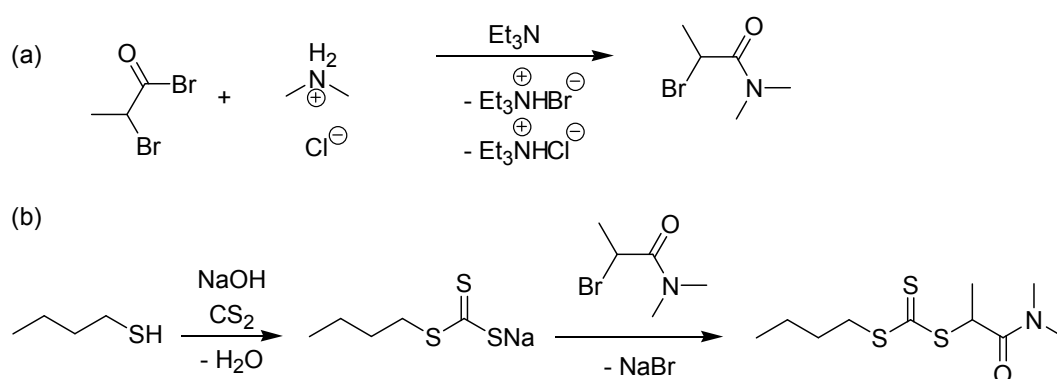
Synthesis of butyl 2-(butylsulfanylthiocarbonylsulfanyl) propionate

Under nitrogen flow, 4.98 g (62.2 mmol) of a 50 wt% aqueous solution of NaOH were added to 5.61 g (62.2 mmol) of 1-butanethiol dissolved in 30 mL THF. Upon dropwise addition of 4.74 g (62.2 mmol) of CS_2 , the white suspension became a clear, bright yellow solution. The reaction mixture was stirred for additional 10 min before 13.0 g (62.3 mmol) of butyl 2-bromo-propionate were added within 10 min. The reaction mixture was stirred at ambient temperature overnight. To the reaction mixture were added 100 mL of water and the aqueous phase was extracted twice with 100 mL of n-hexane. The combined hexane phases were washed with water and dried with anhydrous MgSO_4 . After evaporation of the solvent the crude product was obtained as orange-colored oil (17.0 g) which did not crystallize in the cold (4°C). The crude product contained two by-products according to TLC. As Kugelrohr distillation led to

decomposition, a fraction (3.7 g) of the raw material was purified by column chromatography (silicagel 60, Merck, 0.040-0.063 mm, eluent: n-hexane). Yield: 3.1 g (79 %).

Elemental analysis ($C_{12}H_{22}O_2S_3$, $M_r = 294.50$): Calc: **C** 48.94, **H** 7.53, **S** 32.66. Found: **C** 48.75, **H** 7.47, **S** 31.73. **MS** (EI, negative ions): $m/z = 294$. **1H -NMR** (300 MHz in $CDCl_3$, δ in ppm): $\delta = 0.92$ (t, 3H + 3H, $CH_3-CH_2^-$), 1.31-1.48 (m, 2H + 2H, $CH_3-CH_2^-$), 1.57-1.72 (m, 2H + 2H + 3H, $-O-C-CH_2^-$, $-S-C-CH_2^-$, $-S-CH(CH_3)-$), 3.36 (t, 2H, $-S-CH_2^-$), 4.13 (t, 2H, $-O-CH_2^-$), 4.81 (q, 1H, $-S-CH(CH_3)-$). **^{13}C -NMR** (75 MHz in $CDCl_3$, δ in ppm): $\delta = 13.5$ ($-O-C-C-C-CH_3$; $-S-C-C-C-CH_3$), 16.9 ($-S-CH(CH_3)-$), 19.0 ($-O-C-C-CH_2^-$), 22.0 ($-S-C-C-CH_2^-$), 29.9 ($-S-C-CH_2^-$), 30.5 ($-O-C-CH_2^-$), 36.8 ($-S-CH_2^-$), 48.0 ($-S-CH(CH_3)-$), 65.6 ($-O-CH_2^-$), 171.1 ($-C(=O)-O-$), 222.0 ($-S-C(=S)-S-$). **FT-IR** (KBr, selected bands, wavenumber in cm^{-1}): 2958, 2931, 2872, 1732, 1455, 1378, 1305, 1247, 1159, 1056, 812.

7.2.3. Synthesis of *N,N*-dimethyl 2-(butylsulfanylthiocarbonylsulfanyl) propionamide (**CTA6**)



Materials

2-bromopropionyl bromide (Fluka, purum $\geq 97.0\%$ AT), dimethylamine hydrochloride (Fluka, purum, $\geq 98\%$ AT), CH_2Cl_2 (Acros, pure, stabilized with 100 ppm amylene), triethylamine (Acros, pure), 1-butanethiol (Acros, 98%), NaOH (Fluka, puriss. p.a., ACS reagent, pellets), CS_2 (Aldrich, 99.9+ %, ACS reagent), THF (Merck, extra pure), $MgSO_4$ (Acros, anhydrous)

Procedure

Synthesis of N,N-dimethyl 2-bromopropionamide with *N,N*-dimethyl 2-chloropropionamide as by-product

N,N-dimethyl 2-bromopropionamide was synthesized according to the procedure by Rademacher et al.²⁶² To a stirred suspension of 9.4 g (115 mmol) of dimethylamine hydrochloride in 150 mL of CH_2Cl_2 were added 26 mL (187 mmol) of Et_3N at 0 °C. After the hydrochloride dissolved almost completely, 2-bromopropionylbromide (10 mL, 95 mmol) was added dropwise and a white suspension formed. The reaction was maintained for 30 min at 0 °C and stirred for 2 h at ambient temperature. The precipitated triethylammonium bromide and chloride was filtered off and washed with CH_2Cl_2 . The collected organic phases were dried over $MgSO_4$ and the solvent was evaporated in vacuo to afford the product as yellow oil. Vacuum distillation at 85 °C (1.0 mbar) gave 11.21 g of a colorless liquid. In the 1H and ^{13}C NMR spectra of the distilled product “extra” peaks were observed, which were attributed to the chloro-substituted propionamide (Br : Cl = 3:1) as by-product due to a Finkelstein reaction. As trithiocarbonate salts are strongly nucleophilic and are efficiently alkylated by bromides as well as by chlorides, it was not

necessary to separate the products. Thus, the 3:1 mixture of bromo- and chloro-substituted propionamide was used for the synthesis of **CTA6**.

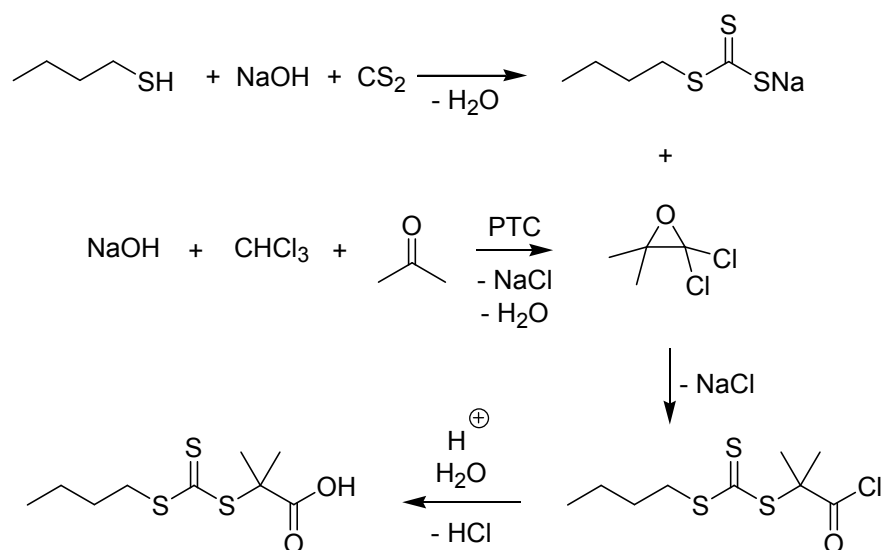
¹H-NMR (300 MHz in CDCl₃, δ in ppm): δ = 1.59 (d, 3H, -CHCl(CH₃-)), 1.75 (d, 3H, CHBr(CH₃-)), 2.99 (d + d, 6H, -N(CH₃)₂), 4.51-4.59 (m, 1H, CHBr(CH₃-), CHCl(CH₃-)). **¹³C-NMR** (75 MHz in CDCl₃, δ in ppm): δ = 20.8 (CHCl(CH₃-), 21.5 (CHBr(CH₃-), 36.0, 37.1 (-N(CH₃)₂, Cl-product), 36.1, 37.3 (-N(CH₃)₂, Br-product), 38.2 (CHBr(CH₃-), 49.3 (CHCl(CH₃-), 168.7 (-C(=O)-O-, Cl-product), 168.9 (-C(=O)-O-, Br-product).

Synthesis of N,N-dimethyl 2-(butylsulfanylthiocarbonylsulfanyl) propionamide

Under nitrogen flow, 3.11 g (38.9 mmol) of a 50 wt% aqueous solution of NaOH were added dropwise to 3.50 g (38.9 mmol) of 1-butanethiol dissolved in 20 mL THF. The dropwise addition of 2.96 g (40 mmol) of CS₂ gave a clear, bright yellow solution. 7.00 g (41.5 mmol) of the mixture of *N,N*-dimethyl 2-bromopropionamide and *N,N*-dimethyl 2-chloropropionamide were added dropwise and white flakes of sodium halide precipitated after a while. The reaction mixture was stirred at ambient temperature over night. 50 mL of water were added and the mixture was extracted two times with 50 mL of hexane. The combined hexane phases were washed with water and dried over anhydrous MgSO₄. The solvent was evaporated and under cooling (4°C) the product crystallized as bright yellow needles. Yield: 9.7 g (94%). The product was pure according to ¹H NMR spectroscopy. Prior to the investigations of the UV-vis characteristics, the product was recrystallized from n-hexane.

m.p. 32 °C. **Elemental analysis** (C₁₀H₁₉NOS₃, M_r = 265.46): Calc: **C** 45.25, **H** 7.21, **N** 5.28, **S** 36.24 Found: **C** 45.28, **H** 7.29, **N** 5.25, **S** 36.53. **MS** (EI, negative ions): m/z = 265. **¹H-NMR** (300 MHz in CDCl₃, δ in ppm): δ = 0.93 (t, 3H, CH₃-CH₂-), 1.42 (m, 2H, -S-C-C-CH₂-), 1.55 (d, 3H, -S-CH(CH₃-), 1.68 (m, 2H, -S-C-CH₂-), 3.02 (s + s, 6H, -N(CH₃)₂), 3.36 (t, 2H, -S-CH₂-), 5.18 (q, 1H, -S-CH(CH₃-). **¹³C-NMR** (75 MHz in CDCl₃, δ in ppm): δ = 13.6 (CH₃-CH₂-), 17.6 (-S-CH(CH₃-), 22.0 (-S-C-C-CH₂-), 29.9 (-S-C-CH₂-), 36.1 (-N(CH₃)₂), 36.9 (-S-CH₂-), 37.4 (-N(CH₃)₂), 46.3 (-S-CH(CH₃-), 170.2 (-C(=O)-N), 223.1 (-S-C(=S)-S-). **FT-IR** (KBr, selected bands, wavenumber in cm⁻¹): 2951, 2928, 2868, 1647, 1491, 1460, 1389, 1081, 1039, 825, 729.

7.2.4. Synthesis of 2-(butylsulfanylthiocarbonylsulfanyl)-2-methyl propionic acid (CTA7)

*Materials*

1-butanethiol (Acros, 98 %), acetone (Acros, p.a.), Aliquat 336 (Acros, average MW = 442 g/mol), NaOH (Acros, p.a., pellets), CS₂ (Aldrich, 99.9+ %, ACS reagent), CHCl₃ (Acros, extra pure, 1% ethanol), HCl (conc., Merck).

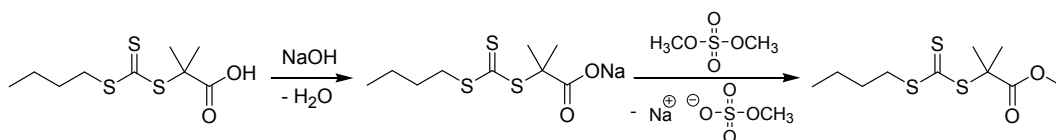
Procedure

CTA7 was synthesized under phase transfer catalysis conditions adopting a procedure by Lai et al.¹⁷⁹ Under nitrogen flow, 3.7 g (41 mmol) of 1-butanethiol, 19.0 g (327 mmol) of acetone and 0.65 g (1.5 mmol) of Aliquat 336 were mixed in a 250-mL three-necked flask. 3.35 g (42 mmol) of a 50 wt% aqueous NaOH solution were added dropwise at 10 °C. Then, 3.04 g (40 mmol) of CS₂ dissolved in acetone (4.3 g) were added to the white suspension and an intense yellow, clear solution formed. The mixture was cooled below 10 °C by an ice bath and CHCl₃ (7.1 g, 59.5 mmol) was added in one portion followed by dropwise addition of 16.0 g of a 50 wt% aqueous NaOH solution. The ice bath was removed after 30 min and the reaction mixture was stirred under nitrogen flow at ambient temperature over night. Then, 60 mL of water and 5 mL of concentrated HCl were added carefully to neutralize the mixture. Acetone was removed by rotary evaporation. The remaining solution was extracted with n-hexane and the combined n-hexane phases were washed with water. After drying over anhydrous MgSO₄, the solvent was removed by rotary evaporation and the raw product solidified as yellow needles (yield: 8.4 g). The raw product contained two minor impurities according to TLC (silicagel, n-hexane/ethyl acetate, 3:2 by volume) but was pure according to ¹H NMR and ¹³C NMR. Prior to polymerizations and for the investigations of the UV-vis characteristics, the product was recrystallized two times from n-hexane.

m.p. 52 °C. **Elemental analysis** (C₉H₁₆O₂S₃, M_r = 252.42): Calc: **C** 42.82, **H** 6.39, **S** 38.11, Found: **C** 42.79, **H** 6.64, **S** 38.17. **MS** (EI, negative ions): m/z = 252. **¹H-NMR** (300 MHz in CDCl₃, δ in ppm): δ = 0.93 (t, 3H, CH₃-CH₂-), 1.42 (m, 2H, -S-C-C-CH₂-), 1.67 (m, 2H, -S-C-CH₂-), 1.72 (s, 6H, -S-C(CH₃)₂-), 3.29 (t, 2H, -S-CH₂-). **¹³C-NMR** (75 MHz in CDCl₃, δ in ppm): δ = 13.6 (CH₃-CH₂-), 22.1 (-S-C-C-CH₂-), 25.2 (-S-C(CH₃)₂-), 29.9 (-S-C-CH₂-), 36.7 (-S-CH₂-), 55.6 (-S-C(CH₃)₂-), 178.7 (-COOH),

220.8 (-S-C(=S)-S-). **FT-IR** (KBr, selected bands, wavenumber in cm^{-1}): 2949, 2924, 2870, 2656, 2551, 1693, 1462, 1419, 1284, 1086, 1049, 916, 816.

7.2.5. Synthesis of methyl 2-(butylsulfanylthiocarbonylsulfanyl)-2-methyl propionate (**CTA8**)



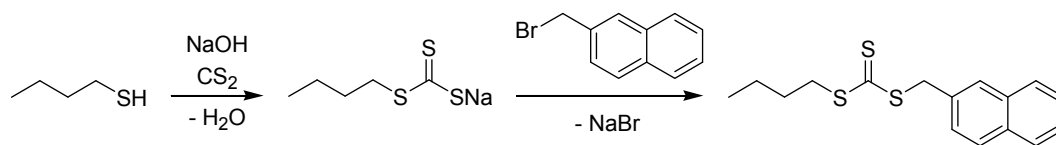
Materials

2-(Butylsulfanylthiocarbonylsulfanyl)-2-methyl propionic acid (**CTA7**), CH_2Cl_2 (Acros, pure, stabilized with 100 ppm amylene), dimethylsulfate (Aldrich, 99+ %), *N,N*-dimethylformamide (DMF) (Fluka, puriss. 99.5 % (GC), anhydrous over molecular sieves), MgSO_4 (Acros, anhydrous).

Procedure

CTA7 was dissolved in CH_2Cl_2 and transferred to a separatory funnel containing purified water. NaOH (0.1 M) was added in understoichiometric amounts to deprotonate the acid but to avoid hydrolysis of the trithiocarbonate. The sodium salt of **CTA7** was extracted into the water phase and the aqueous solution was separated and lyophilized. 2.5 g (9.1 mmol) of the sodium salt were dissolved in 10 mL of anhydrous DMF and transferred to a 25-mL round bottom flask. Under stirring, 3.5 g (27.8 mmol) of dimethylsulfate were added dropwise at ambient temperature. After complete addition, the mixture was stirred at ambient temperature for 1.5 h and at 30 °C for 19 h. Water (20 mL) was added to the reaction mixture and the product was extracted with 100 mL of hexane. The organic phase was washed with 5 wt% aqueous NaHCO_3 and brine. After drying over anhydrous MgSO_4 , the solvent was evaporated and the raw product was obtained as deep yellow oil (2.5 g). TLC (eluent: n-hexane) of the crude product disclosed three side products. Purification by column chromatography (silicagel 60, Merck, 0.040-0.063 mm, eluent: n-hexane) gave the pure product as an orange liquid (1.2 g, 48 %).

Elemental analysis ($\text{C}_{10}\text{H}_{18}\text{O}_2\text{S}_3$, $M_r = 266.44$): Calc: **C** 45.08, **H** 6.81, **S** 36.10. Found: **C** 44.81, **H** 6.99 **S** 35.93. **MS** (EI, negative ions): $m/z = 266$. **$^1\text{H-NMR}$** (300 MHz in CDCl_3 , δ in ppm): $\delta = 0.92$ (t, 3H, $\text{CH}_3\text{-CH}_2\text{-}$), 1.40 (m, 2H, $\text{-S-C-C-CH}_2\text{-}$), 1.65 (m, 2H, $\text{-S-C-CH}_2\text{-}$), 1.68 (s, 6H, $\text{-S-C(CH}_3)_2\text{-}$), 3.28 (t, 2H, $\text{-S-CH}_2\text{-}$), 3.70 (s, 3H, -O-CH_3). **$^{13}\text{C-NMR}$** (75 MHz in CDCl_3 , δ in ppm): $\delta = 13.6$ ($\text{CH}_3\text{-CH}_2\text{-}$), 22.1 ($\text{-S-C-C-CH}_2\text{-}$), 25.3 ($\text{-S-C(CH}_3)_2\text{-}$), 29.9 ($\text{-S-C-CH}_2\text{-}$), 36.6 ($\text{-S-CH}_2\text{-}$), 53.0 (-O-CH_3), 55.8 ($\text{-S-C(CH}_3)_2\text{-}$), 173.5 (-C(=O)-O-), 221.5 (-S-C(=S)-S-). **FT-IR** (KBr, selected bands, wavenumber in cm^{-1}): 2956, 2930, 2872, 1733, 1463, 1432, 1382, 1260, 1152, 1125, 1055, 813.

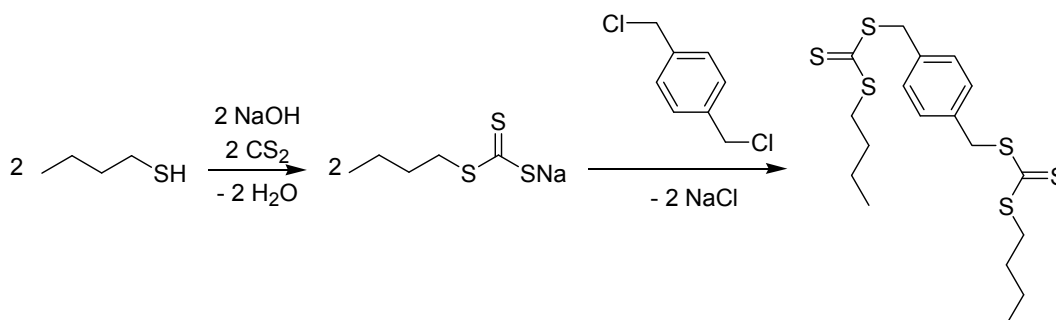
7.2.6. Synthesis of *S*-butyl-*S'*-naphthalen-2-ylmethyl trithiocarbonate (**CTA10**)**Materials**

1-butanethiol (Acros, 98%), NaOH (Acros, p.a., pellets), CS₂ (Aldrich, 99.9+%, ACS reagent), 2-bromomethyl naphthalene (Aldrich, 96%), THF (Merck, extra pure), MgSO₄ (Acros, anhydrous)

Procedure

Under nitrogen flow, 3.35 g (42 mmol) of a 50 wt% aqueous solution of NaOH were added dropwise to 3.7 g (41 mmol) of 1-butanethiol dissolved in 20 mL of THF. CS₂ (3.04 g, 40 mmol) was added dropwise at ambient temperature to the white suspension of precipitated thiolate and a clear, bright yellow solution formed. After stirring for 10 min, 8.8 g (39.8 mmol) of 2-bromomethyl naphthalene dissolved in 20 mL of THF were added. The reaction mixture was stirred over night at ambient temperature. Then, 100 mL of water were added and the solution was extracted with *n*-hexane. The hexane phase was washed with brine and dried over anhydrous MgSO₄. After the organic phase was concentrated, it was left at -20 °C to crystallize. The product crystallized as bright, light yellow needles and was pure according to ¹H and ¹³C NMR spectroscopy. Yield: 8.36 g (67 %).

Elemental analysis (C₁₆H₁₈S₃, M_r = 306.51): Calc: **C** 62.70 **H** 5.92 **S** 31.38, Found: **C** 62.70, **H** 6.03, **S** 31.74. **MS** (EI, negative ions): *m/z* = 306. **¹H-NMR** (300 MHz in CDCl₃, δ in ppm): δ = 0.95 (t, 3H, CH₃-), 1.45 (m, 2H, -S-C-C-CH₂-), 1.70 (m, 2H, -S-C-CH₂-), 3.40 (t, 2H, -S-CH₂-), 4.79 (s, 2H, -CH₂-aryl), 7.42-7.51 (m, 3H, naphthyl), 7.79-7.83 (m, 4H, naphthyl). **¹³C-NMR** (75 MHz in CDCl₃, δ in ppm): δ = 13.6 (CH₃-), 22.1 (-S-C-C-CH₂-), 30.0 (-S-C-CH₂-), 36.8 (-S-CH₂-), 41.6 (-CH₂-naphthyl), 126.3, 127.0, 127.7, 128.2, 128.5 (CH naphthyl), 132.6, 132.8, 133.3 (C naphthyl), 223.7 (-S-C(=S)-S-). **FT-IR** (KBr, selected bands, wavenumber in cm⁻¹): 2956, 2924, 2856, 1419, 1229, 1192, 1088, 1053, 812, 758.

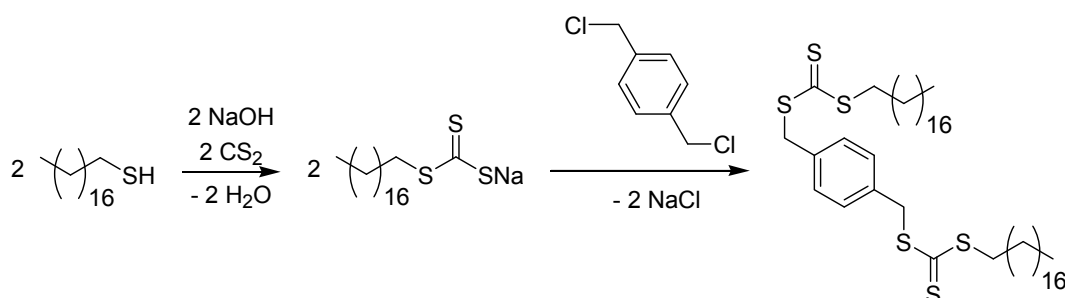
7.2.7. Synthesis of 1,4-bis(butyl trithiocarbonato methyl) benzene (**CTA12**)**Materials**

1-butanethiol (Acros, 98%), NaOH (Acros, p.a., pellets), CS₂ (Aldrich, 99.9+ %, ACS reagent), 1,4-bis(chloromethyl) benzene (Acros, 96%), THF (Merck, extra pure), MgSO₄ (Acros, anhydrous).

Procedure

Under nitrogen, 16.0 g (80 mmol) of a 20 wt% aqueous solution of NaOH were added dropwise at ambient temperature to 7.2 g (80 mmol) of 1-butanethiol dissolved in 5 mL of THF and a clear solution was obtained under vigorous stirring. Then, CS₂ (6.1 g, 80 mmol) was added and the solution became intensely orange. A solution of 7.0 g (40 mmol) of 1,4-bis(chloromethyl) benzene dissolved in 40 mL of THF was added dropwise over 30 min. The solution turned slightly turbid. After stirring over night under nitrogen at ambient temperature, water was added to the mixture. The reaction mixture was extracted with n-hexane several times. The combined hexane phases were washed with brine, dried over anhydrous MgSO₄ and the solution was concentrated by rotary evaporation. Crystallization from n-hexane afforded the bright yellow crystalline product. Yield: 7.4 g (43 %).

m.p. 32 °C. **Elemental analysis** (C₁₈H₂₆S₆, M_r = 434.79): Calc: **C** 49.72, **H** 6.03, **S** 44.25. Found: **C** 49.76, **H** 6.05, **S** 44.81. **MS** (EI, negative ions): m/z = 434. **¹H-NMR** (300 MHz in CDCl₃, δ in ppm): δ = 0.94 (t, 6H, -CH₃), 1.44 (m, 4H, -S-C-C-CH₂-), 1.69 (m, 4H, -S-C-CH₂-), 3.38 (t, 4H, -S-CH₂-), 4.59 (s, 4H, -CH₂-aryl), 7.28 (s, 4H, aryl). **¹³C-NMR** (75 MHz in CDCl₃, δ in ppm): δ = 13.6 (CH₃-), 22.0 (-S-C-C-CH₂-), 30.0 (-S-C-CH₂-), 36.8 (-S-CH₂-), 40.8 (-CH₂-aryl), 129.5 (CH aryl), 134.8 (C aryl), 223.5 (-S-C(=S)-S-). **FT-IR** (KBr, selected bands, wavenumber in cm⁻¹): 2956, 2916, 2856, 1419, 1229, 1088, 1053, 812, 758.

7.2.8. *Synthesis of 1,4-bis(octadecyl trithiocarbonato methyl) benzene (CTA13)**Materials*

1-octadecanethiol (Acros, 96%), NaOH (Acros, p.a., pellets), CS₂ (Aldrich, 99.9+ %, ACS reagent), 1,4-bis(chloromethyl) benzene (Acros, 96%), THF (Merck, extra pure), MgSO₄ (Acros, anhydrous), CHCl₃ (Acros, pure, stabilized with 1 % ethanol)

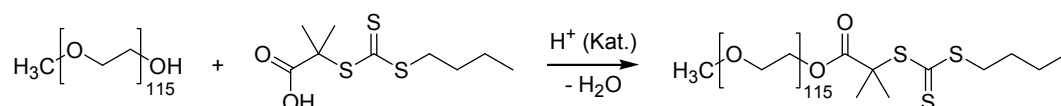
Procedure

Under nitrogen flow, 10.0 g (40 mmol) of a 16 wt% aqueous NaOH solution were added dropwise at ambient temperature to a vigorously stirred solution of 1-octadecanethiol (11.5 g, 40 mmol) in THF (20 mL). The thiolate precipitated as white solid. Then, CS₂ (3.1 g, 40 mmol) was added dropwise at ambient temperature and a deep yellow, clear solution was obtained. 3.5 g (20 mmol) of 1,4-bis(chloromethyl) benzene were dissolved in 20 mL of THF and added slowly to the reaction mixture. Upon addition of the halide, the product precipitated and the reaction mixture turned into a thick paste. To improve mixing of reagents, 80 mL of THF were added. The mixture was stirred over night at 45°C. The precipitated solid was filtered off and washed several times with THF. The raw product was dissolved in

CHCl₃ and dried over anhydrous MgSO₄. The solution was concentrated under slight heating and then left at ambient temperature to crystallize. A light yellow, solid product (7.5 g, 45%) was obtained.

Elemental analysis (C₄₆H₈₂S₆, M_r = 827.53): Calc: **C** 66.76, **H** 9.99, **S** 23.25. Found: **C** 66.63, **H** 10.46, **S** 23.36. **¹H NMR** (300 MHz in CDCl₃, δ in ppm): δ = 0.88 (t, 6H, -CH₃), 1.06-1.46 (m, 60H, -C(2)H₂ - C(16)H₂-), 1.65-1.75 (m, 4H, -S-C-CH₂-), 3.36 (t, 4H, -S-CH₂-), 4.58 (s, -CH₂-aryl), 7.28 (s, 4H, aryl). **¹³C NMR** (75 MHz in CDCl₃, δ in ppm): δ = 14.1 (-CH₃), 22.7 (-CH₂-CH₃), 28.0, 28.8, 29.1, 29.3, 29.4, 29.5, 29.7 (methylene), 31.9 (-S-C-CH₂-), 37.1 (-S-CH₂-), 40.9 (-CH₂-aryl), 129.5 (CH aryl), 134.8 (C aryl), 223.6 (-S-C(=S)-S-). **FT-IR** (KBr, selected bands, wavenumber in cm⁻¹): 2955, 2916, 2850, 1472, 1074, 1063, 837, 822, 719.

7.2.9. Synthesis of PEO monomethyl ether 2-(butylsulfanylthiocarbonylsulfanyl)-2-methyl propionate (CTA14)



Materials

2-(Butylsulfanylthiocarbonylsulfanyl)-2-methyl propionic acid (**CTA7**), PEO monomethyl ether (M_r = 5000) (Fluka), toluene (Acros, p.a.), p-toluenesulfonic acid monohydrate (Fluka, puriss., for acetyl determination).

Procedure

CTA14 was prepared according to the procedure by Z. Ma et al.²⁶⁵ 10.0 g (2 mmol) of PEG monomethyl ether were transferred to a 500 mL round bottom flask and dissolved in 200 g of toluene. Traces of water were removed by azeotropic distillation (60 mL of toluene were distilled off). To the flask were added 38 mg (0.2 mmol) of p-toluenesulfonic acid and 2.52 g (10 mmol) of **CTA7**. The mixture was stirred for two days under reflux and the reaction water was removed using a soxhlet extractor filled with dry molecular sieve (3Å). The product was isolated by slow addition of the reaction mixture to 400 mL of vigorously stirred diethyl ether. The precipitated polymer was collected by vacuum filtration. Under slight warming, the yellow polymer was redissolved in 40 mL of acetone and precipitated in 500 mL of hexane. The supernatant was colorless which proved the removal of excess **CTA7**. After vacuum filtration, the product was dissolved in water, filtered and lyophilized. The product was obtained as yellow powder (9.3 g, 86%).

m.p. 60 °C. **¹H-NMR** (300 MHz in CDCl₃, δ in ppm): δ = 0.92 (t, 3H, -CH₂-CH₃), 1.34-1.47 (m, 2H, -S-C-C-CH₂-), 1.58-1.71 (m, 2H + 6H, -S-C-CH₂- + -S-C(CH₃)₂-), 3.27 (t, 2H, -S-CH₂-), 3.37 (s, 3H, -O-CH₃), 3.38-3.88 (m, 460H, -O-CH₂-) 4.24 (t, 2H, -CH₂-O-C(=O)-). **FT-IR** (KBr, selected bands, in cm⁻¹): 2887, 1468, 1344, 1281, 1242, 1113, 962, 843.

7.3. UV-vis spectroscopic analysis of CTAs

7.3.1. Determination of λ_{\max} and the molar absorptivity ϵ

The UV-vis absorption characteristics of the synthesized CTAs were studied in a variety of solvents. The maximum absorbance wavelengths λ_{\max} and the molar absorptivities ϵ of the π - π^* - as well as the n - π^* -transitions of the thiocarbonyl bond were determined. Solutions of the CTAs were prepared in n-hexane, n-butyl acetate, CH_2Cl_2 , and CH_3OH . Measurements in CH_3CN and 1-butanol were performed only for selected samples. The used solvents were all spectrophotometric grade. In order to determine ϵ of the intense π - π^* -absorption band, solutions were prepared by diluting a stock solution. Six solutions of different concentrations were prepared for each determination of the molar absorptivity. The molar absorptivities ϵ at the maximum absorption wavelength λ_{\max} were determined by a linear fit of absorbance vs. concentration. The correlation coefficients of the linear fits (R^2) were better than 0.99.

7.3.2. Synthesis of polymers for the evaluation of end-group analysis

In order to evaluate the accuracy of molar mass determination by end-group analysis (chapter 3.5), two polymer samples, namely poly(n-butyl acrylate) (polyBuA) and poly(*N,N*-dimethyl acrylamide) (polyDMA), were synthesized by RAFT polymerization. The experimental conditions for their preparation using **CTA7** as RAFT agent are summarized in Table 7.1.

Table 7.1 Preparation of polymers at 65°C for the evaluation of end-group analysis

entry	polymer	monomer [mmol]	CTA7 [mol x 10 ⁵]	AIBN [mol x 10 ⁵]	solvent	polym. time [h]	yield [g]
1	polyBuA	156	78.1	7.8	60 g toluene	3	5.1
2	polyDMA	204	101	5.1	100 g THF	2	9.9

Polymer polyBuA was precipitated in methanol and dried in vacuo. The polymerization mixture of polyDMA was dialyzed against purified water and lyophilized.

7.4. Polymerizations

7.4.1. Reagents

The monomers oligo(ethylene oxide) monomethylether acrylate ($M_r = 454$) (**M1**), *N,N*-dimethyl acrylamide (**M2**), and *1H,1H,2H,2H*-tetrahydroperfluorodecyl acrylate (**M7**) were purchased from Aldrich. *N*-isopropyl acrylamide (**M4**), *n*-butyl acrylate (**M5**) and 2-ethylhexyl acrylate (**M6**) were purchased from Acros. Monomer *N*-acryloyl pyrrolidine (**M3**) was synthesized by J. Kristen (University of Potsdam, Golm) according to a literature procedure^{29, 289} and stored at -20°C under N_2 in the dark. Monomers **M2**, **M5** and **M6** were purified by vacuum distillation from CaH_2 and stored at -20°C under N_2 in the dark. **M4** was recrystallized twice from hexane/benzene (1:1 by volume) to remove the inhibitor. **M1** and **M7** were (vacuum) filtered over a column with basic alumina (Merck, activity I, 0.063-0.200 mm) to remove the inhibitor prior to polymerization. 2,2'-Azobis(isobutyronitrile) (**AIBN**) (98%) was purchased from Acros and recrystallized from methanol. Initiators **V-501** and **V-40** were gifts from Wako and used as received. THF (Merck, extra pure) was distilled from Na/K to remove the inhibitor and peroxides. Solvents used for polymerization were analytical grade. Dialysis tubes "ZelluTrans" (nominal molar mass cut off 4000-6000 D) were purchased from Roth.

7.4.2. Synthesis of double-thermoresponsive block copolymers

Synthesis of macroCTAs

The conditions for the synthesis of the acrylamide-based homo- and block copolymers are summarized in Table 7.1. In a typical procedure for the synthesis of macroCTA (**M4**)₁₁₀ (entry 2, Table 7.2), *N*-isopropyl acrylamide (12.1 g, 107 mmol), **CTA1** (147.7 mg, $5.29 \cdot 10^{-4}$ mol), **AIBN** (17.9 mg, $1.09 \cdot 10^{-4}$ mol) and toluene (41 mL) were transferred to a 100-mL Schlenk flask equipped with a magnetic stirrer. The sample was deoxygenated by three freeze-pump-thaw cycles and the flask refilled with N_2 . The flask was immersed in a preheated oil bath (65°C) and stirred for the required polymerization time. The polymerization was stopped by cooling the flask rapidly in a dry ice/acetone mixture. The polymer was purified by three precipitations into diethyl ether to remove unreacted monomer. Finally, the polymer was dissolved in deionized water, filtered and lyophilized. MacroCTAs (**M4**)₁₁₀ and (**M2**)₁₃₉ were obtained as pink powders and were characterized by ^1H NMR spectroscopy, SEC and UV-vis spectroscopy.

Synthesis of di- and triblock copolymers

In the syntheses of di- and triblock copolymers, the monomer to macroCTA ratio ($[\text{M}]/[\text{macroCTA}]$) was set to 200 according to the concentration of end-groups determined from vis spectroscopy. The amounts of monomer, macroCTA, initiator and solvent used for polymerizations are listed in Table 7.2. In a typical procedure, monomer **M2**, macroCTA (**M4**)₁₁₀ and THF were placed in a Schlenk flask. The amount of initiator was dosed from a freshly prepared stock solution of **AIBN** in THF. The sample was deoxygenated by three freeze-pump-thaw cycles (followed by purging with N_2) and polymerized in a preheated oil bath (65°C) for 6 h. The polymerization was stopped by cooling the flask rapidly in a dry ice/acetone mixture. The diblock copolymer was isolated by repeated precipitation from acetone solution into *n*-hexane. After collecting the polymer by vacuum filtration, the polymer was

dissolved in deionized water, filtered to remove dust and lyophilized. The diblock copolymer was obtained as a light pink powder. For the synthesis of triblock copolymers, an analogous procedure was applied.

Table 7.2 Polymerization conditions for the synthesis of double-thermoresponsive ABC triblock copolymers and their precursors (65 °C)

entry	polymer	monomer [mmol]	CTA or macroCTA [mol x 10 ⁵]	AIBN [mol x 10 ⁵]	solvent	polym. time [h]	yield [g]
1	(M2) ₁₃₉	M2 121	CTA1 59.8	12.2	36 mL toluene	7.5	6.8
2	(M4) ₁₁₀	M4 107	CTA1 52.9	10.9	41 mL toluene	13	3.4
3	(M3) ₅₂	M3 8	CDTB 8	1.6	5 mL toluene	25	57
4	(M2) ₁₃₉ -(M4) ₅₂	M4 29	(M2) ₁₃₉ 14.5 (2.0 g)	2.9	35 mL toluene	12	2.3
5	(M4) ₁₁₀ -(M2) ₅₂	M2 32	(M4) ₁₁₀ 15.7 (2.0 g)	3.3	11 mL THF	6	2.3
6	(M4) ₁₁₀ -(M3) ₇₀	M3 13	(M4) ₁₁₀ 6.5 (0.8 g)	1.3	8 mL THF	6	1.1
7	(M2) ₁₃₉ -(M4) ₅₂ -(M3) ₂₈	M3 9	(M2) ₁₃₉ -(M4) ₅₂ 4.2 (1.5 g)	0.8	9 mL THF	12	1.9
8	(M4) ₁₁₀ -(M2) ₅₂ -(M3) ₆₉	M3 13	(M4) ₁₁₀ -(M2) ₅₂ 6.6 (1.5 g)	1.3	8 mL THF	12	2.3
9	(M4) ₁₁₀ -(M3) ₇₀ -(M2) ₆₄	M2 4	(M4) ₁₁₀ -(M3) ₇₀ 2.6 (0.6 g)	0.4	8 mL THF	12	0.7

7.4.3. Synthesis of triphilic block copolymers

The experimental conditions for the synthesis of the amphiphilic ABC triblock copolymers and their precursors are given in Table 7.3. Conversions were estimated gravimetrically based on the amount of recovered polymer after purification. All polymers were characterized by ¹H NMR spectroscopy, SEC and UV-vis spectroscopy. The data of their molar mass characterization are presented in Table 5.1.

Synthesis of the hydrophobic macroCTA

For the synthesis of the hydrophobic macroCTA (M6)₁₂₀ (entry 5, Table 7.3), 2-ethylhexyl acrylate (20 g, 109 mmol), CTA7 (137 mg, 5.43·10⁻⁴ mol), AIBN (8.9 mg, 5.43·10⁻⁵ mol) and toluene (60 g) were transferred to a 250-mL round-bottom flask equipped with a magnetic stirrer and a rubber septum. The polymerization mixture was deoxygenated by purging with N₂ for 45 min. The flask was immersed in a preheated oil bath and stirred for 4 h at 65 °C. The polymerization was stopped by cooling the flask rapidly in a dry ice/acetone mixture. The polymer was isolated by precipitation into cold methanol and the obtained yellow glue was washed several times with methanol. In order to remove residual solvent and monomer, the sample was lyophilized from benzene solution. The macroCTA (M6)₁₂₀ was obtained as a bright yellow, viscous paste.

Synthesis of hydrophilic macroCTAs

In a typical procedure for the synthesis of the hydrophilic macroCTA polyM1, monomer M1 (19.8 g, 43.6 mmol), CTA7 (110 mg, 4.36·10⁻⁴ mol), initiator V-501 (6.2 mg, 2.2·10⁻⁵ mol) and a mixture of deionized water and methanol (60 g, 1:1 by wt.) were transferred to a 250-mL round-bottom flask

equipped with a magnetic stirrer and a rubber septum. The polymerization mixture was deoxygenated by purging with N₂ for 45 min. The flask was immersed in a preheated oil bath and stirred for 2 h at 69 °C. The polymerization was stopped by cooling the flask rapidly in a dry ice/acetone mixture. Unreacted macromonomer was removed by dialyzing the polymerization mixture against deionized water for 5 days. The aqueous solution of macroCTA (**M1**)₇₀ was lyophilized after filtration and the polymer was obtained as a bright yellow, viscous paste.

Table 7.3 Polymerization conditions for the synthesis of triphilic ABC triblock copolymers and their precursors

entry	polymer	monomer [mmol]	CTA or macroCTA [mol x 10 ⁵]	initiator [mol x 10 ⁵]	solvent	polym. temp. [°C]	polym. time [h]	yield [g]
1	(M1) ₇₀	M1 43.6	CTA7 4.36	V-501 2.2	H ₂ O (30 g) MeOH (30 g)	69	2.0	12.2
2	(M1) ₈₅	M1 52.4	CTA7 43.6	V-501 2.2	H ₂ O (37 g) MeOH (27 g)	69	2.0	9.3
3	(M2) ₁₄₃	M2 204	CTA7 101	AIBN 5.1	100 g THF	65	2.0	9.9
4	(M2) ₃₈₄	M2 204	CTA7 49.9	AIBN 2.5	100 g THF	65	4.0	12.7
5	(M6) ₁₂₀	M6 109	CTA7 54.3	AIBN 5.4	60 g toluene	65	4.0	11.2
6	(M1) ₇₀ -(M5) ₈₃	M5 33.5	(M1) ₇₀ 12.6 (4.0 g)	AIBN 1.3	20 g toluene	65	3.2	5.2
7	(M1) ₇₀ -(M6) ₁₄₀	M6 33.6	(M1) ₇₀ 12.6 (4.0 g)	AIBN 1.3	20 g toluene	65	3.2	5.7
8	(M1) ₈₅ -(M7) ₂₄	M7 4.1	(M1) ₈₅ 10.3 (4.0 g)	V-40 1.0	10 g TFT	88	5.5	4.5
9	(M2) ₁₄₃ -(M5) ₆₂	M5 18.1	(M2) ₁₄₃ 6.9 (1.0 g)	AIBN 0.9	11 g THF	65	1.5	1.4
10	(M2) ₃₈₄ -(M6) ₁₉	M6 6.8	(M2) ₃₈₄ 2.6 (1.0 g)	AIBN 0.4	11 g THF	65	2.0	1.0
11	(M6) ₁₂₀ -(M1) ₅₀	M1 41.0	(M6) ₁₂₀ 17.9 (4.0 g)	AIBN 1.9	110 g toluene	65	2.5	8.0
12	(M6) ₁₂₀ -(M1) ₁₀₉	M1 48.5	(M6) ₁₂₀ 17.9 (4.0 g)	AIBN 1.9	97 g toluene	65	5.0	14.7
13	(M1) ₇₀ -(M5) ₈₃ -(M7) ₁₃	M7 1.5	(M1) ₇₀ -(M5) ₈₃ 3.8 (2.0 g)	AIBN 0.8	15 g TFT	65	19	2.4
14	(M1) ₇₀ -(M6) ₁₄₀ -(M7) ₁₃	M7 0.8	(M1) ₇₀ -(M6) ₁₄₀ 4.0 (2.0 g)	AIBN 0.4	12 g TFT	65	19	2.0
16	(M6) ₁₂₀ -(M1) ₅₀ -(M7) ₄₀	M7 1.8	(M6) ₁₂₀ -(M1) ₅₀ 4.3 (2.0 g)	AIBN 1.0	15 g TFT	65	19	1.8
17	(M6) ₁₂₀ -(M1) ₁₀₉ -(M7) ₂₅	M7 2.1	(M6) ₁₂₀ -(M1) ₁₀₉ 5.0 (4.0 g)	AIBN 1.1	20 g TFT	65	19	4.8
18	PEO-(M5) ₂₂	M5 24.2	CTA14 42 (2.1 g)	AIBN 2.0	20 g THF	65	2.7	2.7
19	PEO-(M6) ₂₄	M6 24.5	CTA14 40 (2.0 g)	AIBN 2.0	17 g THF	65	2.3	3.7
20	PEO-(M5) ₂₂ -(M7) ₂	M7 2.1	PEO-(M5) ₂₂ 10.3 (1.5 g)	V-40 1.0	10 g TFT	88	5.5	1.6
21	PEO-(M6) ₂₄ -(M7) ₂	M7 1.3	PEO-(M6) ₂₄ 6.3 (1.0 g)	V-40 0.6	8 g TFT	88	5.5	1.1

Synthesis of amphiphilic di- and triblock copolymers

For the synthesis of di- and triblock copolymers, the specific macroCTAs, monomers, initiator and solvents were engaged as listed in Table 7.3. The data of their molar mass characterization are presented in Table 5.1. In the synthesis of di- and triblock copolymers, the ratios of monomer to macroCTA ($[M]/[\text{macroCTA}]$) and macroCTA to initiator were set according to the concentration of end-groups determined from UV spectroscopy.

In a typical procedure for the synthesis of diblock copolymers, macroCTA **(M6)₁₂₀** (4.0 g, $1.91 \cdot 10^{-4}$ mol), monomer **M1** (18.6 g, 41 mmol), AIBN (3.1 mg, $1.91 \cdot 10^{-5}$ mol) and toluene (110 g) were transferred to a 250-mL round-bottom flask equipped with a magnetic stirrer and a rubber septum. The flask was immersed in a preheated oil bath and stirred for 2.5 h at 65 °C. The polymerization was stopped by cooling the flask rapidly in a dry ice/acetone mixture. The solvent was removed by rotary evaporation and the polymerization mixture was redissolved in THF. The unreacted macromonomer was removed by dialyzing this solution against deionized water (nominal molar mass cut off 4000-6000 D) for 5 days. Upon solvent exchange, the solution turns into a milky emulsion. After filtration to remove dust, the emulsion was lyophilized. The diblock copolymer was obtained as a clear, yellow paste. The lyophilized diblock copolymer is directly soluble in water and forms an opaque solution.

In a typical procedure for the synthesis of triblock copolymers, the amphiphilic diblock macroCTA **(M6)₁₂₀-(M1)₅₀** (2.0 g, $4.26 \cdot 10^{-5}$ mol), monomer **M7** (0.94 g, 1.81 mmol), AIBN (1.6 mg, $9.7 \cdot 10^{-6}$ mol) and the solvent α,α,α -trifluorotoluene (TFT) (15 g) were transferred to a 50-mL round-bottom flask equipped with a magnetic stirrer and a rubber septum. The polymerization mixture was deoxygenated by purging with N₂ for 20 min. The flask was immersed in a preheated oil bath and stirred for 19 h at 65 °C. The polymerization was stopped by cooling the flask rapidly in a dry ice/acetone mixture. After polymerization, the reaction mixture foamed upon shaking. Most of the solvent TFT was removed by rotary evaporation. The precipitation of the triblock copolymer in diethyl ether and methanol was attempted. However, the polymer did not precipitate as a macroscopic phase but formed a stable dispersion. Therefore, the unreacted fluorinated monomer was removed by dialyzing the block copolymer solution against ethanol for 3 days. The dialysis bags were swollen in deionized water prior to dialysis against ethanol. Finally, the polymer solution was dialyzed against deionized water to remove ethanol, filtered and lyophilized. The syntheses of amphiphilic block copolymers starting from oligomeric PEO macroCTA were performed analogously to the synthesis of di- and triblock copolymers.

7.5. Preparation and analysis of micellar solutions

7.5.1. Solutions of thermoresponsive polymers

Water used for the preparation of micellar solutions was purified by a Millipore Qplus water purification system (resistance of 18 M Ω -cm). Solutions of the thermoresponsive block copolymers for DLS and turbidimetry measurements were prepared by dissolving the polymer in purified water, generally with a concentration of 1.0 g/L. In the slow heating protocol, temperature dependent DLS experiments were run with a heating program from 25°C to 65°C in steps of 1.0 °C, equilibrating the samples for 10 min at each step. In the alternative fast heating protocol, polymer solutions were put in a quartz glass cuvette at room temperature, placed in a heating bath of the desired measuring temperature, and equilibrated in the bath for 10 min before being transferred to the particle sizer which was preheated to the measuring temperature. For annealing measurements, the solutions were kept at 45°C for several days and reanalyzed after 24 h and 48 h.

7.5.2. Micellar solutions of amphiphilic block copolymers

Micellar solutions of amphiphilic triblock copolymers were prepared starting from a common solvent. Different methods for the preparation of micellar solutions were applied. In method A, 50 mg of the block copolymer were dissolved in THF (20 g). The solutions were stirred for at least 1 h to ensure complete dissolution. Then, 10 g of purified water (resistance of 18 M Ω -cm) were added dropwise under stirring to induce the formation of micelle-like aggregates. The excess of THF was slowly evaporated at ambient conditions. Finally, the concentration of the solution was adjusted to 0.5 wt%.

In the alternative preparation procedure, method B, 25 mg of the block copolymer were dissolved in 10 g of THF and stirred for 1 h at ambient conditions. In a separate vial, 5 g of purified water (resistance of 18 M Ω -cm) were weighed. The THF solution and the purified water were transferred to a water bath preset to 70 °C. Under stirring, the THF solution was added dropwise to the purified water. After complete addition, the aqueous solution was stirred for 1 h more at 70°C in order to remove residual THF. Finally, the samples were removed from the water bath and cooled to ambient temperature. The concentration of the solution was adjusted to 0.5 wt%.

Additionally, micellar solutions prepared by protocol A were annealed for 9-25 d at 78°C and reanalyzed by cryo-TEM (protocol C).

8. BIBLIOGRAPHY

1. Bates, F. S.; Fredrickson, G. H., *Annu. Rev. Phys. Chem.* **1990**, *41*, 525-557.
2. Halperin, A.; Alexander, S., *Macromolecules* **1989**, *22*, 2403-2412.
3. Nagarajan, R.; Ganesh, K., *J. Chem. Phys.* **1989**, *90*, 5843-5856.
4. Yuan, X.-F.; Masters, A. J.; Price, C., *Macromolecules* **1992**, *25*, 6876-6884.
5. Gao, Z.; Eisenberg, A., *Macromolecules* **1993**, *26*, 7353-7360.
6. Price, C.; Chen, E. K. M.; Stubbersfield, R. B., *Eur. Polym. J.* **1987**, 649.
7. Linse, P., *Macromolecules* **1994**, *27*, 6404-6417.
8. Riess, G., *Prog. Polym. Sci.* **2003**, *28*, 1107-1170.
9. Jain, S.; Bates, F. S., *Science* **2003**, *300*, 460-464.
10. Zhang, L.; Eisenberg, A., *J. Am. Chem. Soc.* **1996**, *118*, 3168-3181.
11. Zhang, L.; Eisenberg, A., *Polym. Adv. Techn.* **1998**, *9*, 677-699.
12. Chen, E.-Q.; Xia, Y.; Graham, M. J.; Foster, M. D.; Mi, Y.; Wu, W.-L.; Cheng, S. Z. D., *Chem. Mater.* **2003**, *15*, 2129-2135.
13. Choucair, A.; Eisenberg, A., *Eur. Phys. J. E* **2003**, *10*, 37-44.
14. Cornelissen, J. J. L. M.; Fischer, M.; Sommerdijk, N. A. J. M.; Nolte, R. J. M., *Science* **1998**, *280*, 1427-1430.
15. Liu, X.; Kim, J.-S.; Wu, J.; Eisenberg, A., *Macromolecules* **2005**, *38*, 6749-6751.
16. Marques, C.; Joanny, J. F.; Leibler, L., *Macromolecules* **1988**, *21*, 1051-1059.
17. Munch, M. R.; Gast, A. P., *Macromolecules* **1988**, *21*, 1366-1372.
18. Munch, M. R.; Gast, A. P., *Macromolecules* **1990**, *23*, 2313-2320.
19. Johner, A.; Joanny, J. F., *Macromolecules* **1990**, *23*, 5299-5311.
20. Liu, S.; Armes, S. P., *Curr. Opin. Colloid Interface Sci.* **2001**, *6*, 249-256.
21. Baskar, G.; Landfester, K.; Antonietti, M., *Macromolecules* **2000**, *33*, 9228-9232.
22. Manguian, M.; Save, M.; Charleux, B., *Macromol. Rapid Commun.* **2006**, *27*, 399-404.
23. Riess, G.; Labbe, C., *Macromol. Rapid Commun.* **2004**, *25*, 401-435.
24. Ferguson, C. J.; Hughes, R. J.; Nguyen, D.; Pham, B. T. T.; Gilbert, R. G.; Serelis, A. K.; Such, C. H.; Hawke, B. S., *Macromolecules* **2005**, *38*, 2191-2204.
25. Burguière, C.; Pascual, S.; Coutin, B.; Polton, A.; Tardi, M.; Charleux, B.; Matyjaszewski, K.; Vairon, J.-P., *Macromol. Symp.* **2000**, *150*, 39-44.
26. Save, M.; Manguian, M.; Chassenieux, C.; Charleux, B., *Macromolecules* **2005**, *38*, 280-289.
27. Drescher, B.; Scranton, A. B.; Klier, J., *Polymer* **2001**, *42*, 49-58.
28. Arotçaréna, M.; Heise, B.; Ishaya, S.; Laschewsky, A., *J. Am. Chem. Soc.* **2002**, *124*, 3787-3793.
29. Mertoglu, M.; Garnier, S.; Laschewsky, A.; Skrabania, K.; Storsberg, J., *Polymer* **2005**, *46*, 7726-7740.
30. Masala, O.; Seshadri, R., *Annu. Rev. Mater. Res.* **2004**, *34*, 41-81.
31. Förster, S.; Plantenberg, T., *Angew. Chem. Int. Ed.* **2002**, *41*, 688-714.
32. Hamley, I. W., *Angew. Chem. Int. Ed.* **2003**, *42*, 1692-1712.
33. Hamley, I. W., *Nanotechnology* **2003**, *14*, R39-R54.
34. Niu, Y.; Yeung, L. K.; Crooks, R. M., *J. Am. Chem. Soc.* **2001**, *123*, 6840-6846.
35. Graeser, M.; Pippel, E.; Greiner, A.; Wendorff, J. H., *Macromolecules* **2007**, *40*, 6032-6039.

36. Whetten, B. R. L.; Khoury, J. T.; Alvarez, M. M.; Murthy, S.; Vezmar, I.; Wang, Z. L.; Stephens, P. W.; Cleveland, C. L.; Luedtke, W. D.; Landman, U., *Adv. Mater.* **1996**, *8*, 428-433.
37. Bruchez, M.; Moronne, M.; Gin, P.; Weiss, S.; Alivisatos, A. P., *Science* **1998**, *281*, 2013-2016.
38. Klingelhöfer, S.; Heitz, W.; Greiner, A.; Oestreich, S.; Förster, S.; Antonietti, M., *J. Am. Chem. Soc.* **1997**, *119*, 10116-10120.
39. Gohy, J.-F.; Willet, N.; Varshney, S.; Zhang, J.-X.; Jérôme, R., *Angew. Chem. Int. Ed.* **2001**, *40*, 3214-3216.
40. Förster, S.; Antonietti, M., *Adv. Mater.* **1998**, *10*, 195-217.
41. Bronstein, L. M.; Sidorov, S. N.; Valetsky, P. M.; Hartmann, J.; Cölfen, H.; Antonietti, M., *Langmuir* **1999**, *15*, 6256-6262.
42. Antonietti, M.; Förster, S.; Hartmann, J.; Oestreich, S., *Macromolecules* **1996**, *29*, 3800-3806.
43. Underhill, R. S.; Liu, G., *Chem. Mater.* **2000**, *12*, 3633-3641.
44. Abes, J. I.; Cohen, R. E.; Ross, C. A., *Mater. Sci. Eng.* **2003**, *C23*, 641-650.
45. Lowe, A. B.; Sumerlin, B. S.; Donovan, M. S.; McCormick, C. L., *J. Am. Chem. Soc.* **2002**, *124*, 11562-11563.
46. Adams, M. L.; Lavasanifar, A.; Kwon, G. S., *J. Pharm. Sci.* **2003**, *92*, 1343-1355.
47. Rösler, A.; Vandermeulen, G. W. M.; Klok, H.-A., *Adv. Drug Delivery Rev.* **2001**, *53*, 95-108.
48. Yang, L.; Alexandridis, P., *Curr. Opin. Colloid Interface Sci.* **2000**, *5*, 132-143.
49. Harada, A.; Kataoka, K., *Prog. Polym. Sci.* **2006**, *31*, 949-982.
50. Kataoka, K.; Harada, A.; Nagasaki, Y., *Adv. Drug Delivery Rev.* **2001**, *47*, 113-131.
51. Kakizawa, Y.; Kataoka, K., *Adv. Drug Delivery Rev.* **2002**, *54*, 203-222.
52. Jeon, S. I.; Lee, J. H.; Andrade, J. D.; De Gennes, P. G., *J. Colloid Interface Sci.* **1991**, *142*, 149-158.
53. Lee, J. H.; Lee, H. B.; Andrade, J. D., *Prog. Polym. Sci.* **1995**, *20*, 1043-1079.
54. Bütün, V.; Wang, X.-S.; de Paz Báñez, M. V.; Robinson, K. L.; Billingham, N. C.; Armes, S. P., *Macromolecules* **2000**, *33*, 1-3.
55. Zhang, Q.; Remsen, E. E.; Wooley, K. L., *J. Am. Chem. Soc.* **2000**, *122*, 3642-3651.
56. Maeda, H.; Wu, J.; Sawa, T.; Matsumura, Y.; Hori, K., *J. Contr. Rel.* **2000**, *65*, 271-284.
57. Marcucci, F.; Lefoulon, F., *Drug Discovery Today* **2004**, *9*, 219-228.
58. Yasugi, K.; Nakamura, T.; Nagasaki, Y.; Kato, M.; Kataoka, K., *Macromolecules* **1999**, *32*, 8024-8032.
59. Weitman, S. D.; Lark, R. H.; Coney, L. R.; Fort, D. W.; Frasca, V.; Zurawski, V. R., Jr.; Kamen, B. A., *Cancer Res.* **1992**, *52*, 3396-3401.
60. Weitman, S. D.; Weinberg, A. G.; Coney, L. R.; Zurawski, V. R., Jr.; Jennings, D. S.; Kamen, B. A., *Cancer Res.* **1992**, *52*, 6708-6711.
61. Hadjichristidis, N.; Iatrou, H.; Pitsikalis, M.; Pispas, S.; Avgeropoulos, A., *Prog. Polym. Sci.* **2005**, *30*, 725-782.
62. Auschra, C.; Stadler, R., *Macromolecules* **1993**, *26*, 2171-2174.
63. Stadler, R.; Auschra, C.; Beckmann, J.; Krappe, U.; Voigt-Martin, I.; Leibler, L., *Macromolecules* **1995**, *28*, 3080-3091.
64. Zheng, W.; Wan, Z.-G., *Macromolecules* **1995**, *28*, 7215-7223.
65. Kříž, J.; Masař, B.; Pleštil, J.; Tuzar, Z.; Pospíšil, H.; Doskočilová, D., *Macromolecules* **1998**, *31*, 41-51.
66. Lei, L.; Gohy, J.-F.; Willet, N.; Zhang, J.-X.; Varshney, S.; Jérôme, R., *Macromolecules* **2004**, *37*, 1089-1094.

67. Yu, G.-e.; Eisenberg, A., *Macromolecules* **1998**, *31*, 5546-5549.
68. Liu, F.; Liu, G., *Macromolecules* **2001**, *34*, 1302-1307.
69. Zhou, Z.; Li, Z.; Ren, Y.; Hillmyer, M. A.; Lodge, T. P., *J. Am. Chem. Soc.* **2003**, *125*, 10182-10183.
70. Erhardt, R.; Zhang, M.; Böker, A.; Zettl, H.; Abetz, C.; Frederik, P.; Krausch, G.; Abetz, V.; Müller, A. H. E., *J. Am. Chem. Soc.* **2003**, *125*, 3260-3267.
71. Patrickios, C. S.; Lowe, A. B.; Armes, S. P.; Billingham, N. C., *J. Polym. Sci., Part A: Polym. Chem.* **1998**, *36*, 617-631.
72. Erhardt, R.; Böker, A.; Zettl, H.; Kaya, H.; Pyckhout-Hintzen, W.; Krausch, G.; Abetz, V.; Müller, A. H. E., *Macromolecules* **2001**, *34*, 1069-1075.
73. Liu, Y.; Abetz, V.; Müller, A. H. E., *Macromolecules* **2003**, *36*, 7894-7898.
74. McCormick, C. L. In *Stimuli-responsive water soluble and amphiphilic polymers*, ACS Symp. Ser., Washington DC, 2001; The American Chemical Society: Washington DC, 2001.
75. Martin, T. J.; Procházka, K.; Munk, P.; Webber, S. E., *Macromolecules* **1996**, *29*, 6071-6073.
76. Gohy, J.-F.; Antoun, S.; Jérôme, R., *Macromolecules* **2001**, *34*, 7435-7440.
77. Lee, A. S.; Gast, A. P.; Bütün, V.; Armes, S. P., *Macromolecules* **1999**, *32*, 4302-4310.
78. Mountrichas, G.; Pispas, S., *J. Polym. Sci., Part A: Polym. Chem.* **2007**, *45*, 5790-5799.
79. Kröger, R.; Menzel, H.; Hallensleben, M. L., *Macromol. Chem. Phys.* **1994**, *195*, 2291-2298.
80. Jiang, J.; Tong, X.; Morris, D.; Zhao, Y., *Macromolecules* **2006**, *39*, 4633-4640.
81. Pouliquen, G.; Tribet, C., *Macromolecules* **2006**, *39*, 373-383.
82. Jiang, J.; Tong, X.; Zhao, Y., *J. Am. Chem. Soc.* **2005**, *127*, 8290-8291.
83. Kirpach, A.; Adolf, D., *Macromol. Symp.* **2006**, *237*, 7-17.
84. Bütün, V.; Armes, S. P.; Billingham, N. C.; Tuzar, Z.; Rankin, A.; Eastoe, J.; Heenan, R. K., *Macromolecules* **2001**, *34*, 1503-1511.
85. Virtanen, J.; Arotçaréna, M.; Heise, B.; Ishaya, S.; Laschewsky, A.; Tenhu, H., *Langmuir* **2002**, *18*, 5360-5365.
86. Xulu, P. M.; Filipcsei, G.; Zrínyi, M., *Macromolecules* **2000**, *33*, 1716-1719.
87. Kuramoto, N.; Shishido, Y.; Nagai, K., *J. Polym. Sci., Part A: Polym. Chem.* **1997**, *35*, 1967-1972.
88. Suzuki, M.; Nakajima, R.; Tsuruta, M.; Higuchi, M.; Einaga, Y.; Yamamoto, K., *Macromolecules* **2006**, *39*, 64-69.
89. Kudaibergenov, S.; Jaeger, W.; Laschewsky, A., *Adv. Polym. Sci.* **2006**, *201*, 157-224.
90. Komatsu, M.; Inoue, T.; Miyasaka, K., *J. Polym. Sci., Part B: Polym. Phys.* **1986**, *24*, 303-311.
91. Somcynsky, T., *Polym. Eng. Sci.* **1982**, *22*, 58-63.
92. Taylor, L. D.; Cerankowski, L. D., *J. Polym. Sci., Part A: Polym. Chem.* **1975**, *13*, 2551-2570.
93. Fujishige, S.; Kubota, K.; Ando, I., *J. Phys. Chem.* **1989**, *93*, 3311-3313.
94. Liu, H. Y.; Zhu, X. X., *Polymer* **1999**, *40*, 6985-6990.
95. Platé, N. A.; Lebedeva, T. L.; Valuev, L. I., *Polymer J. Jpn.* **1999**, *31*, 21-27.
96. Kan, C.-W.; Doherty, E. A. S.; Barron, A. E., *Electrophoresis* **2003**, *24*, 4161-4169.
97. Xu, J.; Jiang, X.; Liu, S., *J. Polym. Sci., Part A: Polym. Chem.* **2008**, *46*, 60-69.
98. Laschewsky, A.; Reka, E. D.; Wischerhoff, E., *Macromol. Chem. Phys.* **2001**, *202*, 276-286.
99. Aoshima, S.; Oda, H.; Kobayashi, E., *J. Polym. Sci., Part A: Polym. Chem.* **1992**, *30*, 2407-2413.
100. Suwa, K.; Morishita, K.; Kishida, A.; Akashi, M., *J. Polym. Sci., Part A: Polym. Chem.* **1997**, *35*, 3087-3094.

101. Meeussen, F.; Nies, E.; Berghmans, H.; Verbrugghe, S.; Goethals, E.; Prez, F. D., *Polymer* **2000**, *41*, 8597–8602.
102. Durme, K. V.; Verbrugghe, S.; Du Prez, F. E.; Van Mele, B., *Macromolecules* **2004**, *37*, 1054-1061.
103. Aseyev, V.; Hietala, S.; Laukkanen, A.; Nuopponen, M.; Confortini, O.; Prez, F. E. D.; Tenhu, H., *Polymer* **2005**, *46*, 7118-7131.
104. Schild, H. G.; Tirrell, D. A., *J. Phys. Chem.* **1990**, *94*, 4352-4356.
105. Wanka, G.; Hoffmann, H.; Ulbricht, W., *Macromolecules* **1994**, *27*, 4145-4159.
106. Zhao, B.; Li, D.; Hua, F.; Green, D. R., *Macromolecules* **2005**, *38*, 9509-9517.
107. Chen, C. H.; Wilson, J.; Chent, W.; Davis, R. M.; Riffler, J. S., *Polymer* **1994**, *35*, 3587-3591.
108. Tachibana, Y.; Kurisawa, M.; Uyama, H.; Kakuchi, T.; Kobayashi, S., *Chem. Commun.* **2003**, 106-107.
109. Rodríguez-Hernández, J.; Chécot, F.; Gnanou, Y.; Lecommandoux, S., *Prog. Polym. Sci.* **2005**, *30*, 691–724.
110. Cölfen, H., *Macromol. Rapid Commun.* **2001**, *22*, 219-252.
111. Garnier, S.; Laschewsky, A., *Colloid Polym. Sci.* **2006**, *284*, 1243-1254.
112. Kubowicz, S.; Baussard, J.-F.; Lutz, J.-F.; Thünemann, A. F.; Berlepsch, H. v.; Laschewsky, A., *Angew. Chem., Int. Ed.* **2005**, *44*, 5262-5265.
113. Garnier, S.; Laschewsky, A., *Macromolecules* **2005**, *38*, 7580-7592.
114. Kadi, M.; Hansson, P.; Almgren, M.; Furó, I., *Langmuir* **2002**, *18*, 9243-9249.
115. Krafft, M. P.; Riess, J. G., *Biochimie* **1998**, *80*, 489-514.
116. Stähler, K.; Selb, J.; Candau, F., *Langmuir* **1999**, *15*, 7565-7576.
117. Kotzev, A.; Laschewsky, A.; Rakotoaly, R., *Macromol. Chem. Phys.* **2001**, *202*, 3257-3267.
118. Kotzev, A.; Laschewsky, A.; Adriaensens, P.; Gelan, J., *Macromolecules* **2002**, *35*, 1091-1101.
119. Weberskirch, R.; Preuschen, J.; Spiess, H. W.; Nuyken, O., *Macromol. Chem. Phys.* **2000**, *201*, 995-1007.
120. Li, Z.; Hillmyer, M. A.; Lodge, T. P., *Macromolecules* **2004**, *37*, 8933-8940.
121. Li, Z.; Hillmyer, M. A.; Lodge, T. P., *Macromolecules* **2006**, *39*, 765-771.
122. Dormidontova, E. E., *Macromolecules* **1999**, *32*, 7630-7644.
123. Zhu, Y.; Li, R. K. Y.; Jiang, W., *Chem. Phys.* **2006**, *327*, 137-143.
124. Chou, S.-H.; Tsao, H.-K.; Sheng, Y.-J., *J. Chem. Phys.* **2006**, *125*, 194903.
125. Xia, J.; Liu, D.; Zhong, C., *Phys. Chem. Chem. Phys.* **2007**, *9*, 5267-5273.
126. Zhong, C.; Liu, D., *Macromol. Theory Simul.* **2007**, *16*, 141-157.
127. Otsu, T.; Nayatani, K., *Makromol. Chem.* **1958**, *27*, 149-156.
128. Otsu, T., *J. Polym. Sci., Part A: Polym. Chem.* **2000**, *38*, 2121–2136.
129. Otsu, T.; Yoshida, M., *Makromol. Chem., Rapid Commun.* **1982**, *3*, 127-132.
130. Otsu, T.; Yoshida, M.; Kuriyama, A., *Polym. Bull.* **1982**, *7*, 45-50.
131. Solomon, D. H.; Rizzardo, E.; Cacioli, P. Eur. Pat. Appl. 135280, 1985.
132. Georges, M. K.; Veregin, R. P. N.; Kazmaier, P. M.; Hamer, G. K., *Macromolecules* **1993**, *26*, 2987-2988.
133. Matyjaszewski, K.; Davis, T. P., *Handbook of Radical Polymerization*. John Wiley and Sons, Inc.: Hoboken, 2002.
134. Hawker, C. J.; Bosman, A. W.; Harth, E., *Chem. Rev.* **2001**, *101*, 3661-3688.

135. Hawker, C. J., Nitroxide Mediated Living Radical Polymerization. In *Handbook of Radical Polymerization*, Matyjaszewski, K.; Davis, T. P., Eds. John Wiley and Sons, Inc.: Hoboken, 2002; pp 463-521.
136. Fischer, H., *Chem. Rev.* **2001**, *101*, 3581-3610.
137. Tang, W.; Fukuda, T.; Matyjaszewski, K., *Macromolecules* **2006**, *39*, 4332-4337.
138. Benoit, D.; Grimaldi, S.; Robin, S.; Finet, J.-P.; Tordo, P.; Gnanou, Y., *J. Am. Chem. Soc.* **2000**, *122*, 5929-5939.
139. Grimaldi, S.; Finet, J.-P.; Le Moigne, F.; Zeghdaoui, A.; Tordo, P.; Benoit, D.; Fontanille, M.; Gnanou, Y., *Macromolecules* **2000**, *33*, 1141-1147.
140. Benoit, D.; Chaplinski, V.; Braslau, R.; Hawker, C. J., *J. Am. Chem. Soc.* **1999**, *121*, 3904-3920.
141. Farcet, C.; Belleneq, J.; Charleux, B.; Pirri, R., *Macromolecules* **2002**, *35*, 4912-4918.
142. Nicolas, J.; Charleux, B.; Guerret, O.; Magnet, S., *Angew. Chem., Int. Ed.* **2004**, *43*, 6186-6189.
143. Schierholz, K.; Givchchi, M.; Fabre, P.; Nallet, F.; Papon, E.; Guerret, O.; Gnanou, Y., *Macromolecules* **2003**, *36*, 5995-5999.
144. Gibbons, O.; Carroll, W. M.; Aldabbagh, F.; Yamada, B., *J. Polym. Sci., Part A: Polym. Chem.* **2006**, *44*, 6410-6418.
145. Grassl, B.; Clisson, G.; Khoukh, A.; Billon, L., *Eur. Polym. J.* **2008**, *44*, 50-58.
146. Benoit, D.; Harth, E.; Fox, P.; Waymouth, R. M.; Hawker, C. J., *Macromolecules* **2000**, *33*, 363-370.
147. Detrembleur, C.; Sciannamea, V.; Koulic, C.; Claes, M.; Hoebeke, M.; Jérôme, R., *Macromolecules* **2002**, *35*, 7214-7223.
148. Couvreur, L.; Lefay, C.; Belleneq, J.; Charleux, B.; Guerret, O.; Magnet, S., *Macromolecules* **2003**, *36*, 8260-8267.
149. Matyjaszewski, K.; Xia, J., Fundamentals of Atom Transfer Radical Polymerization. In *Handbook of Radical Polymerization*, Matyjaszewski, K.; Davis, T. P., Eds. John Wiley and Sons, Inc.: Hoboken, 2002; pp 523-628.
150. Kato, M.; Kamigaito, M.; Sawamoto, M.; Higashimura, T., *Macromolecules* **1996**, *28*, 1721-1723.
151. Wang, J.-S.; Matyjaszewski, K., *J. Am. Chem. Soc.* **1995**, *117*, 5614-5615.
152. Wang, J.-S.; Matyjaszewski, K., *Macromolecules* **1995**, *28*, 7901-7910.
153. Teodorescu, M.; Matyjaszewski, K., *Macromolecules* **1999**, *33*, 4826-4831.
154. Jiang, J.; Lu, X.; Lu, Y., *J. Polym. Sci., Part A: Polym. Chem.* **2007**, *45*, 3956-3965.
155. Moad, G.; Rizzardo, E.; Thang, S. H., *Polymer* **2008**, *49*, 1079-1131.
156. Chiefari, J.; Chong, Y. K.; Ercole, F.; Krstina, J.; Jeffery, J.; Le, T. P. T.; Mayadunne, R. T. A.; Meijs, G. F.; Moad, C. L.; Moad, G.; Rizzardo, E.; Thang, S. H., *Macromolecules* **1998**, *31*, 5559-5562.
157. Mayadunne, R. T. A.; Rizzardo, E.; Chiefari, J.; Krstina, J.; Moad, G.; Postma, A.; Thang, S. H., *Macromolecules* **2000**, *33*, 243-245.
158. Moad, G.; Chiefari, J.; Chong, Y. K.; Krstina, J.; Mayadunne, R. T. A.; Postma, A.; Rizzardo, E.; Thang, S. H., *Polym. Int.* **2000**, *49*, 993-1001.
159. Charmot, D.; Corpart, P.; Adam, H.; Zard, S. Z.; Biadatti, T.; Bouhadir, G., *Macromol. Symp.* **2000**, *150*, 23-32.
160. Perrier, S.; Takolpuckdee, P., *J. Polym. Sci., Part A: Polym. Chem.* **2005**, *43*, 5347-5393.
161. Barner-Kowollik, C.; Vana, P.; Davis, T. P., The Kinetics of Free-Radical Polymerization. In *Handbook of Radical Polymerization*, Matyjaszewski, K.; Davis, T. P., Eds. John Wiley and Sons, Inc.: Hoboken, 2002; pp 187-261.
162. Barner-Kowollik, C.; Buback, M.; Charleux, B.; Coote, M. L.; Drache, M.; Fukuda, T.; Goto, A.; Klumperman, B.; Lowe, A. B.; McLeary, J. B.; Moad, G.; Monteiro, M. J.; Sanderson, R. D.; Tonge, M. P.; Vana, P., *J. Polym. Sci., Part A: Polym. Chem.* **2006**, *44*, 5809-5831.

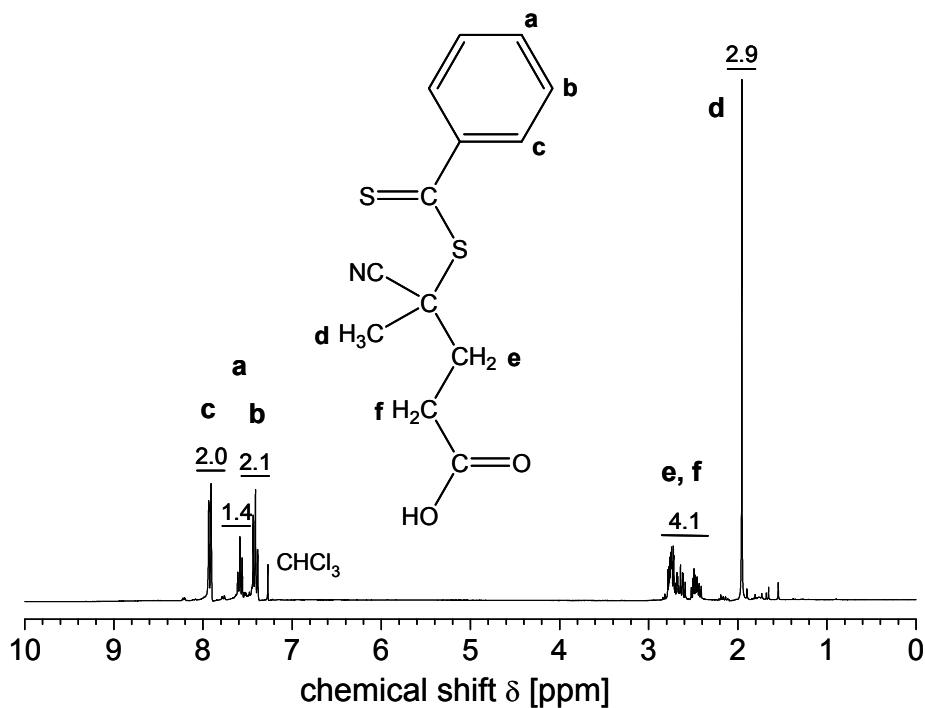
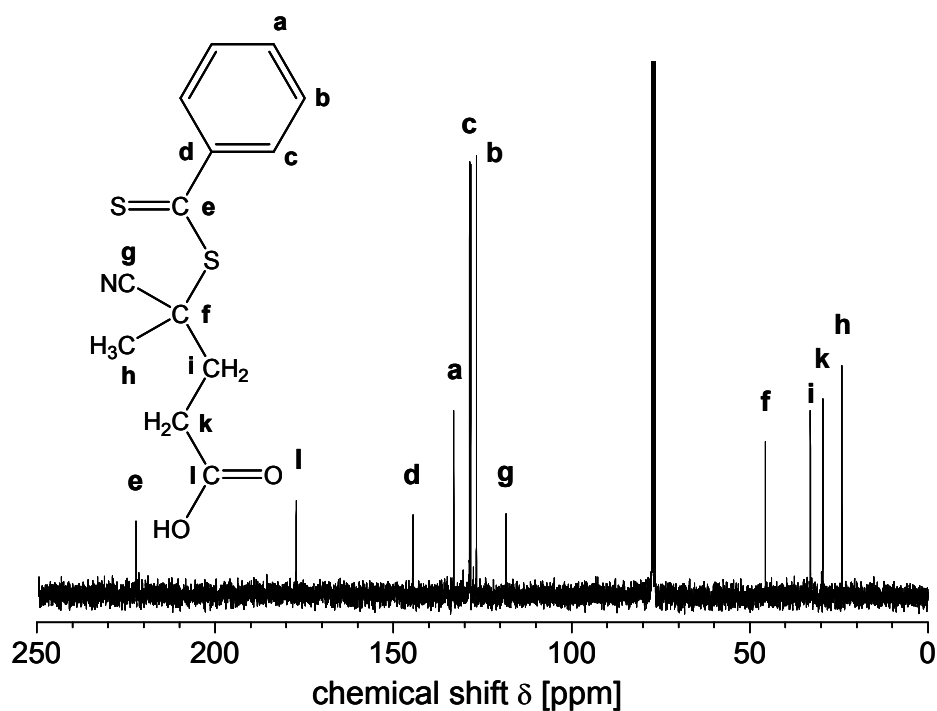
163. Monteiro, M. J.; Brouwer, H. d., *Macromolecules* **2001**, *34*, 349-352.
164. Feldermann, A.; Ah Toy, A.; Davis, T. P.; Stenzel, M. H.; Barner-Kowollik, C., *Polymer* **2005**, *46*, 8448-8457.
165. Barner-Kowollik, C.; Vana, P.; Quinn, J. F.; Davis, T. P., *J. Polym. Sci., Part A: Polym. Chem.* **2002**, *40*, 1058-1063.
166. Chiefari, J.; Mayadunne, R. T. A.; Moad, C. L.; Moad, G.; Rizzardo, E.; Postma, A.; Skidmore, M. A.; Thang, S. H., *Macromolecules* **2003**, *36*, 2273-2283.
167. Chong, Y. K.; Krstina, J.; Le, T. P. T.; Moad, G.; Postma, A.; Rizzardo, E.; Thang, S. H., *Macromolecules* **2003**, *36*, 2256-2272.
168. Monteiro, M. J., *J. Polym. Sci., Part A: Polym. Chem.* **2005**, *43*, 3189-3204.
169. Rizzardo, E.; Chen, M.; Chong, B.; Moad, G.; Skidmore, M.; Thang, S. H., *Macromol. Symp.* **2007**, *248*, 104-116.
170. Barner, L.; Davis, T. P.; Stenzel, M. H.; Barner-Kowollik, C., *Macromol. Rapid Commun.* **2007**, *28*, 539-559.
171. Baussard, J.-F.; Habib-Jiwan, J.-L.; Laschewsky, A.; Mertoglu, M.; Storsberg, J., *Polymer* **2004**, *45*, 3615-3626.
172. Mertoglu, M.; Laschewsky, A.; Skrabania, K.; Wieland, C., *Macromolecules* **2005**, *38*, 3601-3614.
173. Lowe, A. B.; McCormick, C. L., *Prog. Polym. Sci.* **2007**, *32*, 283-351.
174. Chen, M.; Ghiggino, K. P.; Mau, A. W. H.; Rizzardo, E.; Thang, S. H.; Wilson, G. J., *Chem. Commun.* **2002**, 2276-2277.
175. Gondi, S. R.; Vogt, A. P.; Sumerlin, B. S., *Macromolecules* **2007**, *40*, 474-481.
176. Becke, F.; Hagen, H. German Patent DE 1274121 (CA 1969; 70: 322, 3573v), 1968.
177. Thiel, W.; Mayer, R., *J. Prakt. Chem.* **1989**, *331*, 243-262.
178. Hörner, D.; Gattow, G., *Z. Anorg. Allg. Chem.* **1978**, *440*, 246-252.
179. Lai, J. T.; Filla, D.; Shea, R., *Macromolecules* **2002**, *35*, 6754-6756.
180. Oae, S.; Yagihara, T.; Okabe, T., *Tetrahedron* **1972**, *28*, 3203-3216.
181. Bouhadir, G.; Legrand, N.; Quiclet-Sire, B.; Zard, S. Z., *Tetrahedron Lett.* **1999**, *40*, 277-280.
182. Thang, S. H.; Chong, Y. K.; Mayadunne, R. T. A.; Moad, G.; Rizzardo, E., *Tetrahedron Lett.* **1999**, *40*, 2435-2438.
183. Leon, N. H.; Asquith, R. S., *Tetrahedron* **1970**, *26*, 1719-1725.
184. Favier, A.; Charreyre, M.-T.; Chaumont, P.; Pichot, C., *Macromolecules* **2002**, *35*, 8271-8280.
185. Zhou, N.; Lu, L.; Zhu, J.; Yang, X.; Wang, X.; Zhu, X.; Zhang, Z., *Polymer* **2007**, *48*, 1255-1260.
186. Hong, C.-Y.; Pan, C.-Y., *Macromolecules* **2006**, *39*, 3517-3524.
187. Kujawa, P.; Segui, F.; Shaban, S.; Diab, C.; Okada, Y.; Tanaka, F.; Winnik, F. M., *Macromolecules* **2006**, *39*, 341-348.
188. Bowes, A.; McLeary, J. B.; Sanderson, R. D., *J. Polym. Sci., Part A: Polym. Chem.* **2007**, *45*, 588-604.
189. Danis, P. O.; Karr, D. E.; Mayer, F.; Holle, A.; Watson, C. H., *Org. Mass Spectrom.* **1992**, *27*, 843-846.
190. Danis, P. O.; Karr, D. E., *Org. Mass Spectrom.* **1993**, *28*, 923-925.
191. Pohl, H. A., *Anal. Chem.* **1954**, *26*, 1614-1616.
192. Fallais, I.; Devaux, J.; Jérôme, R., *J. Polym. Sci., Part A: Polym. Chem.* **2000**, *38*, 1618-1629.
193. Ma, Y.; Agarwal, U. S.; Vekemans, J. A. J. M.; Sikkema, D. J., *Polymer* **2003**, *44*, 4429-4434.
194. Postma, A.; Davis, T. P.; Donovan, A. R.; Li, G.; Moad, G.; Mulder, R.; O'Shea, M. S., *Polymer* **2006**, *47*, 1899-1911.

195. Ran, R.; Yu, Y.; Wan, T., *J. Appl. Polym. Sci.* **2007**, *105*, 398–404.
196. Wang, Z.; He, J.; Tao, Y.; Yang, L.; Jiang, H.; Yang, Y., *Macromolecules* **2003**, *36*, 7446-7452.
197. Mayadunne, R. T. A.; Jeffery, J.; Moad, G.; Rizzardo, E., *Macromolecules* **2003**, *36*, 1505-1513.
198. Thomas, D. B.; Convertine, A. J.; Hester, R. D.; Lowe, A. B.; McCormick, C. L., *Macromolecules* **2004**, *37*, 1735-1741.
199. Favier, A.; Ladavière, C.; Charreyre, M.-T.; Pichot, C., *Macromolecules* **2004**, *37*, 2026-2034.
200. Schilli, C.; Lanzendörfer, M. G.; Müller, A. H. E., *Macromolecules* **2002**, *35*, 6819-6827.
201. Nakayama, M.; Okano, T., *Biomacromolecules* **2005**, *6*, 2320-2327.
202. Qiu, X.-P.; Winnik, F. M., *Macromol. Rapid Commun.* **2006**, *27*, 1648-1653.
203. Scales, C. W.; Convertine, A. J.; McCormick, C. L., *Biomacromolecules* **2006**, *7*, 1389-1392.
204. Vana, P.; Davis, T. P.; Barner-Kowollik, C., *Macromol. Rapid Commun.* **2002**, *23*, 952–956.
205. Xu, J.; He, J.; Fan, D.; Tang, W.; Yang, Y., *Macromolecules* **2006**, *39*, 3753-3759.
206. Qiu, X.-P.; Winnik, F. M., *Macromolecules* **2007**, *40*, 872-878.
207. Fabian, J.; Scheithauer, S.; Mayer, R., *J. Prakt. Chem.* **1969**, *311*, 45-60.
208. Rach, W.; Gattow, G., *Z. Anorg. Allg. Chem.* **1988**, *565*, 47-53.
209. Fabian, J.; Viola, H.; Mayer, R., *Tetrahedron* **1967**, *23*, 4323-4329.
210. Petiau, M.; Fabian, J., *J. Mol. Struct.* **2001**, *538*, 253-260.
211. Destarac, M.; Charmot, D.; Franck, X.; Zard, S. Z., *Macromol. Rapid Commun.* **2000**, *21*, 1035-1039.
212. Alberti, A.; Benaglia, M.; Laus, M.; Sparnacci, K., *J. Org. Chem.* **2002**, *67*, 7911-7914.
213. Fabian, J., *Theoret. Chim. Acta* **1968**, *12*, 200-205.
214. Baussard, J.-F. Ph. D. thesis, Université Catholique de Louvain, Louvain-La-Neuve, Belgium, 2004.
215. Otsu, T.; Kuriyama, A., *Polym. Bull.* **1984**, *11*, 135-142.
216. Reichardt, C., *Chem. Rev.* **1994**, *94*, 2319-2358.
217. Kamlet, M. J.; Abboud, J. L.; Taft, R. W., *J. Am. Chem. Soc.* **1977**, *99*, 6027-6038.
218. Taft, R. W.; Abboud, J. M.; Kamlet, M. J.; Abraham, M., *J. Solution Chem.* **1985**, *74*, 153-186.
219. Kamlet, M. J.; Abboud, J.-L. M.; Abraham, M. H.; Taft, R. W., *J. Org. Chem.* **1983**, *48*, 2877-2887.
220. Schmitt, B. Ph. D. thesis, Universität Mainz, 1999.
221. Duan, Q.; Miura, Y.; Narumi, A.; Shen, X.; Sato, S.-I.; Satoh, T.; Kakuchi, T., *J. Polym. Sci., Part A: Polym. Chem.* **2006**, *44*, 1117-1124.
222. Aspée, A.; García, O.; Maretti, L.; Sastre, R.; Scaiano, J. C., *Macromolecules* **2003**, *36*, 3550-3556.
223. Chen, M.; Ghiggino, K. P.; Mau, A. W. H.; Rizzardo, E.; Sasse, W. H. F.; Thang, S. H.; Wilson, G. J., *Macromolecules* **2004**, *37*, 5479-5481.
224. Chen, M.; Ghiggino, K. P.; Mau, A. W. H.; Sasse, W. H. F.; Thang, S. H.; Wilson, G. J., *Macromolecules* **2005**, *38*, 3475-3481.
225. Chen, M.; Ghiggino, K. P.; Thang, S. H.; Wilson, G. J., *J. Chin. Chem. Soc.* **2006**, *53*, 79-83.
226. Zhou, N.; Lu, L.; Zhu, X.; Yang, X.; Wang, X.; Zhu, J.; Zhou, D., *Polym. Bull.* **2006**, *57*, 491-498.
227. Burtscher, D.; Saf, R.; Slugovc, C., *J. Polym. Sci., Part A: Polym. Chem.* **2006**, *44*, 6136-6145.
228. Furyk, S.; Zhang, Y.; Ortiz-Acosta, D.; Cremer, P. S.; Bergbreiter, D. E., *J. Polym. Sci., Part A: Polym. Chem.* **2006**, *44*, 1492-1501.
229. Xia, Y.; Burke, N. A. D.; Stöver, H. D. H., *Macromolecules* **2006**, *39*, 2275-2283.

230. Talrose, V.; Stern, E. B.; Goncharova, A. A.; Messineva, N. A.; Trusova, N. V.; Efimkina, M. V., UV/Visible Spectra. In *NIST Chemistry WebBook, NIST Standard Reference Database Number 69*, Linstrom, P. J.; Mallard, W. G., Eds. National Institute of Standards and Technology: Gaithersburg MD, 20899 (<http://webbook.nist.gov>), June 2005.
231. Moad, G.; Chong, Y. K.; Postma, A.; Rizzardo, E.; Thang, S. H., *Polymer* **2005**, *46*, 8458-8468.
232. Li, M.; De, P.; Gondi, S. R.; Sumerlin, B. S., *J. Polym. Sci., Part A: Polym. Chem.* **2008**, *46*, 5093-5100.
233. Perrier, S.; Takolpuckdee, P.; Mars, C. A., *Macromolecules* **2005**, *38*, 2033-2036.
234. Triftaridou, A. I.; Vamvakaki, M.; Patrickios, C. S., *Polymer* **2002**, *43*, 2921-2926.
235. Kyriacou, M. S.; Hadjiyannakou, S. C.; Vamvakaki, M.; Patrickios, C. S., *Macromolecules* **2004**, *37*, 7181-7187.
236. Zhang, W.; Shi, L.; Ma, R.; An, Y.; Xu, Y.; Wu, K., *Macromolecules* **2005**, *38*, 8850-8852.
237. Aubrecht, K. B.; Grubbs, R. B., *J. Polym. Sci., Part A: Polym. Chem.* **2005**, *43*, 5156-5167.
238. Chong, Y. K.; Le, T. P. T.; Moad, G.; Rizzardo, E.; Thang, S. H., *Macromolecules* **1999**, *32*, 2071-2074.
239. Schild, H. G., *Prog. Polym. Sci.* **1992**, *17*, 163-249.
240. Savariar, E. N.; Thayumanavan, S., *J. Polym. Sci., Part A: Polym. Chem.* **2004**, *42*, 6340-6345.
241. Kuramoto, N.; Shishido, Y.; Nagai, K., *Macromol. Rapid Commun.* **1994**, *15*, 441-444.
242. Winnik, F. M.; Ringsdorf, H.; Venzmer, J., *Macromolecules* **1990**, *23*, 2415-2416.
243. Costa, R. O. R.; Freitas, R. F. S., *Polymer* **2002**, *43*, 5879-5885.
244. Winnik, F. M.; Ottaviani, M. F.; Bossmann, S. H.; Garcia-Garibay, M.; Turro, N. J., *Macromolecules* **1992**, *25*, 6007-6017.
245. Winnik, F. M.; Ottaviani, M. F.; Bossmann, S. H.; Pan, W.; Garcia-Garibay, M.; Turro, N. J., *Macromolecules* **1993**, *26*, 4577-4585.
246. Mori, T.; Shiota, Y.; Minagawa, K.; Tanaka, M., *J. Polym. Sci., Part A: Polym. Chem.* **2005**, *43*, 1007-1013.
247. Sumerlin, B. S.; Donovan, M. S.; Mitsukami, Y.; Lowe, A. B.; McCormick, C. L., *Macromolecules* **2001**, *34*, 6561-6564.
248. Donovan, M. S.; Lowe, A. B.; Sumerlin, B. S.; McCormick, C. L., *Macromolecules* **2002**, *35*, 4123-4132.
249. Donovan, M. S.; Sanford, T. A.; Lowe, A. B.; Sumerlin, B. S.; Mitsukami, Y.; McCormick, C. L., *Macromolecules* **2002**, *35*, 4570-4572.
250. Mitsukami, Y.; Donovan, M. S.; Lowe, A. B.; McCormick, C. L., *Macromolecules* **2001**, *34*, 2248-2256.
251. Yang, Z.; Pickard, S.; Deng, N.-J.; Raymond J. Barlow; Attwood, D.; Booth, C., *Macromolecules* **1994**, *27*, 2371-2379.
252. Hua, F.; Jiang, X.; Zhao, B., *Macromolecules* **2006**, *39*, 3476-3479.
253. Yusa, S.-i.; Shimada, Y.; Mitsukami, Y.; Yamamoto, T.; Morishima, Y., *Macromolecules* **2004**, *37*, 7507-7513.
254. Convertine, A. J.; Lokitz, B. S.; Vasileva, Y.; Myrick, L. J.; Scales, C. W.; Lowe, A. B.; McCormick, C. L., *Macromolecules* **2006**, *39*, 1724-1730.
255. Sugihara, S.; Kanaoka, S.; Aoshima, S., *J. Polym. Sci., Part A: Polym. Chem.* **2004**, *42*, 2601-2611.
256. Lutz, J.-F.; Laschewsky, A., *Macromol. Chem. Phys.* **2006**, *206*, 813-817.
257. Brandrup, J.; Immergut, E. H.; Grulke, E. A., *Polymer Handbook*. 4th ed.; John Wiley & Sons, Inc.: Hoboken, New Jersey, 1999.

258. Fijten, M. W. M.; Paulus, R. M.; Schubert, U. S., *J. Polym. Sci., Part A: Polym. Chem.* **2005**, *43*, 3831-3839.
259. Downer, A.; Eastoe, J.; Pitt, A. R.; Simister, E. A.; Penfold, J., *Langmuir* **1999**, *15*, 7591-7599.
260. Eastoe, J.; Paul, A.; Rankin, A.; Wat, R.; Penfold, J.; Webster, J. R. P., *Langmuir* **2001**, *17*, 7873-7878.
261. Pai, T. S. C.; Barner-Kowollik, C.; Davis, T. P.; Stenzel, M. H., *Polymer* **2004**, *45*, 4383-4389.
262. Rademacher, J. T.; Baum, M.; Pallack, M. E.; Brittain, W. J.; William J. Simonsick, J., *Macromolecules* **2000**, *33*, 284-288.
263. Hirao, A.; Sugiyama, K.; Yokoyama, H., *Prog. Polym. Sci.* **2007**, *32*, 1393-1438.
264. Blagodatskikh, I. V.; Sutkevich, M. V.; Sitnikova, N. L.; Churochkina, N. A.; Pryakhina, T. A.; Philippova, O. E., *J. Chromat. A* **2002**, *976*, 155-164.
265. Ma, Z.; Lacroix-Desmazes, P., *J. Polym. Sci., Part A: Polym. Chem.* **2004**, *42*, 2405-2415.
266. Guyot, B.; Ameduri, B.; Boutevin, B.; Melas, M.; Viguier, M.; Collet, A., *Macromol. Chem. Phys.* **1998**, *199*, 1879-1885.
267. Stenzel, M. H.; Barner-Kowollik, C.; Davis, T. P.; Dalton, H. M., *Macromol. Biosci.* **2004**, *4*, 445-453.
268. Bertin, P. A.; Watson, K. J.; Nguyen, S. T., *Macromolecules* **2004**, *37*, 8364-8372.
269. Vamvakaki, M.; Palioura, D.; Spyros, A.; Armes, S. P.; Anastasiadis, S. H., *Macromolecules* **2006**, *39*, 5106-5112.
270. Cui, H.; Hodgdon, T. K.; Kaler, E. W.; Abezgauz, L.; Danino, D.; Lubovsky, M.; Talmon, Y.; Pochan, D. J., *Soft Matter* **2007**, *3*, 945-955.
271. Letchford, K.; Burt, H., *Eur. J. Pharm. Biopharm.* **2007**, *65*, 259-269.
272. Gaucher, G.; Dufresne, M.-H.; Sant, V. P.; Kang, N.; Maysinger, D.; Leroux, J.-C., *J. Contr. Rel.* **2005**, *109*, 169-188.
273. Vangeyte, P.; Gautier, S.; Jerome, R., *Colloids Surf. A* **2004**, *242*, 203-211.
274. Yu, Y.; Zhang, L.; Eisenberg, A., *Macromolecules* **1998**, *31*, 1144-1154.
275. Shen, H.; Eisenberg, A., *J. Phys. Chem. B* **1999**, *103*, 9473-9487.
276. Gaumet, M.; Vargas, A.; Gurny, R.; Delie, F., *Eur. J. Pharm. Biopharm.* **2008**, *69*, 1-9.
277. Won, Y.-Y.; Davis, H. T.; Bates, F. S., *Macromolecules* **2003**, *36*, 953-955.
278. Danino, D.; Bernheim-Groswasser, A.; Talmon, Y., *Colloids Surf. A* **2001**, *183-185*, 113-122.
279. Zheng, Y.; Won, Y.-Y.; Bates, F. S.; Davis, H. T.; Scriven, L. E.; Talmon, Y., *J. Phys. Chem. B* **1999**, *103*, 10331-10334.
280. Won, Y.-Y.; Brannan, A. K.; Davis, H. T.; Bates, F. S., *J. Phys. Chem. B* **2002**, *106*, 3354-3364.
281. Won, Y.-Y.; Davis, H. T.; Bates, F. S.; Agamalian, M.; Wignall, G. D., *J. Phys. Chem. B* **2000**, *104*, 7134-7143.
282. Lin, E. K.; Gast, A. P., *Macromolecules* **1996**, *29*, 390-397.
283. Semenov, A. N.; Nyrkova, I. A.; Khokhlov, A. R., *Macromolecules* **1995**, *28*, 7491-7500.
284. Lodge, T. P.; Hillmyer, M. A.; Zhou, Z.; Talmon, Y., *Macromolecules* **2004**, *37*, 6680-6682.
285. Edmonds, W. F.; Li, Z.; Hillmyer, M. A.; Lodge, T. P., *Macromolecules* **2006**, *39*, 4526-4530.
286. Skrabania, K.; von Berlepsch, H.; Böttcher, C.; Laschewsky, A., *publication in preparation*.
287. Nakano, M.; Matsumoto, K.; Matsuoka, H.; Yamaoka, H., *Macromolecules* **1999**, *32*, 4023-4029.
288. Le, T. P. T.; Moad, G.; Rizzardo, E.; Thang, S. H. Intern Pat Appl 1998: PCT WO9801478 [CA 1998: 15390]. 1998.
289. Parrod, J.; Elles, J., *J. Polym. Sci.* **1958**, *24*, 411-416.

Appendix 1: NMR spectra of chain transfer agents (CTAs)

Figure A1.1 ^1H NMR spectrum of CTA1 in CDCl_3 Figure A1.2 ^{13}C NMR spectrum of CTA1 in CDCl_3

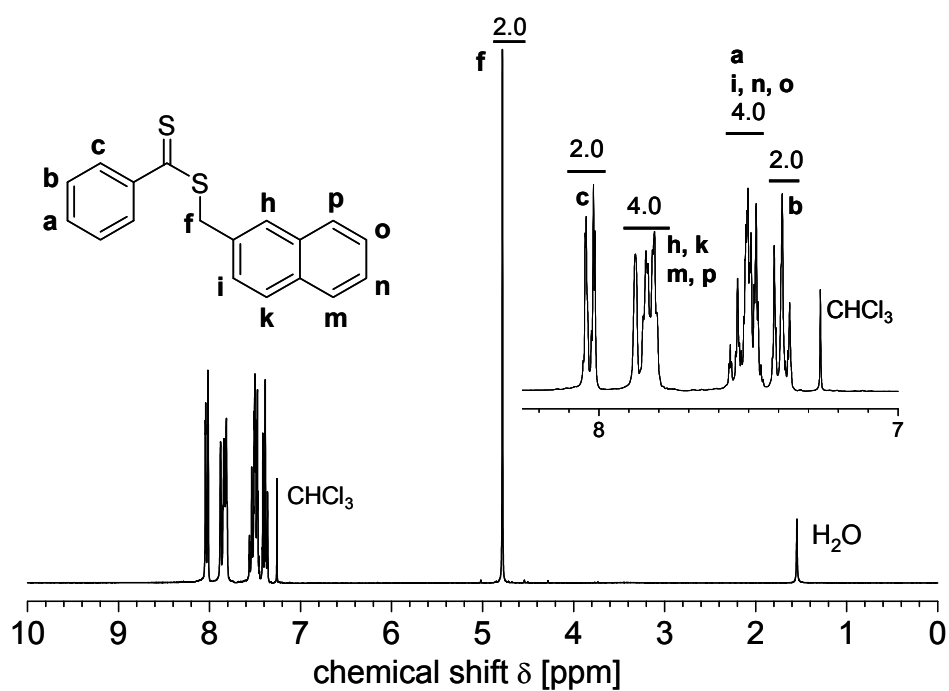


Figure A1.3 ^1H NMR spectrum of CTA2 in CDCl_3

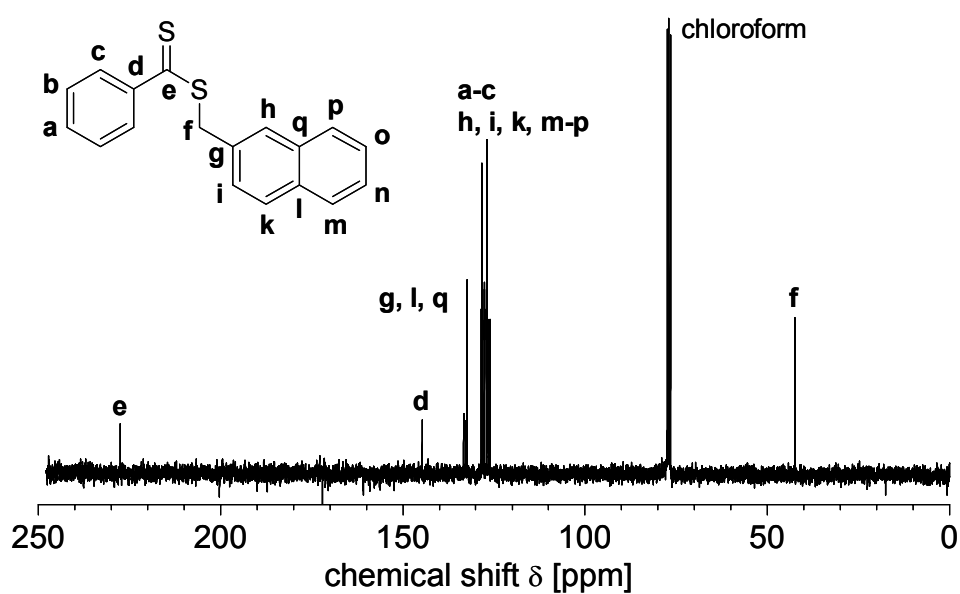


Figure A1.4 ^{13}C NMR spectrum of CTA2 in CDCl_3

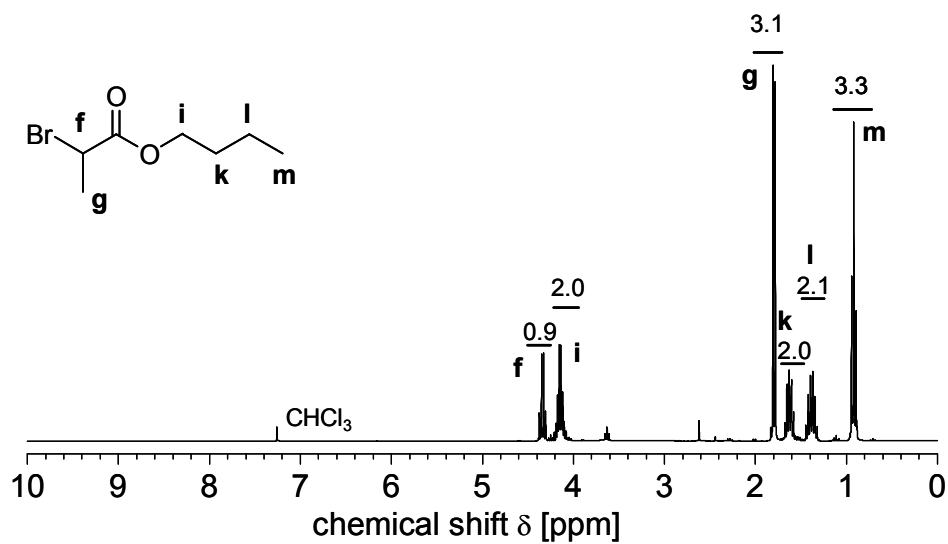


Figure A1.5 ^1H NMR spectrum of butyl 2-bromo-propionate in CDCl_3

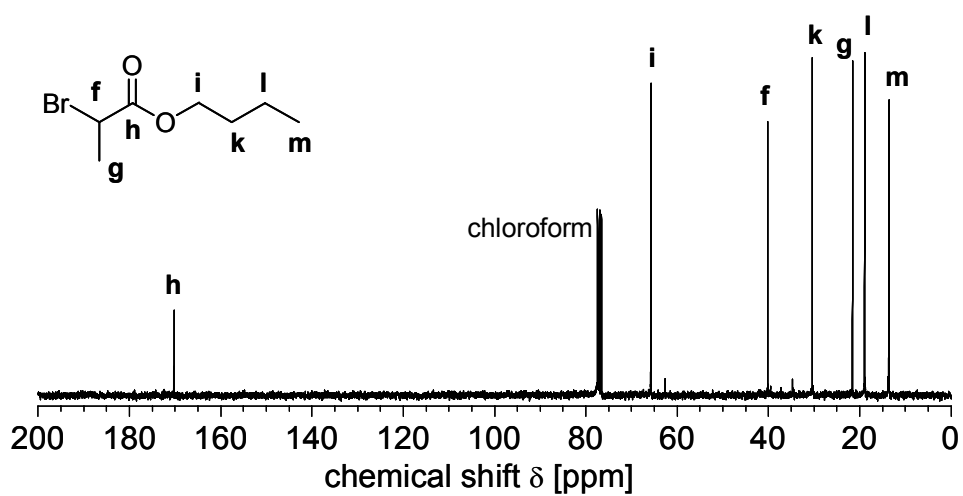


Figure A1.6 ^{13}C NMR spectrum of butyl 2-bromo-propionate in CDCl_3

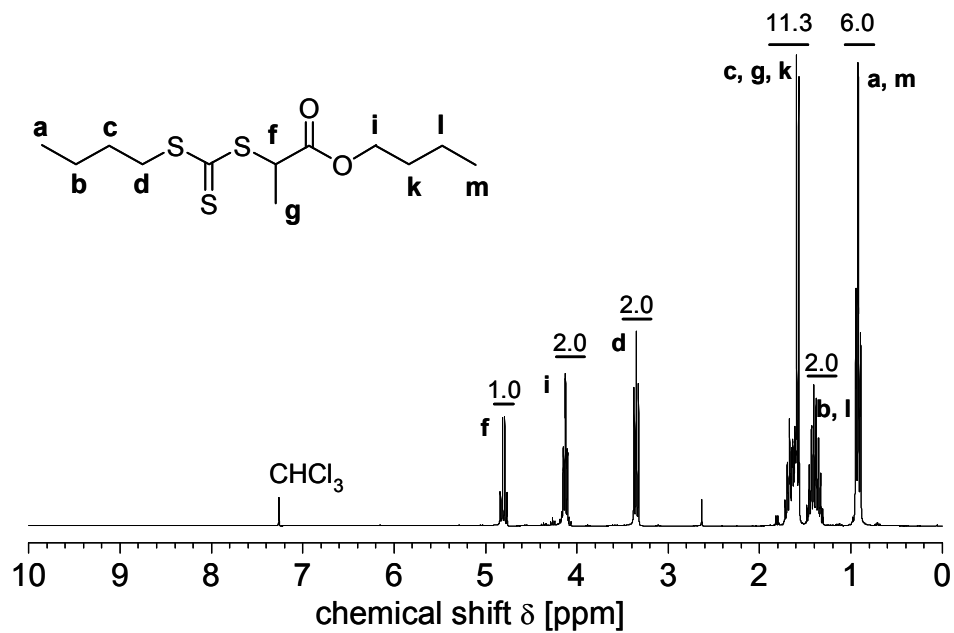


Figure A1.7 ^1H NMR spectrum of CTA5 in CDCl_3

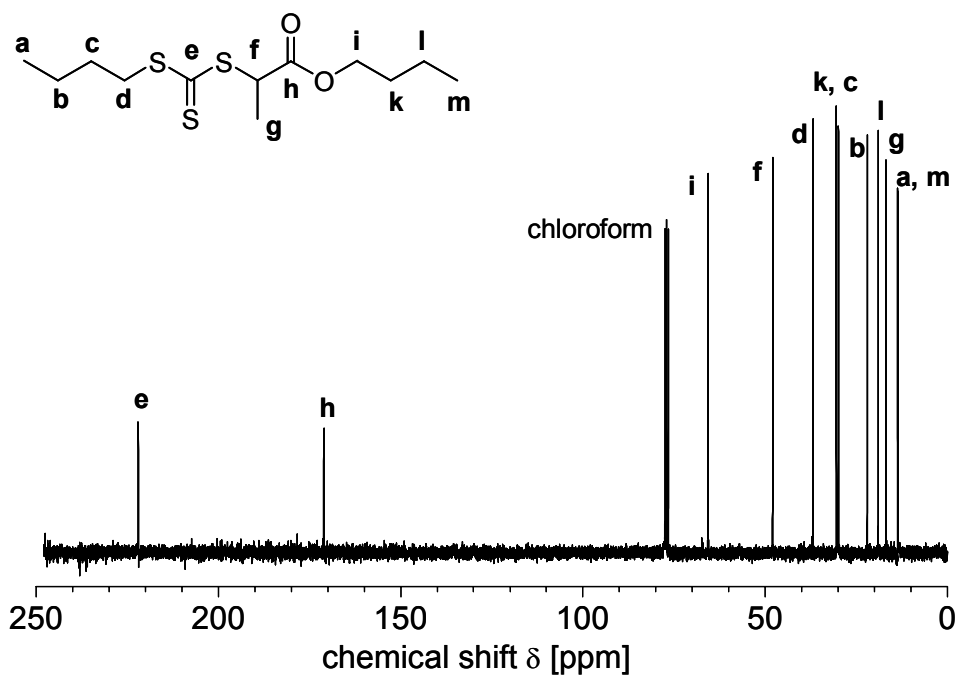


Figure A1.8 ^{13}C NMR spectrum of CTA5 in CDCl_3

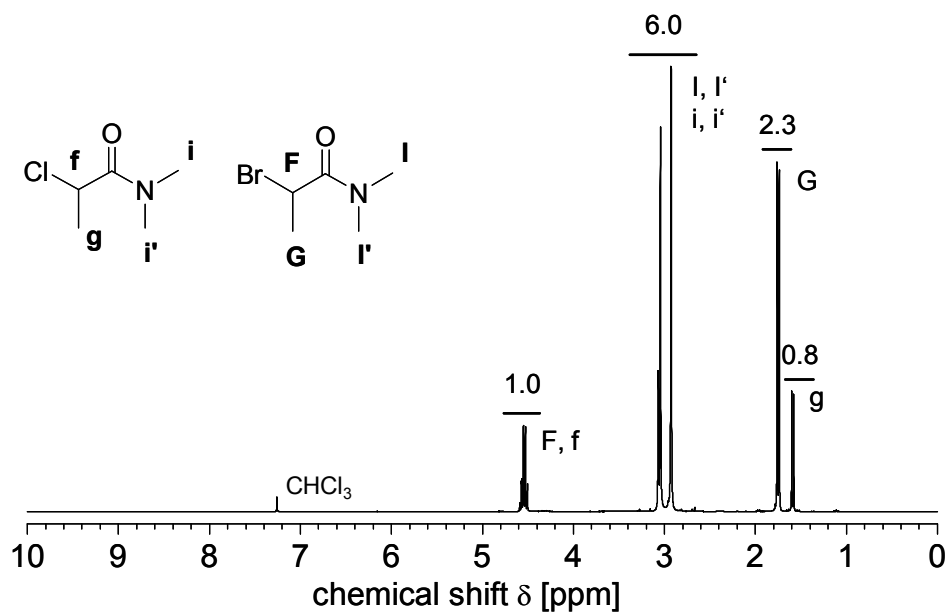


Figure A1.9 ^1H NMR spectrum of N,N -dimethyl 2-bromo-propionamide with N,N -dimethyl 2-chloro-propionamide as by-product in CDCl_3

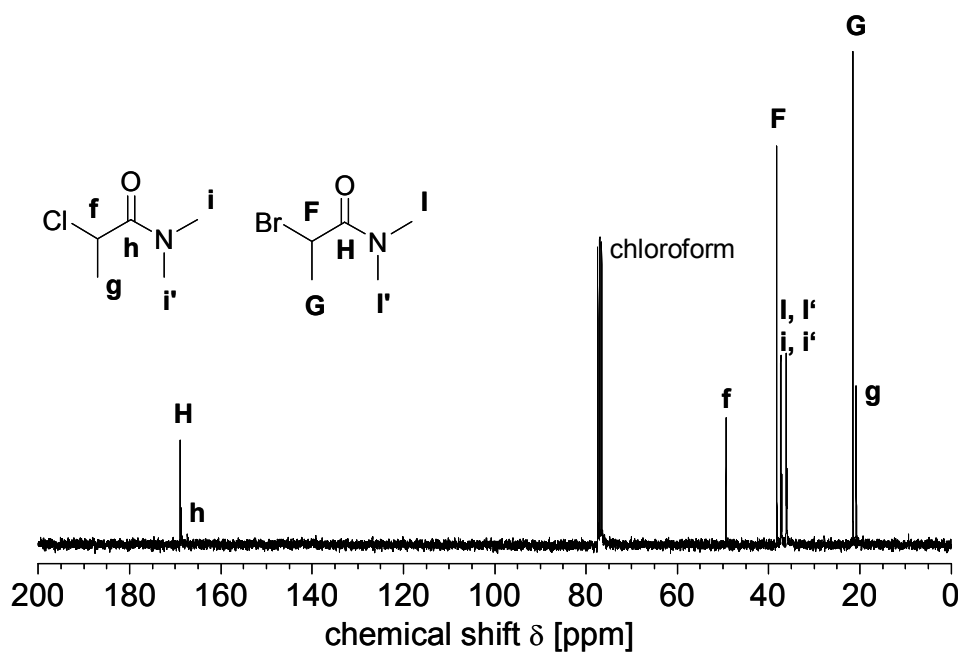


Figure A1.10 ^{13}C NMR spectrum of N,N -dimethyl 2-bromo-propionamide with N,N -dimethyl 2-chloro-propionamide as by-product in CDCl_3

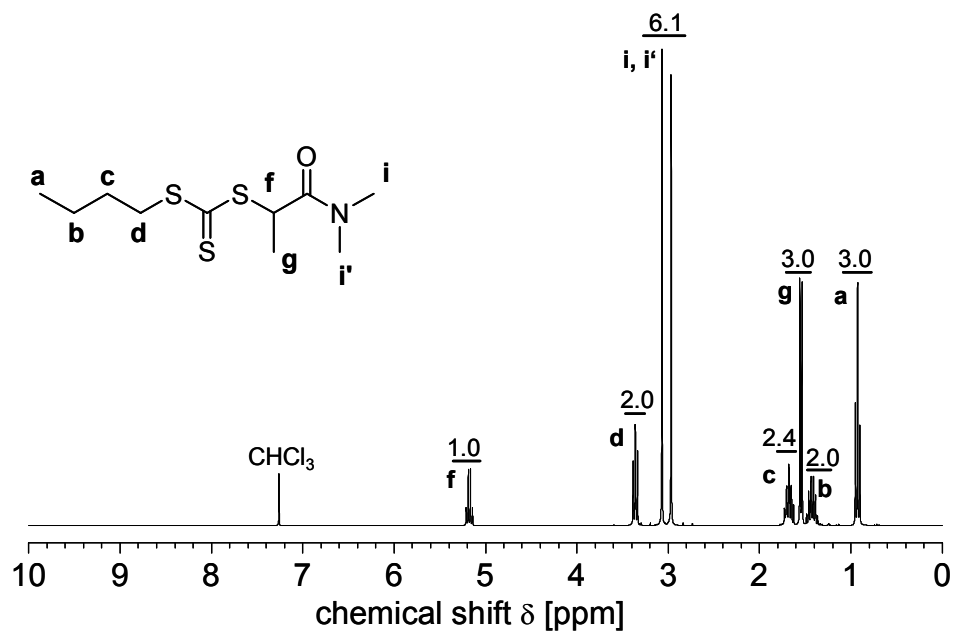


Figure A1.11 ¹H NMR spectrum of CTA6 in CDCl₃

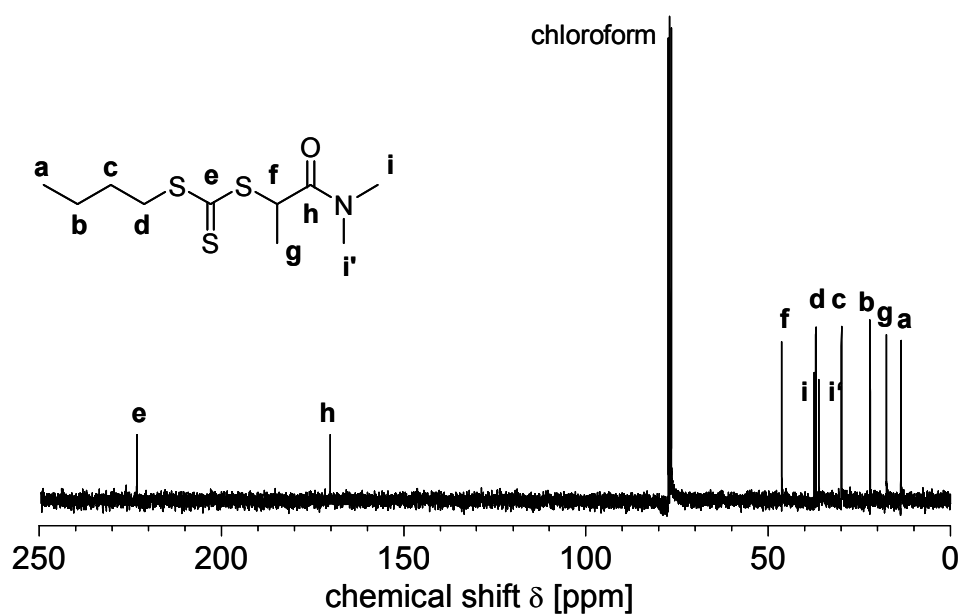


Figure A1.12 ¹³C NMR spectrum of CTA6 in CDCl₃

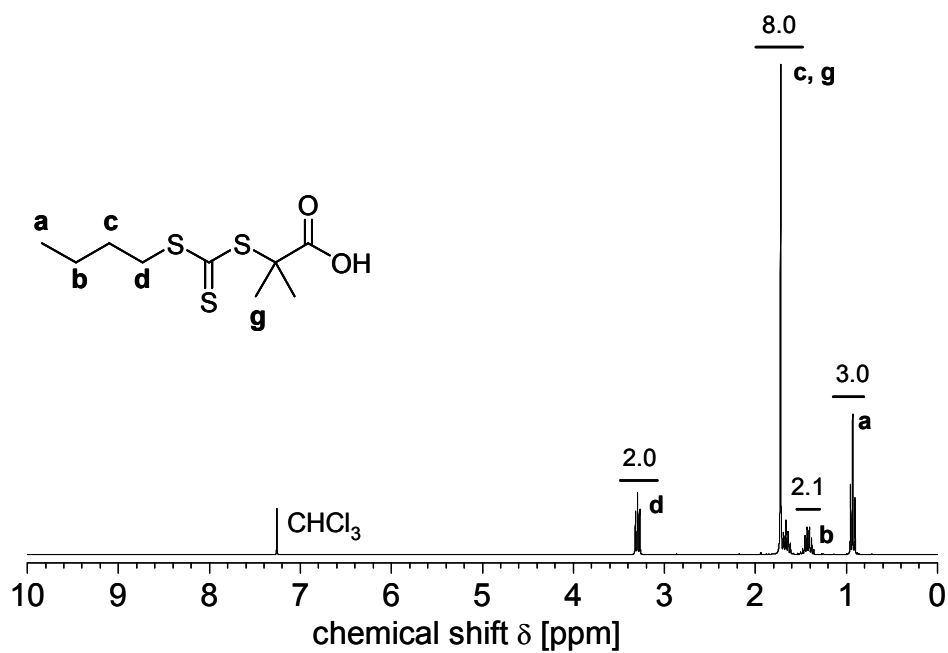


Figure A1.13 ¹H NMR spectrum of CTA7 in CDCl₃

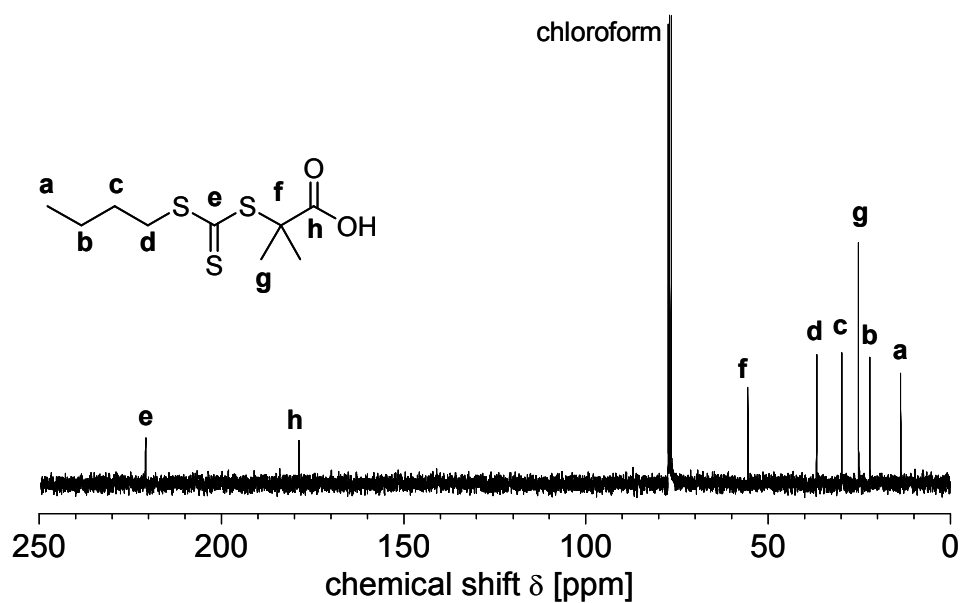


Figure A1.14 ¹³C NMR spectrum of CTA7 in CDCl₃

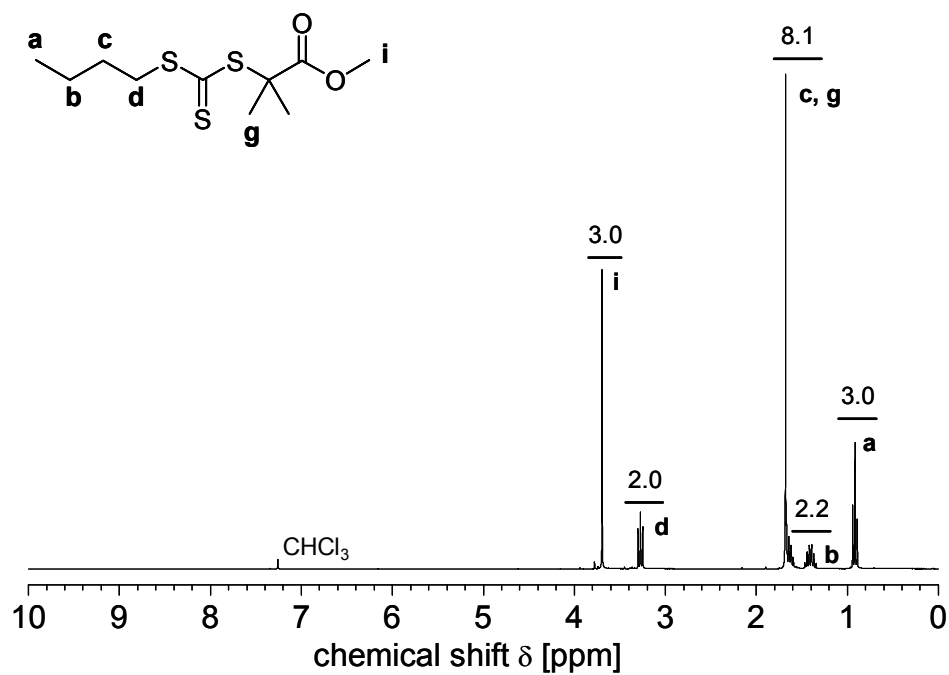


Figure A1.15 ¹H NMR spectrum of CTA8 in CDCl₃

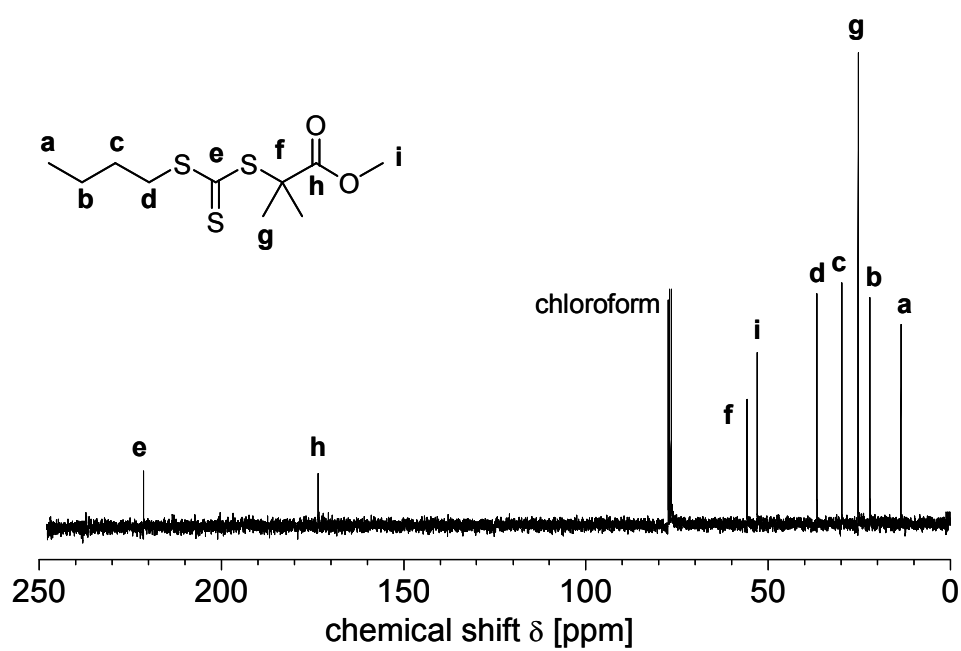


Figure A1.16 ¹³C NMR spectrum of CTA8 in CDCl₃

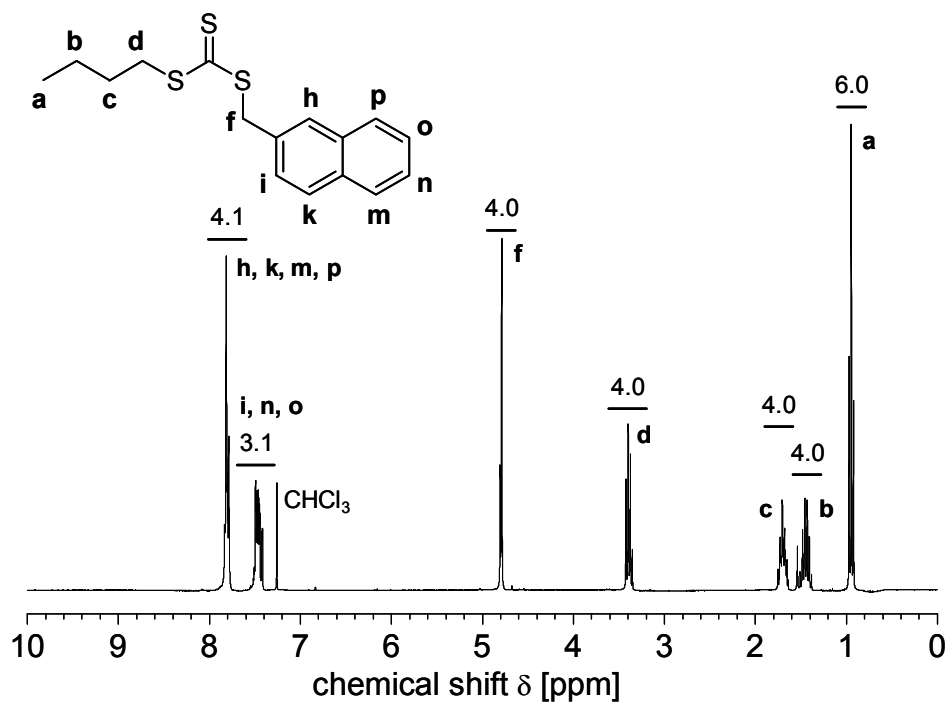


Figure A1.17 ¹H NMR spectrum of CTA10 in CDCl₃

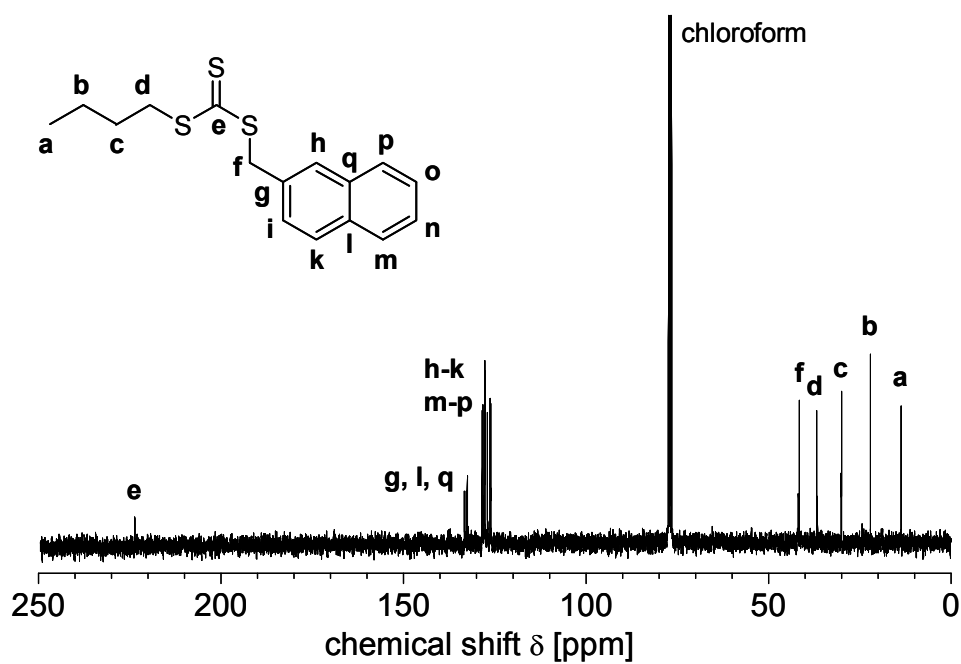


Figure A1.18 ¹³C NMR spectrum of CTA10 in CDCl₃

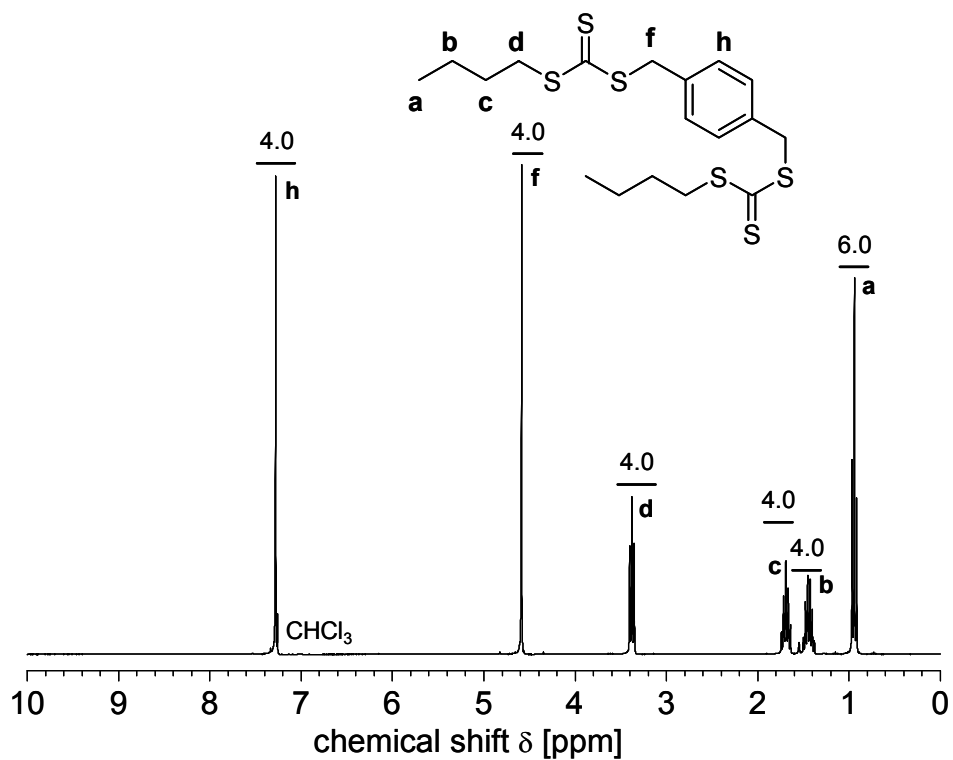


Figure A1.19 ^1H NMR spectrum of CTA12 in CDCl_3

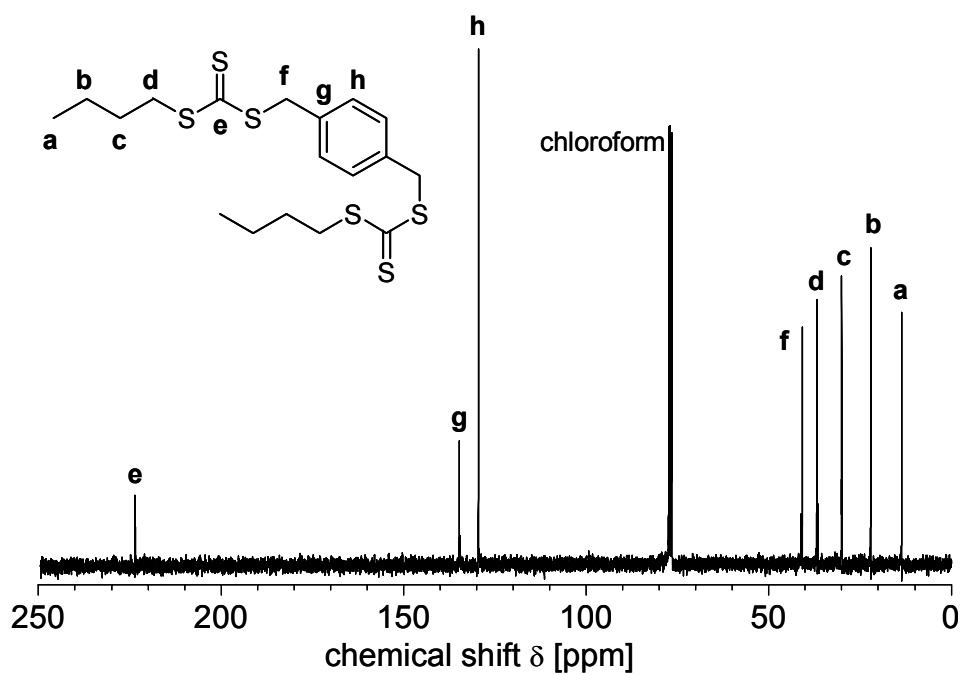


Figure A1.20 ^{13}C NMR spectrum of CTA12 in CDCl_3

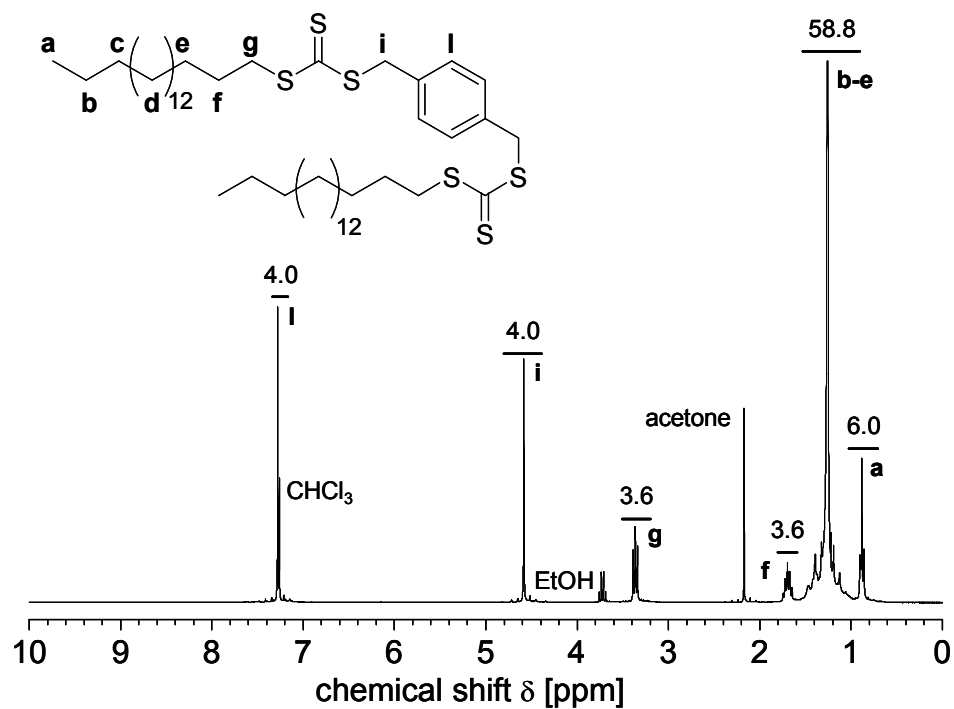


Figure A1.21 ¹H NMR spectrum of CTA13 in CDCl₃

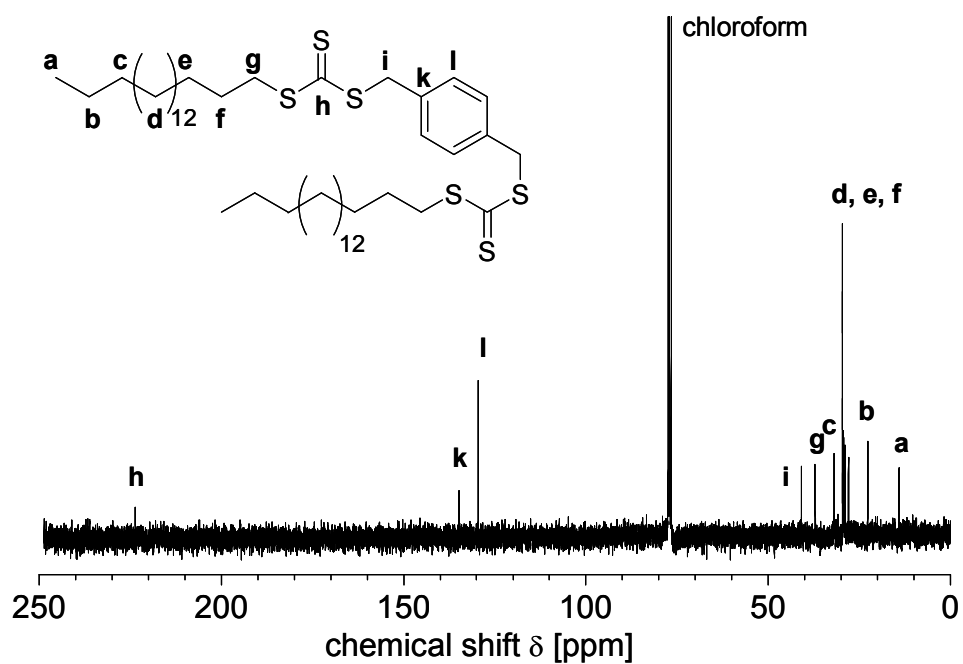


Figure A1.22 ¹³C NMR spectrum of CTA13 in CDCl₃

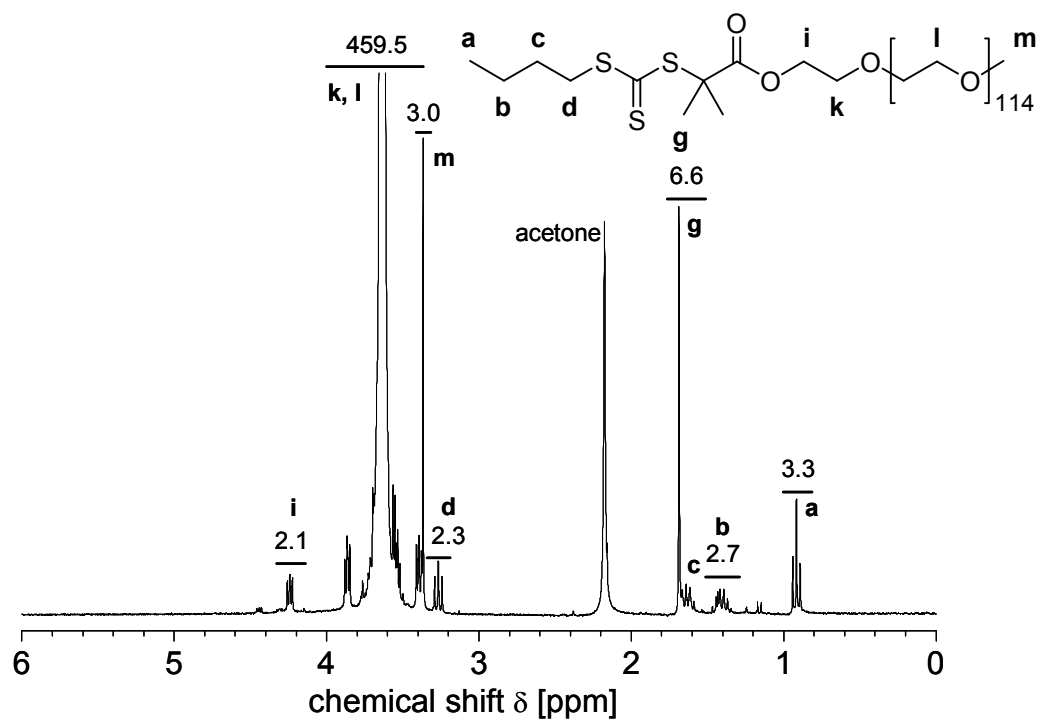
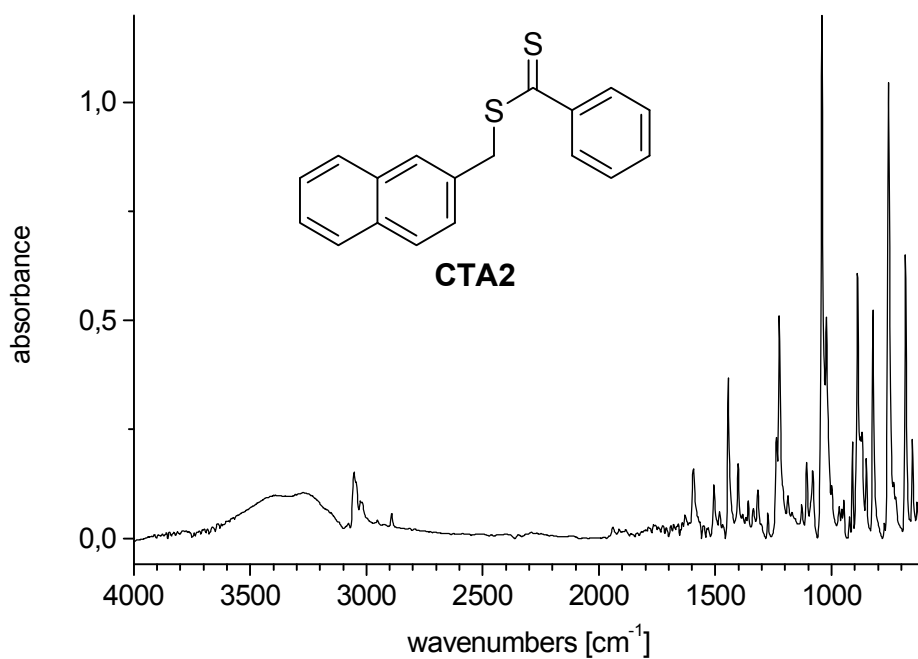
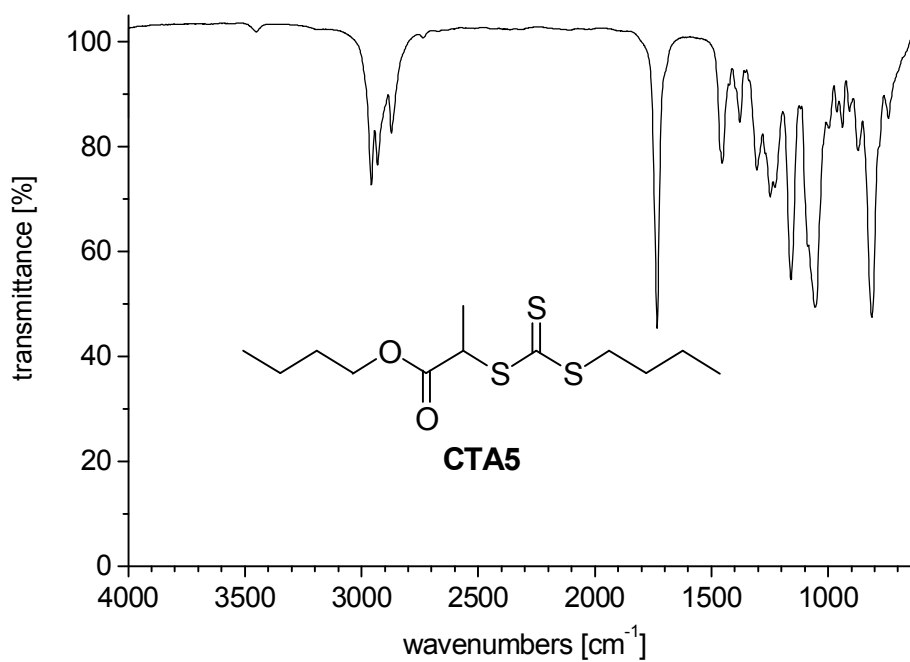


Figure A1.23 ^1H NMR spectrum of CTA14 in CDCl_3

Appendix 2: IR-spectra of CTAs

Figure A2.1 FT-IR spectrum of **CTA2** (KBr pellet)Figure A2.2 FT-IR spectrum of **CTA5** (KBr pellet)

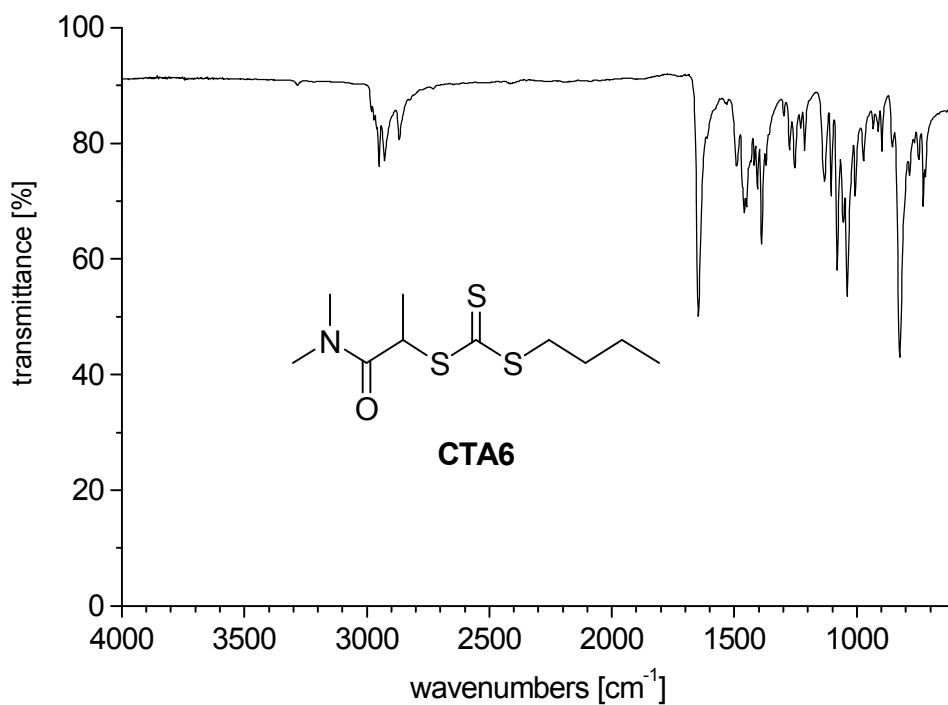


Figure A2.3 FT-IR spectrum of **CTA6** (KBr pellet)

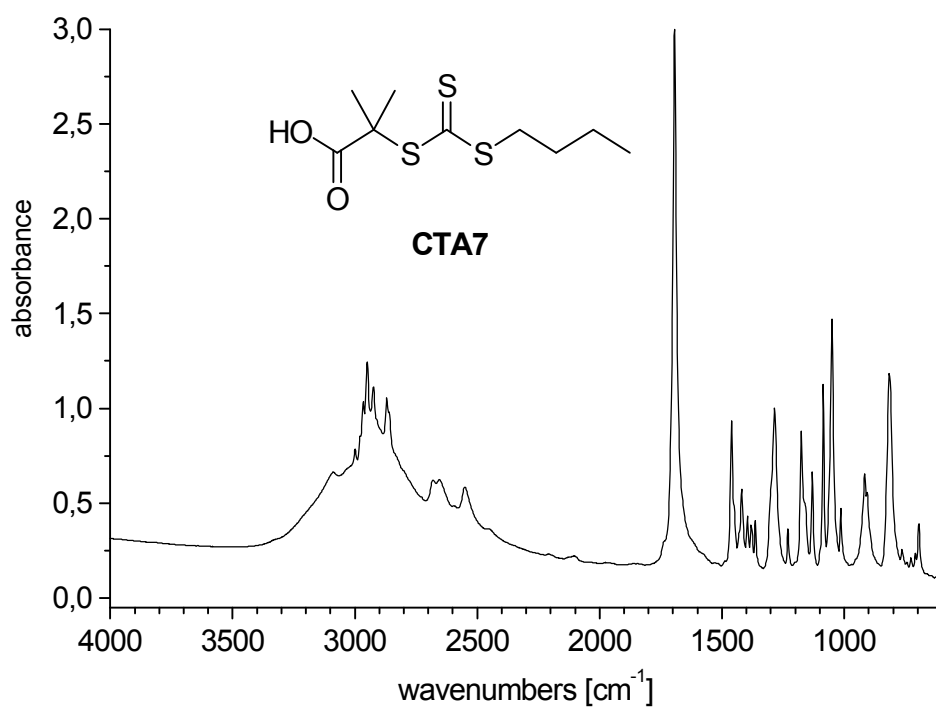


Figure A2.4 FT-IR spectrum of **CTA7** (KBr pellet)

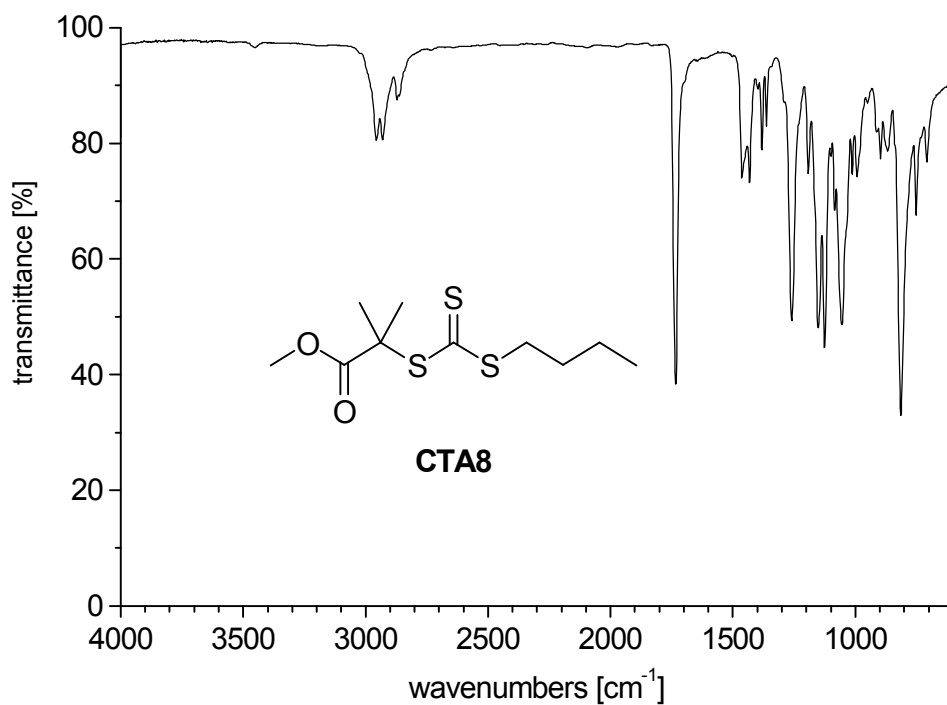


Figure A2.5 FT-IR spectrum of **CTA8** (KBr pellet)

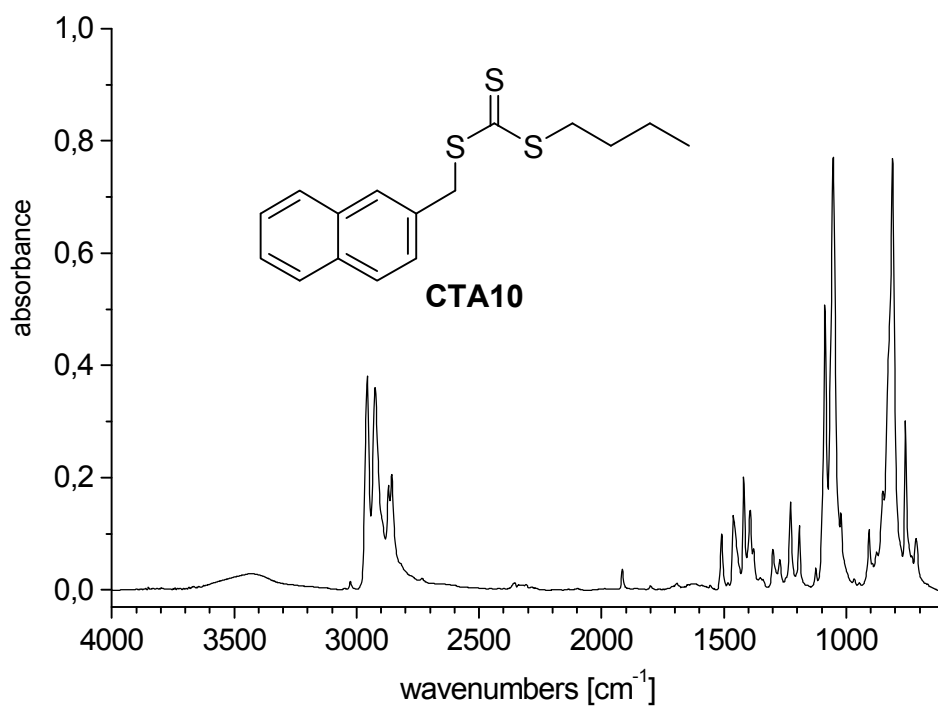


Figure A2.6 FT-IR spectrum of **CTA10** (KBr pellet)

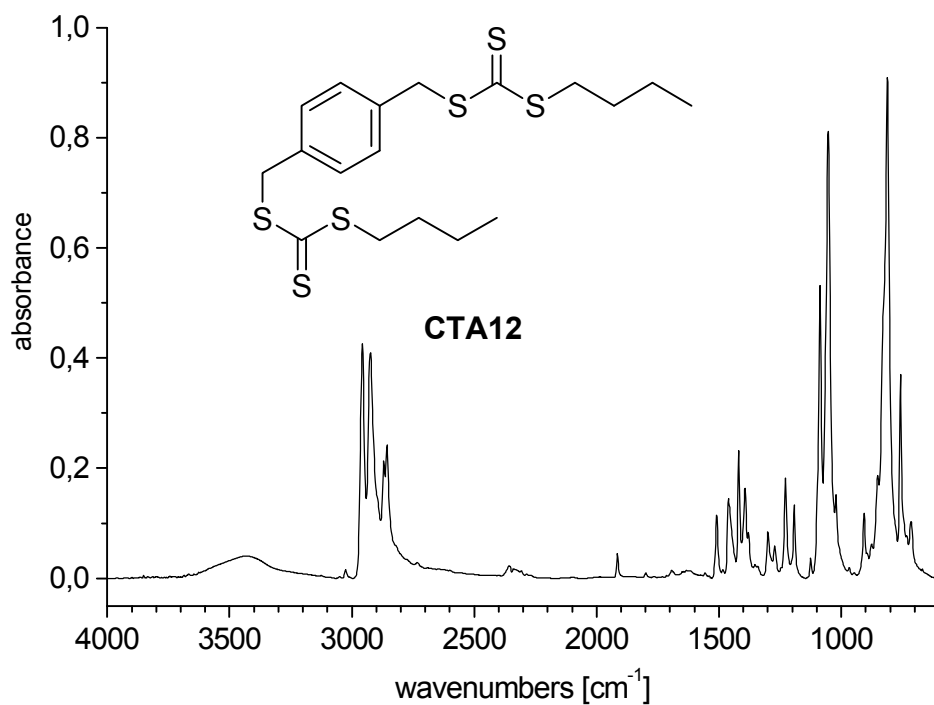


Figure A2.7 FT-IR spectrum of CTA12 (KBr pellet)

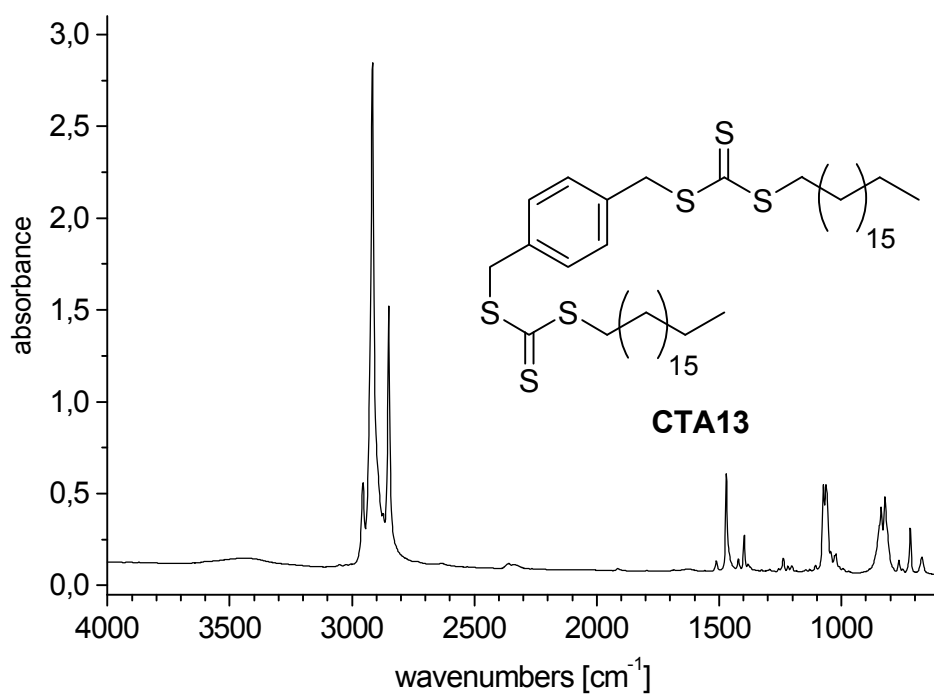


Figure A2.8 FT-IR spectrum of CTA13 (KBr pellet)

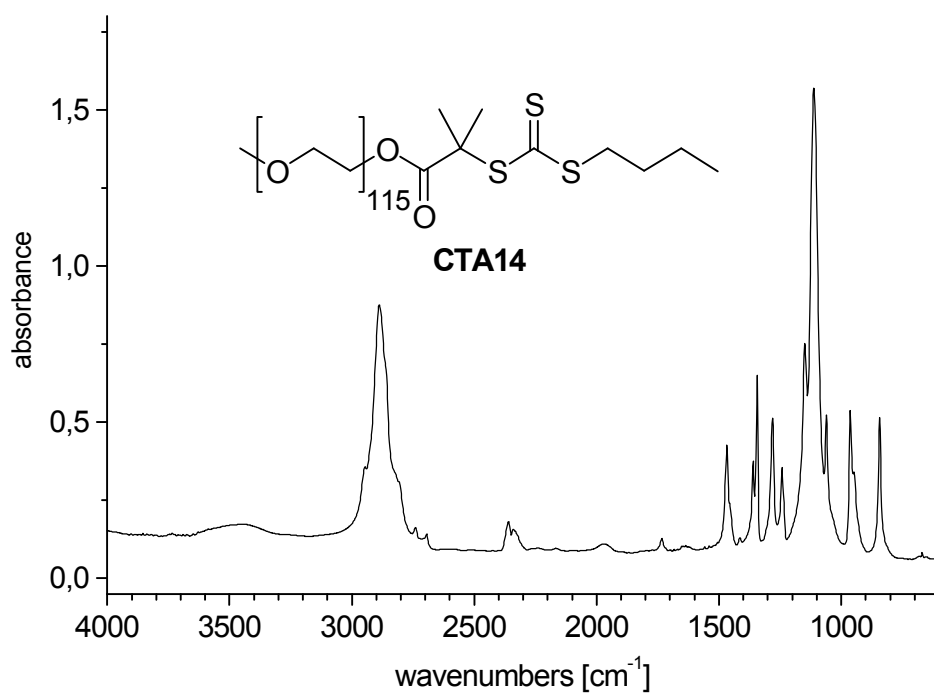


Figure A2.9 FT-IR spectrum of CTA14 (KBr pellet)

Appendix 3: Cryo-TEM micrographs of amphiphilic block copolymers

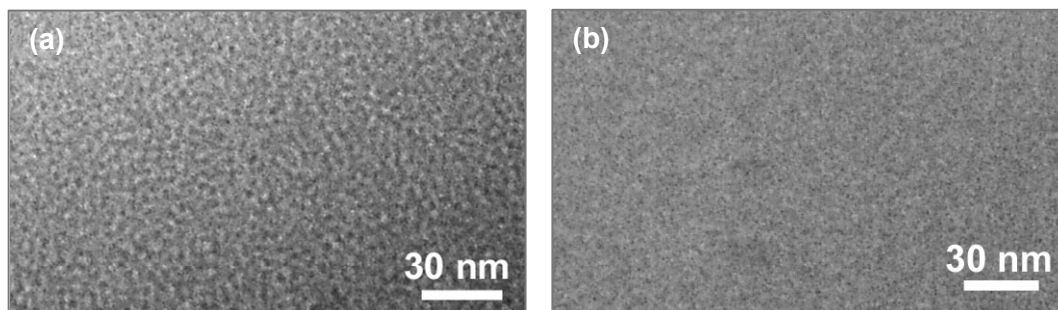


Figure A3.1 Cryo-TEM micrographs of 0.5 wt% aqueous solutions of PEO homopolymers. (a) comb polymer $(\mathbf{M1})_{70}$ (b) linear PEO ($M \sim 20,000$ g/mol).

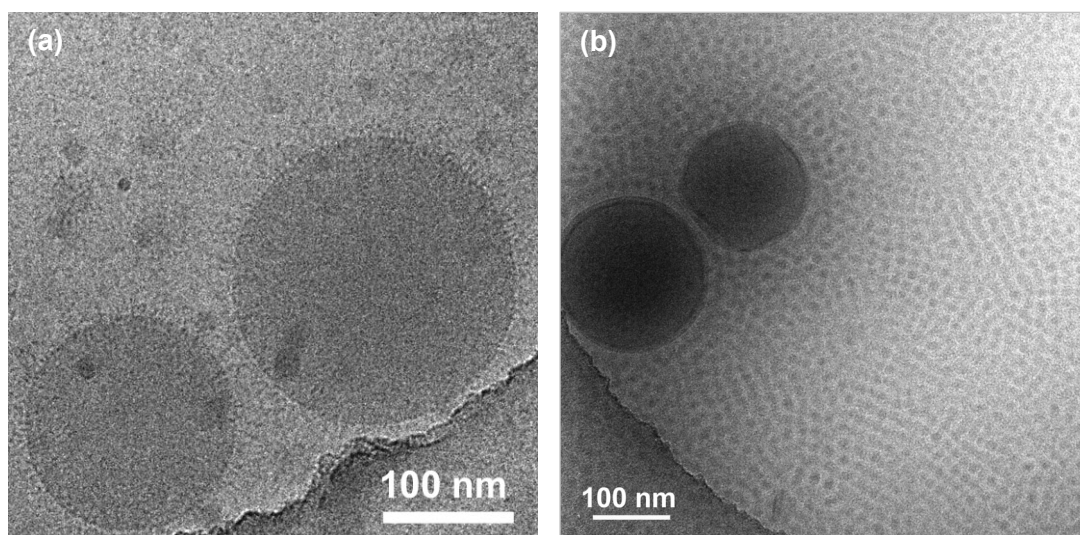


Figure A3.2 Large spherical objects observed for 0.5 wt% aqueous solution of block copolymers (a) $(\mathbf{M6})_{120}$ - $(\mathbf{M1})_{50}$ (b) $\text{PEO}-(\mathbf{M5})_{22}$ - $(\mathbf{M7})_2$.

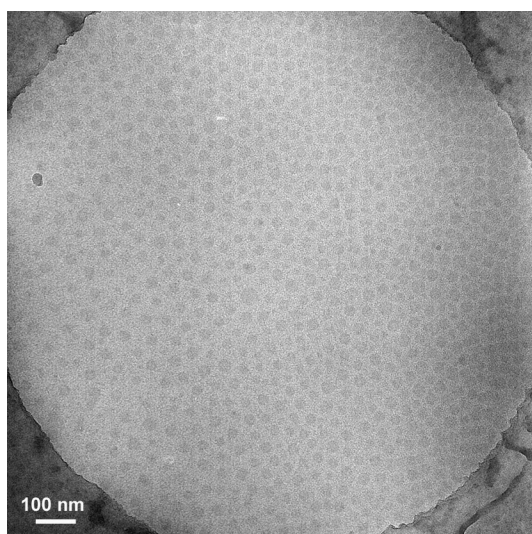


Figure A3.3 Cryo-TEM micrograph of $(\mathbf{M6})_{120}$ - $(\mathbf{M1})_{109}$ (0.5 wt% in H_2O).

Appendix 4: List of figures

- Figure 1.1** Association of AB diblock copolymers into spherical micelles in a selective solvent for the A block
- Figure 1.2** Morphologies of spherical block copolymer micelles
- Figure 1.3** Modification of solid surfaces by block copolymers and block copolymer micelles: (a) Soluble block A interacts with surface (b) Insoluble block B interacts with surface.
- Figure 1.4** Various architectures of ABC triblock copolymers
- Figure 1.5** Micelle morphologies of ABC triblock copolymers in selective solvents: (a) “onion” micelle (b) Janus micelle.
- Figure 1.6** Repeating units of stimuli-responsive polymers
- Figure 1.7** Phase separation in mixtures of hydrocarbon (HC) and fluorocarbon (FC) amphiphiles: (a) mixture of HC and FC surfactants (b) mixture of a standard phospholipid and a HC/FC diblock.
- Figure 1.8** Macromolecular design of multi-compartment micellar systems
- Figure 1.9** Morphologies of micellar cores found for multi-compartment polymeric micelles: (a) spherical and (b) disk-like core-shell-corona micelles (c) segmented worm-like micelle (d) “hamburger” micelle and (e) sphere-on-sphere morphology. For clarity, the hydrophilic corona is omitted.
- Figure 1.10** Nitroxyl-mediated polymerization: (a) Mechanism (b) Examples of typical nitroxyls.
- Figure 1.11** Mechanism of ATRP polymerization
- Figure 1.12** General structure of a RAFT agent
- Figure 1.13** Mechanism of RAFT polymerization
- Figure 1.14** Resonance structures of the intermediate radical in dithiobenzoate-mediated RAFT polymerization
- Figure 1.15** Models for rate retardation in RAFT polymerization by: (a) irreversible and (b) reversible cross-termination.
- Figure 1.16** Resonance structures of (a) dithiocarbamates and (b) xanthates
- Figure 1.17** Effect of the block sequence on the chain transfer step in the synthesis of block copolymers by RAFT: (a) polymerization of a methacrylate monomer using a polyacrylate macroCTA (b) polymerization of an acrylate monomer with a polymethacrylate macroCTA.
- Figure 2.1** Guidelines for the selection of RAFT agents for various polymerizations. For Z, addition rates decrease and fragmentation rates increase from left to right. For R, fragmentation rates decrease from left to right. Dashed lines indicate partial control.
- Figure 2.2** Frequently used synthetic routes to thiocarbonylthio compounds
- Figure 2.3** CTAs studied by UV-vis spectroscopy
- Figure 3.1** General structures of CTAs and macroCTAs
- Figure 3.2** The categories of RAFT agents according to their Z group
- Figure 3.3** Macromolecular CTAs and their corresponding low-molar mass model compounds with a similar substitution pattern

- Figure 3.4** UV-vis spectra of **CTA6** (solid line) and **CTA7** (dashed line) in CH₃OH
- Figure 3.5** UV spectra of model CTAs and macroCTAs: (a) **CTA6** and a poly(*N,N*-dimethyl acrylamide) macroCTA in CH₃OH (b) **CTA5** and a poly(*n*-butyl acrylate) macroCTA in *n*-butyl acetate. Solid line: model CTA, dashed line: macroCTA.
- Figure 3.6** UV-vis spectra of CTAs with naphthalenyl-2-methyl R groups: (a) **CTA2** (b) **CTA10**. Solid line: in *n*-hexane, dashed line: in CH₂Cl₂.
- Figure 3.7** UV spectra of **CTA10** (solid line), **CTA5** (dotted line) (both in CH₂Cl₂) and 2-ethyl naphthalene (dashed line).
- Figure 4.1** Effect of temperature on the amphiphile architectures of double-thermoresponsive triblock copolymers
- Figure 4.2** Monomers and CTA used for the synthesis of double-thermoresponsive triblock copolymers
- Figure 4.3** ¹H NMR spectrum of triblock copolymer **(M4)₁₁₀-(M3)₇₀-(M2)₆₄** in D₂O
- Figure 4.4** SEC elugrams of macroCTAs: (a) **(M2)₁₃₉** and (b) **(M4)₁₁₀** according to RI (dashed line) and UV (solid line) detection. Eluent: *N*-methyl pyrrolidone (0.05 M LiBr).
- Figure 4.5** SEC elugrams of the acrylamide-based ABC triblock copolymers and their respective precursors according to RI response (eluent: 0.05 LiBr in *N*-methyl pyrrolidone): (a) **(M4)₁₁₀-(M3)₇₀-(M2)₆₄** (b) **(M4)₁₁₀-(M2)₅₂-(M3)₆₉** (c) **(M2)₁₃₉-(M4)₅₂-(M3)₂₈**.
- Figure 4.6** Thermo-responsive behavior of polymer **(M3)₅₂** in water: (a) Temperature dependent transmittance of an aqueous solution (0.3 wt%) at 670 nm. Closed triangles: heating (1.0°C/min); open triangles: cooling (1.0°C/min) (b) Clouding temperatures for aqueous solutions of **(M3)₅₂** (0.3 wt%) as a function of NaCl concentration.
- Figure 4.7** Thermo-responsive behavior of a 0.1 wt% aqueous solution of a 1:1:1 (by weight) mixture of **(M4)₁₁₀**, **(M3)₅₂** and **(M2)₁₃₉** as followed by turbidimetry. Solid squares: heating (1.0°C/min); open squares: cooling (1.0°C/min).
- Figure 4.8** Thermo-responsive behavior of 0.1 wt% aqueous solutions of diblock copolymers as followed by turbidimetry: (a) **(M4)₁₁₀-(M3)₇₀** (b) **(M4)₁₁₀-(M2)₅₂** (c) **(M2)₁₃₉-(M4)₅₂**. Closed circles: heating (1.0°C/min); open circles: cooling (1.0°C/min).
- Figure 4.9** Thermo-responsive behavior of 0.1 wt% aqueous solutions of triblock copolymers as followed by turbidimetry: (a) **(M4)₁₁₀-(M3)₇₀-(M2)₆₄** (b) **(M4)₁₁₀-(M2)₅₂-(M3)₆₉** (c) **(M2)₁₃₉-(M4)₅₂-(M3)₂₈**. Closed squares: heating (1.0°C/min), open squares: cooling (1.0°C/min).
- Figure 4.10** Thermo-responsive behavior of a 0.1 wt% aqueous solution of a 1:1 (by weight) mixture of **(M2)₁₃₉-(M4)₅₂** and **(M3)₅₂** as followed by turbidimetry. Closed squares: heating (1.0°C/min), open squares: cooling (1.0°C/min).
- Figure 4.11** Temperature dependent ¹H NMR spectra of double-thermoresponsive triblock copolymers in D₂O at 25°C, 45°C and 65°C: (a) **(M4)₁₁₀-(M3)₇₀-(M2)₆₄** (b) **(M4)₁₁₀-(M2)₅₂-(M3)₆₉** (c) **(M2)₁₃₉-(M4)₅₂-(M3)₂₈**.
- Figure 4.12** Temperature dependent evolution of particle sizes (Z-average) of 0.1 wt% aqueous solutions of ternary block copolymers as followed by DLS: (a) **(M4)₁₁₀-(M3)₇₀-(M2)₆₄** (b) **(M4)₁₁₀-(M2)₅₂-(M3)₆₉** (c) **(M2)₁₃₉-(M4)₅₂-(M3)₂₈**.
- Figure 4.13** Chain topologies of triblock copolymers with associating end blocks: (a) flower-like micelle (b) interconnected micelles (c) dangling chain ends.

- Figure 4.14** Evolution of particle size distributions for 0.1 wt% aqueous solutions of triblock copolymers according to the slow heating protocol: (a) $(\mathbf{M4})_{110}\text{-}(\mathbf{M3})_{70}\text{-}(\mathbf{M2})_{64}$ (b) $(\mathbf{M4})_{110}\text{-}(\mathbf{M2})_{52}\text{-}(\mathbf{M3})_{69}$ (c) $(\mathbf{M2})_{139}\text{-}(\mathbf{M4})_{52}\text{-}(\mathbf{M3})_{28}$.
- Figure 4.15** Evolution of particle size distributions for 0.1 wt% aqueous solutions of triblock copolymers according to the fast heating protocol: (a) $(\mathbf{M4})_{110}\text{-}(\mathbf{M3})_{70}\text{-}(\mathbf{M2})_{64}$ (b) $(\mathbf{M4})_{110}\text{-}(\mathbf{M2})_{52}\text{-}(\mathbf{M3})_{69}$ (c) $(\mathbf{M2})_{139}\text{-}(\mathbf{M4})_{52}\text{-}(\mathbf{M3})_{28}$.
- Figure 4.16** Annealing of 0.1 wt% aqueous solutions of triblock copolymers obtained by the slow and fast heating protocol at 45°C: (a) $(\mathbf{M4})_{110}\text{-}(\mathbf{M3})_{70}\text{-}(\mathbf{M2})_{64}$ (b) $(\mathbf{M4})_{110}\text{-}(\mathbf{M2})_{52}\text{-}(\mathbf{M3})_{69}$ (c) $(\mathbf{M2})_{139}\text{-}(\mathbf{M4})_{52}\text{-}(\mathbf{M3})_{28}$. Particle size distributions after thermal equilibration (solid line), after annealing for 24 h (dashed line) and 48 hours (dotted line).
- Figure 5.1** Monomers used for the synthesis of triphilic ABC block copolymers
- Figure 5.2** CTAs used for the synthesis of triphilic ABC block copolymers
- Figure 5.3** SEC elugrams of triphilic ABC triblock copolymers and their precursors (eluent: THF, flow rate: 1.0 mL min⁻¹, RI detection): (a) $(\mathbf{M1})_{70}\text{-}(\mathbf{M5})_{83}\text{-}(\mathbf{M7})_{13}$ (b) $(\mathbf{M1})_{70}\text{-}(\mathbf{M6})_{140}\text{-}(\mathbf{M7})_{13}$ (c) $(\mathbf{M6})_{120}\text{-}(\mathbf{M1})_{50}\text{-}(\mathbf{M7})_{40}$ (d) $(\mathbf{M6})_{120}\text{-}(\mathbf{M1})_{109}\text{-}(\mathbf{M7})_{25}$. (i), (ii) and (iii) are homopolymer, di- and triblock copolymer, respectively.
- Figure 5.4** SEC elugrams of ABC triblock oligomers prepared from a linear PEO macroCTA (eluent: THF, flow rate 1.0 mL min⁻¹, RI detection): (a) $\text{PEO}\text{-}(\mathbf{M5})_{22}\text{-}(\mathbf{M7})_2$ (b) $\text{PEO}\text{-}(\mathbf{M6})_{24}\text{-}(\mathbf{M7})_2$. (i), (ii) and (iii) are homopolymer, di- and triblock copolymer, respectively.
- Figure 5.5** ¹H NMR spectrum of polymer $(\mathbf{M6})_{120}\text{-}(\mathbf{M1})_{50}\text{-}(\mathbf{M7})_{40}$ in CDCl₃
- Figure 5.6** Differential scanning calorimetry (DSC) traces of (a) homopolymers: (i) $(\mathbf{M1})_{70}$, (ii) $(\mathbf{M6})_{120}$, (ii) **polyM7** and (b) triblock copolymer $(\mathbf{M6})_{120}\text{-}(\mathbf{M1})_{50}\text{-}(\mathbf{M7})_{40}$.
- Figure 5.7** DSC analyses of block copolymers: (a) Traces of $\text{PEO}\text{-}(\mathbf{M5})_{22}\text{-}(\mathbf{M7})_2$ (cooling and 2nd heating run, 20 K/min) (b) Magnified parts of the DSC traces (2nd heating, 20 K/min) of polymers (i) $\text{PEO}\text{-}(\mathbf{M5})_{22}$ and (ii) $\text{PEO}\text{-}(\mathbf{M5})_{22}\text{-}(\mathbf{M7})_2$.
- Figure 5.8** Comparison of the ¹⁹F NMR spectra of the fluorinated monomer **M7** and an ABC triblock copolymer in different solvents: (a) monomer **M7** in CDCl₃ (b) $(\mathbf{M6})_{120}\text{-}(\mathbf{M1})_{50}\text{-}(\mathbf{M7})_{40}$ in CDCl₃ (c) $(\mathbf{M6})_{120}\text{-}(\mathbf{M1})_{50}\text{-}(\mathbf{M7})_{40}$ in THF. Internal reference: α,α,α-trifluorotoluene (TFT).
- Figure 5.9** ¹H NMR spectra of triblock copolymer $(\mathbf{M1})_{70}\text{-}(\mathbf{M5})_{140}\text{-}(\mathbf{M7})_{13}$ in (a) CDCl₃ and in (b) D₂O
- Figure 5.10** Comparison of particle size distributions in 0.5 wt% aqueous solutions of triblock copolymers (solid line) compared to the aggregates of their precursor diblock copolymers (dashed line) as studied by DLS: (a) $(\mathbf{M1})_{70}\text{-}(\mathbf{M5})_{83}\text{-}(\mathbf{M7})_{13}$ (b) $(\mathbf{M1})_{70}\text{-}(\mathbf{M6})_{140}\text{-}(\mathbf{M7})_{13}$ (c) $\text{PEO}\text{-}(\mathbf{M5})_{22}\text{-}(\mathbf{M7})_2$ (d) $\text{PEO}\text{-}(\mathbf{M6})_{24}\text{-}(\mathbf{M7})_2$ (e) $(\mathbf{M6})_{120}\text{-}(\mathbf{M1})_{50}\text{-}(\mathbf{M7})_{40}$ (f) $(\mathbf{M6})_{120}\text{-}(\mathbf{M1})_{109}\text{-}(\mathbf{M7})_{25}$.
- Figure 5.11** Cryo-TEM micrographs of 0.5 wt% aqueous solutions of amphiphilic diblock copolymers: (a) $(\mathbf{M6})_{120}\text{-}(\mathbf{M1})_{50}$ (b) $(\mathbf{M1})_{70}\text{-}(\mathbf{M7})_{24}$.
- Figure 5.12** Cryo-TEM micrographs of 0.5 wt% aqueous solutions of amphiphilic triblock copolymers prepared at ambient conditions: (a) $(\mathbf{M1})_{70}\text{-}(\mathbf{M5})_{83}\text{-}(\mathbf{M7})_{13}$ (b) $(\mathbf{M1})_{70}\text{-}(\mathbf{M6})_{140}\text{-}(\mathbf{M7})_{13}$.
- Figure 5.13** Cryo-TEM micrographs of 0.5 wt% aqueous solutions of amphiphilic triblock copolymers after thermal treatment: (a) $(\mathbf{M1})_{70}\text{-}(\mathbf{M5})_{83}\text{-}(\mathbf{M7})_{13}$ after preparation by protocol A and annealing for 25 d at 78°C (protocol C) (b) $(\mathbf{M1})_{70}\text{-}(\mathbf{M6})_{140}\text{-}(\mathbf{M7})_{13}$ dispersed by protocol B.

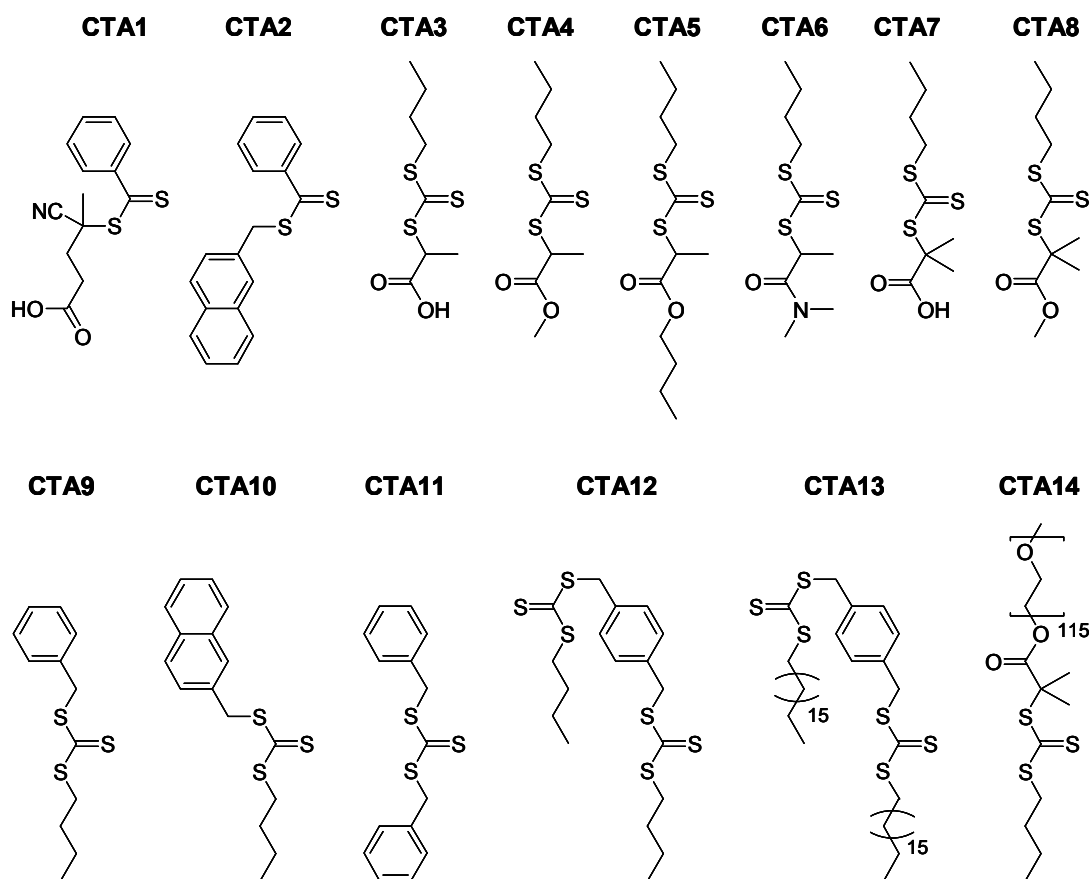
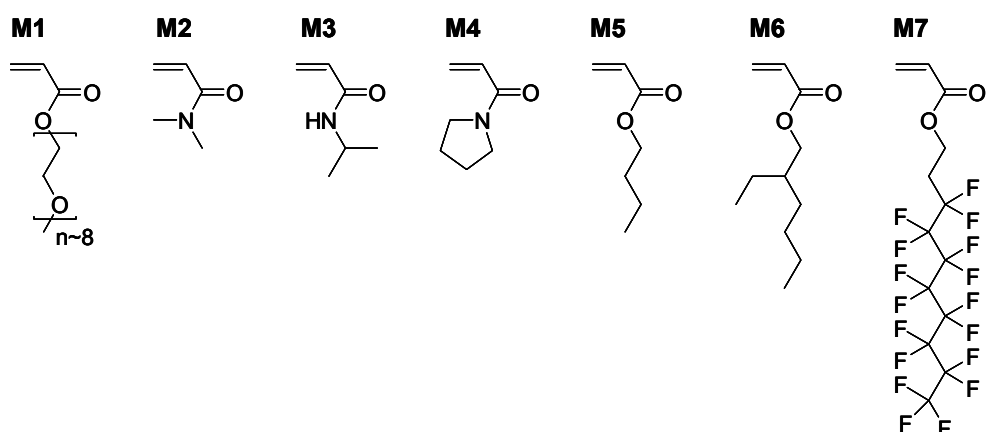
- Figure 5.14** Cryo-TEM micrographs of ABC triblock oligomers with a linear PEO chain (0.5 wt% in water): **PEO-(M5)₂₂-(M7)₂** dispersed at (a) 25°C and (b) 70°C. **PEO-(M6)₂₄-(M7)₂** dispersed at (c) 25°C and (d) 70°C.
- Figure 5.15** Cryo-TEM micrographs of triblock copolymer **(M6)₁₂₀-(M1)₅₀-(M7)₄₀** (0.5 wt% in water): (a) dispersed at 25°C (protocol A) (b) after dispersion at 25°C and annealing for 25 d at 78°C (protocol C) (c) dispersed at 70°C (protocol B).
- Figure 5.16** Micellar aggregates of triblock copolymer **(M6)₁₂₀-(M1)₁₀₉-(M7)₂₃** (0.5 wt% in water): Morphologies (a) and (b) were found for protocol A. Morphologies (c) and (d) evolved after annealing for 25 d at 78°C (protocol C).
- Figure A1.1** ¹H NMR spectrum of **CTA1** in CDCl₃
- Figure A1.2** ¹³C NMR spectrum of **CTA1** in CDCl₃
- Figure A1.3** ¹H NMR spectrum of **CTA2** in CDCl₃
- Figure A1.4** ¹³C NMR spectrum of **CTA2** in CDCl₃
- Figure A1.5** ¹H NMR spectrum of butyl 2-bromo-propionate in CDCl₃
- Figure A1.6** ¹³C NMR spectrum of butyl 2 bromo-propionate in CDCl₃
- Figure A1.7** ¹H NMR spectrum of **CTA5** in CDCl₃
- Figure A1.8** ¹³C NMR spectrum of **CTA5** in CDCl₃
- Figure A1.9** ¹H NMR spectrum of *N,N*-dimethyl 2-bromo-propionamide with *N,N*-dimethyl 2-chloro-propionamide as by-product in CDCl₃
- Figure A1.10** ¹³C NMR spectrum of *N,N*-dimethyl 2-bromo-propionamide with *N,N*-dimethyl 2-chloro-propionamide as by-product in CDCl₃
- Figure A1.11** ¹H NMR spectrum of **CTA6** in CDCl₃
- Figure A1.12** ¹³C NMR spectrum of **CTA6** in CDCl₃
- Figure A1.12** ¹H NMR spectrum of **CTA7** in CDCl₃
- Figure A1.14** ¹³C NMR spectrum of **CTA7** in CDCl₃
- Figure A1.15** ¹H NMR spectrum of **CTA8** in CDCl₃
- Figure A1.16** ¹³C NMR spectrum of **CTA8** in CDCl₃
- Figure A1.17** ¹H NMR spectrum of **CTA10** in CDCl₃
- Figure A1.18** ¹³C NMR spectrum of **CTA10** in CDCl₃
- Figure A1.19** ¹H NMR spectrum of **CTA12** in CDCl₃
- Figure A1.20** ¹³C NMR spectrum of **CTA12** in CDCl₃
- Figure A1.21** ¹H NMR spectrum of **CTA13** in CDCl₃
- Figure A1.22** ¹³C NMR spectrum of **CTA13** in CDCl₃
- Figure A1.23** ¹H NMR spectrum of **CTA14** in CDCl₃
- Figure A2.1** FT-IR spectrum of **CTA2** (KBr pellet)
- Figure A2.2** FT-IR spectrum of **CTA5** (KBr pellet)
- Figure A2.3** FT-IR spectrum of **CTA6** (KBr pellet)
- Figure A2.4** FT-IR spectrum of **CTA7** (KBr pellet)

-
- Figure A2.5** FT-IR spectrum of **CTA8** (KBr pellet)
- Figure A2.6** FT-IR spectrum of **CTA10** (KBr pellet)
- Figure A2.7** FT-IR spectrum of **CTA12** (KBr pellet)
- Figure A2.8** FT-IR spectrum of **CTA13** (KBr pellet)
- Figure A2.9** FT-IR spectrum of **CTA14** (KBr pellet)
- Figure A3.1** Cryo-TEM micrographs of 0.5 wt% aqueous solutions of PEO homopolymers. (a) comb polymer **(M1)₇₀** (b) linear PEO (M ~ 20,000 g/mol).
- Figure A3.2** Large spherical objects observed for 0.5 wt% aqueous solution of block copolymers (a) **(M6)₁₂₀-(M1)₅₀** (b) **PEO-(M5)₂₂-(M7)₂**.
- Figure A3.3** Cryo-TEM micrograph of **(M6)₁₂₀-(M1)₁₀₉** (0.5 wt% in H₂O).

Appendix 5: List of tables

- Table 3.1** Maximum absorption wavelengths (λ_{\max} , in nm) and molar absorptivities (ϵ , in $\text{L mol}^{-1} \text{cm}^{-1}$) for a variety of thiocarbonylthio compounds taken from the literature
- Table 3.2** Maximum absorption wavelengths (λ_{\max}) of the π - π^* - and n - π^* -absorption band of the thiocarbonyl bond for the studied dithiobenzoates and trithiocarbonates in a variety of solvents
- Table 3.3** Molar absorptivities ϵ (in $\text{L mol}^{-1} \text{cm}^{-1}$) due to the π - π^* - and n - π^* -transition of the thiocarbonyl bond for the studied dithiobenzoates and trithiocarbonates in a variety of solvents
- Table 3.4** Solvent polarity parameters
- Table 3.5** Molar mass determination of polymers used for the evaluation of end-group analysis
- Table 4.1** Characterization of the poly(acrylamide) homo- and block copolymers
- Table 4.2** Dynamic light scattering analysis of 0.1 wt% aqueous solutions of double-thermoreponsive triblock copolymers prepared by the slow and fast heating protocol
- Table 5.1** Characterization of triphilic ABC triblock copolymers and their precursors
- Table 5.2** Thermal analysis of homo- and triblock copolymers by differential scanning calorimetry (DSC)
- Table 5.3** Dynamic light scattering analysis of homo- and block copolymer solutions (4.0 g/L) in various organic solvents
- Table 5.4** Dynamic light scattering analysis of 0.5 wt% aqueous solutions of diblock copolymers prepared at 25°C
- Table 5.5** Dynamic light scattering analysis of 0.5 wt% aqueous solutions of triblock copolymers prepared at 25°C (protocol A) and 70°C (protocol B)
- Table 5.6** Characteristics of the micellar aggregates of amphiphilic di- and triblock copolymers as studied by cryo-TEM
- Table 7.1** Preparation of polymers for the evaluation of end-group analysis
- Table 7.2** Polymerization conditions for the synthesis of double-thermoreponsive ABC triblock copolymers and their precursors (65°C)
- Table 7.3** Polymerization conditions for the synthesis of triphilic ABC triblock copolymers and their precursors

Appendix 6: Structures of the CTAs, monomers and initiators used

Chain transfer agents**Monomers****Initiators**